



Universiteit
Leiden
The Netherlands

Molecular characterization of copper-dependent enzymes involved in *Streptomyces* morphology

Petrus, Maria Louise Catharina

Citation

Petrus, M. L. C. (2016, February 18). *Molecular characterization of copper-dependent enzymes involved in Streptomyces morphology*. Retrieved from <https://hdl.handle.net/1887/37863>

Version: Corrected Publisher's Version

License: [Licence agreement concerning inclusion of doctoral thesis in the Institutional Repository of the University of Leiden](#)

Downloaded from: <https://hdl.handle.net/1887/37863>

Note: To cite this publication please use the final published version (if applicable).

Cover Page



Universiteit Leiden



The handle <http://hdl.handle.net/1887/37863> holds various files of this Leiden University dissertation

Author: Petrus, Marloes

Title: Molecular characterization of copper-dependent enzymes involved in *Streptomyces* morphology

Issue Date: 2016-02-18

Molecular characterization of
copper-dependent enzymes involved
in *Streptomyces* morphology

Marloes Petrus

Cover & layout design: Marloes Petrus

Funding statement: My PhD position at the university was supported by the grant awarded to prof P.J.J. Hooykaas on the occasion of his appointment to KNAW Academy Professor

Printed by Ridderprint BV, Ridderkerk, the Netherlands

ISBN: 978-94-6299-258-0

Molecular characterization of copper-dependent enzymes involved in *Streptomyces* morphology

Proefschrift

ter verkrijging van

de graad van Doctor aan de Universiteit Leiden,

op gezag van Rector Magnificus prof. mr. C.J.J.M. Stolker,

volgens besluit van het College voor Promoties

te verdedigen op donderdag 18 februari 2016

klokke 15:00 uur

door

Maria Louise Catharina Petrus

geboren te Heemskerk, Nederland

8 januari 1988

Promotor: Prof. dr. G.P. van Wezel

Copromotor: Dr. D. Claessen

Promotiecommissie: Prof. dr. P.J.J. Hooykaas

Prof. dr. T. Palmer

Prof. dr. H.P. Spaink

Prof. dr. M. Ubbink

Prof. dr. H.A.B. Wösten

Voor mijn ouders

Contents

Chapter 1	General introduction	9
Chapter 2	Pivotal roles for <i>Streptomyces</i> cell surface polymers in morphological differentiation, attachment and mycelial architecture	15
Chapter 3	Analysis of two distinct mycelial populations in liquid-grown <i>Streptomyces</i> cultures using a flow cytometry-based proteomics approach	31
Chapter 4	GlxA is a new structural member of the radical copper oxidase family and is required for glycan deposition at hyphal tips and morphogenesis of <i>Streptomyces lividans</i>	49
Chapter 5	The DyP-type peroxidase DtpA is a Tat-substrate required for GlxA maturation and morphogenesis in <i>Streptomyces</i>	73
Chapter 6	Use of an innovative peptidoglycan-independent platform for the characterization of the glycan produced by CslA	99
Chapter 7	General discussion	121
	Nederlandse samenvatting	131
	References	143
	Curriculum vitae	159
	Publications	161

1

General introduction

Soil bacteria of the genus *Streptomyces* have been studied for more than a century, during which a paradigm shift has occurred. They were initially described as the causative agent of potato scab, a plant disease of root and tuber crops that makes vegetables unsuitable for sale and therefore cause a great economic impact (Güssow, 1914; Millard, 1922). However, during the 1940s streptomycetes were seen in a much more positive light when they became of key interest due to their capability to produce antibiotics. Of these antibiotics streptomycin was the first to be able to combat *Mycobacterium tuberculosis* (Schatz *et al.*, 1944), a discovery for which Selman Waksman was awarded the Nobel Prize in 1952.

Over half of the antibiotics nowadays used in the clinic are produced by streptomycetes. In addition, these bacteria produce a wide variety of other natural compounds used as anticancer, immunosuppressive, antifungal and antihelminthic agents (Hopwood, 2007). Besides the medical interest for streptomycetes and their metabolites there is also a strong interest in the use of these bacteria for the production of industrial proteins. Especially important are the enzymes produced to utilize naturally occurring polymers such as cellulose, mannan, chitin, xylan, starch and agar, and which can be explored for the conversion of renewable energy sources (Vrancken and Anné, 2009). Additionally, streptomycetes are the preferred host for the production of a number of heterologous proteins since they possess efficient protein secretion systems, via which the products are directly released in the culture broth. This greatly facilitates purification, and increases the downstream processing efficiency. Due to the relatively low levels of extracellular proteolytic activity *Streptomyces lividans* is preferred over other *Streptomyces* species as a production host (Vrancken and Anné, 2009).

The Streptomyces life cycle

Streptomycetes belong to the phylum of Actinobacteria, which are Gram-positive bacteria with a relatively high G+C content in their DNA. Bacteria from this phylum exhibit a wide variety of cellular morphologies from coccoid (e.g. *Micrococcus*), rods (*Conexibacter*, *Demequina*) and rod-cocci (e.g. *Arthrobacter*) to more complex forms such as coryneform (*Corynebacterium*), bifurcating or branching cells (*Bifidobacterium*, *Propionibacterium*), and branching mycelial forms (e.g. *Nocardia*, *Frankia*, *Thermobifida*; Goldman and Green, 2008). Streptomycetes belong to the group with the most complex morphology by forming differentiating mycelia that produce drought-resistant spores (Hopwood, 2007). Growth initiates with the germination of a spore, leading to the formation of threadlike structures called hyphae. These hyphae grow via extension of the hyphal tips and by the formation of new branches at some distance behind the growing tip. Occasional crosswalls divide the vegetative hyphae into long multigenomic compartments. This creates a tightly interwoven network of hyphae called a vegetative mycelium (Flårdh and Buttner, 2009). The energy necessary for growth is generated by conversion of organic materials present in the soil that become available upon the secretion of a wide variety of polymer-degrading enzymes (Chater *et al.*, 2010). When nutrients become depleted the reproductive phase is initiated, leading to the formation of an aerial mycelium that is established on top of the vegetative mycelium. Autolytic degradation of the vegetative mycelium by programmed cell death provides the nutrients for this developmental step, while the simultaneous production of antibiotics protects against opportunistic bacteria (Rioseras *et al.*, 2014). Eventually, an astonishing cell division event converts the freestanding aerial hyphae into chains of some hundred unigenomic spores. These spores are easily dispersed and may give rise to new colonizing mycelia.

The complex life cycle of *Streptomyces* is subject to extensive regulation. Most famous are two classically described classes of genes responsible for distinct stages of differentiation: The *bld* (bald) genes are required for the transition from vegetative to aerial growth (Merrick, 1976), while the *whi* (white) genes subsequently contribute to the formation of mature grey-pigmented spores (Chater, 1972). One example of an important *bld* gene is *bldN* for an extracytoplasmic function family sigma factor, which, amongst others, regulates the expression of the chaplin and rodlin proteins (Claessen *et al.*, 2003; Elliot *et al.*, 2003; den Hengst *et al.*, 2010; Bibb *et al.*, 2012). These cell surface proteins decorate the aerial structures, thereby providing surface hydrophobicity and rigidity (see below).

Morphogenesis in submerged cultures

The production of secondary metabolites and enzymes typically occurs in large bioreactors. Mycelial morphology in liquid environments is species-specific and influenced by

environmental conditions. Some species form mostly dispersed, highly fragmenting mycelia, while others establish open mycelial networks (also referred to as mats) or dense clumps of intertwined hyphae called pellets (Paul and Thomas, 1998; van Dissel *et al.*, 2014). Only several species are able to sporulate in liquid environments, including *Streptomyces venezuelae* and *Streptomyces griseus* (Bewick *et al.*, 1976; Kendrick and Ensign, 1983). In bioreactors, morphology is tightly coupled to optimal production of secondary metabolites and enzymes. It is generally accepted that growth as pellets is preferred for the production of antibiotics (Vecht-Lifshitz *et al.*, 1990; Martin and Bushell, 1996; Sarrà *et al.*, 1999). Conversely, optimal enzyme production occurs when the mycelium grows in a more dispersed manner (van Wezel *et al.*, 2006). However, these different morphologies also put constraints on the abilities to maximize product yields. For example, the relatively large size and high hyphal density of pellets limits the transfer of nutrients to the inner parts of these structures, which will decrease growth rate and productivity. On the other hand, open mycelial networks severely increase the viscosity of the culture broth. The ability to control the morphology of *Streptomyces* in liquid-grown environments is therefore key to improve industrial fermentation.

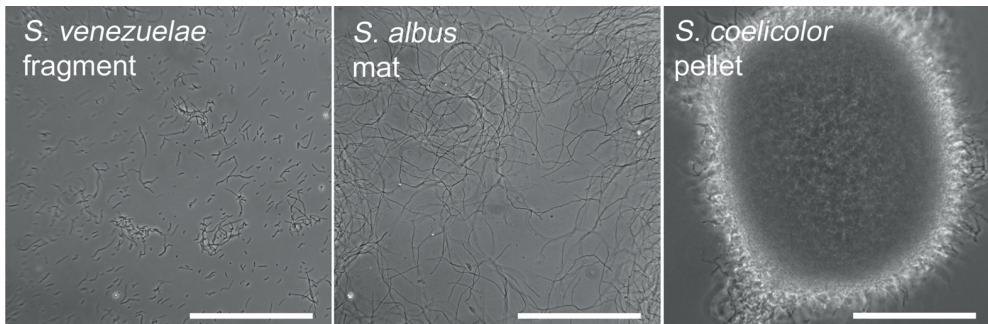


Figure 1. Distinct morphologies of *Streptomyces* species in liquid-grown cultures, namely fragments (*S. venezuelae*), mycelial mats (*S. albus*) and pellets (*S. coelicolor*). Scale bar, 100 μm . Figure is reproduced with permission from van Dissel *et al.* (2014).

Outline of the thesis

Although streptomycetes have been studied for several decades, relatively little is known about the genetic determinants influencing their morphology in liquid-grown cultures. The work presented in this thesis focuses on structural cell surface macromolecules. A better understanding of their role in shaping mycelial morphology should enable us to create optimized production strains and to improve fermenter set-up, which together will promote industrial scale production with streptomycetes.

Cell surface macromolecules act at the interface between the cell and its environment and are crucial for growth and development. **Chapter 2** reviews how *Streptomyces* cell surface polymers function in the formation of reproductive aerial structures, the attachment of hyphae to abiotic surfaces and in generating pellet shape. The review introduces several components that are further studied in the research chapters of this thesis. These components include the extracellular chaplin and rodlin proteins, which are known to play multiple roles during growth and development. They are instrumental for lowering the water surface tension to allow hyphae to escape the aqueous environment, for decorating the *Streptomyces* aerial structures with a hydrophobic rodlet layer, and for attachment of hyphae to hydrophobic surfaces. The polysaccharide produced by the cellulose synthase-like protein CslA is another important extracellular macromolecule required for morphogenesis. This polysaccharide is thought to provide structural rigidity to growing hyphal tips, and is required for the formation of dense pellets. Together, these extracellular macromolecules provide protection and stability to a growing *Streptomyces* colony, resembling the situation in a biofilm of unicellular bacteria where extracellular polymeric substances protect a group of closely collaborating cells.

So far the study of *Streptomyces* pellet formation is mainly based on microscopic analysis, which limits the number of particles that can be analysed. However, to quantitatively describe the growth and development of pellets, a more robust and high-throughput analysis method is desired. **Chapter 3** describes the use of the Complex Object Parametric Analyser and Sorter (COPAS) for analysing pellets in streptomycetes. The COPAS platform is a flow cytometry-based technique designed for measuring objects that are too large to be analysed with conventional cytometry approaches. Use of this technique revealed that liquid-grown *Streptomyces* cultures contain two distinct populations of pellets that not only differ in size, but also appear to have separate roles in growth and production. In addition, a number of mutants is presented, all of which are affected in synthesis of cell surface macromolecules, and thereby leading to pronounced effects on pellet size.

One of the genes that strongly influences pellet size and morphology is *csIA*. The *csIA* gene is located in an operon upstream of *glxA*, which encodes a radical copper oxidase with

homology to fungal galactose oxidases. **Chapter 4** discusses the role of *csIA* and *glxA* in *Streptomyces* morphogenesis. Mutant strains lacking either of these genes fail to synthesize and accumulate a glycan at hyphal tips, and as a consequence neither form pellets in liquid-grown cultures, nor aerial hyphae on solid media. GlxA is a membrane-associated enzyme with a unique tertiary structure. The crystal structure indicates that the active site contains a mononuclear copper (Cu) ion and a tyrosyl-cysteine cross-link. The formation of this cross-link and the incorporation of a Cu ion are fundamental for GlxA functionality and depend on the activity of the copper chaperone Sco. The change from immature GlxA (without a Tyr-Cys cross-link) to mature GlxA (with a Tyr-Cys cross-link) is visible by a shift in electrophoretic mobility, which is presented in **Chapter 5**. This chapter also describes the roles of the other genes of the *sco* operon in morphogenesis. This led to the discovery of a novel DyP-type peroxidase, called DtpA, which appears to be crucial for maintaining the GlxA maturation status. We show that DtpA functions as a peroxidase in the presence of the hydrogen peroxide-producing enzyme GlxA. Deletion of *dtpA* results in loss of GlxA maturation and blocks development, both of which can be overcome by the addition of Cu to the medium. DtpA contains a so-called Tat signal peptide, which directs this protein to the twin-arginine translocation machinery for export. Interestingly, the developmental block in *tat* mutants can be overcome by extracellular complementation with Cu, which again restores the maturation defect of GlxA. This work suggests a Cu-trafficking pathway and Tat-dependent secretion of DtpA, which links this protein to CslA and GlxA-dependent morphogenesis.

Chapter 6 describes the attempts to characterize the glycan produced by CslA. Sequence analysis shows that CslA is a processive glycosyltransferase with a structural fold similar to the cellulose synthase BcsA from *Rhodobacter sphaeroides*. Chemical characterization of the polymer produced by CslA appears to be hampered by the excess of peptidoglycan present in the cell wall. Therefore, a peptidoglycan-independent glycan production platform is presented based on *S. viridifaciens* L-forms that can grow without a peptidoglycan-based cell wall. Preliminary results using this system indicate that the glycan produced by CslA may contain *N*-acetylgalactosamine. This production platform may also be used for the synthesis and purification of glycans from other bacterial sources that in their endogenous hosts are only produced in limited amounts.

Our current understanding how *Streptomyces* morphology is controlled, based on the published literature and the data described in this thesis, is discussed in **Chapter 7**. This Chapter also contains a summary of the thesis.

2

Abstract

Cells that are part of a multicellular structure are typically embedded in an extracellular matrix, which is produced by the community members. These matrices, the composition of which is highly diverse between different species, are typically composed of large amounts of extracellular polymeric substances, including polysaccharides, proteins, and nucleic acids. The functions of all these matrices are diverse: they provide protection, mechanical stability, mediate adhesion to surfaces, regulate motility, and form a cohesive network in which cells are transiently immobilized. In this review we discuss the role of matrix components produced by streptomycetes during growth, development and attachment. Compared to other bacteria it appears that streptomycetes can form morphologically and functionally distinct matrices using a core set of building blocks.

This chapter was published as:

Marloes L.C. Petrus and Dennis Claessen (2014) Antonie van Leeuwenhoek 106: 127-139.

Pivotal roles for *Streptomyces* cell surface polymers in morphological differentiation, attachment and mycelial architecture

Introduction

Bacteria belonging to the genus *Streptomyces* are present in a large number of environments, but most notably in the soil (Hopwood, 2007). Unlike most other bacteria, streptomycetes form a so-called mycelium that consists of branched filaments that grow by tip extension (Flårdh and Buttner, 2009). This mycelium invades and colonizes the soil environment and secretes numerous enzymes that facilitate break down of plant material, which yields nutrients that can be used as food for the growing mycelium (Chater *et al.*, 2010). When nutrients become limiting, a developmental switch occurs during which hyphae start to escape the moist environment and grow into the air. These so-called aerial hyphae can further differentiate into long chains of spores, which can withstand the adverse conditions. Following their dispersal, these spores will reinitiate growth in suitable environments.

Streptomycetes not only grow in moist substrates or in the air but they may also grow over and attach to hydrophobic surfaces such as the leaf of a plant or the skin of an animal. Attachment could contribute to the effective degradation of substrates by saprophytic streptomycetes. Furthermore, attachment of microbes to host surfaces is crucial for initiation of infections. Whether adherence to surfaces is required for the establishment of infections by pathogenic streptomycetes, such as the plant pathogen *Streptomyces scabies* or the human pathogen *Streptomyces somaliensis*, is unknown. In this review, we will discuss the mechanisms that enable streptomycetes to leave the aqueous environment and to grow into the air or to attach to hydrophobic surfaces. We will particularly focus on cell surface-associated polymers, which turn out to have multiple functions in the biology of these organisms.

The role of chaplins and rodlines in aerial growth

The transition from vegetative to aerial growth is characterized by a dramatic change in the surface properties of the hyphae. Whereas vegetative hyphae are hydrophilic, aerial hyphae are hydrophobic due to the assembly of an additional outer surface layer or matrix, called the rodlet layer (Wildermuth *et al.*, 1971; Claessen *et al.*, 2004). The rodlet layer has an amphipathic nature: the hydrophilic side faces the cell wall, while the hydrophobic side is exposed to the air (Elliot and Talbot, 2004; Bokhove *et al.*, 2013). This sheath encapsulates aerial hyphae, leading to the formation of a periplasmic-like compartment that probably contributes to drought resistance by ensuring hydration of the cell walls (Chater *et al.*, 2010). In addition, this surface layer might prevent hyphae from growing back into the aqueous environment. The hydrophobic side of the rodlet layer is characterized by thin fibrils. These fibrils are formed by the assembly of so-called chaplin proteins, for *coelicolor hydrophobic aerial proteins*, after the model streptomycete (i.e. *Streptomyces coelicolor*) in which they were first discovered (Claessen *et al.*, 2003; Elliot *et al.*, 2003). Rather than being deposited randomly at the hyphal surface, these fibrils are often aligned into pairs (rodlets; Fig. 1). This process is mediated by the activity of the rodlin proteins RdIA and RdIB (Claessen *et al.*, 2002; Claessen *et al.*, 2004). Although under ‘normal laboratory conditions’ RdIA and RdIB are not required for aerial growth, it was recently established that an intact rodlet layer is important for aerial growth under osmotic stress conditions, which streptomycetes might encounter occasionally in heterogenic soil environments (de Jong *et al.*, 2012). This might explain why these genes are conserved in most streptomycetes, the only known exception being *Streptomyces avermitilis* (Claessen *et al.*, 2004).

Two types of chaplin proteins exist that differ in length. *S. coelicolor* produces five so-called short chaplins (i.e ChpD-H) that consist of about 55 amino acids, and three longer variants,

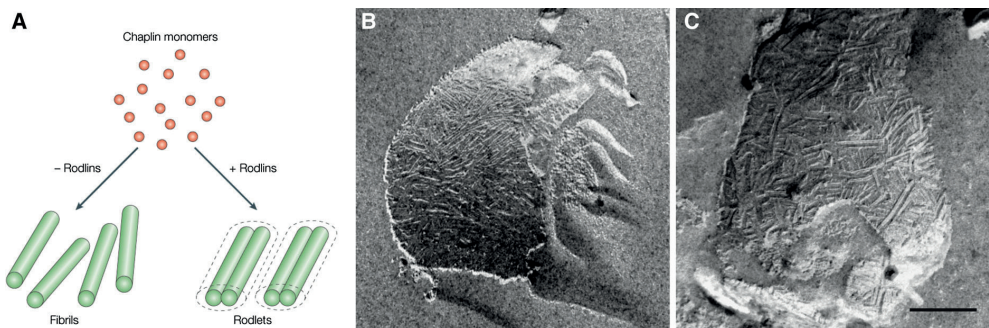


Figure 1. The formation of rodlets in *Streptomyces coelicolor*. **(A)** The formation of rodlets results from the interplay between rodlines and chaplins. Without rodlines, chaplins assemble into fibrils that are randomly deposited on the outer surface of aerial hyphae and spores, as observed in the *S. coelicolor* Δ rdIAB strain **(B)**. In the presence of rodlines, these fibrils are organized into rodlet structures **(C)**. Bar represents 200 μ m. Panels are reproduced, with permission, from Gebbink *et al.* (2005) (A) and Claessen *et al.* (2003) (B, C).

ChpA-C, that are about 230 amino acids in length. All chaplin proteins contain a signal sequence for secretion by the Sec translocation machinery, followed by one (ChpD-H) or two (ChpA-C) so-called chaplin domains (annotated as DUF320 domains (Yeats *et al.*, 2003)). The chaplin domains are mostly hydrophobic and contain three conserved GN motifs, spaced 12-13 amino acids apart (Elliot *et al.*, 2003). These motifs likely contribute to structuring of the domains, of which the central part is predicted to form β -strands, while the termini are likely to form random coil segments (Elliot *et al.*, 2003; Bokhove *et al.*, 2013). The long chaplins have an additional C-terminal signal that is recognized by sortases, which covalently couple their substrates to the growing cell wall (Elliot *et al.*, 2003; Hopwood, 2007; Duong *et al.*, 2012; Schneewind and Missiakas, 2012).

Genes encoding chaplin proteins have been identified in all sequenced *Streptomyces* genomes, each of which typically contains multiple copies. Deletion of the chaplin genes highlighted their importance for aerial growth. In a strain lacking all chaplin genes, aerial growth was severely impaired (Claessen *et al.*, 2004; Capstick *et al.*, 2007). The few aerial hyphae that were formed were devoid of any surface structure, and were found to be lying on top of the vegetative mycelium presumably due to their hydrophilic nature (Claessen *et al.*, 2004). These results demonstrate that the chaplin protein fibrils not only provide surface hydrophobicity, but also rigidity to the aerial hyphae. Notably, three chaplins appear to be invariably present in streptomycetes, which are ChpC, ChpE, and ChpH (Di Berardo *et al.*, 2008). Indeed, elegant work from the Elliot lab indicates that these three chaplins are sufficient to raise a substantial aerial mycelium. Further characterization of this so-called “minimal chaplin strain” indicated that ChpH is the major polymerization unit contributing to aerial growth and the formation of surface fibers (Di Berardo *et al.*, 2008). Furthermore, the long chaplin ChpC probably serves as a cell wall anchor required for tethering the chaplin fibrils to the cell surface. Replacing ChpC and ChpH for ChpA and ChpD, which too are a long and short chaplin respectively, also leads to a strain that is able to raise aerial hyphae and assemble a rodlet layer, albeit less efficiently. This reduction probably relates to the reduced expression of the *chpA* and *chpD* genes when compared to *chpC* and *chpH*, with the latter genes being constitutively expressed during growth (Claessen *et al.*, 2003; Elliot *et al.*, 2003).

ChpE probably has a unique function in the assembly process. It is the only short chaplin lacking two cysteine residues, which are otherwise conserved in all chaplin domains, the only other exception being the C-terminal domain of ChpB. Experiments using synthetic versions of the short chaplins indicate that ChpE, like the other short chaplins, can individually form fibrillar structures *in vitro* (Sawyer *et al.*, 2011). This indicates that the cysteine residues are not essential for chaplin fibril formation, although these residues were shown to be important for the formation of aerial hyphae and rodlets (Di Berardo *et al.*, 2008). The cysteine residues could play a role in the formation of oligomers. Consistent with this idea is the observation that homodimers of ChpH or ChpF were identified in purified chaplins

from cell walls (Sawyer *et al.*, 2011). Such oligomers might serve as nuclei that stimulate fibril formation *in vivo*. Interestingly, *chpE* could only be deleted in a strain lacking the rodlin genes, or the other chaplin genes, but not individually in the wild-type strain (Di Berardo *et al.*, 2008). Taken together, these results would be consistent with a model in which the rodlin proteins coordinate and stimulate chaplin polymerization, while ChpE delays this process, perhaps by interfering with the formation of oligomers. The loss of coordinated assembly in the absence of ChpE could negatively affect development and rodlet formation, and could possibly even be toxic. Unraveling how these chaplins, in conjunction with the rodlin proteins, ultimately cooperate in rodlet formation, is an important challenge for the future.

Chaplins assemble into amyloid fibrils

Proteins that function outside the cell, such as the chaplin proteins, are challenged by relatively harsh, non-physiological conditions. In these environments proteins spontaneously adopt the conformation of lowest free energy that is kinetically accessible to them (Sawyer *et al.*, 2012). Many proteins thus end up forming so-called amyloid protein fibrils (Gebblink *et al.*, 2005; Blanco *et al.*, 2012; Gras and Dennis, 2014). These fibrils have the capacity to bind dyes such as Congo Red and Thioflavin T, which have subsequently been used to visualize and identify amyloids, although these dyes are often not very specific (Khurana *et al.*, 2001). Conclusive evidence to demonstrate that a protein fibril is an amyloid is obtained by diffraction analysis (Kirschner *et al.*, 1986). Amyloid fibrils share a common structure, which is called the cross- β structure, where β -sheets run parallel to the axis of the fibre and hydrogen-bonded β -strands run perpendicular to the fibre axis (Blake and Serpell, 1996; Sunde *et al.*, 1997). Indeed, this cross- β structure conformation was also shown for the chaplin proteins, both individually and in mixtures, showing that chaplins form amyloid fibrils (Sawyer *et al.*, 2011; Sawyer *et al.*, 2012; Bokhove *et al.*, 2013).

Amyloid-forming proteins typically have one or several so-called amyloid domains, consisting of short stretches of amino acids that drive the assembly process (Pastor *et al.*, 2007). Indeed, the conserved ChpH protein contains two of these domains. *In vitro* studies using synthetic versions of these domains indicate that they both can assemble into amyloid fibrils (Capstick *et al.*, 2011). However, *in vivo* these two domains appear to be functionally different. Whereas both domains are required for the formation of aerial hyphae, only the C-terminal domain was required for rodlet formation (Capstick *et al.*, 2011). This could indicate that the C-terminus interacts with other factors that coordinate, or stimulate rodlet formation, as observed with other functional amyloids (Hammer *et al.*, 2007).

Recently, high-resolution electron microscopy in combination with diffraction analyses and secondary structure predictions led to the proposition of a model how chaplins might be

organized into amyloid fibrils (Bokhove *et al.*, 2013; Fig. 2). This model is based on the observation that chaplin fibrils have a diameter of approximately 7 nm, and are highly asymmetric: the hydrophobic side of the fibrils is curved, while the hydrophilic side is relatively flat. In the proposed model, 17 residues present in each chaplin domain are predicted to form a hydrophobic core consisting of β -strands, which is air-exposed. In contrast, the termini of the chaplin proteins are predicted to form hydrophilic random coils that orient towards the aqueous face (or the cell wall). Notably, the curved side of the fibrils would be too large to be spanned by the hydrophobic core of an individual chaplin domain. Therefore, the model suggests that two short chaplin proteins (or occasionally one large chaplin containing two chaplin domains) are oriented in a head-to-head fashion to form the repeating unit of the fiber (Fig. 2). By stacking repeating units in the direction of the fiber, large β -sheets are formed, which are stabilized by hydrogen bonds. Diffraction analysis suggested that these fibrils would only contain parallel β -sheets (Bokhove *et al.*, 2013). Although the model is supported by the current data we have on chaplins, definite proof would be obtained using crystallography approaches. However, crystals are typically difficult

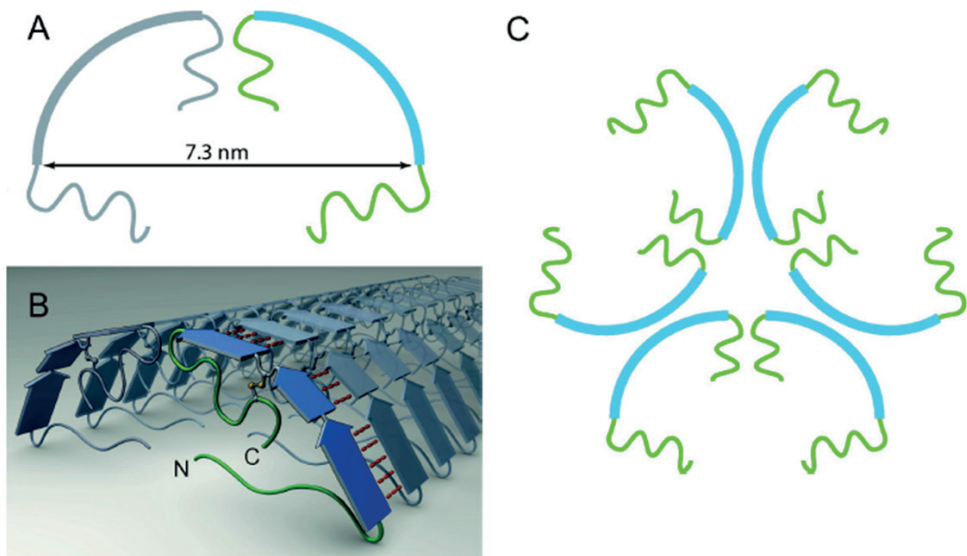


Figure 2. Proposed model for the organization of chaplin monomers into amyloid fibrils. **(A)** Chaplin fibrils, with a diameter of 7.3 nm, are formed by the assembly of repeating units that contain two chaplin monomers oriented in a head-to-head fashion. The hydrophobic side (blue) of the fibrils is curved and exposed to the air, while the hydrophilic side (green) is relatively flat and submerged in the solvent. **(B)** Stacking of the repeating units in the fibril yields an extended parallel β -sheet structure in the direction of the fibril axis. This structure is probably stabilized by the hydrogen bonds (red dashes) formed between the β -strands of adjacent units. The cysteine residues (in yellow) form an intramolecular bridge, thereby connecting the C-terminal part of the protein to the central β -strand. **(C)** Chaplin fibrils can assemble into larger, 12 nm-wide fibres, which can be formed by bundling of three 7.3 nm-wide fibrils. In these larger fibres, the hydrophobic surfaces are buried within the fibre, while the hydrophilic surfaces are exposed to the liquid. Figure is reproduced, with permission, from Bokhove *et al.* (2013).

to obtain with proteins that tend to assemble at high concentrations, such as the chaplins.

The role of chaplins and SapB in escape of aerial hyphae

The first step in the formation of aerial structures is the escape of hyphae from the aqueous environment into the air. However, the medium-air interface, which is characterized by a high surface tension, poses a barrier for aerial growth, despite the capacity of hyphae to generate considerable turgor pressure. In order to overcome this barrier, streptomycetes secrete ChpE and ChpH in the environment, which help to reduce the surface tension (Claessen *et al.*, 2003; Willey *et al.*, 2006). *In vitro* experiments indicated that chaplins can reduce the surface tension, within minutes, from 72 to 24 mJ m⁻², making them among the most potent natural surfactants known (Claessen *et al.*, 2003; Sawyer *et al.*, 2011). Lowering of the water surface tension coincides with the appearance of a light-reflecting membrane at the medium-air interface (Claessen *et al.*, 2003). Recent data indicates that this membrane is amphipathic and asymmetric: the hydrophilic side, which faces the aqueous environment is relatively flat, while the hydrophobic side is exposed to the air and characterized by thin fibrils (Bokhove *et al.*, 2013). At physiological pH, this membrane is rigid considering the fact that it can be lifted from the water-air interface without rupturing. Intuitively, this strength would contradict its supportive role in the escape of hyphae. This apparent discrepancy might be explained by assuming that the surface tension-reducing activity and the formation of rigid fibrils are consecutive steps in the chaplin assembly process. This idea was strengthened by the observation that an unprecedented surface activity of chaplins was observed at elevated pH, coinciding with the formation of a semi-liquid membrane, rather than the rigid membrane formed at neutral pH (Ekkers *et al.*, 2014). The semi-liquid membrane was suggested to represent a trapped intermediate in the assembly process. As such, assembly of chaplins would be strikingly similar to the assembly of a class of fungal proteins known as hydrophobins, which also proceeds via distinct intermediates (de Vocht *et al.*, 2002). Like filamentous streptomycetes, filamentous fungi form reproductive aerial structures after a period of vegetative growth. In a similar manner as chaplins facilitate aerial growth in streptomycetes, the SC3 hydrophobin of *Schizophyllum commune* is secreted in the environment to lower the water surface tension thus enabling aerial growth (Wösten *et al.*, 1999). Moreover, fungal aerial hyphae secrete the SC3 protein that assembles, like chaplins, into fibrillar structures on the cell surface thereby rendering the hyphal surface hydrophobic (Wösten *et al.*, 1993). These data show a striking similarity in the mode-of-action between chaplins and SC3, which are completely unrelated in terms of amino acid sequence, and which can thus be considered a classical example of evolutionary convergence.

Chaplins are not the only surfactants involved in the escape of *Streptomyces* aerial hyphae. Prior to the formation of aerial structures by *S. coelicolor*, the small lantibiotic-like peptide SapB is secreted by vegetative hyphae to facilitate aerial growth (Willey *et al.*, 1991; Tillotson

et al., 1998). Likewise, SapB analogues have been discovered in other streptomycetes, including SapT of *Streptomyces tendae* (Kodani *et al.*, 2005) and AmfS of *Streptomyces griseus* (Ueda *et al.*, 2002), although other SapB orthologues are presumably synthesized by most, if not all streptomycetes. Recent evidence from the Willey lab indicates that the SapB precursor peptide RamS, encoded by the *ramS* gene, is produced constitutively and regardless of medium composition (Gaskell *et al.*, 2012). However, post-translational modification of RamS only occurs under certain conditions, which is regulated by RamR

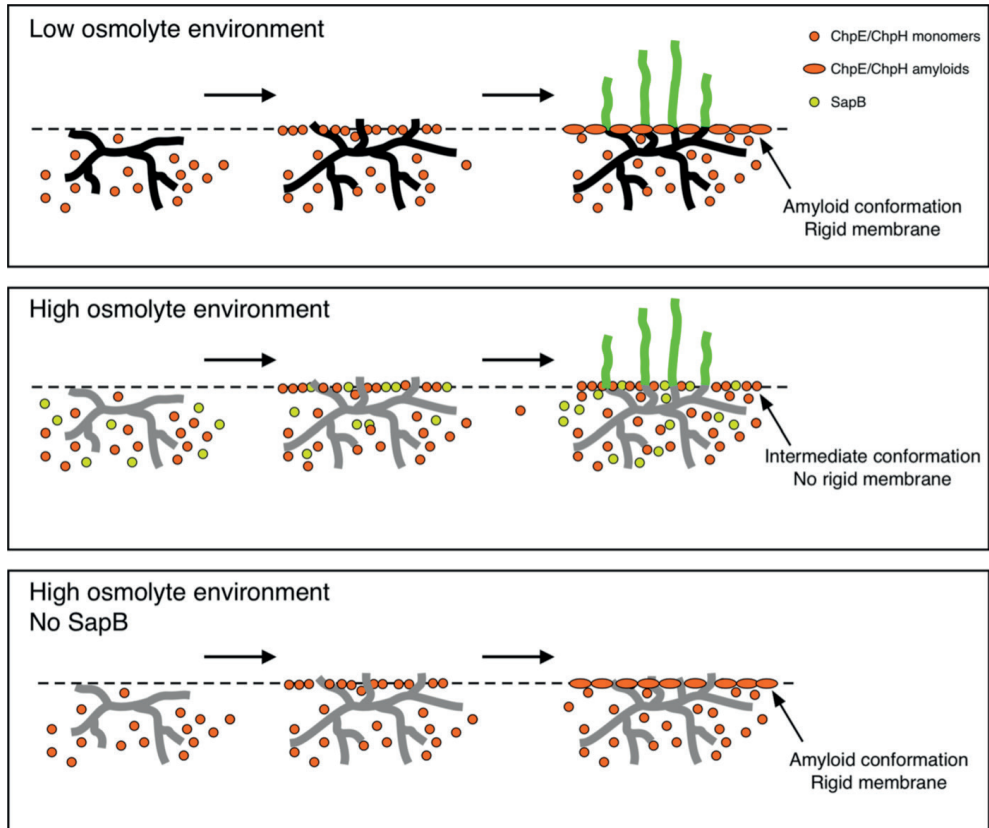


Figure 3. The role of chaplins and SapB in initiation of aerial growth. During vegetative growth the chaplins ChpE and ChpH are secreted into the aqueous environment. These small chaplins accumulate at the air-medium interface due to their amphipathic nature. Initial assembly of ChpE and ChpH leads to the formation of a semi-liquid (non-amyloidal) membrane, which strongly reduces the water surface tension. As more chaplin monomers reach the air-medium interface, the transition towards the amyloidal confirmation is induced, leading to a rigid interfacial chaplin membrane. Under this condition, the high turgor pressure within the hyphae enables them to grow into the air (A). SapB is secreted by vegetative hyphae in high osmolarity media, together with ChpE and ChpH. The presence of SapB at the interface delays the formation of a rigid chaplin membrane. This allows hyphae to escape the aqueous environment despite the reduced turgor pressure (B). Without SapB, chaplin self-assembly results in the formation of a rigid amyloid membrane, hampering aerial growth due to the low turgor pressure of hyphae (C). Vegetative hyphae with a high turgor pressure are highlighted in black, while hyphae with a low turgor pressure are grey-colored. Aerial hyphae are drawn in green.

(Kodani *et al.*, 2004; Gaskell *et al.*, 2012).

Like ChpE and ChpH, SapB has surfactant-like properties. However, unlike the chaplins, SapB appears to be important only for development on rich media that typically contain high amounts of osmolytes such as sucrose, or KCl (Willey *et al.*, 2006; Capstick *et al.*, 2007; de Jong *et al.*, 2012; Fig. 3). Only under such conditions can the mature SapB peptide be identified in the medium, unlike its presence on the spore surface, which is medium-independent (de Jong *et al.*, 2012). Because hyphal turgor pressure is reduced in medium with high osmolarity, vegetative hyphae might have problems in breaching the chaplin membrane formed at the medium-air interface. Perhaps secreted SapB intercalates in the developing chaplin membrane and thereby delays, or prevents the transition towards the rigid end conformation (Fig. 3). This would lead to the formation of a membrane, perhaps equivalent to the semi-liquid chaplin membrane observed at elevated pH, that is easier to breach.

The role of chaplins in fimbriae formation and attachment

Functional amyloids are most abundantly mentioned in the context of bacterial adhesion to (a)biotic surfaces (Alteri *et al.*, 2007; Dueholm *et al.*, 2010; Romero *et al.*, 2010). Like other bacteria, streptomycetes are capable of adhering to a variety of surfaces, which could be instrumental for invasive growth, or for the efficient degradation of substrates, for example dead plant material. Also, attachment could be important for establishing infections by plant pathogenic streptomycetes, such as *Streptomyces ipomoeae* or *S. scabies*. Strong attachment of *S. coelicolor* is observed in so-called liquid static cultures, coinciding with the formation of an extracellular matrix, that is quite distinct from the rodlet matrix identified on aerial hyphae (van Keulen *et al.*, 2003; de Jong, Wösten, *et al.*, 2009). The attachment-associated matrix is characterized by fimbrial structures that appear to be connected to the hyphal surface via protrusions present along the adhering hyphae (Fig. 4). Formation of fimbriae is dependent on the presence of the chaplins, inferring that fimbriae are, at least partially, composed of these proteins (de Jong, Wösten, *et al.*, 2009). Indeed, without chaplins fimbriae are no longer formed, and which concomitantly also prevents hyphae from adhering to the surface (Fig. 4). Similar results were obtained with a mutant strain lacking the *bltN* gene, which encodes an extracytoplasmic function sigma factor required for the expression of the chaplin genes (Elliot *et al.*, 2003; Bibb *et al.*, 2012).

Intriguingly, when a chaplin-containing solution was incubated for 7 days, long fibers were observed with a diameter of approximately 12 nm, as opposed to the 7 nm-wide fibrils observed at the water-air interface (Bokhove *et al.*, 2013). These fibers had a cross- β structure and are very reminiscent of the fimbrial structures observed in attachment. These larger fibers, however, appear to consist of bundled 7 nm-wide fibrils, which indeed were

occasionally observed emanating from partially unwound fibers (Bokhove *et al.*, 2013). To mediate attachment to hydrophobic surfaces fimbriae probably require partial unfolding or unwinding to expose the hydrophobic sides of the individual chaplin fibrils, which are expected to be buried in the interior of the hydrophilic fimbriae. Taken together, these data demonstrate that chaplin fibrils can assemble into higher order assemblies, which can have very different roles in growth and development of streptomycetes.

Like chaplins, fungal hydrophobins are also involved in attachment (Kershaw and Talbot, 1998; Lugones *et al.*, 2004). However, while chaplin fibrils are organized into fimbriae, hydrophobin-mediated attachment is quite different. Using *Sch. commune* as an example, attachment depends on assembly of the SC3 hydrophobin into an amphipathic membrane at the interface between the hypha and the hydrophobic surface (Wösten *et al.*, 1994).

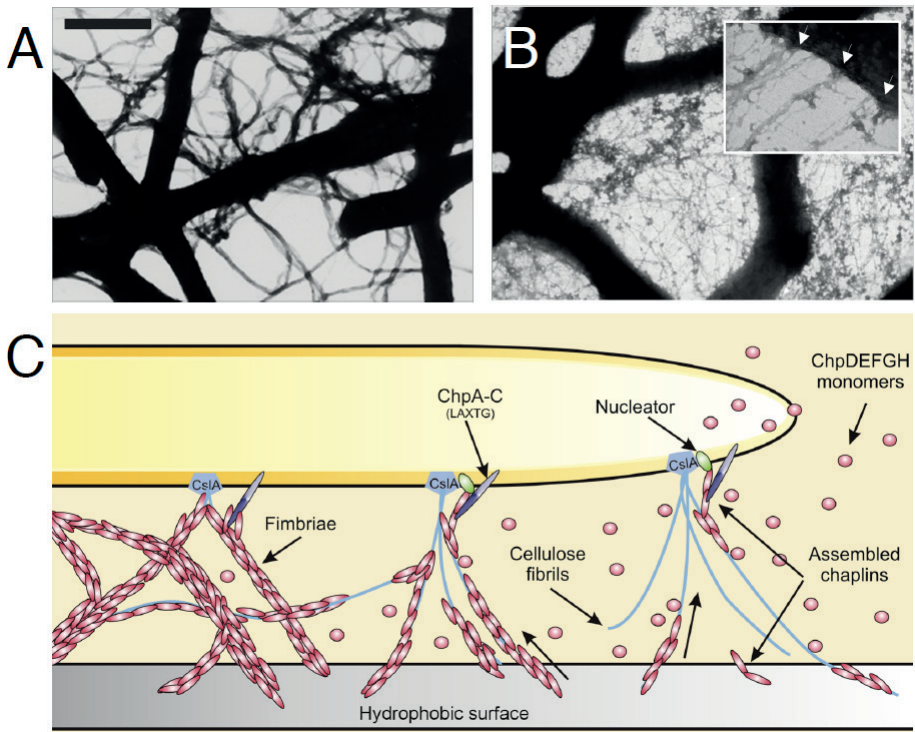


Figure 4. Attachment of hyphae to hydrophobic surfaces is mediated by amyloid fimbriae. **(A)** Attachment of hyphae coincides with the formation of fimbriae that assemble into a matrix in between the adhering hyphae. **(B)** Fimbriae are no longer formed in the absence of chaplins. Instead, thin cellulose-like filaments emerge from the spike-shaped protrusions that serve as an anchoring platform for the fimbriae (see arrows in inset, right panel). Bar represents 2.5 μm or 125 nm (inlay). **(C)** Proposed model for the role of chaplins and cellulose in fimbriae formation in *S. coelicolor*. Thin cellulose-like fibrils produced by CslA extend from spike-shaped protrusions and serve as an anchoring platform for fimbriae. Secreted chaplins assemble into amyloids when contacting assembled chaplin fibrils or a hydrophobic surface. Association of chaplin amyloids and the cellulose-like fibrils leads to the formation of fimbriae. Partial unwinding of the hydrophilic fimbriae possibly exposes the hydrophobic parts that mediate the interaction with the hydrophobic surface. Panels are reproduced, with permission, from de Jong *et al.* (2009).

This membrane would render the hyphal surface (partially) hydrophobic, thereby increasing compatibility with the hydrophobic surface to which the hypha adheres. This process is thus very similar to the mechanism by which these proteins decorate fungal aerial hyphae (Talbot, 1997). Hydrophobin-mediated attachment has been shown to underlie the pathogenicity of *Magnaporthe grisea* (Talbot *et al.*, 1993; Talbot *et al.*, 1996), which makes it tempting to speculate that chaplins may also be involved in establishing pathogenic interactions.

The role of beta-glucans in attachment and differentiation

Multicellular communities of bacteria are typically held together by a variety of extracellular polymers. In addition to amyloid fibrils, these often include polysaccharides, lipids and nucleic acids (Claessen *et al.*, 2014 and references therein). For instance, cellulose was shown to be important for adhesion of the plant pathogen *Agrobacterium tumefaciens* to plant tissue (Matthysse, 1986). Furthermore, cellulose is an important component of the extracellular matrix of *Escherichia coli* and pathogenic *Salmonella* species (Zogaj *et al.*, 2001; White *et al.*, 2003; Serra *et al.*, 2013). Notably, also adhesion of streptomycetes involves a cellulose-like glycan, which is synthesized by the cellulose synthase-like protein CslA (Xu *et al.*, 2008; de Jong, Wösten, *et al.*, 2009). Attachment of hyphae was significantly reduced in mutant strains lacking the corresponding *cslA* gene. Interestingly, the *cslA* mutant produced fimbriae that were indistinguishable from those of the wild type, both in terms of morphology and number, which indicates that CslA is not essential for fimbriae formation (de Jong, Wösten, *et al.*, 2009). Instead, the glycan was shown to be important for proper anchoring of the fimbriae to the adhering hyphae (Fig. 4). This was concluded from the fact that CslA is active at sites that connect fimbriae to the adhering hyphae, and the detachment of wild-type fimbriae from the hyphal surface by cellulase activity. This led to a model in which CslA produces a cellulose-like glycan, which serves as an anchoring platform for the chaplin amyloids. Indeed, these glycan structures were visible at protrusion sites along the hyphae in the absence of chaplins (Fig. 4). Anchoring probably also involves the large chaplins, which could co-assemble with the short chaplins into amyloidal fimbriae. The sorting signals present in ChpA-C could then contribute to covalent anchoring of the fimbriae to the cell wall of adhering hyphae, in addition to glycan-mediated anchoring (Fig. 4).

Genes involved in bacterial cellulose synthesis are typically organized in an operon, containing the *bcsABCD* genes (Römling, 2002). However, the organization of the *cslA* gene cluster is quite different. *Streptomyces* lacks the c-di-GMP binding protein BcsB, which is essential for the synthesis of cellulose according to the currently accepted model (Ross *et al.*, 1991, and see below). Furthermore, *cslA* is translationally coupled to *glxA*, which encodes a radical copper oxidase with weak homology to galactose oxidases (Whittaker and Whittaker, 2006). This atypical gene organization is only found in the myxobacterium *Stigmatella aurantiaca*, where deletion of either *fbfA* or *fbfB* hampers fruiting body formation following starvation

(Silakowski *et al.*, 1996; Silakowski *et al.*, 1998). Notably, in addition to being important for surface attachment, the CslA protein is also required for development. Deletion of the *csIA* gene, or the downstream located *glxA* gene in *S. coelicolor* causes a developmental block on media containing high levels of osmolytes, such as sucrose (Xu *et al.*, 2008; Liman *et al.*, 2013). Importantly, omitting the sucrose restored aerial growth in the *glxA* mutant strain, but not in the *csIA* mutant (Liman *et al.*, 2013). Considering the fact that the *glxA* gene was also shown to have a *csIA*-independent promoter, these data suggest that CslA and GlxA have different functions in morphogenesis (Liman *et al.*, 2013). However, both proteins could still cooperate in the same pathway leading to morphogenesis, at least under some conditions. In growing hyphae, both CslA and GlxA are present at the hyphal tip (Xu *et al.*, 2008; Liman *et al.*, 2013). Notably, deletion of the *glxA* gene leads to a lack of CslA-produced glycan at the hyphal tips (Chaplin *et al.*, 2015). This would be consistent with a role for GlxA in maturation of the glycan, which in turn is required for its proper placement and/or function. Despite its presence at the hyphal tip, the function of the polymer is largely unknown. One hypothetical role could be that such a polymer stimulates the assembly of chaplins into amyloid fibrils and thereby affect the formation of aerial hyphae. A similar role has been described in *Sch. commune*, where the extracellular glycan schizophyllan, stimulates conversion of SC3 monomers into functional amyloids (Scholtmeijer *et al.*, 2009). Alternatively, the CslA-produced polymer could play a role in providing rigidity to hyphal tips. Polar growth, as exerted by filamentous bacteria, requires constant cell wall remodeling at apical sites (Flårdh, 2003a). As a result, these sites are prone to damage, which could be counterbalanced by synthesis of a glycan that provides additional strength (Xu *et al.*, 2008; Chater *et al.*, 2010). This additional rigidity might be of critical importance for aerial growth in high osmolyte environments, perhaps due to the reduced turgor pressure in hyphae under such conditions. Future characterization of the polymer will be necessary to unravel its precise role and mode-of-action during *Streptomyces* growth and development.

Regulation of extracellular matrix production during growth and development

In many bacteria the transition from a motile to a surface-attached lifestyle is coordinated by the second messenger bis-(3'-5')-cyclic dimeric guanosine monophosphate (c-di-GMP for short). This molecule stimulates the biosynthesis of matrix components in biofilms (Hengge, 2009). c-di-GMP was discovered in 1987 as an activator of cellulose synthesis in *Gluconacetobacter xylinus* (formerly *Acetobacter xylinum*; Ross *et al.* 1991), and was subsequently shown to play a similar role in *E. coli* and *Salmonella* species (Simm *et al.*, 2004). Intracellular c-di-GMP levels are increased by diguanylate cyclases (DGCs) that synthesize c-di-GMP from two molecules of GTP, while c-di-GMP-specific phosphodiesterases (PDEs) degrade this second messenger. DGC activities are associated with conserved GGDEF domains, while c-di-GMP-specific PDE activity is associated with so-called EAL protein

domains. Although a large number of c-di-GMP-metabolizing enzymes contain both GGDEF and EAL domains, most of these proteins possess only one enzymatic activity (Hengge, 2009; Tran *et al.*, 2011; Hull *et al.*, 2012). Interestingly, *S. coelicolor* contains a number of proteins putatively involved in c-di-GMP metabolism (Tran *et al.*, 2011). Three of the GGDEF domain-containing proteins, *cdgA*, *cdgB* and SCO5511 are direct targets of the central developmental regulator BldD (den Hengst *et al.*, 2010), which is required for morphological differentiation (den Hengst *et al.*, 2010). Overexpression of *cdgA* or *cdgB* inhibits aerial mycelium formation, likely due to increased levels of c-di-GMP (den Hengst *et al.*, 2010; Tran *et al.*, 2011). In agreement, deletion of the c-di-GMP-degrading PDEs RmdA and RmdB also leads to a development arrest (Hull *et al.*, 2012). Taken together, these studies show that c-di-GMP signaling is important for control of development in *Streptomyces*. Whether c-di-GMP levels regulate matrix production in streptomycetes, as observed in other bacteria, remains to be elucidated. In this respect, however, it is interesting to note that the developmental arrest of the *csIA* mutant is shared with a *cdgB* mutant strain (Tran *et al.*, 2011).

Roles for extracellular surface polymers in pellet formation

Industrial-scale production of important secondary metabolites, such as antibiotics, occurs in large bioreactors. Growth of streptomycetes in such conditions, as opposed to solid-grown or liquid standing cultures, is characterized by the formation of large clumps, or pellets, consisting of interconnected hyphae (van Wezel *et al.*, 2006; Celler *et al.*, 2012). Formation of pellets might be caused by surface-to-surface contact between smaller particles, which as a result can become very large (several millimeters in diameter (Tresner *et al.*, 1967; Vecht-Lifshitz *et al.*, 1990)). As a consequence, growth occurs predominantly at the outer surface of pellets as oxygen and/or nutrient depletion hamper growth in the central region (Celler *et al.*, 2012; Nieminen *et al.*, 2013). Indeed, work from the Manteca lab has indicated that programmed cell death (PCD)-like events occur in the central part of pellets (Manteca *et al.*, 2008; Rioseras *et al.*, 2014). While PCD probably creates space for new hyphal growth, this also poses a serious threat for pellet integrity, in particular considering the presence of strong shear stress forces applied in bioreactors. It is therefore reasonable to assume that extracellular substances contribute to the cohesion of hyphae in pellets. Indeed, Kim and Kim described that DNase treatment of pellets leads to their disintegration (Kim and Kim, 2004). As such, extracellular DNA (eDNA), supposedly released during autolysis of hyphae in the central part of pellets, could hold hyphae together, in a way reminiscent of the role of eDNA in various biofilm matrices (Whitchurch *et al.*, 2002; Kim and Kim, 2004; Barnes *et al.*, 2012). Similarly, a role for the polysaccharide hyaluronic acid was proposed (Kim and Kim, 2004). More recent evidence indicates that also the CslA-produced polymer is involved in pellet architecture (Xu *et al.*, 2008; van Veluw *et al.*, 2012). In contrast to the dense pellets formed in the wild-type strain, mycelium of the *csIA* mutant had an open structure (Xu *et al.*,

2008). Furthermore, the chaplin proteins were shown to be involved in control of pellet size (van Veluw *et al.*, 2012). Interestingly, cell surface polymers might be interesting targets for the industrial improvement of strains, considering the fact that the morphology and size of pellets is important for productivity (Wardell *et al.*, 2002; van Wezel *et al.*, 2006; van Veluw *et al.*, 2012). Taken together, these results indicate that extracellular surface polymers are involved in shaping *Streptomyces* pellets.

Uncharacterized cell envelope polymers

Throughout this review we focused on the extracellular matrix of streptomycetes, with special emphasis on polymers that have a structural role in morphogenesis. However, there are several other understudied cell envelope components where we know surprisingly little about. Although many actinomycetes typically have membrane-anchored lipoglycans, lipoteichoic acids have recently been characterized in streptomycetes (Rahman *et al.*, 2009; Cot *et al.*, 2011) and these polymers can be presumed to project into the cell envelope from the membrane. In addition, other carbohydrate-based polymers may be incorporated in the cell envelope, including a putative cell wall glycan that is produced upon cell wall stress (Hong *et al.*, 2002) and also teichoic acids (Weidenmaier and Peschel, 2008; Potekhina *et al.*, 2011), teichuronic acids (Schäffer and Messner, 2005; Tul'skaya *et al.*, 2011) and teichulosonic acids (Tul'skaya *et al.*, 2011; Ostash *et al.*, 2014). The latter three comprise a group of anionic polymers that are largely responsible for the negative charge of the cell wall. As such, they have been implied to function in the homeostasis of cations (Hughes *et al.*, 1973). Studies in various bacteria demonstrate that such anionic polymers play key roles in important biological processes including, amongst others, control of cell shape, cell division, biofilm formation, and protein secretion (reviewed in Weidenmaier and Peschel, 2008). In streptomycetes, teichoic acids were shown to be important for spore wall formation (Kleinschnitz *et al.*, 2011). In contrast, roles for teichuronic and teichulosonic acids in streptomycetes are unknown, despite their presence in the cell envelope (Shashkov *et al.*, 2002; Ostash *et al.*, 2014). Uncovering their function seems like an important challenge for the future.

Concluding remarks

We have here discussed the different extracellular matrix polymers produced by streptomycetes. These polymers have evolved to fulfill a wide range of functions in streptomycetes. They are involved in the transition from vegetative to aerial growth, provide aerial hyphae with a water-repellent surface layer, mediate attachment of hyphae to hydrophobic surfaces, and are involved in constructing pellets. Although the key players have been identified, relatively little is known how these molecules cooperate *in vivo*. Although

chaplins can self-assemble into fibrils at hydrophilic-hydrophobic interfaces, without the involvement of other molecules, the *in vivo* situation appears to be more complex. In natural settings, chaplin amyloids form higher-order structures with distinct morphologies and functions, but the underlying mechanisms have not been explored. For instance, how the rodlin proteins contribute to the chaplin polymerization process during formation of aerial hyphae, which thereby become decorated with pairwise aligned rodlets, is completely unknown. Similarly, how the chaplin fibrils are organized into fimbrial structures that firmly associate with adhering hyphae needs further exploration. A better understanding of the molecular mechanisms underlying chaplin assembly will be essential to unravel common features, but also differences, with other functional amyloids and might simultaneously provide new insights into the complex extracellular biology of streptomycetes.

3

This chapter was published as:

G. Jerre van Veluw ‡, Marloes L.C. Petrus ‡, J. Gubbens ‡, Richard de Graaf, Inez P. de Jong, Gilles P. van Wezel, Han A.B. Wösten and Dennis Claessen (2012). *Applied Microbiology and Biotechnology* 96: 1301-1312. ‡ These authors contributed equally to the work

Abstract

Streptomyces are proficient producers of enzymes and antibiotics. When grown in bioreactors, these filamentous microorganisms form mycelial pellets that consist of interconnected hyphae. We here employed a flow cytometry approach designed for large particles (COPAS) and demonstrate that liquid-grown *Streptomyces* cultures consist of two distinct populations of pellets. One population consists of mycelia with a constant mean diameter of approximately 260 μm , whereas the other population contains larger mycelia whose diameter depends on the strain, the age of the culture and medium composition. Quantitative proteomics analysis revealed that 37 proteins differed in abundance between the two populations of pellets. Stress-related proteins and biosynthetic proteins for production of the calcium-dependent antibiotic CDA were more abundant in the population of large mycelia, while proteins involved in DNA topology, modification or degradation were overrepresented in the population of small mycelia. Deletion of genes for the cellulose synthase-like protein CslA and the chaplins affected the average size of the population of large pellets but not that of small pellets. Considering the fact that the production of enzymes and metabolites depends on pellet size, these results provide new leads towards rational strain design of *Streptomyces* strains tailored for industrial fermentations.

Analysis of two distinct mycelial populations in liquid-grown *Streptomyces* cultures using a flow cytometry-based proteomics approach

Introduction

Streptomycetes are Gram-positive mycelial soil bacteria that are commercially very attractive for the production of a wide range of natural products such as antibiotics, anticancer agents and immunosuppressants (Hopwood, 2007). Moreover, streptomycetes produce a plethora of enzymes that allow them to utilize almost any naturally occurring polymer, such as cellulose, mannan, chitin, xylan, starch, glycan and agar. Many of these enzymes are industrially important for the conversion of renewable energy sources (Vrancken and Anné, 2009). Unlike unicellular bacteria, which grow exponentially by binary fission with a constant generation time (Errington *et al.*, 2003), streptomycetes grow by hyphal extension, with branching adding the exponential component. During growth, vegetative hyphae are divided into compartments by cross-walls (Chater and Losick, 1997; Jakimowicz and Van Wezel, 2012). The reproductive phase is initiated by the erection of sporogenic structures called aerial hyphae, which differentiate following a complex cell division event whereby the multigenomic hyphae are converted into chains of unigenomic spores. Aerial hyphae are formed only on solid-grown cultures, giving the colonies their characteristic white and fluffy appearance (Kelemen and Buttner, 1998; Flärdh and Buttner, 2009). The transition from vegetative to aerial growth is accompanied by the production of an extracellular protein layer, composed of chaplins and rodmins, that makes aerial hyphae hydrophobic (Claessen *et al.*, 2002; Claessen *et al.*, 2003; Elliot *et al.*, 2003; Claessen *et al.*, 2004). During the formation of aerial hyphae numerous secondary metabolites are produced, including many antibiotics (van Wezel and McDowall, 2011).

Industrial-scale production with streptomycetes occurs in large bioreactors. Under these conditions, pellets are formed that consist of interconnected hyphae (Celler *et al.*, 2012).

Such mycelial pellets have very different sizes. Elongation and branching of hyphae, as well as fragmentation and lysis are regarded as factors controlling the size and morphology of these multicellular structures (Nielsen and Johansen, 1995; Nielsen, 1996). Moreover, the cell wall plays an important role in pellet architecture. Overexpression of the actinomycete-specific cell division protein SsgA, which controls septum-site localization (Willemse *et al.*, 2011) and several aspects of cell wall homeostasis (Noens *et al.*, 2007), leads to increased fragmentation and hence smaller pellets. Interestingly, this is accompanied by a strongly increased enzyme production (van Wezel *et al.*, 2006). Likewise, the absence of the cellulose synthase-like protein CslA in *Streptomyces coelicolor* (Xu *et al.*, 2008; de Jong, Wösten, *et al.*, 2009) has a profound effect on mycelial growth, leading to a significant decrease in pellet size. CslA produces a polysaccharide polymer at the hyphal tip, which has been suggested to be cellulose (Xu *et al.*, 2008; de Jong, Wösten, *et al.*, 2009). This secreted polysaccharide is thought to maintain the integrity of the hyphal tip that is subject to constant remodeling due to ongoing cell wall synthesis orchestrated by DivIVA (Flärdh, 2003b). Taken together, these observations show the importance of the cell wall in the establishment and stability of pellet architecture.

Flow cytometry has been used to study populations of single-celled organisms (Hutter and Eipel, 1979; Phillips and Martin, 1983). This method could not be used for the multicellular pellets of *Streptomyces* that are simply too large to pass the nozzle. Recently, the COPAS (Complex Object Parametric Analyzer and Sorter) platform has been used to analyze pellets of the fungus *Aspergillus niger* with sizes ranging from 30-750 microns (de Bekker *et al.* 2011). We here for the first time use this platform to analyze bacterial multicellular structures. Our work demonstrates that *Streptomyces* liquid cultures consist of two distinct populations of pellets that differ in size. Stress-related proteins are more abundant in the population of large pellets, while proteins involved in DNA topology, modification or degradation are more abundant in the population of small pellets. The size of the larger pellets, but not that of the smaller pellets, was species- and medium-dependent.

Materials and Methods

Strains and culture conditions

The strains used in this study are shown in Table S1. Media were prepared as described (Kieser *et al.*, 2000). *Streptomyces* species were grown at 30 °C on solid R5 or MS agar plates, or as shaken cultures (180 rpm) in 250 ml flasks equipped with coil springs containing 100 ml YEME, TSBS, R5 with glucose, or NMMP defined medium containing glucose. Liquid media were inoculated with 10⁶ spores ml⁻¹.

Flow cytometry using the COPAS Plus

Pellets were harvested and fixed with 4% formaldehyde for 30 min on ice. They were washed twice with phosphate-buffered saline (PBS) and stored at -20 °C until further use. Pellets were analyzed based on size (time-of-flight [TOF]) using a COPAS Plus profiler equipped with a 1-mm nozzle (Union Biometrica, Holliston, MA). The flow design of the COPAS Plus is such that pellets pass the laser beam over their longitudinal axis. All data points with an extinction [EXT] ≥ 25 (thus excluding single hyphae and debris) were used for subsequent analysis.

Statistical analysis

The statistical analyses were performed as described by van Veluw et al., (2012). Briefly, the log-transformed datasets were fit by a probability distribution assuming two normal distributions (Vinck *et al.*, 2005). This model determines five parameters: the participation fraction (p), two means (μ_1 ; μ_2) and two standard deviations (σ_1 ; σ_2). For each parameter the 95% confidence interval (CI) estimate was obtained by refitting with the model after bootstrapping (1000 replicates) using the open source Scilab language. Datasets with non-overlapping CI's of the mean and a $0.025 < p < 0.975$ were considered to be derived from a culture with two populations of pellets.

Proteomics analysis

Mycelia from 48 h old YEME-grown cultures were washed in PBS and sorted using the COPAS Plus. Proteomics experiments were carried out as detailed in Gubbens *et al.* (2012). Briefly, size-fractionated mycelia were sonicated for 5 min at 12 W output power using 5 s on / 5 s off intervals in 100 mM Tris/HCl (pH 7.5), 10 mM MgCl₂ and 5 mM dithiothreitol (DTT), after which the debris was removed by centrifugation (16,000 *g* for 10 min at 4 °C). 110 μ g of total protein per sample was precipitated using chloroform/methanol (Wessel and Flügge, 1984). Protein samples were digested with trypsin as described (Piette *et al.*, 2005) and dried in a vacuum concentrator. Samples were then labeled using stable isotope dimethyl labeling on-column using Sep-Pak C18 200 mg columns (Waters) as described (Boersema *et al.*, 2009). Labeled peptides were mixed 1:1, dried and dissolved in ~ 1 mL 5% formic acid. The mixture was fractionated by cationic exchange (SCX) using a polysulfoethyl A column (PolyLC, 100 x 2.1 mm, particle size 5 μ m, average pore size 200 Å, column volume 0.346 ml), and 0.5 ml sample loaded on the column. Mobile phases were SCX A (10 mM KH₂PO₄, 20% (v/v) acetonitrile, pH 3) and SCX B (10 mM KH₂PO₄, 20% (v/v) acetonitrile, 0.5 M KCl, pH 3). Peptides were fractionated at a flow rate of 250 μ l/min with a gradient of 0-18% SCX B in 18 CV, 18-30% SCX B in 6 CV, and 30-100% SCX B in 5 CV. In total, 24 peptide fractions were

collected for LC-MS analysis on an LTQ-Orbitrap setup. Data analysis was performed using MaxQuant 1.2.2.5 (Cox and Mann, 2008). MS/MS spectra were searched against the UniProt *S. coelicolor* reference proteome set (organism 100226, excluding SCP1 plasmid proteins, version 2012_06) with a false discovery rate of 1% for both proteins and peptides, and an additional second peptide search was performed (Cox *et al.*, 2011). Low-scoring versions of already identified peptides were retained for quantification and the minimum peptide ratio count for quantification was set to three. For all expression ratios a B significance (Cox and Mann, 2008) was calculated using Perseus 1.3.0.4 (part of the MaxQuant suite) and results filtered based on a Benjamini-Hochberg false discovery rate of 5%. Subsequently, proteins with a significant expression ratio that was based on only three or four quantification events and a variability of >150% were removed, since these quantifications could be regarded as dubious. Protein descriptions were taken from StrepDB (The *Streptomyces* Annotation Server, <http://strepdb.streptomyces.org.uk>).

Results

Application of large particle flow cytometry for size fractionation of mycelia

S. coelicolor forms pellets of variable size in liquid-grown cultures (Fig. 1A). To analyze the size distribution, large particle flow cytometry was deployed using a COPAS Plus. *S. coelicolor* pellets were analyzed on the basis of their time of flight (TOF) in milliseconds (Fig. 1B). To relate the pellet diameter to TOF, 27 pellets were measured by microscopy (Fig. 1C). This revealed a relationship between TOF and pellet diameter whereby the diameter equals $0.57 \times \text{TOF} + 159 \mu\text{m}$.

To analyze the size distribution of the *S. coelicolor* pellets, the TOF of the events with an extinction ≥ 25 were divided by the mean TOF of the population. Mathematical modeling of the pooled data of biological triplicates showed that the pellet size in liquid-grown cultures

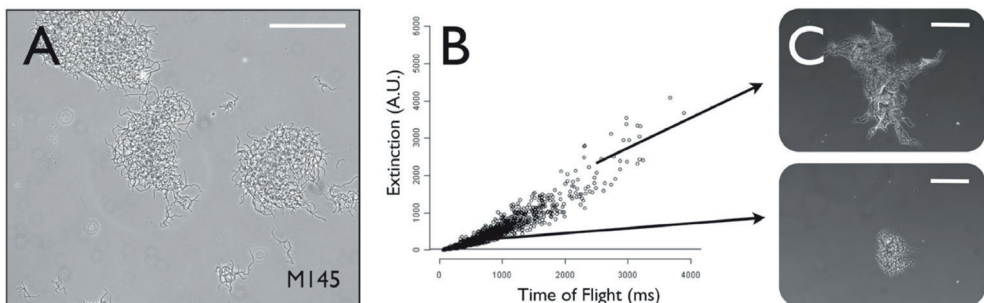


Figure 1. Heterogeneity in pellet size in liquid-grown YEME cultures of *S. coelicolor*. Size distribution of pellets (A) was analysed by COPAS (B). The COPAS technology allows separation of colonies according to size (C). Bars represent $400 \mu\text{m}$ (A) and $300 \mu\text{m}$ (C).

was not normally distributed when YEME, NMMP, R5, or TSBS were used as growth medium. Instead, the size distribution could be fitted assuming the existence of two normally distributed populations (Fig. 2; Table 1). These two populations were observed between day 1 and day 7 (Fig. 2; Table 1). The average diameter (μ_1) of small pellets was 266 μm ($\pm 10\%$) regardless of the medium that was used or the age of the cultures. In contrast, the average diameter (μ_2) of large pellets varied in time (e.g. varying between 454 and 728 μm in TSBS).

A difference in the diameter of large pellets was also observed between different media (varying from 457 μm in case of NMMP to 728 μm in case of TSBS medium (Table 1). The populations of large pellets formed in R5- and YEME-grown cultures reached their maximal size (521 μm in case of R5 and 474 μm in case of YEME medium; Table 1) after 48 h of growth, after which their size decreased to 346 and 304 μm , respectively. In contrast, in TSBS medium the pellets decreased in size after 24 h of growth. Unlike in other media, in minimal medium (NMMP) the diameter of the large pellets increased, after an initial decrease (Table 1). The largest pellets in NMMP-grown cultures (457 μm) were detected after 7 days of growth. Taken together, these data show that the size of the large pellets formed by *S. coelicolor* is dynamic in time and depends on the medium composition.

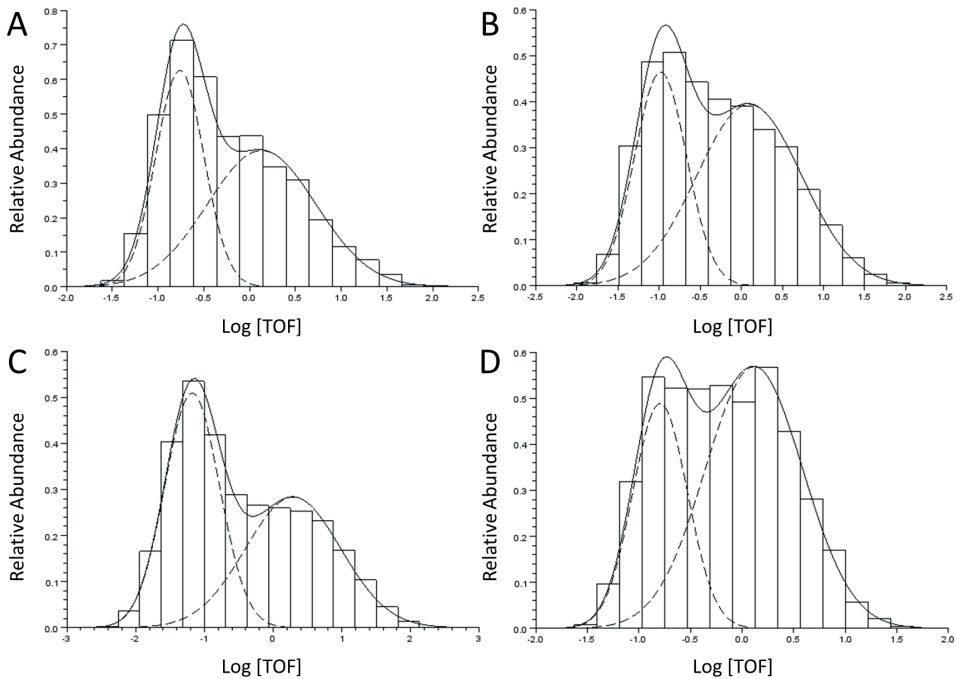


Figure 2. Relation of medium and size distribution of pellets in liquid-grown cultures. *S. coelicolor* was grown for 24 h in NMMP with glucose (A), R5 (B), TSBS (C) or YEME (D). Two populations of pellets that differ in size were detected in all media (see also Table 1).

Table 1. Heterogeneity between pellets in liquid-grown cultures of *S. coelicolor*. Heterogeneity is defined as non-overlapping confidence intervals (CI) of the mean diameter of both populations (μ_1 and μ_2) and a confidence interval of the participation fraction (PF) between 0.025-0.975.

Medium	Time (h)	μ_1 (μm)	95% CI μ_1	μ_2 (μm)	95% CI μ_2	PF1	95% CI PF1
NMMP	24	260	258 - 262	405	399 - 413	0.413	0.391 - 0.437
	48	285	284 - 287	347	331 - 365	0.791	0.711 - 0.850
	72	281	278 - 284	364	358 - 373	0.551	0.507 - 0.608
	96	285	282 - 289	347	333 - 363	0.630	0.520 - 0.725
	168	278	275 - 281	457	443 - 477	0.585	0.550 - 0.626
R5	24	261	257 - 264	458	446 - 475	0.368	0.334 - 0.409
	48	256	254 - 259	521	507 - 537	0.363	0.340 - 0.391
	72	259	256 - 261	450	438 - 465	0.550	0.522 - 0.579
	96	256	253 - 260	398	387 - 410	0.511	0.469 - 0.553
	168	251	249 - 254	346	338 - 354	0.483	0.437 - 0.531
TSBS	24	290	287 - 294	728	693 - 761	0.507	0.478 - 0.536
	48	285	281 - 290	629	609 - 650	0.457	0.427 - 0.486
	72	281	276 - 285	581	559 - 603	0.489	0.449 - 0.523
	96	274	270 - 279	477	463 - 493	0.456	0.416 - 0.496
	168	271	268 - 275	454	440 - 469	0.506	0.467 - 0.546
YEME	24	246	243 - 250	376	364 - 388	0.324	0.272 - 0.377
	48	257	253 - 261	474	458 - 494	0.316	0.276 - 0.362
	72	254	250 - 259	408	395 - 425	0.360	0.306 - 0.423
	96	248	246 - 251	366	357 - 376	0.383	0.344 - 0.427
	168	242	238 - 245	304	289 - 324	0.703	0.592 - 0.805

Two populations of pellets could also be distinguished in liquid-grown cultures of *Streptomyces lividans*, and the more phylogenetically distant species *Streptomyces scabies* and *Streptomyces griseus* (Fig. 3; Table 2). The average diameter of small pellets (μ_1) remained constant in time and was similar for all streptomycetes (averaging $256 \mu\text{m} \pm 10\%$). In contrast, the average size of the large pellets (μ_2) fluctuated in case of *S. lividans* and *S. scabies* (Fig. 4; Table 2). Less variation was observed for *S. griseus*. This again shows that streptomycetes form two different populations of pellets in liquid-grown cultures, with a dynamic size distribution for large pellets, while that of the small pellets is constant.

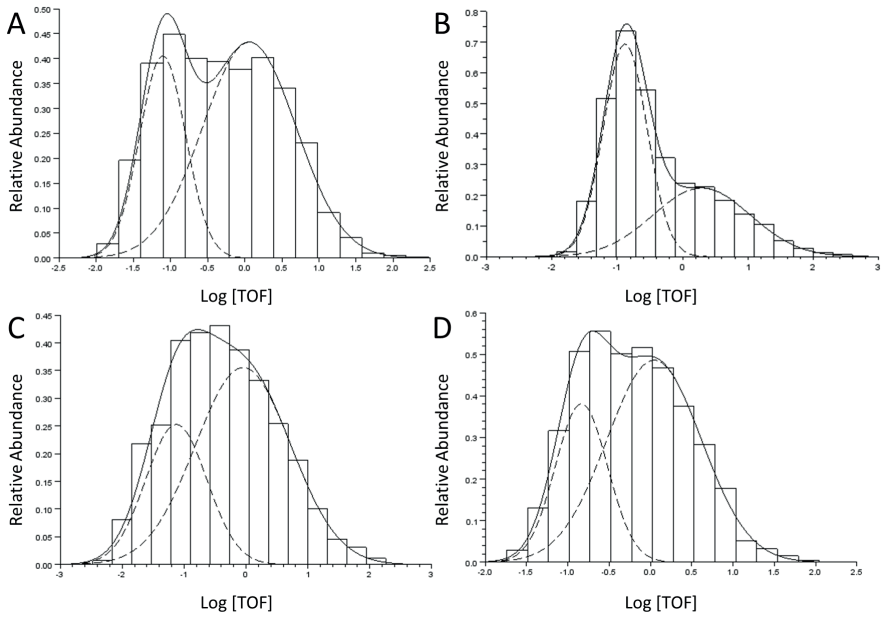


Figure 3. Size distributions of pellets of liquid-grown cultures of *S. coelicolor* (A), *S. lividans* (B), *S. scabies* (C), and *S. griseus* (D) grown for 48 h in YEME medium. Two populations of pellets that differ in size are detected in all strains.

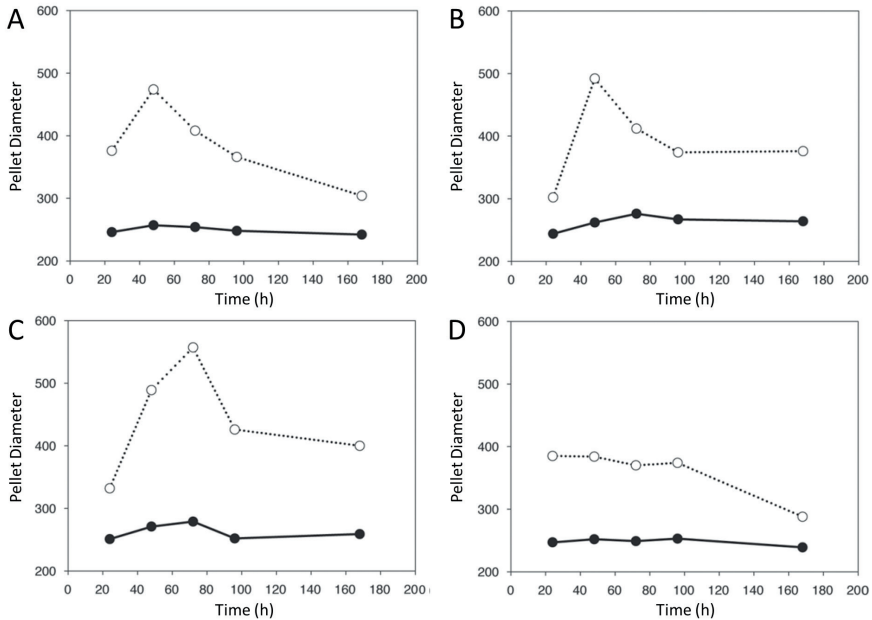


Figure 4. Dynamics of pellet size in time in liquid-grown YEME cultures of *S. coelicolor* (A), *S. lividans* (B), *S. scabies* (C), and *S. griseus* (D).

Table 2. Heterogeneity between pellets in liquid-grown YEME cultures of different *Streptomyces* strains. Heterogeneity is defined as non-overlapping confidence intervals (CI) of the mean diameter of both populations (μ_1 and μ_2) and a confidence interval of the participation fraction (PF) between 0.025-0.975.

Strain	Time (h)	μ_1 (μm)	95% CI μ_1	μ_2 (μm)	95% CI μ_2	PF1	95% CI PF1
<i>S. coelicolor</i>	24	246	243 - 250	376	364 - 388	0.324	0.272 - 0.377
	48	257	253 - 261	474	458 - 494	0.316	0.276 - 0.362
	72	254	250 - 259	408	395 - 425	0.360	0.306 - 0.423
	96	248	246 - 251	366	357 - 376	0.383	0.344 - 0.427
	168	242	238 - 245	304	289 - 324	0.703	0.592 - 0.805
<i>S. lividans</i>	24	244	233 - 266	302	285 - 399	0.457	0.238 - 0.916
	48	262	260 - 264	492	475 - 511	0.582	0.558 - 0.609
	72	276	269 - 284	412	396 - 446	0.446	0.369 - 0.553
	96	267	263 - 272	374	365 - 385	0.520	0.465 - 0.577
	168	264	258 - 272	376	365 - 390	0.431	0.360 - 0.518
<i>S. scabies</i>	24	251	247 - 258	332	320 - 356	0.564	0.479 - 0.694
	48	271	258 - 286	489	462 - 525	0.313	0.235 - 0.410
	72	279	267 - 298	557	499 - 715	0.526	0.418 - 0.692
	96	252	247 - 258	426	410 - 446	0.349	0.298 - 0.408
	168	259	253 - 265	400	383 - 423	0.491	0.422 - 0.567
<i>S. griseus</i>	24	247	215 - 281	385	293 - 1971	0.629	0.163 - 0.967
	48	252	248 - 256	384	374 - 398	0.302	0.256 - 0.363
	72	249	247 - 252	370	363 - 378	0.424	0.387 - 0.461
	96	253	248 - 259	374	360 - 389	0.397	0.324 - 0.471
	168	239	236 - 243	288	270 - 316	0.749	0.588 - 0.871
ΔcslA	24	238	235 - 244	271	263 - 300	0.603	0.455 - 0.871
	48	244	242 - 248	312	307 - 318	0.328	0.278 - 0.396
	72	255	251 - 258	378	369 - 388	0.391	0.349 - 0.436
	96	255	250 - 259	328	320 - 338	0.466	0.388 - 0.542
	168	245	243 - 248	310	296 - 329	0.760	0.677 - 0.827
$\Delta\text{chpABCDEFGH}$	24	259	247 - 269	344	306 - 462	0.743	0.490 - 0.921
	48	268	261 - 276	404	384 - 429	0.531	0.450 - 0.618
	72	266	261 - 388	388	372 - 409	0.406	0.329 - 0.500
	96	260	256 - 355	355	343 - 368	0.484	0.411 - 0.558
	168	270	262 - 281	379	360 - 417	0.553	0.439 - 0.720

Synchronous spore germination and pellet heterogeneity

To exclude that differences in spore germination could contribute to culture heterogeneity, we inoculated *S. coelicolor* cultures with spores that had been pre-germinated by 10 min heat shock at 50°C followed by pre-incubation in rich 2xYT media (Kieser *et al.*, 2000). Phase contrast microscopy showed that indeed the pre-germination procedure resulted in near-synchronous spore germination (not shown). The size distribution of pellets after 24 h of growth again revealed two distinct populations of pellets (Fig. 5), strongly suggesting that germination efficiency did not play a role in culture heterogeneity. Consistent with this idea, a bimodal distribution was also observed in a $\Delta nepA$ mutant strain (Fig. 5C) that germinates synchronously (de Jong *et al.*, 2009). Two populations of pellets were also detected when mycelium rather than spores was used as the inoculum (data not shown). Taken together, these data show that pellets are heterogeneous in size regardless of the inoculum.

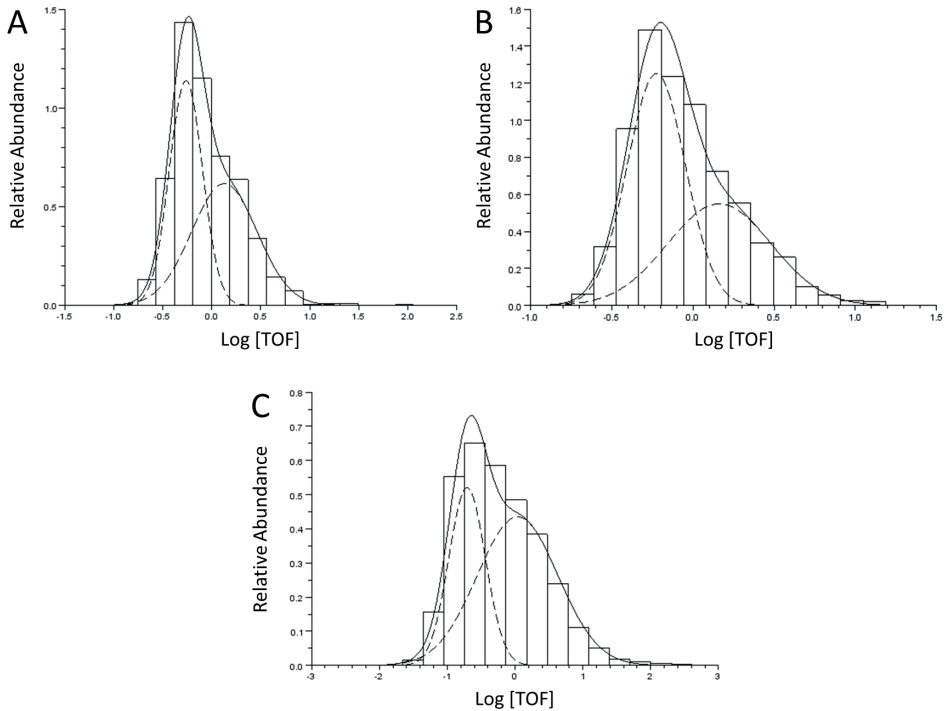


Figure 5. The effect of synchronous spore germination on the size distribution of *S. coelicolor* pellets in YEME medium. Two populations of pellets were detected after 24 h using untreated (A) or heat-shocked (B) spores. Two populations that differ in size are also detected in the *nepA* mutant whose spores germinate more synchronously (C).

Deletion of genes for cell surface-related proteins affects the average diameter of large pellets

A *csIA* mutant strain was previously shown to form smaller pellets (Xu *et al.*, 2008). Yet, again two populations were detected in this strain throughout growth (Table 2). The average size of the small pellets was about 250 μm , similar to that observed for the parental wild-type *S. coelicolor* strain. In contrast, sizes of the large pellets were different from the parent. After 24 h, the average size of the large *csIA* pellets was 271 μm compared to 376 μm for the parental strain (Table 2). A comparable difference was detected after 48 h with 312 μm for the *csIA* mutant and 474 μm for the parent. At later time points the differences decreased until the sizes were almost identical after 168 h (310 μm for the *csIA* mutant and 304 μm for the parent).

Pellets of the $\Delta\text{chpABCDEFGHIH}$ strain were analyzed to investigate the role of chaplins in the size of pellets in liquid-grown cultures (Table 2). Like the parent *S. coelicolor* M145, two distinct populations of pellets could be distinguished. The small pellets had a diameter of approximately 265 μm irrespective of culture age and this was similar to that of parental strain (Table 2). In contrast, the large pellets formed by the $\Delta\text{chpABCDEFGHIH}$ mutants were 404 μm in diameter, which is significantly smaller than the 474 μm observed for the parent strain after 48 h (Table 2). However, the size difference was less pronounced than observed for the *csIA* mutant.

Comparative proteomics of size-fractionated mycelia

One important application of the cell sorting technology described above is cytomics, in other words: the application of -omics technology on different cell types (*i.e.* small and large pellets). As proof of concept, and to determine protein profiles in the different populations, we applied quantitative proteomics using stable isotope dimethyl labeling on size-fractionated mycelial pellets from YEME liquid cultures. Using this approach, relative abundance ratios of 1149 proteins could be determined with at least 3 independent quantification events. Interestingly, only 37 proteins (3.2%) were found to be significantly different between the two populations; 17 were significantly overrepresented in the large pellets relative to the small pellets, and 20 were significantly underrepresented (Table 3).

Many of the proteins that were either overrepresented or underrepresented in the large versus the small mycelial pellets could be tentatively assigned to specific functional classes. Several stress-related proteins are overrepresented in the list of targets that are more abundant in the population of large pellets, which may be explained by reduced oxygen availability. The protein that is most strongly (around 30-fold) enhanced in the larger pellets is SCO0913 or EgtD. The *egtD* gene is the last gene of the *egtABCD* operon, which is involved

in the biosynthesis of the rare amino acid ergothioneine. Only a few microorganisms can synthesize this molecule, notably actinobacteria (including mycobacteria) and filamentous fungi (Seebeck, 2010). The role of ergothioneine in microbes is unclear, but the molecule has antioxidant properties (Cheah and Halliwell, 2012). Other stress-related proteins include those encoded by genes in the region around the response regulator gene SCO0204 (Table S2). Our recent studies revealed that SCO0204 controls development and oxidative stress (van Rossum et al., manuscript in preparation). SCO0204 probably has a similar regulon as DosR, which is the oxygen-sensitive dormancy response regulator in *Mycobacterium tuberculosis* (Chauhan et al., 2011; Gerasimova et al., 2011). One important target that is significantly more abundant in large pellets and part of the SCO0204 regulon is the universal stress protein USP (SCO0200).

Table 3. Proteins under- and overrepresented in the large mycelia relative to the small mycelia.

Fold change (2log value)	Independent quantification events	SCO number	Description
Proteins underrepresented in the population of large mycelia			
-4.8	3	SCO0917	Putative oxygenase
-4.4	7	SCO5289	CvnA5 Putative two component sensor kinase
-3.7	18	SCO4860	Putative secreted hydrolase
-3.5	5	SCO2157	Putative aminotransferase
-2.3	3	SCO3686	Putative uncharacterized protein
-2.0	13	SCO1551	Putative eukaryotic-type protein kinase
-2.0	6	SCO5104	Putative uncharacterized protein
-1.9	10	SCO6762	Putative phytoene dehydrogenase
-1.8	5	SCO2613	Putative membrane protein
-1.7	5	SCO4091	BldC Putative DNA-binding protein
-1.6	3	SCO2236	YoeB Toxin
-1.4	6	SCO6811	Putative secreted protein
-1.1	9	SCO5803	LexA repressor
-0.9	5	SCO4092	HrpA ATP-dependent helicase
-0.9	13	SCO5497	Putative uncharacterized protein
-0.9	4	SCO5698	Putative uncharacterized protein
-0.9	4	SCO7507	Putative dioxygenase
-0.8	4	SCO3748	F40 Cold shock protein
-0.8	9	SCO0436	RpmF2 50S ribosomal protein L32-2
-0.8	13	SCO4711	RpsQ 30S ribosomal protein S17

Fold change (2log value)	Independent quantification events	SCO number	Description
Proteins overrepresented in the population of large mycelia			
0.8	56	SCO0200	Universal stress protein (USP)
0.8	18	SCO0179	Putative zinc-containing dehydrogenase
0.9	5	SCO1384	Putative uncharacterized protein
1.0	17	SCO0617	Probable phosphoketolase
1.0	7	SCO0174	Putative DNA-binding protein
1.0	6	SCO3236	AsnO L-asparagine oxygenase
1.0	5	SCO5389	Putative uncharacterized protein
1.0	3	SCO5869	Putative uncharacterized protein
1.1	17	SCO3230	CdaPSI CDA peptide synthetase I
1.2	12	SCO0201	Putative integral membrane protein
1.4	7	SCO3945	CydA Putative cytochrome oxidase subunit I
1.4	4	SCO3231	CdaPS2 CDA peptide synthetase II
1.5	4	SCO6273	Putative type I polyketide synthase
1.7	26	SCO7511	Gap2 Glyceraldehyde 3-phosphate dehydrogenase
3.4	6	SCO4252	Putative uncharacterized protein
4.4	4	SCO4060	Putative uncharacterized protein
4.9	5	SCO0913	Putative uncharacterized protein

Interestingly, also proteins for biosynthesis of the glycopeptide calcium-dependent antibiotic (CDA) were more abundant in the population of large pellets, consistent with the observation that antibiotics are preferentially produced in larger pellets (Wardell et al., 2002). These proteins included the CDA peptide synthase I and II (SCO3230 and SCO3231) and a secreted hydrolase (SCO3233) that is also included in the CDA biosynthetic machinery (Table S3; Bentley et al., 2002). The biosynthetic proteins for the antibiotics actinorhodin and undecylprodigiosin were not detected.

Several of the hits in the list of less abundant proteins in large pellets are related to DNA topology, modification or degradation. These include the SOS response regulator LexA (SCO5803; Kelley, 2006) and the DNA helicase HrpA (SCO4092). The list further contained the cysteine desulfurase DndA (SCO2157), the pyridine nucleotide-disulphide oxidoreductase SCO6811, and the top hit SCO0917 (30-fold less abundant in larger pellets). The latter encodes a luciferase-type flavin monooxygenase, the gene for which is immediately upstream of and probably coregulated with the *uvrA*-like gene SCO0918. *UvrA* is part of the bacterial nucleotide excision repair system (Sancar, 1996). Besides HrpA (SCO4092), also the genetically adjacent *BldC* (SCO4091) was identified as a protein underrepresented in the larger pellets. *BldC* is a developmental control protein required for the onset of

morphological differentiation of streptomycetes, via a yet unknown mechanism (Hunt et al., 2005). Interestingly, three sensory kinases were less abundant in the population of large pellets, including SCO1551, SCO5289, and SCO5104, which is a multi-domain protein that carries a histidine kinase domain found in, among others, DNA gyrases and topoisomerases, several GAF and PAS sensory domains and a domain found in sigma factors. Taken together, these data show significant differences in protein abundance in different pellet populations.

Discussion

A major complicating factor in the use of streptomycetes for industrial fermentation is that, like filamentous fungi, these microorganisms grow as intricate networks of branched hyphae, producing characteristic filamentous multicellular structures referred to as pellets. This results in high viscosity of the fermentation broth, and the concomitant low yield per unit of time is a major bottleneck for industrial applications. Understanding how morphology correlates to the production of natural products and enzymes is of great importance for industry-scale production. Large pellets typically produce antibiotics (Wardell *et al.*, 2002), while small fragments optimally produce enzymes (van Wezel *et al.*, 2006). These results imply that changing the relative abundance of smaller or larger pellets, as appropriate, might improve yield. Heterogeneity of cultures is a common trait in microbial communities, perhaps because heterogeneous populations have increased fitness as compared to homogeneous populations. One of the best-studied examples is the sporulation process in *Bacillus subtilis* (Errington, 2003). Sporulation is an irreversible process that is initiated when nutrients become limiting. When sporulation starts, not all cells enter this process, leading to two different populations of cells: sporulating and non-sporulating cells (Smits *et al.*, 2006). The relevance of sporulation is evident for individual cells: these structures are highly resistant to harsh environmental conditions, thereby ensuring maintenance of the species. However, the non-sporulating cells can continue to grow on nutrients that are released during cell lysis and sporulate later, or resume growth when new nutrients become available (Veening *et al.*, 2008). As such, this diversification in two populations of cells benefits the entire population. Heterogeneity is also evident in solid-grown sporulating cultures of streptomycetes. For instance, a vertical cross-section through an individual colony reveals that only the vegetative mycelium in the central part of the colony forms the red-pigmented antibiotic undecylprodigiosin (Chater, 1998). The presence of (sporulating) aerial hyphae on top of such colonies introduces another form of heterogeneity (Chater, 1998). We here show that heterogeneity is also present in liquid-grown cultures, where it is characterized by the presence of two distinct populations of pellets.

The presence of two populations of pellets in liquid cultures of streptomycetes was observed irrespective of media composition and culture age. The pellet diameter in the population of small pellets was similar between the tested streptomycetes and was also not affected

by culture age (i.e. between day 1 and day 7) and medium composition. In contrast, the mean size of the population of large pellets did vary. Pellet size is affected by parameters such as the geometry of the flask or bioreactor, the composition of the growth medium, pH, temperature, and the stirring speed (Tough and Prosser, 1996; Cui *et al.*, 1998; Celler *et al.*, 2012). Our data suggest that these parameters would impact in particular the population consisting of large pellets and not that of the small ones. Deletion of genes for the cellulose synthase-like protein CslA and for the chaplin cell surface proteins affected only the size of the large pellets. The observed decrease in their size implies that the cell surface has a critical role in establishing or maintaining pellet architecture. Taken together, these data suggest that the population of small pellets is an intrinsic property of growth of streptomycetes not influenced by environmental conditions and cell wall components. In contrast, the diameter of large pellets is determined by such factors and also differs between *Streptomyces* species.

So far, it is not clear how the heterogeneity in pellet size is established. The size of fungal pellets is influenced by aggregation of spores (primary aggregation) and of germlings (secondary aggregation; Lin, Grimm, Wulkow, Hempel, & Krull, 2008). This implies that the pellet size depends on the surface properties of both spores and hyphae (van Veluw *et al.*, 2012). Significantly, in *Streptomyces* two populations of pellets were observed irrespective whether spores or mycelium were used as an inoculum. This implies that heterogeneity is not the result of spore aggregation. The large pellets might result from the aggregation of small pellets. Heterogeneity in surface properties of the small pellets may result in distinct populations. This is consistent with the important role that cell surface proteins have on pellet size.

In terms of application, we demonstrate here that the COPAS technology allows, among others, a comparison between different bacterial cell types (i.e. small and large pellets), also known as cytomics. Cytomics is a promising technology applied frequently in the eukaryotic field (Kumar and Borth, 2012), and we feel this may form an important asset in the design of producer strains with improved productivity. Application of quantitative proteomics demonstrated relatively small differences between small and large pellets. Out of the over 1100 proteins that could be quantified in the mycelial fractions, the abundance of only 37 was significantly different (17 were more abundant and 20 were less abundant in large mycelia relative to small mycelia). The production of antibiotics and proteins is affected by pellet size, but it is yet unknown what the molecular basis for this phenomenon is. For instance, the production of erythromycin by *Saccharopolyspora erythraea* (closely related to *Streptomyces*) requires larger pellets for optimal yields (Wardell *et al.*, 2002). We indeed showed that biosynthetic proteins for the production of the antibiotic CDA were enhanced in the large pellets. Several oxidative stress-related proteins were also overrepresented in the population of large pellets. This is most likely explained by the enhanced oxygen stress in large mycelial pellets due to mass transfer problems (Celler *et al.*, 2012). Notably, several

proteins encoded by genes in the chromosomal region between SCO0168-0208, most of which belong to the regulon of the response regulator SCO0204, were also enhanced in larger pellets. This includes the important stress protein USP, and we anticipate that this protein may play an important role in mycelial stress management. SCO0204 itself is an oxygen sensory protein (van Rossum et al., manuscript in preparation) and together with the sensory kinase SCO0203 it forms a two-component system that is orthologous to the DevS-DevR two-component system controlling dormancy in *Mycobacterium* species (Chao et al., 2010).

Many of the proteins that were less abundant in large pellets related to DNA topology, modification or degradation, including the SOS response regulator LexA (Kelley, 2006) and the DNA helicase HrpA. While the fact that BldC (SCO4091), encoded by a gene adjacent to that for HrpA, was also less abundant is perhaps suggestive, it is yet unknown if this regulator of morphogenesis is functionally related to *hrpA*. Other DNA metabolism-related proteins were the cysteine desulfurase DndA and the pyridine nucleotide-disulphide oxidoreductase SCO6811. The relatively high abundance of these proteins in small mycelia may be explained by the generally faster growth in small pellets, which presumably requires more intensive DNA replication, folding/unfolding and quality control.

Summarizing, we successfully applied the COPAS technology to size fractionate liquid-grown mycelia of streptomycetes, which revealed that *Streptomyces* cultures consist of two different mycelial types. This allowed us to identify differences in protein abundance depending on mycelium size. The initial data set obtained in this work provides insight into proteins that may play a role in growth and stress management of liquid-grown mycelia. This also provides strong validation for the applicability of our approach. The efficiency and reproducibility of the sorting process was highlighted by the highly similar protein profiles obtained from biologically independent replicate experiments. Besides size fractionation, flow cytometry also allows fractionation of mycelia based on fluorescence intensity or a combination of fluorescence intensity and size (de Bekker et al., 2011). Our work therefore opens new avenues for the cell biological research on streptomycetes.

Acknowledgements

Marloes Petrus and Dennis Claessen were appointed at IBL from the award to Prof. Dr. P.J.J. Hooykaas as Academy Professor. Jerre van Veluw created the scripts for analysis of two populations of pellets and assisted with the COPAS analysis. Jacob Gubbens assisted with proteomics and prepared the proteomics pipe-line. Bogdan Florea and Hermen Overkleeft are thanked for help with mass spectroscopy. Han Wösten en Gilles van Wezel gratefully acknowledge the Dutch Applied Research Council (STW) for continuing financial support.

Supporting information

Table S1. Strains used in this study

Organism	Strain	Description	Reference or source
<i>S. coelicolor</i>	M145	M145 Wild-type SCP1- SCP2-	Kieser <i>et al.</i> , 2000
	Δ <i>cslA</i>	<i>sco2836::Tn5062</i>	de Jong <i>et al.</i> , 2009
	Δ <i>chpABCDEFGHIH</i>	<i>chpAD::scar chpB::vph chpCH::aadA</i> <i>chpE::scar chpF::scar chpG::aac(3)IV</i>	Claessen <i>et al.</i> , 2004
	Δ <i>nepA</i>	<i>nepA::aac(3)IV</i>	de Jong <i>et al.</i> , 2009
<i>S. griseus</i>	ATCC 13273	Wild-type	ATCC
<i>S. lividans</i>	1326	Wild-type	Kieser <i>et al.</i> , 2000
<i>S. avermitilis</i>	ATCC 31267	Wild-type	ATCC
<i>S. scabies</i>	ISP5078	Wild-type	Gift from Prof. R. Loria

Table S2. Changes in the abundance of proteins encoded by genes around the response regulator gene *SCO0204* in the large mycelia relative to the small mycelia.

Fold change ($^2\log$ value)	Independent quantification events	SCO number	Description
0.5	32	SCO0167	Putative uncharacterized protein
0.6	15	SCO0168	Possible regulator protein
-0.1	9	SCO0171	Nicotinate phosphoribosyltransferase
1.0	7	SCO0174	Putative DNA-binding protein
0.8	18	SCO0179	Putative zinc-containing dehydrogenase
0.5	15	SCO0198	Putative uncharacterized protein
0.7	28	SCO0199	Putative alcohol dehydrogenase
0.8	56	SCO0200	Putative uncharacterized protein
1.2	12	SCO0201	Putative integral membrane protein
0.0	10	SCO0203	Putative two-component sensor
0.4	31	SCO0204	Putative luxR family two-component response regulator
0.4	27	SCO0208	Pyruvate phosphate dikinase

Table S3. Changes in the abundance of proteins encoded by genes of the *cda* gene cluster in the large mycelia relative to the small mycelia.

Fold change (² log value)	Independent quantification events	SCO number	Description
-0.2	5	SCO3226	AbsA2 Two component system response regulator
1.1	17	SCO3230	CdaPSI CDA peptide synthetase I
1.4	4	SCO3231	CdaPS2 CDA peptide synthetase II
0.6	9	SCO3233	Putative hydrolase
1.0	6	SCO3236	AsnO L-asparagine oxygenase

4

This Chapter was published as:

Amanda K. Chaplin, Marloes L.C. Petrus, Giulia Mangiameli, Michael A. Hough, Dimitri A. Svistunenko, Peter Nicholls, Dennis Claessen, Erik Vijgenboom and Jonathan A.R. Worrall (2015). *Biochemical Journal* 469: 433-444

Abstract

Streptomyces lividans displays a distinct dependence on copper to fully initiate morphological development. Evidence has accumulated to implicate the participation of an extracytoplasmic cuproenzyme in morphogenesis. Here we show that GlxA is this cuproenzyme. GlxA is membrane associated and has an active site consisting of a mononuclear copper and a cross-linked Tyr-Cys co-factor. The domain organisation of the tertiary structure defines GlxA as a new structural member of the mono-copper oxidase family, with copper coordination geometry similar to, but spectroscopically distinct from fungal galactose oxidase. Electron paramagnetic resonance spectroscopy reveals that the oxidation of cupric GlxA generates a protein radical residing on the Tyr-Cys cross-link. A variety of canonical galactose oxidase substrates (including D-galactose) were tested but none were readily turned over by GlxA. A *glxA* null-mutant leads to loss of glycan accumulation at hyphal tips and consequently a drastically changed morphology both on solid substrates and in liquid-grown environments, a scenario similarly observed in the absence of the neighbouring glycan synthase CsIA. The *glxA* mutant phenotype cannot be rescued by addition of copper suggesting it is the enzymatic action of GlxA on the glycan that is required for development and morphology. From a biotechnology perspective the open mycelium morphology observed with the *glxA* mutant in submerged culture has implications for use as an enzyme production host.

GlxA is a new structural member of the radical copper oxidase family and is required for glycan deposition at hyphal tips and morphogenesis of *Streptomyces lividans*

Introduction

Streptomycetes are filamentous monoderm soil bacteria that form networks of branching hyphae called mycelia. These organisms display a complex developmental life cycle on solid substrates. Following spore germination a vegetative mycelium is established that in response to nutrient depletion and other signals initiates both secondary metabolite production and morphological differentiation (Flårdh and Buttner, 2009; van Dissel *et al.*, 2014). This leads to the formation of aerial hyphae that will develop into chains of spores. The richness and varied production of secondary metabolites in streptomycetes is coordinated with development and these metabolites have long been a source of interest due to their pharmaceutical properties (Flårdh and Buttner, 2009; van Dissel *et al.*, 2014). Streptomycetes also hold promise as a large scale production host in biotechnology for the heterologous production of proteins and enzymes at high levels for therapeutic, scientific, diagnostic and agricultural purpose (Anné *et al.*, 2012). *Streptomyces lividans* is a preferred choice as an industrial host primarily due to its low level of endogenous extracellular proteolytic activity. As a production host the morphology of the mycelial growth in submerged culture is important as this can play a significant role in its production capacity (van Dissel *et al.*, 2014).

Copper (Cu) is an essential redox-active metal ion in living organisms. In *S. lividans* a distinct dependence on the bioavailability of Cu in order to fully initiate morphological development is known (Keijser *et al.*, 2000; Fujimoto *et al.*, 2012; Blundell *et al.*, 2013). *In vitro* studies have revealed that two extracytoplasmic Cu metallochaperones, ECuC and Sco, facilitate a Cu trafficking pathway whereby the Sco protein can receive Cu from ECuC and deliver it to the Cu_A site of an aa₃-type cytochrome *c* oxidase (CcO). Mutant analysis in *S. lividans* has revealed that morphological development proceeds in the absence of ECuC ($\Delta ecuc$) and CcO

(Δcco), but not in the absence of Sco (Δsco). While $\Delta ecuc$ and Δsco significantly reduce CcO activity, these data indicate that morphological development is not linked to impaired CcO activity (Blundell *et al.*, 2013). Notably the addition of exogenous Cu to the Δsco mutant rescues development (Blundell *et al.*, 2013). This implies that a branched Cu trafficking pathway is prevalent under Cu homeostasis conditions in *S. lividans*, whereby Sco is most certainly required to act as a Cu chaperone for CcO and possibly for other extracytoplasmic cupro-proteins/enzymes that trigger formation of aerial hyphae (Blundell *et al.*, 2014).

Analysis of the *S. lividans* genome has revealed a number of genes that encode for putative extracytoplasmic cuproenzymes (Worrall and Vijgenboom, 2010; Cruz-Morales *et al.*, 2013). One of these, SLI_3188, has a weak sequence homology with the secreted fungal cuproenzyme galactose oxidase (Gox), with putative ligands to the Cu ion (two Tyr and two His residues) seemingly conserved (Supplementary Fig. S1). Gox houses a catalytic unit, which combines two distinct redox centres; a mononuclear Cu site capable of one electron redox cycling and a Tyr-Cys cofactor, whereby a Cys residue is cross-linked to one of the Cu coordinating Tyr residue and can form a stable protein radical (Whittaker and Whittaker, 1988; Whittaker and Whittaker, 1990; Ito *et al.*, 1991; Whittaker and Whittaker, 1993; Ito *et al.*, 1994; Lee *et al.*, 2008). This redox unit enables the two-electron oxidation of a range of D-isomers of primary alcohols (including the C6-hydroxymethyl group of mono- and polysaccharides) to aldehydes with the reduction of dioxygen to hydrogen peroxide (Avigad *et al.*, 1962). The physiological function of Gox remains unknown, but the broad substrate specificity inherent in this cuproenzyme suggests that maintaining hydrogen peroxide production in the extracytoplasmic environment may be important for function.

In *S. coelicolor* a homologous gene to SLI_3188, annotated as *glxA*, is required for aerial hyphae development under conditions of osmotic stress (Liman *et al.*, 2013). The *glxA* gene is the distal gene in an operon with *csIA*, which encodes a family 2 glycosyltransferase that synthesizes a glycan at hyphal tips (Xu *et al.*, 2008; Petrus and Claessen, 2014). Orthologs of *glxA* and *csIA* are present in all streptomycetes and several other actinobacteria with some species having paralogs e.g. *S. griseus* and *S. albus*. The genetic locus contains several other genes encoding enzymes implicated in glycan processing, including a Cu-containing lytic polysaccharide monooxygenase, suggesting a role of GlxA in polysaccharide modification or synthesis. In the present study we show that GlxA is a membrane-associated cuproenzyme with a mononuclear Cu site and a Tyr-Cys redox cofactor. However, GlxA is distinct from fungal Gox through a unique tertiary structure, atypical spectroscopic properties, and a lack of enzymatic activity with a range of 'classical' Gox substrates. As observed in the absence of *csIA*, we find that a *glxA* null-mutant stalls aerial hyphae development on solid media, lacks the hyphal tip glycan and has a dramatically different morphology in liquid-grown cultures. The latter is of particular interest in respect to the use of *S. lividans* as a cell factory for protein production.

Experimental

Mycelium washes, fractionation and GlxA detection

S. lividans 1326 was grown in TSBS for 18 h at 30 °C with shaking at 200 rpm. Mycelium was harvested in 1.5 ml aliquots by centrifugation at 15,000 g for 10 min and stored at -80 °C until required. Mycelium aliquots were first resuspended in 25 mM Tris/HCl pH 7.5, 100 mM NaCl centrifuged at 25,000 g and the supernatant was kept as the 100 mM NaCl wash. The pellet was resuspended in buffer containing 1 M NaCl, incubated for 30 min on ice and centrifuged at 25,000 g, which produced the 1 M NaCl wash. For mycelium extracts the suspended mycelium pellets were sonicated (Bioruptor, 12 cycles 30 s on, 30 s off). The soluble (S30) and insoluble fractions (P30) were obtained by centrifugation at 30,000 g. The supernatant (S30) was subjected to a second centrifugation step at 100,000 g to remove all membrane particles and ribosomes to give the S100 and P100 fractions. The pellets (P30 and P100) was resuspended in buffer containing 1 % Triton X-100, incubated on ice for 30 min and centrifuged again at 30,000 g and 100,000 g, respectively to separate triton soluble (P30-TS, P100-TS) and insoluble (P30-TP, P100-TP) fractions. Fractions obtained were run on 10 % SDS-PAGE and blotted to Hybond-P membranes for immuno-detection of GlxA and EF-Tu1. The antibodies against GlxA were a kind gift of James W. Whittaker (Oregon Health & Science University, USA). The EF-Tu1 antibodies were raised in rabbits against *S. ramocissimus* EF-Tu1 (Vijgenboom *et al.*, 1994). Incubation with antibodies (GlxA antibodies 10,000 x diluted and EF-Tu1 antibodies 5,000 x diluted) was carried out for 18 h at 4 °C with gentle rocking in PBS with 5 % milk (FrisoLac Extra, FrieslandCampina). The bound antibodies were detected with GARAP (Sigma) as the secondary antibody and NBT/BCIP as the substrate. Digital images were taken of the Western blots and total signal intensities were determined with Image J (Schneider *et al.*, 2012).

*Creation of the *S. lividans* $\Delta cslA$ and $\Delta glxA$ null-mutants, complementation plasmids and monitoring growth morphology*

The $\Delta glxA$ and $\Delta cslA$ mutant was prepared and isolated as previously described (Blundell *et al.*, 2013). In the $\Delta glxA$ mutant, nucleotides +60 to +1916 relative to the start codon of *SLI_3188* were replaced by a 62 nt scar of the *loxP* recombination site including two *XbaI* sites. In the $\Delta cslA$ mutant, nucleotides +79 to +1827 relative to the start of *SLI_3187* were replaced. The mutant is consistent with the one described by Xu *et al.* (2008). Plasmid pGlxA contains the *glxA* ORF (*SLI_3188*) and the promoter region (-545 to -1) upstream of *cslA* (*SLI_3187*). For surface growth the agar media R5 (Kieser *et al.*, 2000) was incubated at 30 °C, and supplemented with Cu as required. Morphology in liquid media was determined following 24 h growth at 30 °C with shaking in flasks equipped with coils containing Tryptic

Soya Broth (TSB) supplemented with 10 % sucrose and Cu as indicated. Samples from liquid cultures were analysed by light microscopy with a Zeiss Standard 25 microscope and digital pictures were taken with an AxioCam camera linked to AxioVision software. All spore stocks were obtained from cultures grown on MS agar plates (Kieser *et al.*, 2000) and stored in 20 % glycerol at -20 °C.

Monitoring glycan production

Glycan production was determined following 24 h growth at 30 °C in 8 well microscopy plates (Lab-TEK II Chambered Coverglass) containing 500µl mNMMP medium [24]. Mycelium was stained by adding 50 µl calcofluor white (CFW) solution (Remel Bactidrop) to each well. After 5min, but within 20 min, stained mycelium was analysed with a laser-scanning confocal microscope (Zeiss LSM5 Exciter/Axio Observer) by excitation with a 405 nm laser, a 405/488 nm beamsplitter and a bandpass emission filter of 420-480 nm. Images were adjusted for brightness and contrast using ImageJ (Schneider *et al.*, 2012).

Cloning, over-expression and purification of GlxA

The *glxA* gene with 200 flanking nt at the 5' and 3' ends was amplified from *S. lividans* 1326 and cloned into a pUC19 vector. This construct was used to create an N-terminal deleted *glxA* for over-expression in *Escherichia coli* by amplifying the *glxA* nt sequence that starts coding for amino acid 35, and restricted using the *Nde*I and *Bam*HI sites of a pET28a vector (Novagen) to create an N-terminal His₆-tagged *glxA* construct. The overexpression and purification of recombinant GlxA are described in Supporting Information.

Preparation of GlxA samples and UV-visible spectroscopy

GlxA concentration was determined by UV-visible spectroscopy (Varian Cary 50 UV-visible spectrophotometer) using an extinction coefficient (ϵ) at 280 nm of 78,730 M⁻¹·cm⁻¹. The various forms of GlxA were prepared through the addition of ~ 5-fold excess of [Fe(CN)₆]³⁻ (Sigma), [Ir(Cl)₆]³⁻ (Acros) or Na₂S₂O₄ (Sigma) followed by removal via a PD-10 column (GE Healthcare).

Crystallisation and structure determination

An ARI-Gryphon 96-well crystallisation robot was used to screen crystallisation conditions for GlxA. A crystal hit was discovered in 0.1 M sodium acetate pH 4.6, 15% PEG 20,000 (PEG suite, Qiagen). Scaling-up and optimisation of GlxA crystals from the initial hit was carried out in 24-well VDX plates (Molecular Dimensions) using the hanging drop vapor

diffusion method at 20 °C. Equal volumes of GlxA solution at a concentration of 15 mg ml⁻¹ and reservoir solution containing 0.1 M sodium acetate pH 4.0, 20% PEG 20,000 were mixed. Crystals suitable for diffraction studies grew within 1 week. A single crystal was transferred to a cryoprotectant solution containing, the respective reservoir solution and 20 % glycerol prior to flash-cooling by plunging into liquid nitrogen. Crystallographic data were measured at the beamline I03, Diamond Light Source, using an X-ray wavelength of 0.979 Å and a Pilatus 6-M-F detector (Dectris). Details of structure determination are given in Supporting Information. Coordinates and structure factors were deposited in the RCSB Protein Data Bank with accession number 4unm. A summary of data and refinement statistics and the quality indicators for the structure are given in Table 1. CAVER analyst 1.0 was used for the identification of tunnels (Kozlikova *et al.*, 2014). Chain B of GlxA was analysed using the tunnel computation tool within CAVER with a starting point defined using the first coordination sphere Cu binding residues (Tyr²⁸⁹, Tyr⁵⁰¹, His⁵⁰², His⁵⁸⁹). Default settings for tunnel analysis were used, including the minimum probe radius set to 0.9 Å.

Table 1. X-ray data processing and refinement parameters. The GlxA crystal structure was in space group $P2_1$ with unit cell parameters 50.4, 126.6, 107.6 Å, 90, 91.1, 90°. Values in parentheses refer to the outermost resolution shell (1.80-1.77 Å).

Resolution (Å)	53.3-1.77
Unique reflections	130533 (21898)
Completeness (%)	99.7 (99.6)
Redundancy	3.6 (3.4)
Rmerge (%)	0.064 (0.633)
Mn(I/sd)	10.5 (2.0)
Wilson B factor (Å ²)	20.5
Rcryst	0.188
Rfree	0.228
RMSD bond lengths (Å)	0.011
RMSD bond angles (°)	1.41
ESU based on ML (Å)	0.096
Ramachandran favoured (%)	95.9
PDB accession code	4unm

EPR spectroscopy

GlxA samples (85-120 µM) for EPR were prepared in duplicate in a mixed buffer system consisting of 10 mM each of Tris, potassium acetate, MES, MOPS and 200 mM KCl with the pH adjusted to 7.0. Wilmad SQ EPR tubes (Wilmad Glass, Buena, NJ) were filled with the GlxA solutions and frozen in methanol kept on dry ice. The tubes were then transferred to liquid nitrogen. All EPR spectra were measured on a Bruker EMX EPR spectrometer (X band) at a modulation frequency of 100 kHz. A spherical high-quality Bruker resonator

ER 122 SP 9703 and an Oxford Instruments liquid helium system were used to measure the low-temperature EPR spectra. Digitising of a published EPR spectrum was performed using Un-Scan-It, v.6, Silk Scientific.

Activity assays

A variety of putative substrates for GlxA were assayed. These included the following monosaccharides; D-galactose, D-glucose, D-sucrose, D-fructose *N*-acetyl-D-glucosamine, and D-glucuronic acid; the disaccharides, D-lactose and D-cellobiose; and the aldehydes and primary alcohols glycolaldehyde, glyoxal and glycerol (all purchased from Sigma). Catalytic turnover was measured using a coupled assay, whereby the production of H₂O₂ by GlxA was detected by the presence of horseradish peroxidase (HRP) (Sigma) and the subsequent oxidation of guaiacol (Sigma). Samples were prepared in 3 ml quartz cuvettes containing 0.1 M sodium phosphate, pH 7.4, 1 mM guaiacol, 1 μ l HRP (10 mg ml⁻¹), 20-30 μ M GlxA and varying concentrations of the individual substrate. The oxidation of guaiacol was monitored at 470 nm using a Hewlett-Packard 8453 diode-array spectrophotometer scanning between 190 and 1100 nm and thermostatted at 25 °C. Plots of turnover rate (k , s⁻¹) versus substrate concentration were constructed, whereby k was calculated from $((\Delta A_{470}/\epsilon_{gc})/t)/[GlxA]$ where ΔA_{470} is the absorbance change at 470 nm upon guaiacol oxidation, ϵ_{gc} is the extinction coefficient of the guaiacol oxidation product taken as 5.57 mM⁻¹ cm⁻¹, t is the time in seconds and $[GlxA]$ is the total millimolar concentration of GlxA in the assay.

Results

GlxA is associated with the membrane

The distribution of GlxA in the soluble and insoluble fractions of liquid grown *S. lividans* mycelium was first determined. Upon thorough mycelium sonication followed by centrifugation steps, a small fraction of GlxA was detected in the soluble protein fraction (S100) with the majority remaining in the pellet fraction (P30 and P100) (Fig. 1A and B). In contrast, the majority of the cytoplasmic marker EF-Tu1 is detected in the soluble fraction (S100) (Fig. 1A and B). Resuspension of the insoluble pellet fraction in buffer containing 1 % Triton X-100 solubilizes a significant amount of GlxA (Fig. 1A and B), indicating that GlxA is not covalently bound to the membrane. However, salt washes did not remove GlxA from intact mycelium (Fig. 1C), but small amounts of EF-Tu1 were detected probably due to some lysis. These data show that GlxA is not a peripheral membrane protein but is firmly associated with the membrane, although not via a covalent bond. These results are in agreement with *in silico* analysis, which predict residues 1-11 of GlxA to be an N-terminal signal peptide (Petersen *et al.*, 2011), with a weak signal peptidase cleavage site between

residues 11-12, followed by a transmembrane helix (residues 12-32), which could function as the membrane anchor (Käll *et al.*, 2004; Bagos *et al.*, 2008).

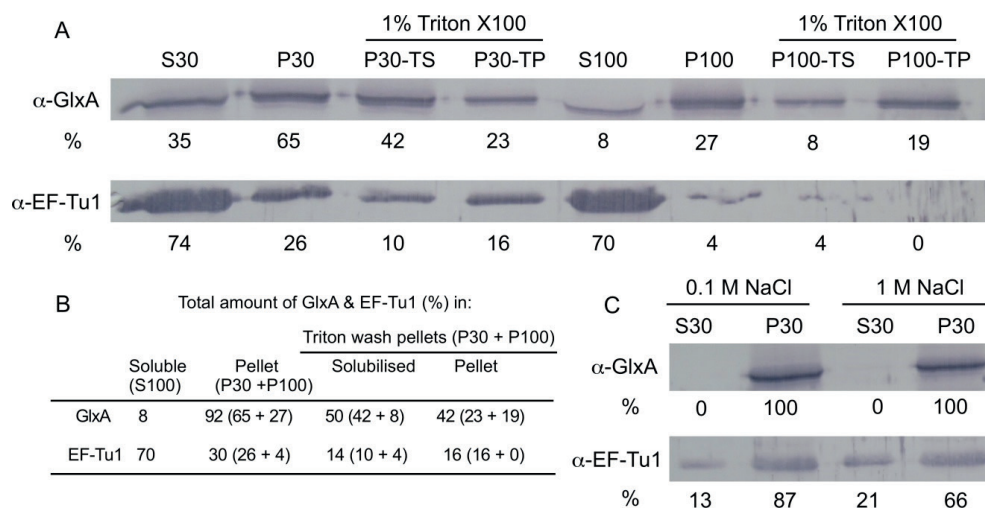


Figure 1. Location of GlxA in the mycelium determined by Western blotting. **A)** Detection of GlxA and EF-Tu1 in the various mycelium fractions. Samples were prepared as described in “Experimental”. The band intensities are expressed as percentages relative to the total amount of GlxA or EF-Tu1 in the S30 plus P30 fraction, of which the intensity was set at 100%. **B)** The Table presents the total soluble (S100), 1% triton soluble (P30-TS + P100-TS) and insoluble fraction (P30-TP + P100-TP) of GlxA and EF-Tu1 expressed in percentage according to (A). **C)** NaCl washes of the intact mycelium. The signals detected in the S30 plus P30 samples of the 100 mM NaCl wash was set at 100%.

The tertiary structure of GlxA consists of three distinct domains

To elucidate the molecular features of GlxA, an N-terminal truncated expression construct (Δ 1-34) for over-expression in *E. coli* was generated, which yielded 45 mg·L⁻¹ of purified GlxA. The crystal structure of GlxA was determined to 1.77 Å resolution and contains two protein molecules in the crystallographic asymmetric unit. Molecule A (residues 38-645) exhibits significantly lower B-factors and higher quality electron density than molecule B, but contains a disordered region between residues 198-206 (not visible in the electron density), whereas the main chain for molecule B was complete between residues 37 and 645. The overall structure of GlxA (Fig. 2) consists of three predominately β -sheet domains. Preceding the first domain are two short N-terminal α -helices (α 1 and α 2), with the α 1 helix orientated approximately perpendicular to the α 2 helix. Domain 1 of GlxA consists of seven Kelch motifs (blades) arranged in a β -propeller tertiary structure (Fig. 2). Each blade of the propeller consists of four anti-parallel β -sheets (*a*, *b*, *c*, *d*) with each sheet connected through variable length loops (Fig. 2). Blades 1 and 2 each possess structural inserts in the loops connecting sheet *b* to sheet *c*. In blade 1 a short platform-like α -helix (α 3) is inserted which has an overall negative charge, whereas in blade 2, sheets *b* and *c* are connected via domain 2 (Fig. 2). Domain 2 consists of 10 β -sheets and 1 short α -helix (α 4). According to the CATH

database (Sillitoe *et al.*, 2013) the domain 2 fold is classified as mainly β , with a β -barrel architecture formed by sheets 1, 3, 4, 8, 9 and 10 (Fig. 2), and a representative domain topology with thrombin, subunit H. Protruding out from the core β -barrel is a long β -hairpin loop (residues 194-210) consisting of β -sheets 6 and 7 (Fig. 2). In molecule A this β -hairpin loop is disordered and not built into the model, whereas this is not the case for molecule B due to stabilising polar interactions with molecule A residues from a symmetry related GlxA molecule in the unit cell (Supplementary Fig. S2). Domain 2 is positioned in the overall tertiary structure such that the β -barrel core lies across the top of approximately half of domain 1 with the β -hairpin loop extending into the solvent (Fig. 2). Further analysis of domain 2 using PDBFold identifies no structures deposited in the PDB with a high structural homology (the highest Q-score obtained was only 0.14). Thus the fold of domain 2 in GlxA is relatively novel compared to known structures. The third domain starts immediately after the seventh Kelch motif and is located at the bottom of domain 1. Domain 3 consists of

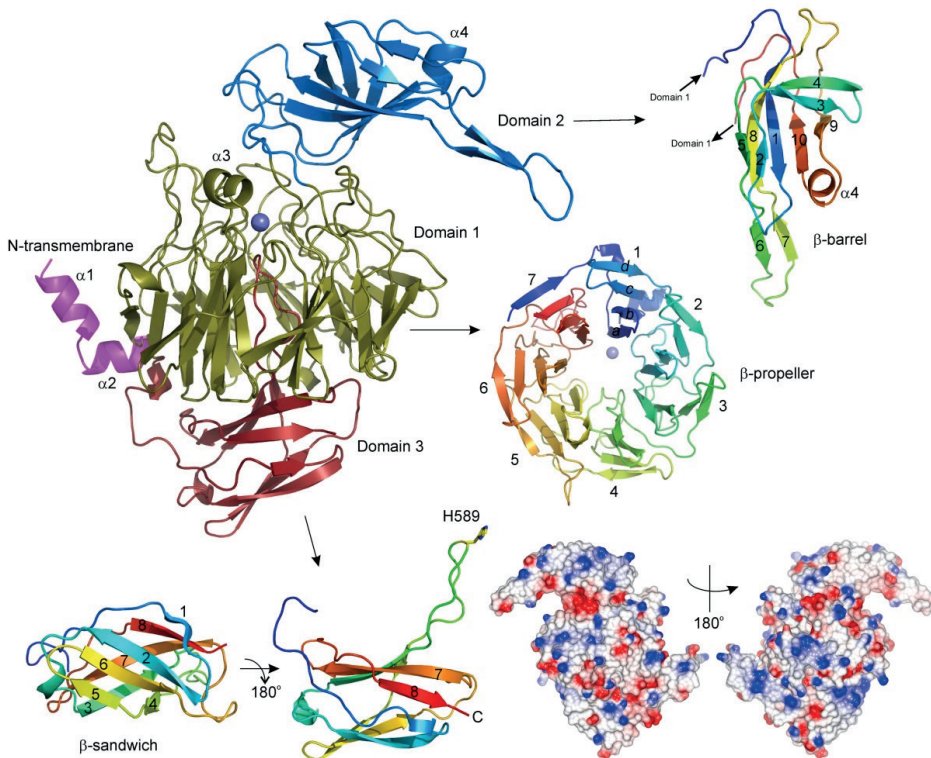


Figure 2. X-ray crystal structure of *S. lividans* GlxA. The three domains forming the tertiary structure are indicated and coloured gold (domain 1), blue (domain 2) and red (domain 3). The four short α -helices present in the structure are labelled. Each domain is shown individually and in more detail as discussed in the main text. The Cu atom is represented as a sphere and electrostatic surface representations in two GlxA orientations are shown. Images were prepared in PyMol and CCP4MG (McNicholas *et al.*, 2011).

8 β -sheets and one short α -helix forming a β -sandwich fold with a high structural homology to domain 3 of Gox (1.18 Å RMSD from superimposition). A loop (residues 583-590 in GlxA) connecting β -sheets 3 and 4 of domain 3 penetrates upwards into domain 1 along the 7-fold symmetry axis and provides one of the ligands (His⁵⁸⁹) to the Cu ion of GlxA (*vide infra*). The charge distribution of GlxA (pI 8.2) is displayed through electrostatic surface representations (Fig. 2), and indicates a rather disperse distribution of charge across the whole molecular surface.

Architecture and spectroscopic properties of the Cu site in GlxA

A well-defined 16σ peak in the σ -weighted $F_o - F_c$ difference map was present in each GlxA chains in the asymmetric unit, into which a Cu ion was modelled. The Cu is coordinated in a square pyramidal geometry with the O_γ of Tyr⁵⁰¹ acting as the axial ligand and the equatorial coordination positions occupied by the O_γ of Tyr²⁸⁹, the $N\epsilon 2$ of His⁵⁰² and His⁵⁸⁹ and a H₂O molecule (Fig. 3A). Bond lengths to the Cu ion are reported in Table 2 together with a comparison to those in Gox. Unbroken electron density is observed between the side chain S_γ atom of Cys¹²¹ and the $C\epsilon 1$ ring atom of Tyr²⁸⁹, providing clear evidence that a cross-linked Tyr-Cys cofactor is formed in GlxA, with a bond length of 1.9 Å (2.0 Å in chain B) (Fig. 3A). Adjacent to Tyr²⁸⁹ is Trp²⁸⁸, which has its side chain indole ring orientated such that the benzene ring is π - π stacking with the phenoxyl ring of Tyr²⁸⁹ with $C^{Tyr} - C^{Trp}$ distances between ~ 3.5 and 4 Å (Fig. 3A).

The UV-Vis absorbance spectrum of the blue-grey Cu(II)-GlxA has a broad, low intensity band in the visible region ($\lambda_{max} \sim 577$ nm) and two distinct shoulders ($\lambda_{max} \sim 362$ and 320 nm) (Fig. 3B). No change to these absorption features in the pH range 4 to 8 was observed, with the addition of Cu(II) ions resulting in only a small absorbance increase in $\lambda_{max} \sim 577$ nm over a 12 h period (Fig. 3B). In contrast the Cu(II)-Gox absorption spectrum has weak intensity bands at $\lambda_{max} 441$ nm attributed to phenolate (Tyr) to Cu(II) ligand-to-metal charge transfer (LMCT) and at $\lambda_{max} 630$ nm arising from mixed Cu ligand field transition and LMCT (Whittaker and Whittaker, 1988; Whittaker and Whittaker, 1993). Addition of the reductant Na₂S₂O₄ bleaches all absorption features (Fig. 3B) with removal of Na₂S₂O₄ and subsequent exposure to air resulting in the return of the Cu(II)-GlxA spectrum. This infers that the Cu is redox active and can cycle between the Cu(II) and Cu(I) states.

The EPR spectrum of Cu(II)-GlxA at pH 7 displays features consistent with an axial Cu(II) g-tensor, $g_{||} = 2.182$ and $g_{\perp} = 2.05$ (Fig. 3C). The strong line on the right from the indicated g_{\perp} region is not a principal g-factor component but an “overshoot” line (Antholine, 2005) occurring for specific orientations of the Cu(II) complexes, subject to particular relationships between the values of $g_{||}$, g_{\perp} and the anisotropic components of the hyperfine interaction of the electron spin ($S = 1/2$) with the Cu nuclear spin ($S = 3/2$), $A_{||}$ and A_{\perp} . The EPR spectrum

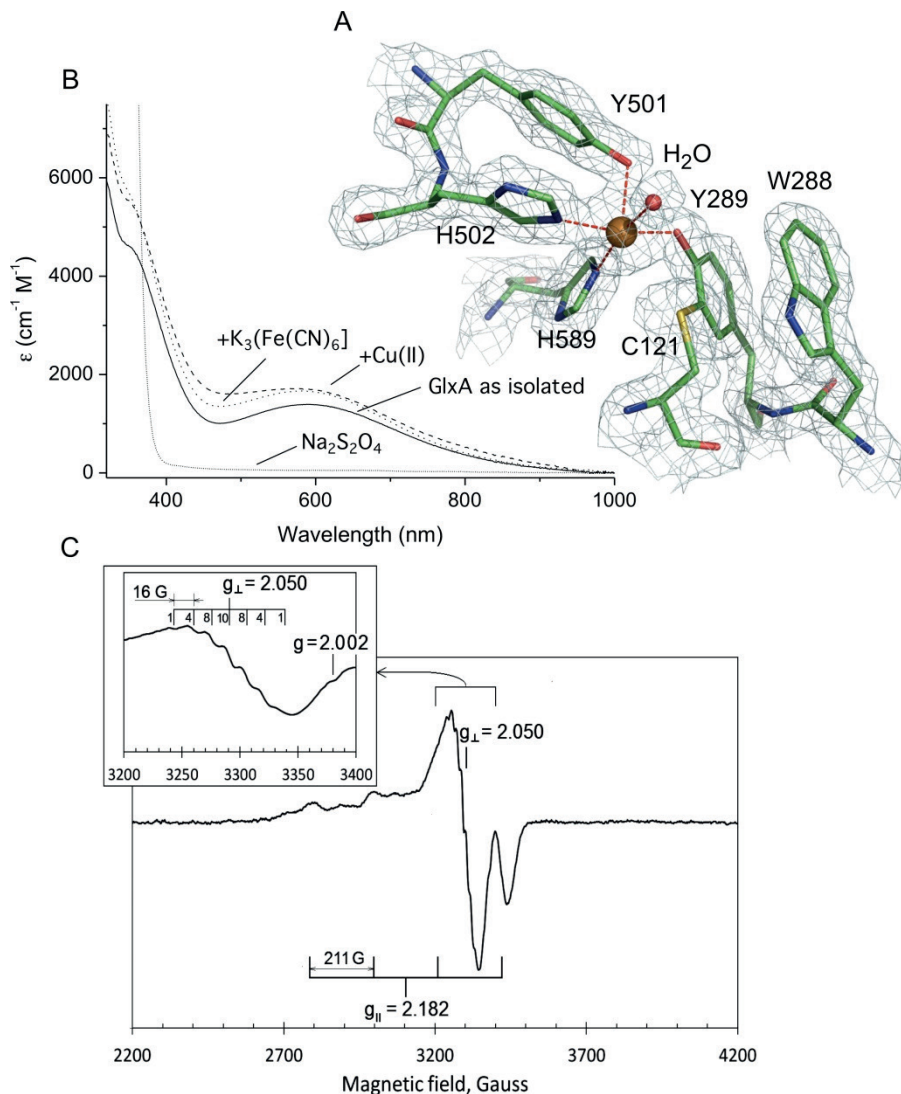


Figure 3. Structure and spectroscopy of the GlxA Cu site. **A)** $2F_o - F_c$ electron-density map contoured at 2σ of the Cu site in GlxA. The Cu ion is represented as a brown sphere with the first coordination sphere ligands to the Cu ion depicted as sticks and the equatorially coordinating H_2O molecule as a red sphere. **B)** Absorbance spectrum at pH 7 and 20 °C of purified GlxA (80 μ M) and following the addition and removal of the oxidant $[Fe(CN)_6]^{3-}$, the reductant $Na_2S_2O_4$ and $Cu(II)SO_4$. **C)** $Cu(II)$ -GlxA EPR spectrum (85 μ M) at pH 7. The g_{\parallel} component shows a hyperfine interaction of the electron spin ($S = 1/2$) with the $I = 3/2$ Cu nuclear spin – four components 1:1:1:1 separated by $A_z^{Cu} = 211$ G. Inset: the g_{\perp} region of the spectrum, which displays unpaired electron ($S = 1/2$) hyperfine interaction of the electron spin with the $Cu(II)$ ligands – seven components of relative intensities 1:4:8:10:8:4:1 separated by 16 G. Instrumental conditions: temperature 10 K, microwave frequency $\nu_{MW} = 9.47$ GHz, microwave power $P = 3.18$ mW, modulation frequency $\nu_M = 100$ kHz, modulation amplitude $A_M = 5$ G, time constant $\tau = 82$ ms, scan rate $V = 22.6$ G \cdot s $^{-1}$, number of scans per spectrum $NS = 1$.

Table 2. Bond lengths of the Cu sites (monomer A and B) in *S. lividans* GlxA and *F. graminearum* Gox (PDB 1gof) (Ito *et al.*, 1994).

GlxA (A/B)		Gox	
Cu-Tyr289 OH	1.84/1.97 Å	Cu-Tyr272 OH	1.93 Å
Cu-Tyr501 OH	2.24/2.14 Å	Cu-Tyr495 OH	2.69 Å
Cu-His502 Nε2	2.13/2.18 Å	Cu-His496 Nε2	2.11 Å
Cu-His589 Nε2	2.18/2.23 Å	Cu-His581 Nε2	2.14 Å
Cu-H ₂ O	2.44/2.50 Å	*Cu-acetate	*2.26 Å
Tyr289-Cys121	1.92/1.97 Å	Tyr-Cys	1.83 Å

*1gof crystallised in acetate buffer pH 4.5 (GlxA acetate buffer pH 4.0), with an acetate molecule found in place of the H₂O molecule in GlxA. In a Gox structure (1gog) (Ito *et al.*, 1991) crystallised in the absence of acetate buffer at pH 7.0 a H₂O molecule is found with a bond length to the Cu ion of 2.81 Å.

line shape is similar to that of Cu(II)-Gox (Whittaker and Whittaker, 2003), which also has an axial Cu(II) g-tensor (Peisach and Blumberg, 1974; Cleveland *et al.*, 1975; Bereman and Kosman, 1977). However, the GlxA spectrum exhibits a more distinctly resolved overshoot line, likely to be a consequence of a smaller g_{\parallel} (2.182 as compared to 2.21-2.23 in Gox). The g_{\perp} component displays a hyperfine interaction of the electron spin with the Cu(II) ligands, which for GlxA gives seven lines with relative intensities of 1:4:8:10:8:4:1 (Fig. 3C, inset) compared to five lines in Gox (Cleveland *et al.*, 1975; Bereman and Kosman, 1977).

Substrate access sites and binding pocket

Due to the buried nature of the Cu site, it is likely that a substrate would have to gain access via a tunnel. CAVER was used to identify tunnels in the GlxA structure (Chovancova *et al.*, 2012; Kozlikova *et al.*, 2014), defined as void pathways leading from a cavity inside GlxA, *i.e.* the Cu site, that transverse to the protein surface. Three tunnels of different lengths were identified (Fig. 4A). The entrance to tunnel I lies between the α 3 helix on the loop connecting sheets *a* and *b* in blade 1 and a well-ordered loop in blade 7 of domain 1 (Fig. 4A and B). The tunnel has an opening of $\sim 8 \times 8$ Å, is void of H₂O molecules and leads directly to the equatorially Cu coordinating H₂O molecule, with a distance to the surface of ~ 10 Å. The dimensions of the surface opening are such that pyranose carbohydrates *e.g.* D-glucose or D-galactose, and also C2 substituted pyranose carbohydrates such as *N*-acetyl-glucosamine would be able to pass. The opening of tunnel II is located beneath the β -hairpin loop of domain 2 (Fig. 4B), with the dimensions of the opening, $\sim 9 \times 7$ Å. A network of six H-bonded H₂O molecules are present in the tunnel that thread down to the Cu coordinating H₂O molecule, with a distance to the surface of ~ 25 Å. Tunnel III spans a large section of domain 1, starting from below the equatorial His ligands and leading to a surface entrance formed by residues Ala¹²⁸, Gly²⁹⁸, Pro³²² and Ser⁶²². The tunnel is lined with a continuous network of well-ordered H₂O molecules (13 in total) and has a distance from the Cu ion to the surface

of ~ 70 Å. A putative substrate pocket is identified above the axial Tyr⁵⁰¹ ligand and is directly accessible from either tunnel I or II (Fig. 4C). The pocket is occupied with several H₂O molecules, all of which are well ordered and form an extensive H-bond network, which also includes a H-bond interaction with the Tyr⁵⁰¹ ligand (Fig. 4C). The pocket is completely polar and is formed from the side chains of 6 amino acids (Fig. 4C). Side-chain H-bonding interactions with the H₂O network in the pocket are apparent for some of the residues (Fig. 4C), with Asn⁸⁸ and Arg⁴⁶⁹, part of the entrance to tunnel I (Fig. 4B), also capable of

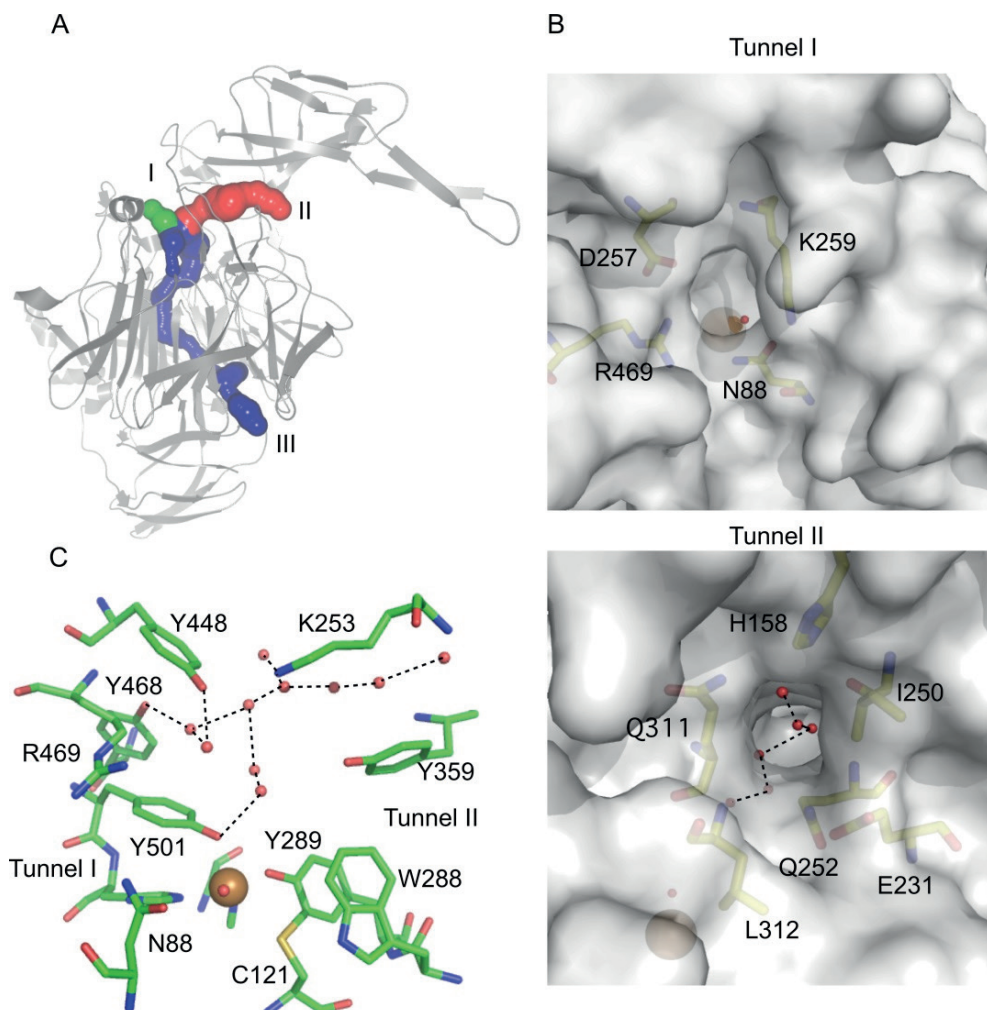


Figure 4. Substrate access channels and binding pocket. **A)** Location of the three surface-to-Cu site tunnels (I, II, III) in *S. lividans* GlxA identified using the programme CAVER (Kozlikova et al., 2014). **B)** Partial transparent surface views of the openings to tunnels I and II. The amino acids forming the openings are labelled and shown as sticks, H₂O molecules are depicted as red spheres and the Cu ion as a brown sphere. In tunnel I the equatorially Cu co-ordinated H₂O molecule is visible, and tunnel II illustrates the H-bonded H₂O network leading from the surface to the Cu site. **C)** The putative substrate-binding pocket in GlxA.

H-bond interactions.

The Tyr-Cys crosslink is redox active

The Tyr-Cys cross-link identified in the GlxA X-ray structure is redox active in Gox. Addition of the oxidants, $[\text{Fe}(\text{CN})_6]^{3-}$ or $[\text{Ir}(\text{Cl})_6]^{3-}$, to Cu(II)-GlxA does not perturb the absorbance spectrum (Fig. 3B) in contrast to Gox where formation of the fully oxidised Cu(II)-Tyr-Cys• form leads to distinct spectral features. However, a change in the EPR spectrum of GlxA following addition of $[\text{Fe}(\text{CN})_6]^{3-}$ is observed, with a 3 component free radical EPR spectrum detected (Fig. 5). The spectrum is very similar to the spectrum of the radical on the Tyr-Cys crosslink reported for Gox (Whittaker and Whittaker, 1990), glyoxal oxidase (Whittaker *et al.*, 1999) and SCO2837p from *S. coelicolor* (Whittaker and Whittaker, 2006) (Fig. 5). This observation taken together with the result of $\text{Na}_2\text{S}_2\text{O}_4$ reduction indicates that the active site of GlxA can access three oxidation states (reduced (Cu(I)), semi-reduced (Cu(II)) and fully oxidised (Cu(II)-Tyr-Cys•) as is the case for Gox and should therefore be able to catalyse the two-electron oxidation of a substrate.

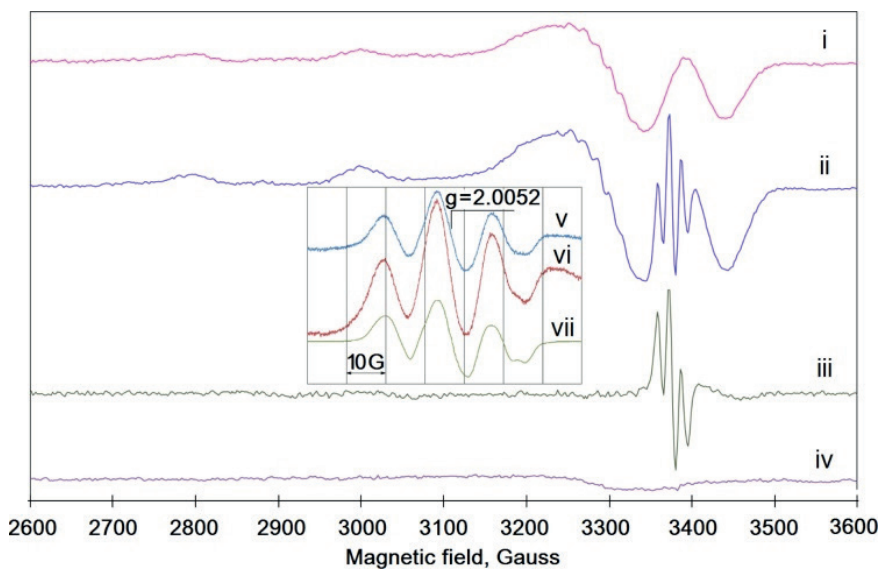


Figure 5. EPR spectra of Tyr-Cys radicals. **i)** As isolated GlxA. **ii)** After $[\text{Fe}(\text{CN})_6]^{3-}$ treatment. **iii)** difference spectrum ($\text{ii} - 1.46 \times \text{i}$) showing the free radical EPR signal in its pure form (the coefficient 1.46 was found empirically to minimize input of other EPR signals to the difference spectrum). **iv)** As in (i), but after $\text{Na}_2\text{S}_2\text{O}_4$ treatment. **Inset:** the same sample as the one used to detect spectrum (ii), was used to measure the free radical EPR signal in greater detail using two different microwave power levels, 50 μW (**v**) and 3.18 mW (**vi**). **vii)** The EPR spectrum of the radical in SCO2837p from *S. coelicolor* (Whittaker and Whittaker, 2006). All spectra were recorded at 40 K using 120 μM of GlxA at pH 7, with the instrumental conditions for i, ii and iv the same as in Fig. 3C and for spectra v and vi as follows: modulation amplitude $A_m = 3$ G, scan rate $V = 0.596$ G s^{-1} . Spectrum vii is a digitised image from (Whittaker and Whittaker, 2006), aligned with the GlxA spectrum on the basis of g-factors, therefore the magnetic field axis is not indicated.

Enzymatic activity of GlxA

A number of compounds were assayed for activity with GlxA using a coupled peroxidase assay (see “Experimental”), with only four showing significant oxidase activity. Fig. 6A reveals that aerobic oxidation rates for D-galactose, D-glucose and glycerol, follow a linear substrate relationship for the concentrations used. From the slopes of these plots, second order rate constants (k_{red}) were determined for D-galactose; $8.4 \times 10^{-3} \text{ M}^{-1}\text{s}^{-1}$, for D-glucose; $8.8 \times 10^{-3} \text{ M}^{-1}\text{s}^{-1}$ and for glycerol; $1.7 \times 10^{-2} \text{ M}^{-1}\text{s}^{-1}$. No activity was observed for the C2 position modified monosaccharide *N*-acetyl-D-glucosamine or for fructose, a 5-membered ring monosaccharide. Likewise D-glucuronic acid gave no activity, illustrating that a C1 glycosidic (aldehyde) group is not effective as reductant when the C6 group is modified (COOH vs CH₂OH). Furthermore, no activity was detected with the disaccharides D-lactose and D-cellobiose. In addition to catalysing the oxidation of primary alcohols, Gox has been reported to convert aldehydes to the corresponding carboxylates (Kelleher and Bhavanandan, 1986). However, the aldehyde, glyoxal, turned over by glyoxal oxidase, also did not give activity with GlxA. In contrast, glycolaldehyde (C₂H₄O₂) the smallest molecule to contain both an aldehyde and a hydroxyl group gave significant activity with GlxA that followed Michaelis-Menten kinetics (Fig. 6B). From these data a K_m for glycolaldehyde of 115 mM and a maximal aerobic turnover (k_{cat}) of 0.14 s^{-1} was determined. The corresponding k_{cat}/K_m value of $1.22 \text{ M}^{-1} \text{ s}^{-1}$ enables a direct comparison with the two monosaccharides and glycerol, with glycolaldehyde reacting 100-times faster.

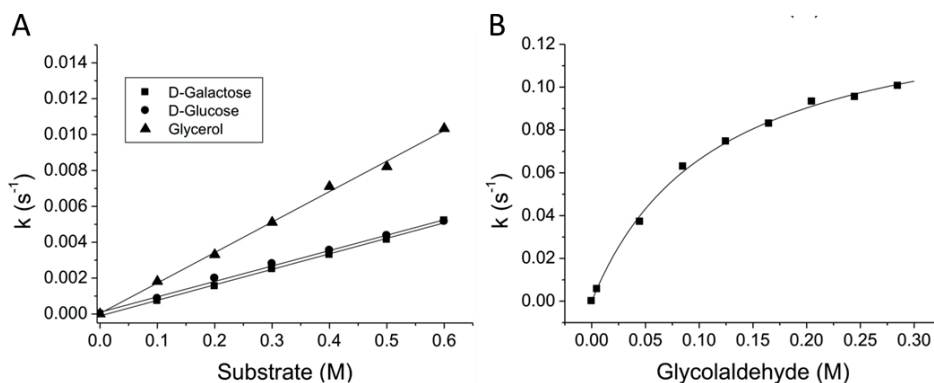


Figure 6. Enzyme activity of *S. lividans* GlxA. **A and B**) Plots of turnover rates (k) for GlxA with four different substrates (25 °C). In (A) the line of best fit through the data points enables a second-order rate constant ($\text{M}^{-1}\text{s}^{-1}$) to be determined. In (B) the data points have been fitted to the Michaelis-Menten equation to yield a K_m value and turnover (k_{cat}) reported in the main text.

GlxA is required for glycan synthesis at hyphal tips and morphogenesis

To investigate a functional role of GlxA, we created a null-mutant in *S. lividans*. Consistent

with previous work in *S. coelicolor*, our *S. lividans glxA* null-mutant has a bald phenotype (*i.e.* no aerial hyphae formation) on solid media, as is also the case for the *csIA* null-mutant (Xu *et al.*, 2008; Liman *et al.*, 2013) (Fig. 7A). Notably, the bald phenotype in the *glxA* and *csIA* null-mutants cannot be rescued upon addition to the medium of exogenous Cu(II) (Fig. S3) as has previously been reported for the Δsco null-mutant (Blundell *et al.*, 2013). Furthermore, the *glxA* and *csIA* mutants have an identical morphology in liquid-grown

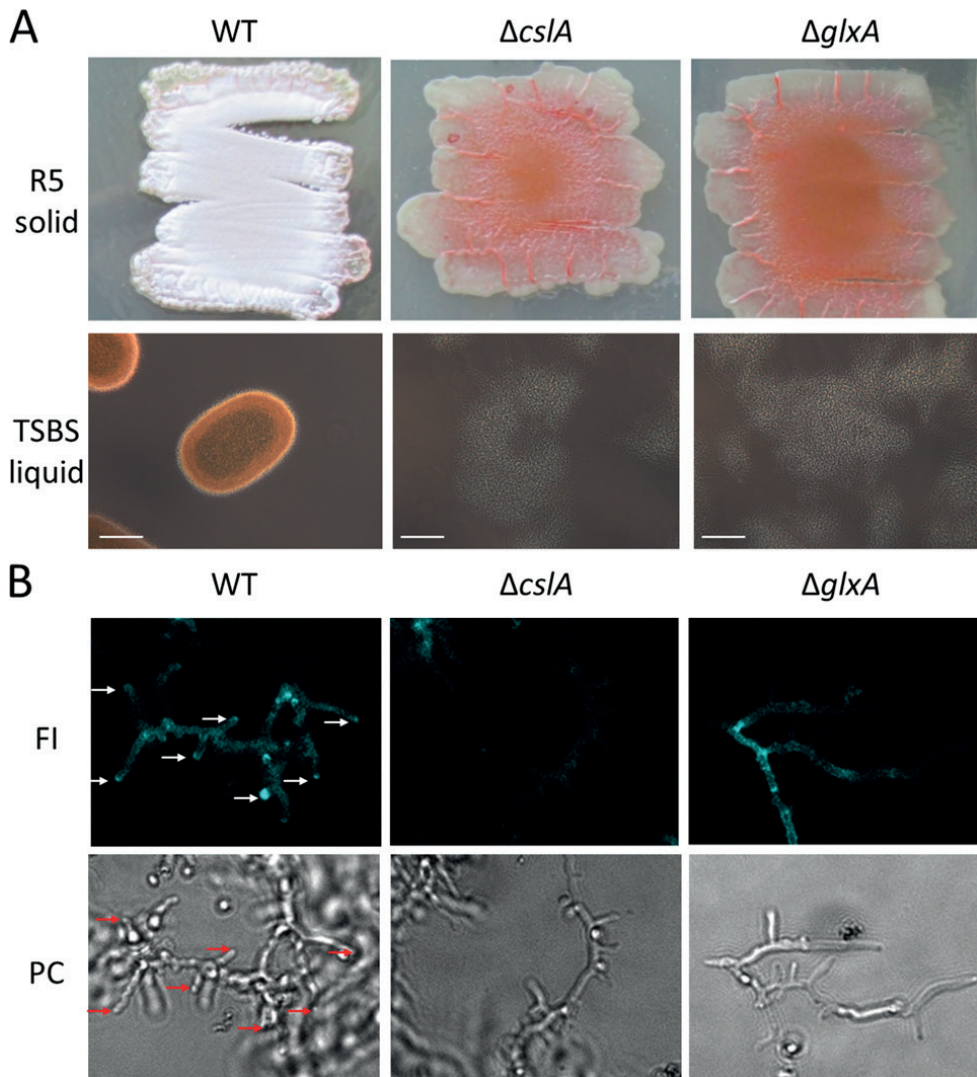


Figure 7. Deletion of *csIA* or *glxA* in *S. lividans* leads to a block in development and abolishes pellet formation and glycan deposition. **A)** Growth on solid R5 medium and pellet formation and dispersed growth in TSBS 24 h liquid cultures. Scale-bar (white line) is 100 μ m. **B)** CFW staining in 24 h mNMMP standing cultures shown in fluorescence image (FI) and phase contrast brightfield (PC). Arrows indicate tip staining that is present in WT cultures but not in mutants.

cultures. Instead of the dense compact pellets seen in WT, the mutants grow with an open mycelium phenotype (van Dissel *et al.*, 2014) (Fig. 7B). The transcriptomes of the *glxA* and the *csIA* mutant as analysed by RNA-seq revealed increased expression of genes related to osmoprotection indicating that the mutants suffer from osmotic stress (data not shown) and is in agreement with the observation of Liman *et al.* (2013). Excitingly, mycelial staining with calcofluor white (CFW), which binds to β -(1-4) glycans indicated that the hyphal tips in both the *csIA* and *glxA* null mutants were no longer stained, in contrast to those of the WT strain (Fig. 7B). This indicates that in addition to CslA, GlxA is required for glycan synthesis or attachment to hyphal tips.

Discussion

Results from the present study reveal that *S. lividans* GlxA is a membrane-associated cuproenzyme required for the production or localisation of the hyphal tip glycan. The spectroscopic properties, tertiary structure and enzymatic profile are all distinctly different to its fungal counterpart Gox, thus making GlxA a new structural and functional member of the mononuclear Cu oxidase family.

From a spectroscopic perspective a number of features in GlxA stand out. In the Cu(II)-GlxA EPR spectrum, the g_{\perp} component displays a hyperfine interaction of the electron spin with the Cu(II) ligands, giving rise to 7 lines with relative intensities 1:4:8:10:8:4:1 yielding a 16 G splitting (Fig. 3C inset). For Cu(II)-Gox, a quintet line structure of relative intensities 1:2:3:2:1 (Cleveland *et al.*, 1975; Bereman and Kosman, 1977) and a distance between the lines typical for a N hyperfine interaction (14-18 G) (Berliner *et al.*, 2001; Kirima *et al.*, 2003) consistent with two His ligands is observed. The source of the additional hyperfine splitting in GlxA is presently unclear and requires further investigation, but would suggest that differences in the electronic properties of the Cu(II) site in GlxA and Gox exist. A further anomaly in the spectroscopic properties between GlxA and Gox is in relation to the spectral observation of the Tyr-Cys• radical. EPR spectroscopy clearly indicates the presence of this radical (Fig. 5) following addition of an oxidant to Cu(II)-GlxA. However, no perturbation of the Cu(II)-GlxA absorbance spectrum is observed as is the case on forming Cu(II)-Tyr-Cys• in Gox. Furthermore, the Cu(II)-GlxA optical spectrum does not resemble that of Cu(II)-Gox (Whittaker and Whittaker, 1988). The coordination geometry of the Cu(II) site in both GlxA and Gox are identical, but as indicated by EPR could be electronically distinct and the possibility of second sphere coordination effects having an effect could be possible. In this respect the most pertinent difference between GlxA and Gox is in the side chain orientation of Trp²⁸⁸ (Trp²⁹⁰ in Gox). In Gox, Trp²⁹⁰ has been proposed to provide an extended aromatic system with its indole ring stacking over the Tyr-Cys bond, stabilising the delocalisation of the radical (Fig. 8D) (Ito *et al.*, 1991; Rogers *et al.*, 2007). However, in GlxA Trp²⁸⁸ no longer has its indole ring stacking with the Tyr-Cys cross-link, but instead has the benzene ring

component π - π stacking with the Tyr²⁸⁹ Cu ligand (Fig. 8D). In combination with a more insulated (buried) Cu site, the re-orientation of the Trp side chain may influence the electronic transitions of the Cu and the radical and result in the markedly different absorbance spectrum for GlxA compared to Gox.

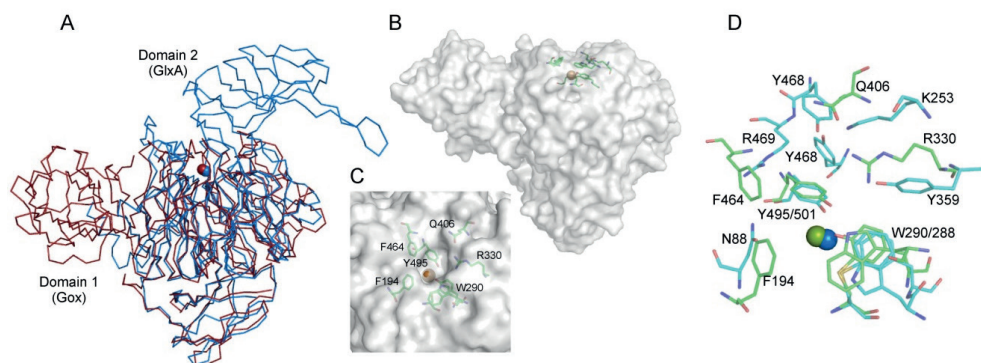


Figure 8. Structural comparison of GlxA with Gox (1gof) (Ito *et al.*, 1991). **A)** Ribbon representation of a superposition of the Ca atoms of GlxA (blue) with Gox (red). The Cu ions are shown as spheres. **B)** Surface representation of Gox, with location of the Cu ion (brown sphere) and residues in the substrate pocket indicated in sticks. **C)** View of the substrate pocket looking down the 7-fold symmetry axis towards domain 3 of Gox. The location of the surface exposed Tyr⁴⁹⁵ Cu ligand and the stacking Trp²⁹⁰ as well as residues forming the substrate pocket are shown in sticks, with the solvent exposed Cu represented as a sphere. **D)** Superposition of the substrate pockets in GlxA (blue) and Gox (green).

The ability to generate 3 oxidation states in GlxA suggests an enzymatic function in *S. lividans*. However, none of the substrates tested exhibit activity with GlxA that is comparable to Gox (with the exception of D-glucose). This is exemplified with D-galactose, the canonical monosaccharide substrate for Gox, where under aerobic conditions a k_{cat}/K_m value of $10^{-3} \text{ M}^{-1}\text{s}^{-1}$ for GlxA is determined, which is a million times lower than for Gox (Baron *et al.*, 1994) and is equivalent to Gox with D-glucose (Sun *et al.*, 2002). The most active substrate tested with GlxA, glycolaldehyde, has a K_m value (115 mM) comparable to Gox for D-galactose (70-80 mM), but a k_{cat}/K_m value > 4-orders of magnitude lower. For Gox the turnover of glycolaldehyde has been reported to be 75 % of the D-galactose rate (Arends *et al.*, 2006). These slow turnover kinetics indicate that GlxA has very different substrate specificity compared to Gox with gross structural differences discussed below a likely discriminant.

The distinctness of the GlxA structure can be appreciated from the superposition with Gox in Fig. 8A. In Gox the domain arrangement and surface flatness of the β -propeller domain (domain 2) contributes to a readily accessible Cu site and substrate binding pocket (Fig. 8B and C) (Ito *et al.*, 1991). This is not the case in GlxA, due to the positioning of domain 2 and the longer loop structures of the Kelch motifs. The more accessible nature of the Cu site in Gox is further apparent by the presence of an acetate ion (a buffer component of the

crystallisation solution) coordinating the Cu in the X-ray structure. Despite crystals of GlxA also being grown from acetate buffer, no evidence for an acetate ion, in or close, to the Cu site is observed, highlighting the protection afforded to the Cu site in GlxA. Furthermore, a very different structural arrangement of the substrate pocket in GlxA compared to Gox is apparent (Fig. 8D). On one side of the Gox pocket, the side chains of residues Arg³³⁰, Gln⁴⁰⁶ and the Nε1 atom of Trp²⁹⁰ are posed to provide H-bonds to the canonical D-galactose substrate, with the opposite side of the pocket formed by the aromatic residues, Phe¹⁹⁴ and Phe⁴⁶⁴, creating an asymmetric polar/apolar substrate pocket. For GlxA the residues in the pocket, with the exception of Trp²⁸⁸, differ and are not spatially conserved (Fig. 8D). Furthermore, Trp²⁸⁸ in GlxA, has its indole ring 'flipped' relative to Trp²⁹⁰ in Gox, making this orientation less favourable from a distance perspective for a substrate H-bond interaction in the pocket (Fig. 8D) (Ito *et al.*, 1994). These differences serve to illustrate that despite the Cu coordination being similar, the substrate pockets between Gox and GlxA contain no conserved features. Therefore substrates displaying high turnover kinetics with Gox are unlikely to be optimally accommodated or positioned in GlxA enabling for similar high turnover rates to be achieved.

The observations from the molecular genetics and CFW staining (Fig. 7) indicate that GlxA is directly involved in the production or localisation of the hyphal tip glycan. Synthesis of this glycan also requires CslA, which is a cellulose synthase-like enzyme encoded by the translationally-coupled gene upstream of *glxA*. This glycan accumulates at apical sites during vegetative growth and is absent in the *cslA* mutant (Xu *et al.*, 2008; de Jong, Wösten, *et al.*, 2009; Petrus and Claessen, 2014), and also in the *glxA* mutant. The molecular identity of this glycan is not yet known, but we propose that GlxA acts to modify it through a two-electron oxidation process. It is tempting to speculate that the orientations of tunnels I and II, both connecting at the Cu site (Fig. 4), could be a key structural feature utilised by GlxA in the oxidation of this glycan. A scenario whereby the nascent glycan produced by CslA is fed down into one of these tunnels, orientated in the substrate pocket, oxidised, and then released through the other tunnel may be envisaged. From a biotechnology perspective the open mycelium structure of the *glxA* and *cslA* null-mutants in liquid-grown cultures is of interest for improvement in the utilization of *S. lividans* as an enzyme production host. It has been shown that a more fragmented and therefore also more open mycelium growth in *Streptomyces* increases enzyme production several fold (van Wezel *et al.*, 2006; van Dissel *et al.*, 2014) and that the absence of other glycans result in a distinct morphology in liquid cultures (van Dissel *et al.*, 2015).

Finally, the inability of the $\Delta glxA$ phenotype to be rescued by Cu, links GlxA to the Cu dependency of *S. lividans* (Fig. S3) and raises the question of how GlxA acquires Cu. Our previous work has inferred that the Cu chaperone Sco delivers Cu to an aa_3 -type CcO and also to an unidentified target, which is required to trigger aerial hyphae growth (Blundell *et*

al., 2013; Blundell *et al.*, 2014). To date no other Sco target except CcO in either eukaryote or prokaryote species has been identified. The possibility therefore arises that the second Sco target in *S. lividans* is GlxA. Further experiments aimed at exploring whether this is the case are planned.

Acknowledgements

We acknowledge the award of a University of Essex Silberrad Scholarship to Amanda Chaplin and the Society of Biology for support of a summer student, Emma Blundell, who assisted in the early stages of this project. Amanda Chaplin cloned, overexpressed and purified recombinant GlxA, crystallized and solved the X-ray structure and performed all spectroscopic and enzymatic activity measurements. Erik Vijgenboom acknowledges NWO/ACTS for grant 053.80.703 in the ERA-IB framework (EIB.08.013 EPOS). Diamond Light Source for access to beamline I03 (East of England Macromolecular Crystallography BAG, MX7461) and use of the JCSG Quality Control Server is acknowledged.

Supporting Information

Introduction

GlxA	1	-----MKD--RAG-----RRRARRFAI-----GTAVVVVALAG-----	25
GOX	1	ASAPIGSAISRNNWAVTCDSAQSGNECNKAIDGNKDTFWHTFYGGANGDKPKPHTYTIIDMKTTQNVNGLSMLPRQDNGWIGRHEVYLSSDG	93
GlxA	26	-----MNGPWLRYRSETEKYHQYKIQIPEYK-----AANGKWEI--EFEEKYRQNTIHAALLRTGK	79
GOX	94	TNWGSPVASGSHFAD-SSTTKYSNFETRPARYVRLVAITEANGQFWTSIAEINVFAQSSYTAPOQPLGRWGPTIDLEIIVPAA---AAIEPTSGR	182
GlxA	80	VLMVAGSGNNQ--DNSDDKQYDTRIDWPVKGTIKK---VPTPSDLFCTGHTQLANGNLLIAGGTRKRYEKLKGDVTKAGGLMVVHNENPDKPITL	168
GOX	183	VLMWSSYRNDAFGGSPGGITLTSWDBSTGIVSDRTVTVTKHDMFCPEISMDGNGQIVVTGGNDA-----	247
GlxA	169	PAGTKFTGKENGKTFVSKDPLVLPRAEKVDFPATGAFVRNDPLGRIYVEAQKSGSAYETGETENDRYVQGLSGADARNTYGIQAKLALDKKDF	261
GOX		-----	
GlxA	262	QGIRDAFEDPVAEKYIKVDPMHEARWYPTLTLGDGKILSVSGLDDIGQLVPGKNEVYDEPKTKAWTYTDKVRQFETYP-----	341
GOX	248	---KKTSLYDSSSDSWIPGPDQVARGYQSSATMSDGRVFTIGGWS--GGVFEKNGEVYSSSKTWTSLPNAKVNEMLTADKQLYRSDNHAW	336
GlxA	342	LFLMQNGKIFYSGANAGYDDVGRTPGVWVDETNRKFTKVPGMSDANMLETANTVLLPPADEKYMVIGGGVGESKLSSEKTRTADLK---	430
GOX	337	LEGWKKGSVEQAGPSTAMNWy---YTSGSGDVKSAGKRSNRGVAPDAMC--GNAVY-DAVKGIILTFGGSPDYQSDATNAHITITGEPG	423
GlxA	431	ADDPKFVDGFSLEKSTRYPQASILPDDSVLVSQGSQDYR--GRGDSNIIQARLYHEDTNEFERVADPLVGRNYHSGSILLPDRGLMFFGSDSLY	522
GOX	424	TSPNTVFASNGLYFARTFHTSVVLPDGGFTITGGQRRIIPFEDSTFVETPEIYVVEQDTFYKQNFNSIVRVHYSISLLELDRGVFVNGG--GLC	515
GlxA	523	ADKANTKPKGFQRIEITYTTPYLYRDSRP----DLSGG--PCTIARGGSGTFTSRAASTVKKVRLIRPSASTHVTDVDQRSIALDFKAD--GDK	608
GOX	516	GDCTT---N--HFDAQIFTEPNLYNSNGNLATRPKITRTSTQSVKVG--GRITISTDSSIASKASLIRYGATHTVNTDQRRIPIHLLTNNNGNS	601
GlxA	609	LTVTVPSSGKNLVQSGWYMMFVTDEGETPSSKAEWVRVP--	645
GOX	602	YSFQVPSDSGVALPGYWMLFVMSAGVPSVASTIRVTQ	639

Figure S1. Clustal omega sequence alignment of *Streptomyces lividans* GlxA with that of *Fusarium graminearum* Gox. Sequence conservation is indicated in grey. * indicates sequence position of ligands to the Cu ion and ^ indicates the Cys that forms the Tyr-Cys crosslink.

Materials and methods

Overexpression and purification of GlxA

GlxA was over-expressed in *E. coli* strain BL21 (DE3) starting from overnight precultures (2 ml 2xYT, 2 µl Kan (50 mg ml⁻¹), 37 °C) that were subsequently used to inoculate 750 ml of medium in 2 L flasks. At an OD600 of 0.6, isopropyl β-D-1-thiogalactopyranoside (IPTG; Melford) was added to a final concentration of 1 mM and the temperature decreased to 25 °C. Cells were harvested after 16 h at 3,501 g and lysed using an EmulsiFlex-C5 cell disrupter (Avestin) followed by centrifugation at 38,724 g for 20 min at 4 °C. The clarified supernatant was loaded to a 5 ml Ni²⁺-NTA Sepharose column (GE Healthcare) equilibrated with Buffer A (50 mM Tris/HCl, 500 mM NaCl, 20 mM imidazole, pH 8.0) and eluted with a linear imidazole gradient using Buffer B (Buffer A with 500 mM imidazole). A single peak at ~20 % Buffer B was eluted from the column and fractions were pooled and dialysed overnight at 4 °C against Buffer C (50 mM Tris/HCl, 150 mM NaCl, pH 8.0). Following dialysis, the N-terminal His6-tag was removed by incubating the protein at room temperature overnight in the presence of 125 U of thrombin (Sigma). The protein/thrombin mixture was reapplied to the Ni²⁺-NTA Sepharose column (GE Healthcare) and the flow-through collected and concentrated at 4 °C using a centricon (vivaspin) with a 30 kDa cut-off. Concentrated protein was loaded to a

S200 Superdex column (GE Healthcare) equilibrated with Buffer C and fractions eluting from the major peak (retention volume ~80 ml consistent with a monomer species with a mass in the region of 70 kDa) were concentrated and used in further studies.

Structure determination of GlxA

Diffraction data obtained from GlxA crystals were indexed using iMosflm (Battye *et al.*, 2011) and scaled and merged using Aimless (Evans and Murshudov, 2013) in the CCP4i suite. The structure of GlxA was solved using a model derived from Chainsaw (Stein, 2008), by using the last common atom function and the PDB entry 2eie as the alignment model. Subsequent molecular replacement produced a solution for one of the two molecules in the asymmetric unit that were predicted from the Matthews coefficient. Model building in ARP/WARP (Perrakis *et al.*, 1999) produced a model for one of these GlxA molecules in the asymmetric unit and this was subsequently used as a search model in PhaserMR (McCoy *et al.*, 2007) to locate the second, less well-ordered molecule. Refinement of the structure was carried out using Refmac5 (Murshudov *et al.*, 1997) in the CCP4i suite, with model building between refinement cycles in Coot (Emsley and Cowtan, 2004). Riding hydrogen atoms were added when refinement of the protein atoms had converged. Structures were verified using the Molprobit server (Davis *et al.*, 2007), the JCSG Quality Control Server and Coot (Emsley and Cowtan, 2004).

Results

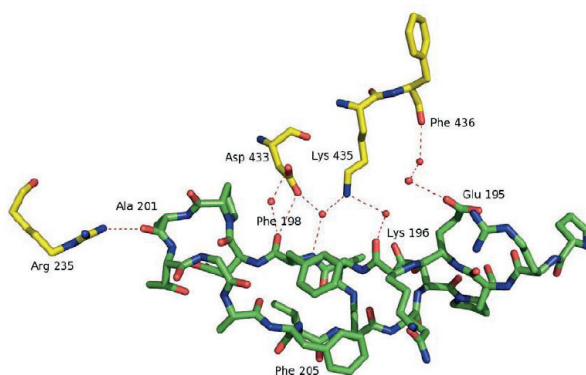


Figure S2. Stabilizing crystal packing interactions for the 6-hairpin loop in chain B of the GlxA structure. Interactions with adjacent molecules are largely solvent-mediated with a small number of direct interactions between amino acids. Note that an additional linkage between the amide nitrogen of Phe²⁰⁵ and Lys³²³ of an adjacent molecule, via a bridging water is omitted from the figure for clarity.

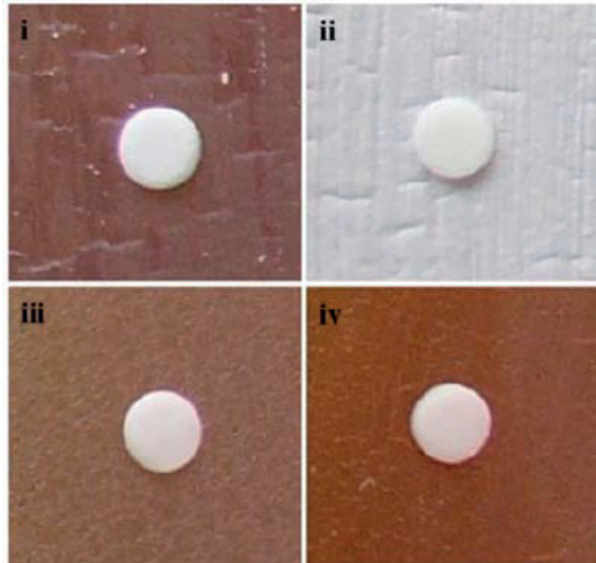


Figure S3. R5 agar plates were inoculated for confluent growth with *S. lividans* WT (i and ii) and Δ glxA mutant (iii and iv) spores and incubated for 24 h at 30 °C. No stimulation of development was observed 24 h incubation time after the addition of a Paper filter disk containing 10 μ l of 10 mM H₂O₂ on top of the young mycelium (i and iii). The WT showed full uniform development after 96 h (ii) but that development was independent of where H₂O₂ was applied. The mutant did not produce aerial hyphae or spores after 96 h (iv). Therefore H₂O₂ cannot induce development in either the WT or the glxA null-mutant.

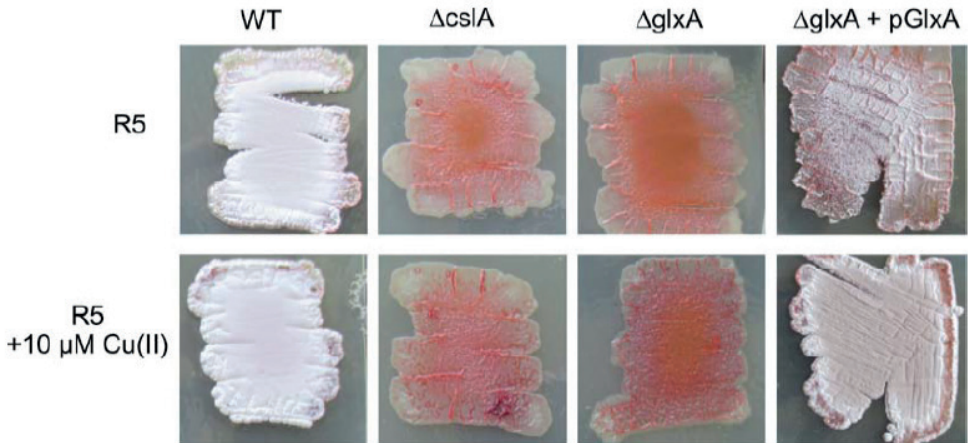


Figure S4. Complementation of the glxA mutant with a low copy plasmid harboring the glxA gene under control of the csIA promoter results in a wild type morphology on both solid and in liquid media (data not shown). The induction of development by Cu observed in the WT strain is also seen in the complemented glxA mutant.

5

Marloes L.C. Petrus, Erik Vijgenboom, Amanda K. Chaplin, Jonathan A.R. Worrall, Gilles P. van Wezel and Dennis Claessen (2016) Open Biology 6: (1) p. 150149

Abstract

The filamentous bacterium *Streptomyces lividans* depends on the radical-copper oxidase GlxA for the formation of reproductive aerial structures and, in liquid environments, for the formation of pellets. Incorporation of copper into the active site is essential for the formation of a cross-linked tyrosyl-cysteine cofactor, which is needed for enzymatic activity. In the present study, we show a crucial link between GlxA maturation and a group of copper-related proteins including the chaperone Sco and a novel DyP-type peroxidase hereinafter called DtpA. Under copper-limiting conditions, the *sco* and *dtpA* deletion mutants are blocked in aerial growth and pellet formation, similarly to a *glxA* mutant. Western analysis showed that GlxA maturation is perturbed in the *sco* and *dtpA* mutants, but both maturation and morphology can be rescued by increasing the bioavailability of copper. DtpA acts as a peroxidase in the presence of GlxA and is a substrate for the Tat translocation pathway. In agreement, the maturation status of GlxA is also perturbed in *tat* mutants, which can be compensated for by the addition of copper, thereby partially restoring their morphological defects. Our data support a model wherein a copper-trafficking pathway and Tat-dependent secretion of DtpA link to the GlxA-dependent morphogenesis pathway.

The DyP-type peroxidase DtpA is a Tat-substrate required for GlxA maturation and morphogenesis in *Streptomyces*

Introduction

Streptomycetes are multicellular bacteria with a complex developmental life cycle. Following the germination of spores, a network of interconnected filaments is established, which is called a vegetative mycelium. This mycelium feeds on nutrients in the soil until they become depleted. This nutrient scarcity triggers the onset of a developmental program leading to the lysis of the vegetative mycelium and the formation of aerial hyphae that erect from the colony surface into the air giving the colony a white, fluffy appearance (Claessen *et al.*, 2006; Flårdh and Buttner, 2009). Differentiation of these reproductive structures leads to the synchronous production of millions of grey-pigmented spores that easily disperse. At the onset of aerial mycelium formation streptomycetes produce a richness of secondary metabolites, including numerous antibiotics, antitumor compounds and anthelmintic agents, that make them of interest for pharmaceutical purposes (Hopwood, 2007; van Wezel and McDowall, 2011). Additionally, due to their competence to directly secrete proteins in the culture broth, streptomycetes hold promise as hosts for the heterologous production of enzymes (Vrancken and Anné, 2009; Anné *et al.*, 2012).

Metabolite and enzyme production typically occurs in large bioreactors. Growth under these conditions is characterized by the formation of large, biofilm-like aggregates of mycelium, called pellets (Nielsen, 1996; van Dissel *et al.*, 2014). Like in biofilms, formation and integrity of these structures depends on the synthesis of extracellular glycans (Kim and Kim, 2004; Petrus and Claessen, 2014; Claessen *et al.*, 2014). Recently, reverse engineering of a non-pelleting strain of *Streptomyces lividans* indicated a crucial role for the newly identified *mat* gene locus, putatively involved in synthesis of an extracellular glycan needed for pellet formation (van Dissel *et al.*, 2015). Deletion of the *mat* genes leads to a dispersed mycelium

with a 60% increase in growth rate and productivity of *S. lividans* (van Dissel *et al.*, 2015). A second extracellular glycan involved in pellet formation is produced by enzymes encoded by the *csIA-glxA* locus (Xu *et al.*, 2008; van Veluw *et al.*, 2012; Chaplin *et al.*, 2015). The *csIA* gene encodes a protein belonging to family 2 of the glycosyl transferases, which contains cellulose and chitin synthases, amongst others (Coutinho *et al.*, 2003). CslA synthesizes a β -(1,4)-glycan at hyphal tips, which is thought to provide protection during the ongoing cell wall remodelling at these sites (Xu *et al.*, 2008). Mutation of *csIA* abolishes pellet formation in liquid-grown cultures but also blocks aerial growth (Xu *et al.*, 2008; van Veluw *et al.*, 2012). The *csIA* gene is located in an operon with the downstream located *glxA* gene. The *csIA-glxA* operon is probably acquired via horizontal gene transfer and is conserved among all streptomycetes, with some species having two copies (Liman *et al.*, 2013). In most streptomycetes this gene cluster also contains a third gene downstream of *glxA*, called *csIZ*, which encodes an endoglucanase (Xu *et al.*, 2008; Liman *et al.*, 2013). Like in the absence of *csIA*, deletion of *glxA* blocks development and abolishes pellet formation, coinciding with the loss of glycan deposition at hyphal tips (Liman *et al.*, 2013; Chaplin *et al.*, 2015). This is consistent with a model in which both proteins cooperatively function in glycan deposition.

GlxA has been recently characterized (Chaplin *et al.*, 2015). The X-ray crystal structure revealed a unique tertiary structure with an active site consisting of a mononuclear copper (Cu) ion and a tyrosyl-cysteine redox cofactor, bearing resemblance to the Cu active site in fungal galactose oxidases (Gox) (Ito *et al.*, 1991). This family of enzymes carry out the two electron oxidation of primary alcohols to aldehydes with the reduction of dioxygen to hydrogen peroxide (Avigad *et al.*, 1962). Unlike Gox, the active site Cu and putative substrate binding pocket is buried in GlxA but can be accessed through channels leading down from three separate surface locations (Chaplin *et al.*, 2015). Notably, no significant *in vitro* enzymatic activity with D-galactose or a range of mono- or disaccharide substrates that are turned over by Gox was detected (Whittaker and Whittaker, 2006; Chaplin *et al.*, 2015). However, GlxA was able to turnover glycolaldehyde, the smallest molecule to contain both an aldehyde and a hydroxyl group. Thus it is likely that the substrate specificity of GlxA is different from that of Gox.

S. lividans strongly depends on Cu to initiate the morphological switch from vegetative to aerial growth (Kieser and Hopwood, 1991; Keijser *et al.*, 2000). Our previous work provided clues for the existence of a Cu-trafficking pathway involved in this process. One of the proteins in this pathway, the Cu chaperone Sco, is required for morphogenesis under conditions of low Cu availability. Notably, morphogenesis of the *sco* mutant is restored by the addition of Cu to the medium (Blundell *et al.*, 2013). Sco receives its Cu ion from the extracytoplasmic Cu chaperone ECuC (Blundell *et al.*, 2014), and, in turn, delivers Cu to the Cu_A site of an $\alpha\alpha_3$ -type cytochrome c oxidase (CcO) and to a second target, possibly the cuproenzyme GlxA, that is required to trigger aerial growth (Blundell *et al.*, 2013; Blundell *et al.*, 2014; Chaplin *et*

al., 2015). In contrast to the *sco* mutant, the *glxA* phenotype (on solid media or in solution) cannot be rescued by the addition of exogenous Cu (Chaplin *et al.*, 2015).

sco (SLI_4214) and *ecuc* (SLI_4213) are the first two genes of an operon that also contains genes for a putative Cu transport protein (SLI_4212) and for a secreted protein with a putative Tat (twin arginine translocation) signal sequence (SLI_4211) (Widdick *et al.*, 2006) and a DyP (dye-decolorizing peroxidase)-type domain (Fujimoto *et al.*, 2012; Blundell *et al.*, 2013; Colpa *et al.*, 2014). DyP are a new class of monohaem peroxidases that are widely distributed amongst bacteria and fungi, but their physiological role remains unclear (Sugano *et al.*, 1999; Singh and Eltis, 2015). Here we show that SLI_4211, hereinafter called *dtpA* (for DyP-type peroxidase A), encodes a protein that functions as a peroxidase in the presence of GlxA and is required for executing the final enzymatic step in the cascade of the GlxA-dependent morphogenesis pathway. Deletion of the *dtpA* gene leads to an arrest in development due to impaired GlxA maturation and function, which can be overcome by the extracellular addition of Cu to the medium. Extracellular complementation with Cu also restores GlxA maturation issues and development in *tat* mutants, thereby connecting Tat-dependent secretion of DtpA to GlxA-dependent morphogenesis. We propose an integrated model how a Cu trafficking pathway and Tat secretion ultimately link to the GlxA-dependent morphogenesis pathway.

Materials and Methods

Bacterial strains and plasmids

All *Streptomyces* strains used in this study are presented in Table 1. Mutants were constructed in *S. lividans* 1326 (*S. lividans* 66, stock number 1326 from the John Innes Centre; Hopwood *et al.*, 1985). The *tat* mutants, kindly provided by Dr. J. Anné and Dr. L. Vanmellaert (Katholieke Universiteit Leuven), were created in the *S. lividans* TK24 background (Schaerlaekens *et al.*, 2001; Schaerlaekens *et al.*, 2004; De Keersmaeker *et al.*, 2005). *Escherichia coli* JM109 was used for routine cloning purposes (Messing *et al.*, 1981). Vectors and constructs are summarized in Table 2.

Growth conditions and media

Streptomyces strains were grown at 30°C (Hopwood *et al.*, 1983). *Streptomyces* spores were isolated from soy flour-mannitol (MS) agar plates (Kieser *et al.*, 2000). For phenotypical characterizations, $\pm 10^6$ spores were plated in square 2x2 cm patches on R5 agar plates, supplemented with 10 μ M CuSO₄, FeSO₄, MnSO₄, ZnSO₄ or Co(NO₃)₂ if necessary. Photographs of plates were taken daily with a compact digital camera (Canon Ixus).

Table 1. *Streptomyces lividans* strains used in this study.

Strains	Description	Reference or source
1326	Wild-type <i>S. lividans</i> 1326	(Hopwood <i>et al.</i> , 1985)
$\Delta csIA$	1326 lacking <i>csIA</i> (marker-less)	(Chaplin <i>et al.</i> , 2015)
$\Delta glxA$	1326 lacking <i>glxA</i> (marker-less)	(Chaplin <i>et al.</i> , 2015)
$\Delta csIZ$	1326 lacking <i>csIZ</i> (marker-less)	This work
Δsco	1326 lacking <i>sco</i> (marker-less)	(Blundell <i>et al.</i> , 2013)
$\Delta ecuc$	1326 lacking <i>ecuc</i> (marker-less)	(Blundell <i>et al.</i> , 2014)
$\Delta dtpA$	1326 lacking <i>dtpA</i> (marker-less)	This work
ΔSLI_4212	1326 lacking <i>SLI_4212</i> (marker-less)	This work
Δcox	1326 <i>SLI_2481-2482::aac(3)IV</i>	(Blundell <i>et al.</i> , 2013)
TK24	<i>S. lividans</i> TK24	(Hopwood <i>et al.</i> , 1983)
$\Delta tatA$	TK24 <i>tatA::aac(3)IV</i>	(De Keersmaecker <i>et al.</i> , 2005)
$\Delta tatB$	TK24 <i>tatB::aac(3)IV</i>	(Schaerlaekens <i>et al.</i> , 2004)
$\Delta tatC$	TK24 <i>tatC::neo</i>	(Schaerlaekens <i>et al.</i> , 2001)

For morphology in liquid-grown cultures, tryptic soy broth with 10% sucrose (TSBS) was used, which was supplemented with 10 μ M CuSO₄ as indicated. Therefore, 250 ml flasks equipped with coils and containing 100 ml TSBS medium were inoculated with 10⁶ spores ml⁻¹. Morphology was determined following 24 h growth at 30°C while shaking at 200 rpm. Samples from liquid-grown cultures were analysed by light microscopy with a Zeiss Standard 25 microscope and digital pictures were taken with an AxioCam linked to AxioVision software.

Construction of the *csIZ*, *dtpA*, and *SLI_4212* mutants

The *csIZ*, *dtpA* and *SLI_4212* null-mutants were created in *S. lividans* 1326 in a two-step process using the unstable pWHM3 plasmid and the Cre-LoxP system as described (Świątek *et al.*, 2012). In the *csIZ* null-mutant nucleotides +15 to +1011 relative to the start codon of *SLI_3188* were replaced with the *loxP-apra* cassette, while in the *dtpA* mutant nucleotides +19 to +1208 relative to the start of *SLI_4211* and in the *SLI_4212* mutant nucleotides -18 to +1932 relative to the start of *SLI_4212* were replaced. The Cre recombinase was used to remove the *loxP-apra* cassette from the obtained mutants, which were then verified by PCR amplification and sequencing. The *dtpA* mutant was complemented by integration of plasmid pMLCP1 (Table 2), which contains the *dtpA* gene under the control of the *sco* promoter. All primers used in this work are shown in Table 3.

Table 2. Vectors and constructs used in this study

Plasmid	Description	Reference or source
SET152	<i>Streptomyces/E.coli</i> shuttle vector. Integrates in <i>Streptomyces</i>	(Bierman <i>et al.</i> , 1992)
pWHM3	<i>Streptomyces/E.coli</i> shuttle vector	(Vara <i>et al.</i> , 1989)
pΔcslZ	pWHM3 derivative containing the flanking regions of the <i>S. lividans</i> <i>cslZ</i> gene (SLI_3189) interspersed by the <i>apra-loxP</i> cassette	This work
pΔdtpA	pWHM3 derivative containing the flanking regions of the <i>S. lividans</i> <i>dtpA</i> gene (SLI_4211) interspersed by the <i>apra-loxP</i> cassette	This work
pΔSLI_4212	pWHM3 derivative containing the flanking regions of the <i>S. lividans</i> SLI_4212 gene interspersed by the <i>apra-loxP</i> cassette	This work
pTDW46	pSET152 derivative containing the <i>dagA</i> gene, where the sequence corresponding to the original DagA signal peptide is replaced by <i>aadA</i> , the streptomycin resistance gene	(Widdick <i>et al.</i> , 2006)
pTDW47	pTDW46 containing a fragment encoding the DagA signal peptide	(Widdick <i>et al.</i> , 2006)
pMLCP1	pSET152 derivative with <i>dtpA</i> under control of the <i>sco</i> promoter	This work
pMLCP2	pTDW46 derivative containing a fragment encoding the putative DtpA signal sequence (MPDQSIPTRSPEATRGTPGPLDSDNPGAATAPEGVSRRLGTAGATGLVGAAGAAAGYAAAPSSAATPLTSLGSGS)	This work
pMLCP3	pTDW46 derivative containing a fragment encoding the CslZ signal sequence (MYGSKPAGNMSRRRAASAAALGAAALLLAGCSSSGDGDKAAGAGITQQPKETDGS)	This work
pMLCP4	pTDW46 derivative containing a fragment encoding the putative ECuC signal sequence (MRRRLAEGPVRRLAGGPVRRRPPALAAVAVIGALTLAGCGSDSGADSASPGAELSVDAAAGS)	This work
pMLCP5	pTDW46 derivative containing a fragment encoding the putative GlxA signal sequence (MKDRAGRARRRFAIGTAVVVALAGMNGPWLGS)	This work
pET4211	pET28a vector with N-terminal His-tag, containing the <i>dtpA</i> (SLI_4211) gene restricted between the <i>NdeI</i> and <i>HindIII</i> sites	This work
pET3188	pET28a vector with N-terminal His-tag, containing the <i>glxA</i> (SLI_3188) gene encoding residues 35-645, restricted between the <i>NdeI</i> and <i>HindIII</i> sites	(Chaplin <i>et al.</i> , 2015)

Table 3. Primers used in this study

Primer name	Primer sequence	Restriction site
SLI_4211.P1	GATCGAATTCTGCTGCGCGGCTCGTACAC	<i>EcoRI</i>
SLI_4211.P2	CATGCTAGAAATGGACTGGTCGGGCATGG	<i>XbaI</i>
SLI_4211.P3	GATCTCTAGACGTGCAGCGCAAGCTGGACC	<i>XbaI</i>
SLI_4211.P4	CATGAAGCTTATGAAGCGCTGCGGAATCCC	<i>HindIII</i>
4211.FW.NdeI	GATCCATATGCCCGACCAGTCCATTCC	<i>NdeI</i>
4211.RV.XbaI	CATGCTAGAGCCTTCAGGGCCGAGATACG	<i>XbaI</i>
4211-F	CTAAATATGGCGACTCCCCTCACCTCGCTC	<i>NdeI</i>
4211-R	CATAAGCTTTCACCCCTCCAGCAGCCGCTGA	<i>HindIII</i>
C121G-F	GTCCGACCTGTTCCGGCACCGGACACA	-
C121G-R	TGTGTCCGGTGCCGAACAGGTCGGAC	-
SLI_4212.P1	GCGGAATTCGGCGCCGACAGCGACAAGC	<i>EcoRI</i>
SLI_4212.P2	GCGTCTAGAGGCGATGGTCTGCGTCAAGGTG	<i>XbaI</i>
SLI_4212.P3	GCGTCTAGAGTGCGGACCTCCGACATCGAC	<i>XbaI</i>
SLI_4212.P4	GCGAAGCTTCTCCGTCGACTCGGTGGCC	<i>HindIII</i>
SLI_3189.P1	GATCGAATTCTGGGTGGGCACGAGCGTCTG	<i>EcoRI</i>
SLI_3189.P2	CATGCTAGATTGCTGCCGTACATCCAACC	<i>XbaI</i>
SLI_3189.P3	GATCTCTAGACTGGCGCAAGGATAAGACAC	<i>XbaI</i>
SLI_3189.P4	CATGAAGCTTGTTCACCGCAAGGAGAACG	<i>HindIII</i>
GlxA_F.NdeI	GATCCATATGAAAGACCGTGCCGGCCGC	<i>NdeI</i>
GlxA_R.BamHI	CATGGGATCCGAGCCACGCCCCGTTTCATCCC	<i>BamHI</i>
CsIZ_F.NdeI	GATCCATATGTACGGCAGCAAGCCGGCCGAAAC	<i>NdeI</i>
CsIZ_R.BamHI	CATGGGATCCGCTCGGTCTCCTTGGGCTGCTG	<i>BamHI</i>
DtpA_F.NdeI	GATCCATATGCCCGACCAGTCCATTCC	<i>NdeI</i>
DtpA_R.BamHI	CATGGGATCCGCTGCCGAGCGAGGTGAGG	<i>BamHI</i>
Ecuc_F1.NdeI	GATCCATATGAGGCGGCTCGCGGAAGG	<i>NdeI</i>
Ecuc_R.BamHI	CATGGGATCCGGCGGCTCGACCGAGAGTTC	<i>BamHI</i>

Cloning and site-directed mutagenesis of DtpA and GlxA

The SLI_4211 gene encoding DtpA was amplified from the genomic DNA of *S. lividans* strain 1326 by PCR using a forward primer (4211-F) with a flanking 5'-*NdeI* restriction site and a reverse primer (4211-R) with a flanking *HindIII* restriction site (Table 3). The resulting PCR product (1,134 bp) was ligated into the *NdeI* and *HindIII* sites of a pET28a (Kan^r) vector (Novagen) to create an N-terminal His₆-tagged construct (pET4211). The C121G variant of GlxA was created using a Quikchange mutagenesis approach using the C121G-F and C121G-R primers and the pET3188 vector as template (Table 3).

Over-expression and purification of DtpA

pET4211 (Kan^r) vector was transformed into *E. coli* BL21 (DE3) cells. Overnight precultures (low salt LB medium; Melford) were successively used to inoculate 1.4 L of high salt LB medium (10 g tryptone, 10 g sodium chloride, 5 g yeast extract per litre) with 50 mg ml⁻¹ kanamycin and grown at 37°C, 180 rpm. At an OD₆₀₀ of 1.2 5-aminolaevulinic acid (0.25 mM final concentration) and iron citrate (100 µM final concentration) were added consecutively for their use as a haem-precursor and iron supplement. Cultures were then induced by adding isopropyl β-D-thiogalactopyranoside (IPTG; Melford) to a final concentration of 0.5 mM and carbon monoxide (CO) gas bubbled through the culture for 20-30 s. Flasks were then sealed and incubated for a further 18 h at 30 °C and 100 rpm. Cells were harvested via centrifugation (10,000 *g*, 10 min, 4 °C) and the cell pellet resuspended in 50 mM Tris/HCl, 500 mM NaCl (Fisher) and 20 mM imidazole (Sigma) at pH 8 (Buffer A). The resuspended cell suspension was lysed using an EmulsiFlex-C5 cell disrupter (Avestin) followed by centrifugation (22,000 *g*, 30 min, 4 °C). The clarified supernatant was loaded onto a 5-ml nickel-nitrilotriacetic acid-Sepharose column (GE Healthcare) equilibrated with Buffer A and eluted by a linear imidazole gradient using Buffer B (Buffer A with 500 mM imidazole). The peak eluting at ~ 40% Buffer B was found to contain DtpA collected pooled and concentrated using a Centricon (VivaSpin) with a 10 kDa cut-off at 4 °C and loaded onto a PD-10 desalting column to remove bound CO and imidazole followed by application to an S200 Sephadex column (GE Healthcare) equilibrated with 20 mM NaPi, 100 mM NaCl, pH 7. A major peak eluted at ~ 77 ml consistent with a monomer species with fractions assessed by SDS-PAGE then concentrated and stored at - 20°C. DtpA concentrations were determined by UV-visible spectroscopy (Varian Cary 60 UV-visible spectrophotometer) using an extinction coefficient (ϵ) at 280 nm of 37,470 M⁻¹ cm⁻¹.

Over-expression and purification of holo- and apo-GlxA proteins

WT GlxA (residues 354-645) and the C121G variant were over-expressed in *E. coli* BL21 (DE3) using the pET3188 vector (Table 2) and purified as previously reported (Chaplin *et al.*, 2015). For the C121G variant no CuSO₄ was added before and after cell lysis so as to produce the apo-form of the variant. The production of apo WT GlxA required the adoption of an autoinduction procedure (Studier, 2005) using the medium 8ZY-4LAC-SUC (Deacon and McPherson, 2011). All plastic and glassware was soaked in 0.1 M EDTA and rinsed extensively with doubly deionised water prior to use to ensure as metal free conditions as possible. LB pre-cultures were used to inoculate 400 ml 8ZY-4LAC-SUC cultures in 2 L baffled flasks with shaking at 180 rpm 25 °C for 48 h. Cells were then harvested and apo-GlxA was purified as previously described (Chaplin *et al.*, 2015). GlxA protein concentrations were determined using an ϵ_{280} of 78,730 M⁻¹ cm⁻¹.

COPAS measurements

Particle analyses using the COPAS Plus profiler were performed as described previously (van Veluw *et al.*, 2012; Petrus *et al.*, 2014). Briefly, pellets were fixed with 4% formaldehyde for 30 min on ice, washed twice with phosphate-buffered saline (PBS), and stored at -20°C until further use. Samples were analysed using a COPAS Plus profiler equipped with a 1-mm nozzle (Union Biometrica, Holliston, MA). Pellets pass the laser beam over their longitudinal axis and data will be collected on the extinction (EXT) and time of flight (TOF) for all objects with a minimum TOF of 40. All experiments were performed in triplicate and at least 2500 pellets were analysed per sample. The mean TOF values of the mutant strains were compared to that of the wild-type strain, which was set to 100%.

Western Blot analyses

Mycelium was harvested from either TSBS liquid-grown cultures after 24 h of growth, or from solid R5 agar plates that had been overlaid with Track Edge membranes (Millipore) after 2 days of growth. The mycelia were washed with 10 mM Tris/HCl pH 7 buffer, and resuspended in 300 μl of the same buffer, followed by sonication on ice using a Bioruptor Plus (Diagenode). Complete lysis was checked by microscope, after which the lysed mycelium was separated into a soluble fraction (supernatant) and an insoluble fraction (pellet) by centrifugation at 16,000 g (4°C). Bradford analysis was used to determine the protein concentrations in the soluble fraction and 10 μg of protein was used for separation by SDS-PAGE on precast 7.5% mini-protean[®] TGX Gels (BioRad) at 100 V for ~ 2 h. Proteins were transferred to PVDF membranes (GE Healthcare) and incubated overnight with EF-Tu1 antibodies (1:5,000; (Vijgenboom *et al.*, 1994)) and/or GlxA polyclonal antibodies (1:10,000). Following one hour of incubation with GARAP (goat anti-rabbit alkaline phosphatase), detection was carried out with NBT/BCIP.

For the detection of recombinant GlxA proteins obtained from *E. coli*, 5 ng protein was used, and PVDF membranes were treated with diluted GlxA antibodies (1:20,000).

UV-vis spectroscopy and coupled peroxidase assay

UV-vis spectra were recorded using a Cary 60 spectrophotometer (Agilent). Hydrogen peroxide (H_2O_2) (Sigma) was prepared as required with concentrations determined using an ϵ_{240} of $43.6 \text{ M}^{-1} \text{ cm}^{-1}$. Resting state DtpA (FeIII) was prepared in 20 mM NaPi pH 7, 100 mM NaCl to a concentration of 10 μM in a 1 ml quartz cuvette (Hellma). Samples for UV-vis spectral analysis were prepared upon additions to the resting state DtpA of: 1 equivalent of H_2O_2 ; 1 equivalent of H_2O_2 followed by addition of 0.2 M glycolaldehyde (Sigma); 20 μM GlxA and 0.2 M glycolaldehyde; 0.2 M glycolaldehyde; 1 equivalent of H_2O_2 followed by 1

equivalent of ferrocyanide ($[\text{Fe}(\text{CN})_6]^{4-}$)

Catalytic turnover was measured using a coupled assay whereby production of H_2O_2 by GlxA in the presence of the substrates glycolaldehyde (0.2 M), D-galactose (0.6 M), D-glucose (0.6 M) and *N*-acetyl-D-glucosamine (0.1 M) (all from Sigma) was tested for in the presence of DtpA or horse radish peroxidase (HRP) and the subsequent oxidation of ABTS (2,2'-azino-bis(3-ethylbenzothiazoline-6-sulphonic acid) (Sigma). Samples were prepared in 1 ml cuvettes containing 20 mM NaPi, 100 mM NaCl, pH 7.0, 30 mM ABTS, 20 μM GlxA, 5 μM DtpA or 1 μl of HRP (10 mg ml^{-1}) and the respective GlxA substrate, with reactions started by addition of GlxA. Oxidation of ABTS was monitored at 436 nm using a Hewlett-packard 8453 diode-array spectrophotometer scanning between 190 and 1100 nm and thermostatted at 30 °C. Turnover rate (k , in s^{-1}) was calculated from $((\Delta A_{436}/\epsilon_{\text{ABTS}})/t)/[\text{GlxA}]$ where ΔA_{436} is the absorbance change at 436 nm upon ABTS oxidation, ϵ_{ABTS} is the extinction coefficient of the ABTS cation radical oxidation product taken as 29.3 $\text{mM}^{-1}\text{cm}^{-1}$, t is the time in s and $[\text{GlxA}]$ is the total millimolar concentration of GlxA in the assay.

Tat-dependent secretion assay

Analysis of Tat-dependent protein secretion was performed as described (Widdick *et al.*, 2006 and 2008). PCR fragments encoding the candidate signal peptides were cloned as *NdeI*-*Bam*HI fragments into pTDW46, which contains the agarase gene lacking its original Tat signal sequence, expressed from the *dagA* promoter (Widdick *et al.*, 2008). The empty plasmid pTDW46 was used as a negative control, while pTDW47 carrying a fragment for the original DagA signal peptide was used as a positive control. Candidate signal sequences were those from CslZ, DtpA, ECuC and GlxA (the putative signal peptide sequences are shown in Table 3). All constructs were transformed to *S. lividans* TK24 and *S. lividans* TK24 ΔtatC . The agarase assay was performed by spotting each strain (1000 spores in a 10 μl drop) on MM-C medium, which contains agar as the sole carbon source (Widdick *et al.*, 2006). After 5 days of growth, plates were overlaid with Lugol solution (Sigma) and staining was recorded by taking digital images after 45 min. Average diameters of clearing zones were calculated from 10 replicates per strain.

Bioinformatics

SLI database numbers refer to the genome of *S. lividans* 66 (alternatively known as 1326, Cruz-Morales *et al.*, 2013). To study the conservation of gene order we used the synteny web service SyntTax (Oberto, 2013). Signal sequence predictions were carried out using PRED-TAT (Bagos *et al.*, 2010) and prediction of the Tat-motif and scores for the peptidase cleavage sites were obtained using TatP (Bendtsen *et al.*, 2005).

Results

Identification and characterization of copper-related morphogenes in S. lividans

The *csA* and *glxA* genes are conserved in streptomycetes and are organized in a larger gene cluster that also contains the *csZ* gene (Fig. S1). In *Frankia* species this gene cluster is located adjacent to a *sco* homologue. Also in certain *Burkholderia* species, Gox-encoding genes co-occur with *sco* genes, suggestive of a direct functional correlation (Fig. S1). In the genome of *S. lividans* 66 (also referred to as *S. lividans* 1326; (Cruz-Morales *et al.*, 2013)), *sco* is located elsewhere on the chromosome as a member of an operon containing the *ecuc*, SLI_4212 and *dtpA* genes (Fig. S1). Given the putative correlation, deletion mutants lacking the majority of the coding sequences of either *csZ*, SLI_4212 or *dtpA* were created as described in the Methods section, and compared to the previously generated mutants lacking *csA*, *glxA*, *ecuc* or *sco* (Fig. 1). In line with earlier work, the *csA* and *glxA* mutants failed to produce aerial hyphae on R5 agar plates, and development could not be restored to the mutants by the addition of 10 μM exogenous CuSO_4 (Fig. 1). In contrast, the *csZ* and SLI_4212 null mutants were identical to the parental strain and formed sporulating aerial hyphae after 3 days of growth. Deletion of *ecuc* led to a slight delay in aerial hyphae formation when compared to the parental strain (Fig. 1). However, in contrast to *sco* mutants, the *ecuc* mutant progressed through development after 6 days, while no aerial hyphae were formed by the *sco* mutant (Fig. S2). Notably, the addition of 10 μM CuSO_4 to the medium rescued

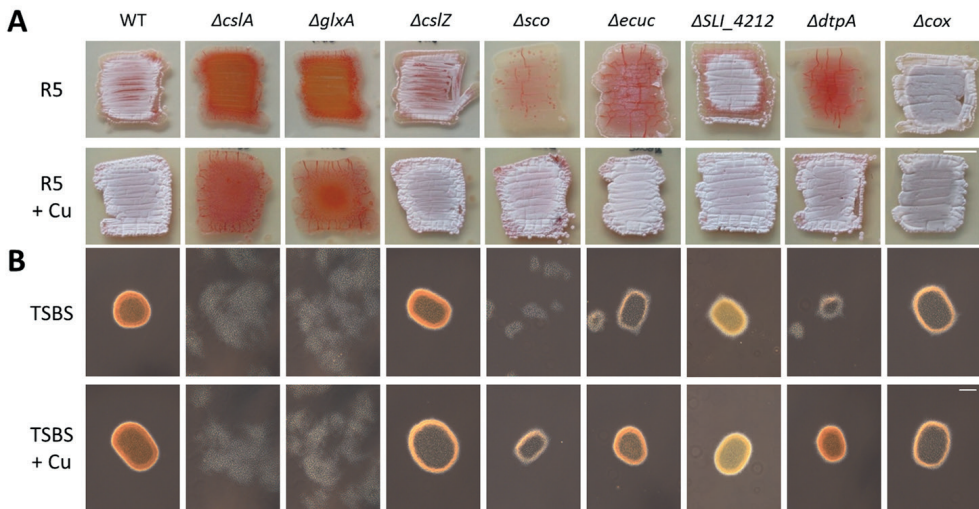


Figure 1. Phenotypic analysis of *S. lividans* strains lacking Cu-related morphogenes. The parental strain *S. lividans* 1326 is indicated as WT. **(A)** Morphology of strains after 3 days of growth on R5 medium in the absence (top row) and presence (bottom row) of 10 μM CuSO_4 . **(B)** Morphology of strains in TSBS medium after 24 h of growth in the absence (top row) and presence (bottom row) of 10 μM CuSO_4 . Scale bar (white line) represents 1 mm (A) or 100 μm (B).

the morphological defects in the *ecuc* and *sco* mutants (Fig. 1, S2). The lack of development of these mutants is not a result of decreased CcO activity since the *cox* mutant, lacking CcO, develops normally (Fig. 1, S2). Interestingly, deletion of *dtpA*, encoding a putative haem peroxidase, also stalled development, which again could be restored by the addition of 10 μM CuSO_4 to the medium (Fig. 1, S2) or by reintroduction of the gene (Fig. S3). Development could not be restored to any of the mutants by the addition 10 μM of FeSO_4 , ZnSO_4 , MnSO_4 or $\text{Co}(\text{NO}_3)_2$ showing that it is a specific effect mediated by the addition of Cu (Fig. S4).

Given the defects of *csIA* and *glxA* mutants in pellet formation, we analysed mycelial morphology of the other mutants lacking copper-related morphogenes both microscopically and quantitatively using a complex object parametric analyser and sorter (COPAS (Xu *et al.*, 2008; van Veluw *et al.*, 2012; Chaplin *et al.*, 2015)). This revealed that the average size of mycelia of the *csIA* and *glxA* mutants decreased to 28% and 31% of those of the parental strain, respectively, and this was not affected by the addition of 10 μM CuSO_4 (Fig. 1B and 2). The *csIZ* and SLI_4212 mutants formed similarly sized pellets as the parental strain both in the presence and absence of additional Cu (Fig. 1B and 2). Interestingly, like in the *csIA* and *glxA* mutants, mycelia of the *sco* mutant were less dense and more open in TSBS cultures (Fig. 1B). Their average size was reduced to 29% of the size of wild-type mycelia (Fig. 2). In contrast to *csIA* an *glxA* mutants, pellet formation was restored to *sco* mutants by extra Cu (Fig. 1B and 2). Deletion of *ecuc* had a relatively minor effect, with the average pellet size reduced to 65% of that of wild-type pellets, while pellet sizes slightly increased to 75% of

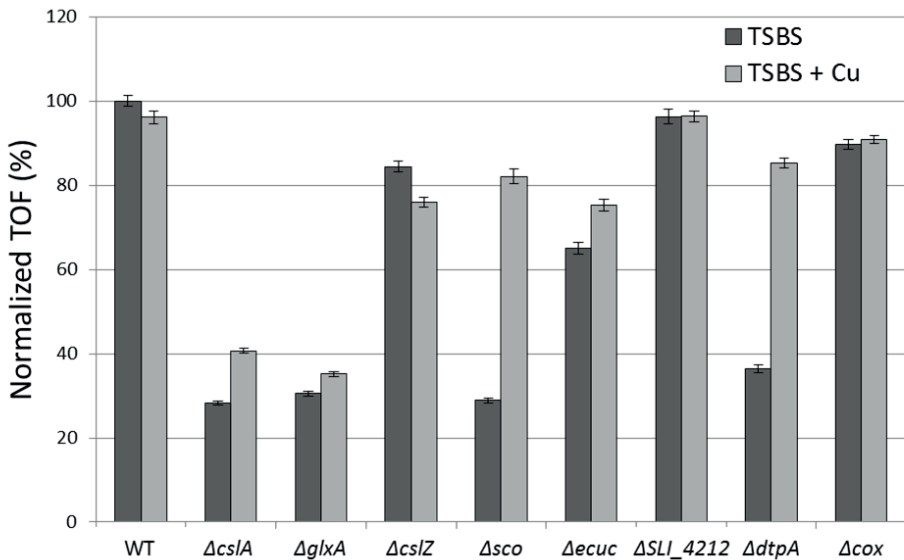


Figure 2. Average pellet sizes of *S. lividans* strains lacking Cu-related morphogenes. Strains were grown for 24 h in TSBS medium in the presence (light-grey bars) or absence (dark-grey bars) of 10 μM CuSO_4 . The average diameter of wild-type pellets obtained from TSBS medium was used as a reference and set to 100%. Error bars indicate 95% confidence intervals of the mean.

wild-type values when copper was added to the cultures (Fig. 1B and 2). Like in the absence of *csIA*, *glxA* and *sco*, deletion of *dtpA* blocked the formation of pellets, yielding mycelia whose average size was reduced to 36% of the size of wild-type mycelia. In the presence of elevated levels of Cu, pellet morphology and size were similar to those of wild-type pellets (Fig. 1B and 2). Taken together, these data indicate that development and pellet morphology strongly depend on *csIA*, *glxA*, *sco* and *dtpA* and the bioavailability of Cu. Furthermore, it suggests an interdependence of the four proteins.

The absence of Sco, ECuC or DtpA affects GlxA maturation

GlxA functionality requires the incorporation of a Cu ion and the formation of a Tyr-Cys cross-link (Chaplin *et al.*, 2015). Previous studies with fungal Gox have indicated that Cu is required to initiate the formation of the Tyr-Cys cross-link. A pre-processed form of Gox (no Tyr-Cys cross-link) is characterised on SDS-PAGE by a slower migrating band than the mature form (Tyr-Cys cross-link formed) (Rogers *et al.*, 2008). To assess whether this maturation affects GlxA mobility, purified apo-, holo-GlxA and a C121G variant were run on an SDS-PAGE gel and migration patterns detected by GlxA polyclonal antibodies. From Fig. 3 it is apparent that apo-GlxA (prepared under Cu-starved conditions) and the C121G variant, in which the cross-linking Cys residue is replaced by a Gly, migrate slower than the holo-GlxA (prepared under Cu-replete conditions). This indicates that the Tyr-Cys cross-link absent in both the apo-GlxA and the C121G variant accounts for this retardation of electrophoretic mobility. Interestingly, both the mature and the immature form of GlxA were detected in mycelia of *S. lividans* 1326 grown in TSBS cultures, with the mature form being more prominent (Fig. 4A).

We then investigated whether the absence of *Sco* would influence the maturation of GlxA.

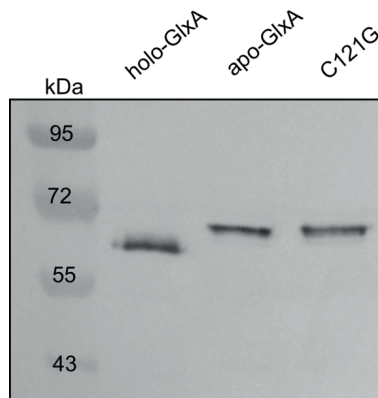


Figure 3. Immunoblot analysis of GlxA maturation from samples over-expressed in *E. coli*. GlxA is over-expressed and purified in either Cu-replete conditions (holo-GlxA) or Cu-starved conditions (apo-GlxA). The C121G variant is unable to form the Tyr-Cys cross-link and migrates together with apo-GlxA, which requires the addition of Cu to form the cross-link. Molecular weight markers are indicated in kDa.

In the absence of Sco, GlxA was exclusively found in its immature form, unlike in the parental strain (Fig. 4A). Interestingly, growth of the *sco* mutant in the presence of 10 μM CuSO_4 led to the accumulation of the mature form of GlxA (Fig. 4A), consistent with the restored formation of pellets (see above). Given the changes in pellet morphology in the *ecuc* and *dtpA* mutant strains, we also verified the maturation pattern of GlxA in these mutants. In the *ecuc* mutant strain, only a small fraction of GlxA was in the mature form, with the majority being immature (Fig. 4A). However, no mature GlxA was identified in the *dtpA* null mutant. Like in the *sco* mutant, the mature form of GlxA reappeared in the *ecuc* and *dtpA* null mutants grown in TSBS supplemented with 10 μM CuSO_4 (Fig. 4A). Deletion of *csIZ*, *SLI_4212* or *cox* did not abolish GlxA maturation (Fig. S5A). Altogether, these data imply Sco, ECuC and DtpA in the GlxA maturation pathway and in pellet morphology under low levels of Cu in liquid-grown cultures.

We also analysed whether the developmental block on solid medium related to GlxA maturation defects. The amount of the mature form of GlxA was strongly decreased in the absence of Sco and DtpA, and could be increased by the addition of 10 μM CuSO_4 to the medium (Fig. 4B). No major changes in the abundance of the mature form of GlxA were observed in the absence of ECuC, *csIZ*, *SLI_4212* and *CcO* (Fig. S5B).

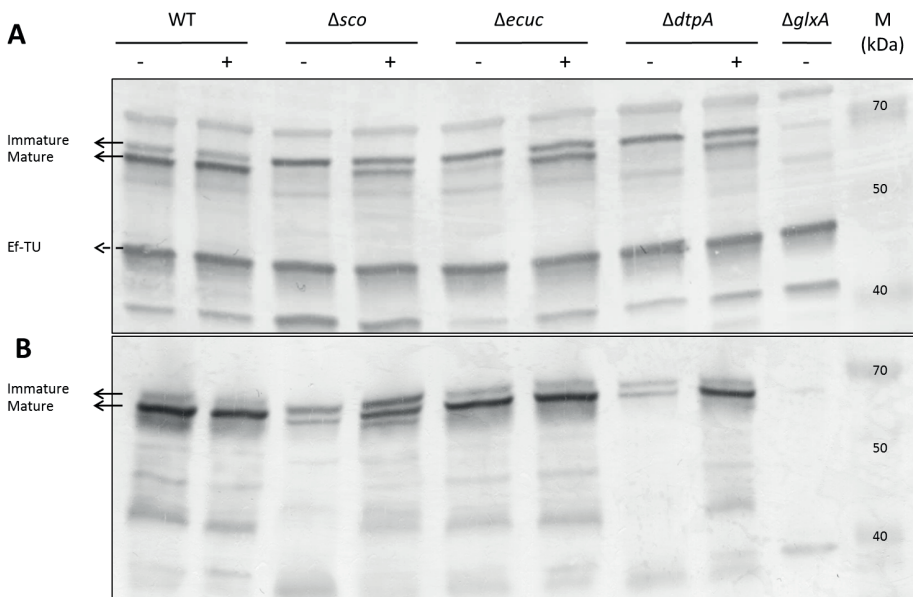


Figure 4. Immunoblot analysis of GlxA maturation in the wild-type strain and Δsco , $\Delta ecuc$ and $\Delta dtpA$ mutants grown for 24 h in TSBS medium (**A**) or grown for 2 days on R5 medium (**B**) in the presence (+) or absence (-) of 10 μM CuSO_4 . The two bands indicated with the solid arrows represent GlxA, the upper band being immature GlxA (no Tyr-Cys cross-link) and the lower band being mature GlxA (with Tyr-Cys cross-link). The band indicated with a dashed arrow indicates Ef-TU, which serves as a control for the total amount of protein loaded on the gel. Molecular weight markers are indicated in kDa.

DtpA acts as a peroxidase in the presence of GlxA

Purified DtpA gave a UV-visible spectrum with absorption maxima at 406 nm (soret band), 502 nm, 635 nm and a shoulder at 540 nm, typical of a resting state ferric (Fe^{III}) haem peroxidase (Kim *et al.*, 1999; Sugano *et al.*, 2007; Chen *et al.*, 2015) (Fig. 5A). Addition of H_2O_2 to resting state DtpA resulted in a shift to 399 nm and flattening of the soret band together with the formation of new absorption maxima at 530, 557, 614 and 644 nm. This indicates that DtpA had undergone a two-electron oxidation process to form compound I ($\text{haem}\bullet + \text{Fe}^{\text{V}}=\text{O}$), which over time and in the absence of a reducing substrate decays to the ferric resting state ($k = 6.7 \times 10^{-3} \text{ s}^{-1}$, data not shown). This behaviour is typical of a peroxidase (Kim *et al.*, 1999; Sugano *et al.*, 2007; Chen *et al.*, 2015), which is consistent with the DyP-type peroxidase motif found in SLI_4211. On mixing equimolar amounts of DtpA and GlxA, no change in the DtpA absorbance spectrum was observed (data not shown). We have previously shown that under aerobic conditions GlxA is relatively inactive with substrates that are readily turned over by fungal Gox (Chaplin *et al.*, 2015). Upon addition of glycolaldehyde to the GlxA:DtpA sample (the best substrate for GlxA (Chaplin *et al.*, 2015)), DtpA compound I is formed within a minute (Fig. 5A), providing direct proof that DtpA is a true peroxidase and GlxA is producing H_2O_2 , which is subsequently used by DtpA. Over a period of time (> 20 min) compound I is transformed to a new species with maxima at 420, 539, 571, 635 and 696 nm. These spectral properties are not consistent with the formation of the one electron reduced compound II peroxidase form, i.e. a ferryl species ($\text{Fe}^{\text{IV}}=\text{O}$), which in the case of DtpA would have given rise to maxima of 419, 528, 557, 621 and 728 nm (Fig. 5A). Instead, the new species has a spectrum that resembles an oxy-ferrous form suggesting that under the conditions employed DtpA eventually becomes fully reduced. The same spectral species is formed upon addition of excess glycolaldehyde to DtpA compound I generated through addition of one equivalent of H_2O_2 , and on addition of excess glycolaldehyde to the resting state ferric enzyme (Fig. S6). This illustrates *in vitro* that glycolaldehyde is acting as a reductant with DtpA, without intermediate formation of compound I. However, when GlxA is present the formation of compound I before transition to the oxy-ferrous form shows that glycolaldehyde is its substrate leading to the production of H_2O_2 .

One possibility that could arise is that GlxA activity is dependent on the type of peroxidase used. Prior to assessing whether GlxA activity could be affected in the presence of DtpA, native PAGE and analytical gel filtration chromatography were used to assess whether a physical interaction occurred. Neither method gave evidence to support a strong interaction between the two proteins (data not shown). To test whether GlxA activity is dependent on DtpA, a coupled peroxidase assay was performed comparing DtpA to horseradish peroxidase (HRP). Fig. 5B compares the turnover rates (k , in s^{-1}) for various substrates in the presence of HRP or DtpA. It is apparent that for all substrates tested no boost in activity occurs when DtpA replaces HRP.

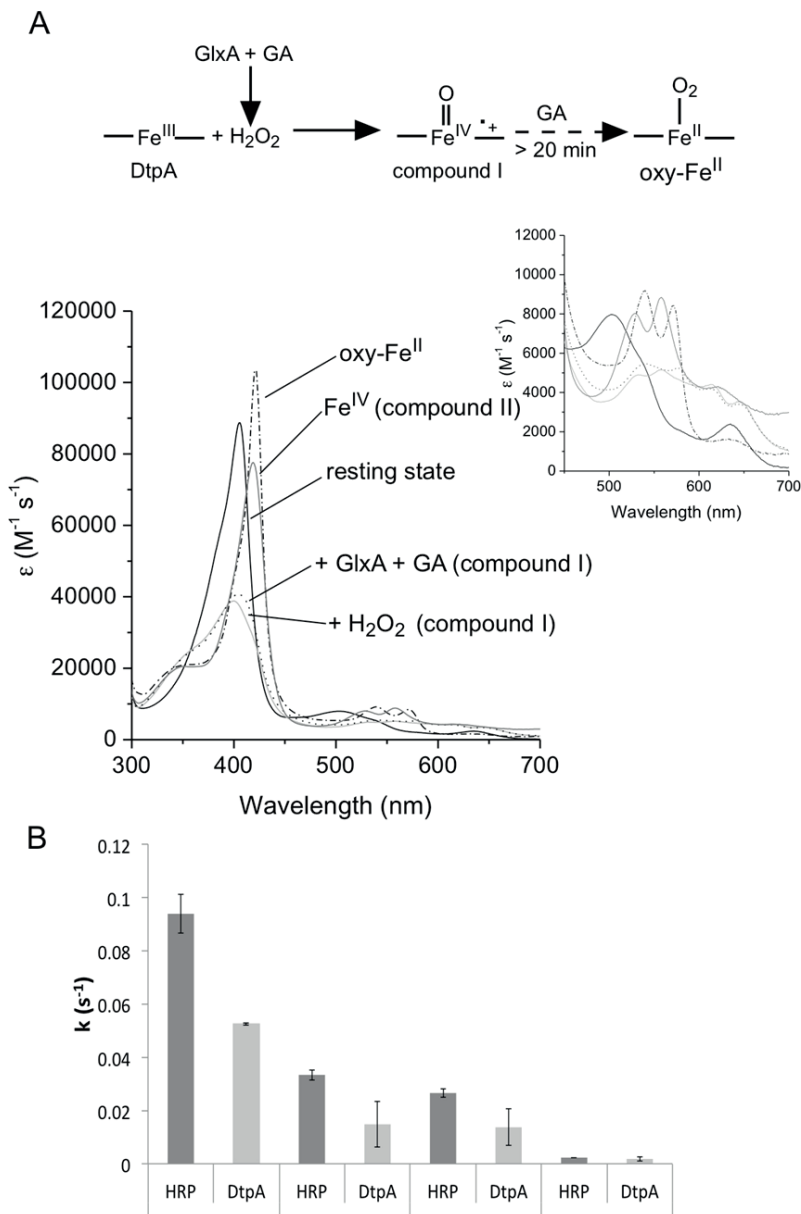


Figure 5. Peroxidase activity of DtpA. **(A)** Static UV-visible spectra of various haem oxidation states of DtpA (20 mM sodium phosphate pH 7, 100 mM NaCl) as illustrated by the reaction scheme. Addition of H_2O_2 (light grey solid line) or GlxA and glycolaldehyde (GA) (dotted line) to resting state DtpA (Fe^{III}) leads to a compound I spectrum. Over time the compound I species is converted to a species with an oxy-ferrous like spectrum (dashed-dot line) in presence of GA. Note that no compound II species is observed in this process. The compound II spectrum shown was generated by formation of compound I followed by addition of $[\text{Fe}(\text{CN})_6]^{4-}$ (dark grey solid line). Inset a zoomed in region of the weaker intensity absorbance bands. **(B)** Turnover rates (k) for GlxA with four different substrates (30 °C) in the presence of HRP or DtpA determined through the subsequent oxidation of ABTS. Error bars indicate the standard deviation from triplicate experiments.

CslZ and *DtpA* are exported via the *Tat* machinery

Proteins that are directed to the twin-arginine translocation (Tat) machineries have signal peptides with a canonical architecture consisting of a relatively basic n-region at the N-terminus, which contains the highly conserved twin-arginine motif. The n-region is followed by a hydrophobic h-region and a polar c region with a signal peptidase recognition site (Palmer and Berks, 2012). Careful analysis of the signal sequence of *DtpA* indicates that it fulfills the criteria for being a Tat substrate (Fig. 6A). Indeed, the PRED-TAT tool for predicting Tat-signals indicates with a reliability score of 0.998 that *DtpA* is exported via the Tat translocation channel. However, TatP predicts that the putative signal peptidase cleavage site of *DtpA*, after position 68 [SSA-AT], is weak with a score of 0.32, well below the cutoff of 0.51.

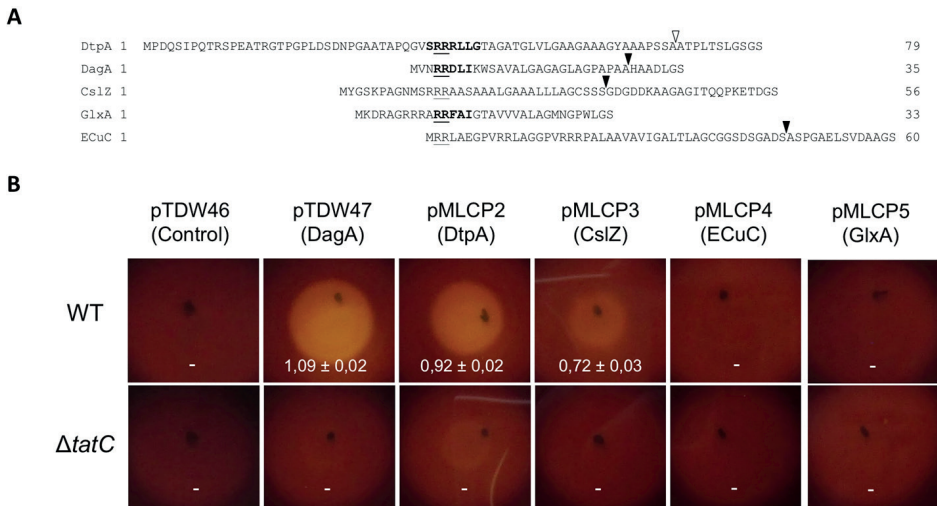


Figure 6. *Tat* dependent protein secretion of *DtpA* and *CslZ* in *S. lividans*. **(A)** N-terminal signal sequence of *S. lividans* *DtpA*, *DagA*, *CslZ*, *GlxA* and *Ecuc* proteins. Bold-face text highlights the twin-arginine motifs predicted by TatP, with the conserved arginines underlined. The solid triangles at the C-termini indicate the predicted strong peptidase cleavage sites, while the open triangle indicates the predicted cleavage site in *DtpA*, which has a low cleavage site score. **(B)** Visualization of extracellular agarase activity after lugol staining of *S. lividans* strains grown on MM-C medium with agar as the sole carbon source. The used strains expressed the *DagA* protein without its signal sequence (pTDW46), or with signal sequences of *DagA* (pTDW47), *DtpA* (pMLCP2), *CslZ* (pMLCP3), *Ecuc* (pMLCP4) or *GlxA* (pMLCP5). Halos are indicative for *DagA* secretion. No halos were observed when the constructs were introduced in the *tatC* mutant. Numbers indicate the mean diameter of clearing zones in cm with the corresponding standard error of the mean.

PRED-TAT also indicates that other proteins encoded by the *cslA-glxA* locus or the *sco* operon could potentially be exported via the Tat secretion machinery, namely *GlxA*, *CslZ* and *ECuC* (Fig 6A). To establish which of these proteins are true Tat substrates, we used a reporter

system that makes use of secretion of the agarase protein DagA, which is a Tat substrate (Widdick *et al.*, 2006 and 2008). If secreted, DagA will degrade agar into its oligosaccharides, visible as a halo surrounding the colony after staining with iodine. Control colonies of *S. lividans* TK24 expressing DagA with its native N-terminal signal sequence, were surrounded by a zone of clearing of 1.09 ± 0.02 cm. Zones of clearing were also observed when the N-terminal signal sequences of CslZ (0.72 ± 0.03 cm) or DtpA (0.92 ± 0.02 cm) were fused to DagA, consistent with the *in silico* prediction (Fig. 6B). In contrast, no halos were found with the putative Tat signal sequences of GlxA and ECuC (Fig. 6B). Furthermore, when DagA fused behind the signal sequences of DtpA or CslZ was expressed in the *tatC* null mutant of *S. lividans*, no zones of clearance were detected (Fig. 6B). Taken together, these results demonstrate that the N-termini of CslZ and DtpA are *bona-fide* Tat signal sequences and that secretion of these two proteins depends on the Tat secretion pathway.

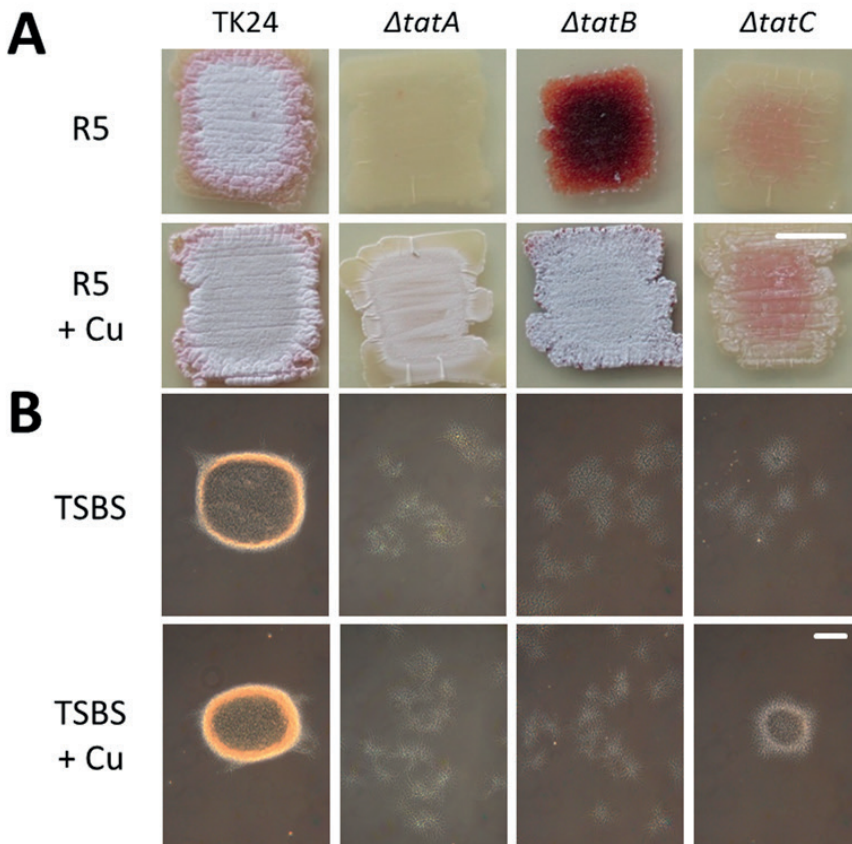


Figure 7. Phenotypic analysis of *S. lividans* *tat* mutant strains. The parental strain *S. lividans* TK24 is indicated as TK24. **(A)** Morphology of strains after 3 days of growth on R5 medium in the absence (top row) and presence (bottom row) of $10 \mu\text{M CuSO}_4$. **(B)** Morphology of strains in TSBS medium after 24 h of growth in the absence (top row) and presence (bottom row) of $10 \mu\text{M CuSO}_4$ (bottom row). Scale bar represents 1 cm (A) or $100 \mu\text{m}$ (B).

The addition of Cu restores GlxA maturation and morphogenesis to *tat* mutants

Considering that the Tat substrate DtpA influences development in a Cu-dependent manner, we speculated that the previously described morphological defects of *tat* mutants (Schaerlaekens *et al.*, 2004; De Keersmaecker *et al.*, 2005) might be restored by the addition of 10 μM CuSO_4 (Fig. 7A). Surprisingly, this addition to R5 agar plates was sufficient to restore aerial growth in the *tatA*, *tatB* and *tatC* mutants. Addition of 10 μM ZnSO_4 , MnSO_4 or $\text{Co}(\text{NO}_3)_2$ did not restore the formation of aerial hyphae when the strains were grown on R5 agar plates, while 10 μM FeSO_4 only slightly improved aerial growth in the *tatB* mutant (Fig. S7). Notably, Western analysis revealed that the addition of 10 μM CuSO_4 led to an increase in the mature form of GlxA in the *tatA* and *tatC* mutants, similarly as observed for the *sco* and *dtpA* mutants on R5 agar plates (Fig. 8A, 4B). In contrast, mature GlxA was detected in the *tatB* mutant irrespective of the presence of 10 μM CuSO_4 . These results support a model in which the morphological defects in the *tatA* and *tatC* mutants on R5 agar plates are related to the failure to secrete DtpA, which consequently affects GlxA maturation.

We also analysed pellet formation and GlxA maturation in liquid-grown TSBS cultures in the presence or absence of additional Cu. As expected, the three *tat* mutants grew as dispersed mycelia in liquid-grown TSBS cultures without added copper. As on R5 agar, the mature form

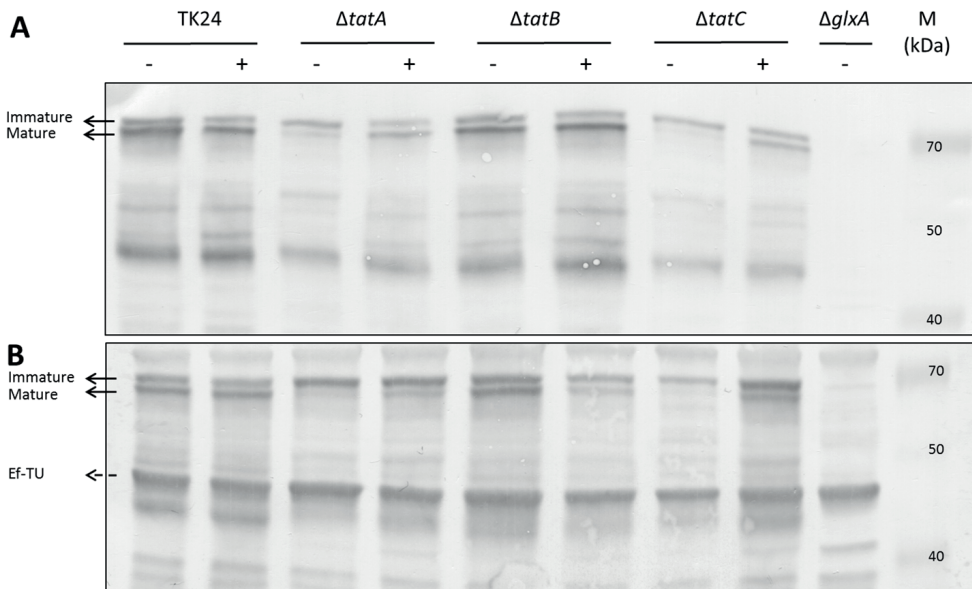


Figure 8. Immunoblot analysis of GlxA maturation in *S. lividans* TK24 and *tat* mutant strains grown 24 h in TSBS medium **(A)** or grown for 2 days on R5 medium **(B)** in the presence (+) or absence (-) of 10 μM CuSO_4 . The two bands indicated with the solid arrows represent GlxA, the upper band being immature GlxA (no Tyr-Cys cross-link) and the lower band being mature GlxA (with Tyr-Cys cross-link). The band indicated with a dashed arrow indicates EF-TU, which serves as a control for the total amount of protein loaded on the gel. Molecular weight markers are indicated in kDa.

of GlxA was present in the *tatB* mutant in TSBS-grown cultures without additional Cu, in contrast to the *tatA* and *tatC* mutants (Fig. 8B). The mature form of GlxA reappeared in the *tatA* and *tatC* mutants grown in the presence of 10 μM CuSO_4 , and restored pellet formation to the *tatC* mutant (Fig. 7B). Taken together, these data demonstrate that failure to secrete DtpA is an important aspect contributing to the morphological defects in the *tat* mutants.

Discussion

Morphological differentiation in streptomycetes is a complex process that depends on environmental conditions and extensive extracellular signalling between hyphae (Chater, 2006; Claessen *et al.*, 2006; Claessen *et al.*, 2014). Over the last decades, a large number of so-called *bld* genes were identified, which are required for development, and in particular on the reference media, namely R2YE (or R5) agar plates. In most cases, the precise function of these genes is not clear. Recently, it was demonstrated that several of the “classical” *bld* mutants are disturbed in desferrioxamine (DFO) biosynthesis (Lambert *et al.*, 2014). DFO is a chelator that recruits iron from the extracellular environment (Berner *et al.*, 1988; Yamanaka *et al.*, 2005). Development in some of the *bld* mutants, and notably *bldJ* and *bldK*, is restored by the addition of exogenous iron to the culture, thereby bypassing the requirement for this chelator. Work from our and other groups has shown that in addition to iron, copper also plays a crucial role in morphogenesis (Kieser and Hopwood, 1991; Ueda *et al.*, 1997; Keijser *et al.*, 2000; Blundell *et al.*, 2014). The work described in this chapter provides further molecular insights into the importance of significant levels of Cu for development, as we here show that many of the genes relating to what we have dubbed the Cu-trafficking pathway are required for aerial hyphae formation – and hence also for reproductive sporulation – when the bioavailability of Cu becomes limiting. A key member of this pathway is GlxA, which requires Cu for formation of a cross-linked Tyr-Cys cofactor and enzymatic activity (Chaplin *et al.*, 2015). We provide evidence that the novel *bld* gene *dtpA* encodes a Tat substrate that is involved in Cu-dependent morphological development. DtpA is required for GlxA maturation, together with the Cu chaperone Sco, and as a haem peroxidase DtpA also provides an interesting link between the copper- and iron-dependent pathways leading to morphogenesis.

The *dtpA* gene is located in a cluster of Cu-related genes that is not only present in streptomycetes, but also in *Frankia* sp. Ccl3, *Thermobifida fusca*, *Nocardioopsis dassonvillei* and *Catenulispora acidiphila*. The clustering of *sco*, *ecuc* and *dtpA* in these organisms infers a functional link between these proteins. Indeed, our work demonstrates that in streptomycetes these genes are all required for morphogenesis under conditions of Cu limitation, which is probably common in many laboratory media and in nature (Newcomb and Rimstidt, 2002). Based on past and current data we propose a model how the Cu chaperones Sco and ECuC function together with DtpA in the GlxA maturation pathway (Fig. 9). Eventually, mature

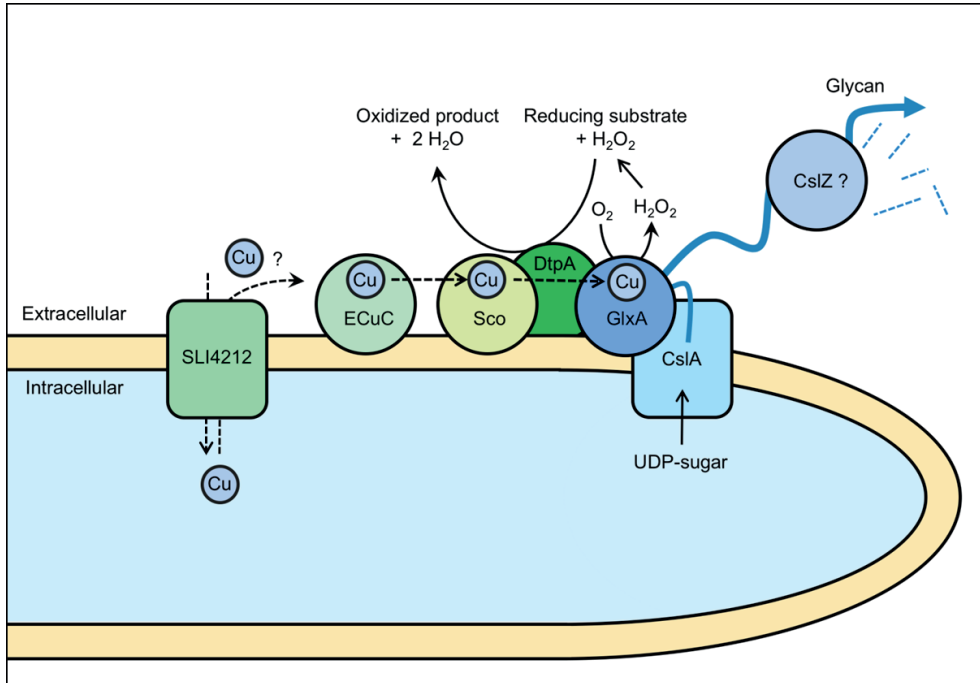


Figure 9. Proposed model for the Cu-dependent morphogenesis pathway in *S. lividans*. Mature GlxA requires the incorporation of a Cu ion and the formation of a Tyr-Cys covalent bond. GlxA receives its Cu from the extracellular chaperone Sco, which in turn receives Cu from the lipoprotein ECuC. The putative Cu transporter SLI_4212 may be involved in shuttling Cu ions over the membrane, although its activity is not essential for GlxA function. DtpA affects the maturation of GlxA, possibly by changing the oxidation state of Cu, or by removal of the reactive H_2O_2 which is generated by GlxA while oxidizing its substrate. Mature GlxA acts cooperatively with the cellulose synthase like protein CslA in formation of an extracellular glycan, which may be processed by CslZ.

GlxA functions together with the CslA protein in the production and modification of an extracellular glycan that plays a crucial role in morphogenesis (Chaplin *et al.*, 2015).

The absence of Sco has a dramatic effect on GlxA maturation, which can be compensated for by the addition of Cu to the medium. This connects well to our earlier work that suggested that Sco acts as the chaperone that provides Cu to GlxA. (Chaplin *et al.*, 2015). Based on genomic context, this may also occur in other species, as previously suggested (Banci *et al.*, 2007). Sco in turn receives its Cu from ECuC (Blundell *et al.*, 2014), and our data indicate that the absence of *ecuc* also affects the correct maturation of GlxA, in particular under oxidizing conditions like in shaken liquid-grown cultures. However, the activity of ECuC is not essential for morphogenesis as the *ecuc* mutant formed a substantial aerial mycelium after prolonged incubation, and also formed pellets, albeit smaller, in liquid-grown cultures. This implies a role for ECuC in ensuring optimal Cu trafficking, but also indicates that Sco can obtain Cu in an ECuC-independent manner depending on the redox state of the environment. Something similar is true for GlxA, which in the absence of both Sco and ECuC can reach its mature

conformation by the addition of Cu. How Cu is sequestered and transferred in the absence of these chaperones is not known and is under further investigation.

Our work clearly indicates that the maturation of GlxA under Cu limiting conditions also depends on DtpA. We hypothesize that DtpA plays a role in Cu transfer, possibly by changing the oxidation state of the redox metal. Such a role would be very similar to that of the Dyp-type peroxidase EfeB in *Bacillus subtilis*, which oxidizes Fe(II) to Fe(III) before cellular uptake (Miethke *et al.*, 2013). *S. lividans* also possesses an *efeB* homologue (SLI_2602), which is located in a gene cluster that contains genes encoding a lipoprotein (SLI_2601/*efeO*) and an iron transporter (SLI_2603/*efeU*). This organization is analogous to the *dtpA* gene cluster that contains genes for the lipoproteins Sco and ECuC and also for a metal transporter, in this case the putative copper transporter SLI_4212. Our data indicate that the *dtpA* gene cluster is tailored towards copper trafficking, while the *efeB* gene cluster more likely regulates iron homeostasis. However, the EfeO protein is reported to have a cupredoxin domain and to bind both Cu and Fe, again inferring cross-talk between both metals in morphological pathways.

Our data also demonstrate that GlxA produces H₂O₂ in the presence of glycolaldehyde, which is the best substrate determined for GlxA (Chaplin *et al.*, 2015). The H₂O₂ is then used by DtpA, thus contributing to protection of the hyphal tip from oxidative damage. Removal of H₂O₂ leads to the formation of DtpA compound I. The conversion of compound I to compound II is not observed in our assay, because of the reducing nature of excess glycolaldehyde leading to slow formation of an oxy-ferrous species. However, compound II is detected in DtpA through the controlled reduction of compound I (as shown in Fig. 5A), indicating that DtpA is behaving as a true peroxidase and that the peroxidation mechanism is operable. Lack of a true substrate for GlxA therefore hampers a fuller investigation into the events occurring after compound I formation, but the formation of the latter clearly indicates a synergy between GlxA and DtpA. Cooperation between an oxidase and peroxidase has been demonstrated in some fungi, for instance between the glyoxal oxidase and manganese peroxidase in *Phanerochaete crassa* (Takano *et al.*, 2009 and 2010) Therefore, the discovery of DtpA might help unravelling the substrate that is converted by GlxA.

Can the Tat substrate DtpA explain the morphological defects of tat mutants?

The Tat secretion pathway is a major route for protein export in streptomycetes in comparison to most other bacteria (Schaerlaekens *et al.*, 2004; Widdick *et al.*, 2006), and resides at the hyphal tip (Willemse *et al.*, 2012). *Streptomyces* mutants lacking *tatA*, *tatB*, or *tatC* have morphological defects in liquid-grown environments, and also fail to develop a robust aerial mycelium (Schaerlaekens *et al.*, 2001; Schaerlaekens *et al.*, 2004; De Keersmaecker *et al.*, 2005; Widdick *et al.*, 2006). Due to the large number of predicted Tat substrates (\pm 145-189;

Rose *et al.*, 2002; Bendtsen *et al.*, 2005; Widdick *et al.*, 2006; Chater *et al.*, 2010) no obvious candidates could be held responsible for these defects, which are undoubtedly caused by multiple missing proteins. However, our work suggests that the Tat-secreted protein DtpA is a crucial substrate that explains some of the morphological defects observed in *tat* mutants.

Adding Cu remarkably improved aerial mycelium formation by *S. lividans tat* mutants, which was also sufficient to restore the formation of pellets, albeit small, in liquid-grown cultures of *tatC* mutants. Western analysis indicated that the levels of mature GlxA in the *tatA* and *tatC* mutants were increased by the addition of Cu to the medium. These results are consistent with a model in which the TatA and TatC components of the Tat translocation machinery facilitate secretion of DtpA at the hyphal tip, where it contributes in the CslA-GlxA-dependent pathway of morphogenesis (Fig. 9). The addition of Cu also stimulated aerial growth in the *tatB* mutant, but this appears to be unrelated to the maturation status of GlxA. We hypothesize that the developmental rescue of the *tatB* mutant by Cu is mediated by an unknown Cu protein that does not necessarily relate to the GlxA-dependent pathway described here. The observed variations in phenotype and GlxA maturation between the different *tat* mutants forms an interesting starting point for further analysis of possible specific roles of the individual Tat proteins in streptomycetes.

Our model suggests that the proteins involved in apical polymer synthesis may be organized in a larger complex. CslA is an integral membrane protein, while GlxA has an N-terminal membrane anchor and is shown to be membrane located (Chaplin *et al.*, 2015). Indeed, both proteins were shown to be tip-localized (Xu *et al.*, 2008; Liman *et al.*, 2013). The chaperones Sco and ECuC are predicted lipoproteins (Worrall and Vijgenboom, 2010), while also DptA may remain anchored to the membrane considering the presence of a transmembrane helix that overlaps with the Tat signal sequence. Given the weak signal peptidase recognition site, this offers the option that DptA remains anchored to the membrane after transport, which is particularly important in liquid environments where the protein could otherwise diffuse away from its proposed action site. Interestingly, the gene adjacent to *sco* encodes a copper-responsive protein with a so-called cohesin domain. Such domains are important for assembly of large macromolecular complexes, most notably the cellulosome of *Clostridium thermocellum* (Shimon *et al.*, 1997). Whether this protein is involved in assembly of a large protein complex involved in hyphal tip glycan deposition is under current investigation.

Acknowledgements

We would like to thank Dr J. Anné and Dr. L Vanmellaert for providing the *tat* mutant strains, Dr. J. Whittaker for the GlxA antibodies and Dr. T. Palmer for the Tat secretion reporter plasmids.

Supplemental information

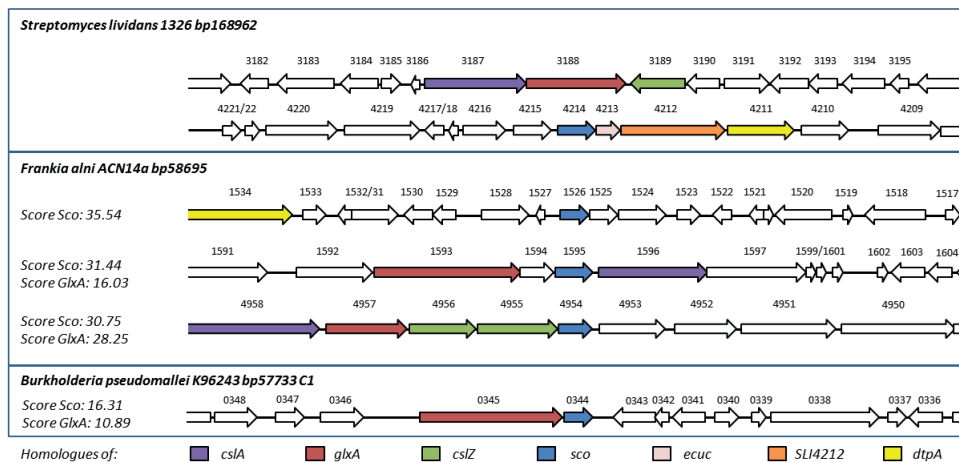


Figure S1. Comparison of the genomic context of the *glxA* and *sco* genes of *S. lividans* with the homologues from *Frankia alni* and *Burkholderia pseudomallei* using SyntTax (Oberto, 2013). *Frankia alni* contains three *sco* homologues, two of which cluster with *glxA* and *cslA* homologues. In *Burkholderia pseudomallei* several *sco* homologues are found, one of which is located immediately downstream of a *glxA*-like gene.

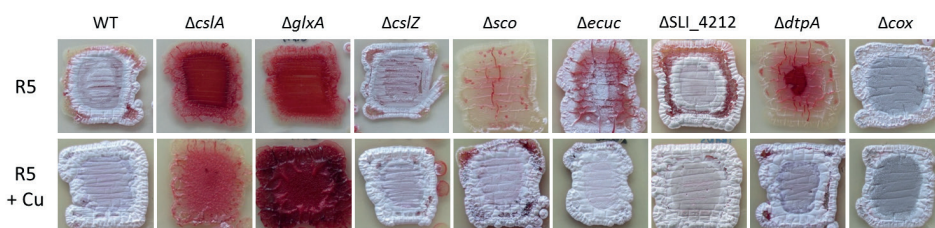


Figure S2. Phenotypic analysis of *S. lividans* strains lacking copper-related morphogenes. Morphology of strains after 6 days of growth on R5 medium in the absence (top row) and presence (bottom row) of $10 \mu\text{M CuSO}_4$.

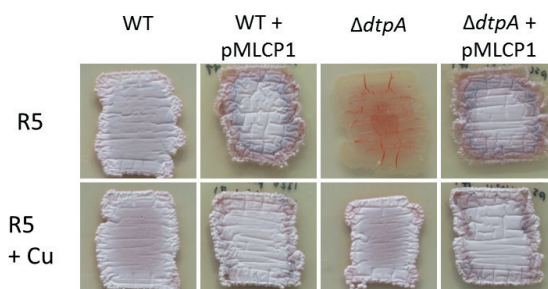


Figure S3. Complementation of the *dtpA* deletion mutant by expressing a copy of *dtpA* under control of the *sco* promoter in the integrating pMLCP1. Strains were grown for 3 days on R5 medium in the absence (top row) and presence (bottom row) of $10 \mu\text{M CuSO}_4$.

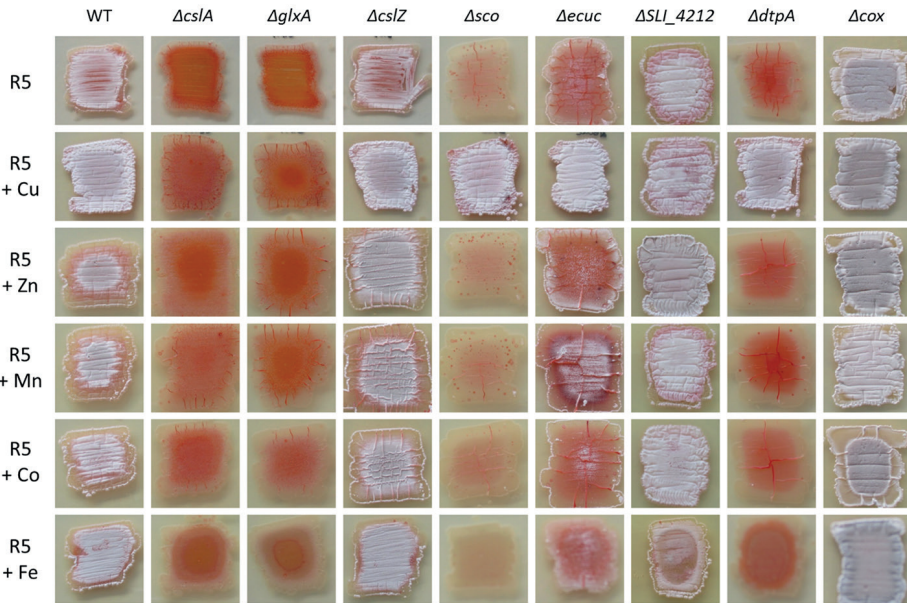


Figure S4. Phenotypic analysis of *S. lividans* strains lacking copper-related morphogenes. Morphology of strains after 3 days of growth on R5 medium (top row) supplemented with 10 μM CuSO_4 (second row), ZnSO_4 (third row), MnSO_4 (fourth row), $\text{Co}(\text{NO}_3)_2$ (fifth row) or FeSO_4 (bottom row).

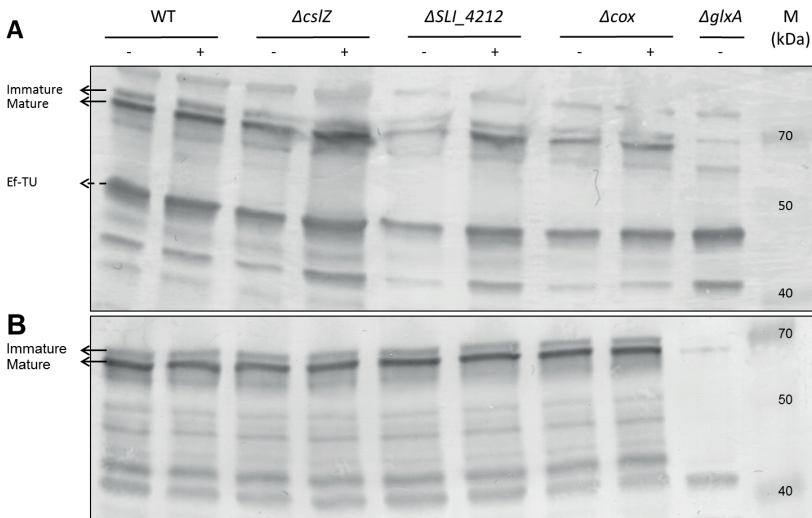


Figure S5. Immunoblot analysis of *GlxA* maturation in the wild-type strain and ΔcslZ , ΔSLI_{4212} and Δcox mutants grown for 24 h in TSBS medium (**A**) or grown for 2 days on R5 medium (**B**) in the presence (+) or absence (-) of 10 μM CuSO_4 . The two bands indicated with the solid arrows represent *GlxA*, the upper band being immature *GlxA* (no Tyr-Cys cross-link) and the lower band being mature *GlxA* (with Tyr-Cys cross-link). The band indicated with a dashed arrow indicates *Ef-TU*, which serves as a control for the total amount of protein loaded on the gel. Molecular weight markers are indicated in kDa.

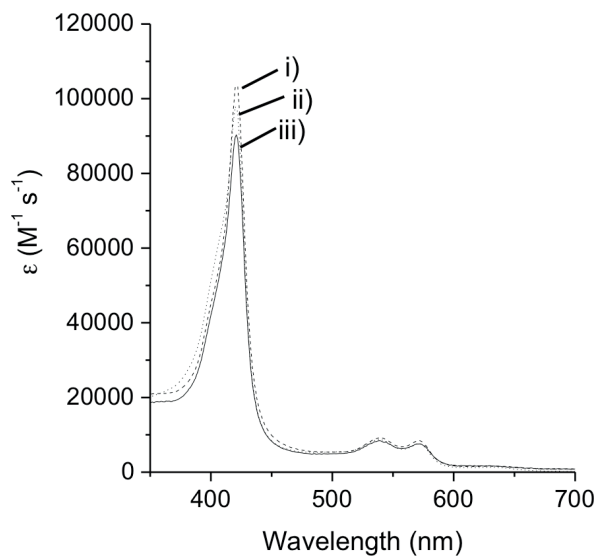


Figure S6. Static UV-visible spectra of oxy-ferrous DtpA (20 mM sodium phosphate pH 7, 100 mM NaCl) generated from i) resting state DtpA, GlxA and 0.2 M glycolaldehyde (GA); ii) resting state DtpA and 0.2 M GA; iii) compound I generated via addition of 1 equivalent of H_2O_2 followed by addition of 0.2 M GA.

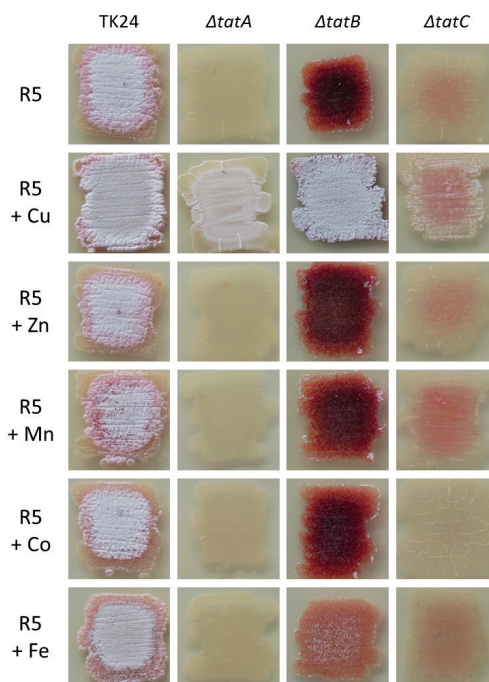


Figure S7. Phenotypic analysis of *S. lividans* *tat* mutant strains. Morphology of strains after 3 days of growth on R5 medium (top row), or R5 medium supplemented with $10 \mu M$ $CuSO_4$ (second row), $ZnSO_4$ (third row), $MnSO_4$ (fourth row), $Co(NO_3)_2$ (fifth row) or $FeSO_4$ (bottom row).

6

Marloes L.C. Petrus, Sander S. van Leeuwen, Karina Ramijan, Karthick B.S.S. Gupta, Wim Jesse, Erik Vijgenboom, Gilles P. van Wezel, Young Choi, Lubbert Dijkhuizen, Dennis Claessen

Abstract

Extracellular polysaccharides are produced by organisms from all kingdoms of life and play crucial roles in their biology. The filamentous bacterium *Streptomyces lividans* produces an extracellular glycan at hyphal tips by the action of the cellulose synthase-like protein CslA. The absence of CslA has a dramatic effect on morphology, as it blocks the formation of pellets in liquid environments and reproductive aerial structures on solid substrates. Despite its importance in morphogenesis, the glycan produced by this enzyme has not been characterized. Using a bioinformatics approach we show that CslA is a processive glycosyltransferase with a three dimensional structure comparable to the cellulose synthase BcsA of *Rhodobacter spaeroides*. However, differences are present in specific motifs involved in substrate and product binding. Subsequent chemical characterization of the polysaccharide was severely hampered by the relative abundance of peptidoglycan. To overcome this hurdle, we developed a cell wall-deficient synthesis platform for glycan characterization. As a proof-of-principle, we used this system to determine the composition of the CslA polymer and show that it may consist of glucose and/or *N*-acetylgalactosamine. We anticipate that this innovative production platform will facilitate characterization of glycans that are only produced in small amounts and for which purification is difficult.

Use of an innovative peptidoglycan-independent platform for characterization of the glycan produced by CslA

Introduction

Cellulose and chitin are the most abundant organic compounds in nature. They are key components of the cell walls of plants, algae, fungi or yeast, but also the exoskeleton of arthropods, where their main function is to provide structural rigidity. Cellulose is also produced by bacteria, where it contributes to the formation of sessile, multicellular growth forms called biofilms (Saxena *et al.*, 1990; Ross *et al.*, 1991; Römling, 2002; Jahn *et al.*, 2011; Römling and Galperin, 2015). Polysaccharide synthesis is catalyzed by glycosyltransferases (GTs) that exhibit a strong specificity for both the donor and the acceptor molecules (Breton *et al.*, 2006; Lairson *et al.*, 2008). For instance, cellulose synthases use UDP-activated glucose residues as donor substrate, while chitin synthases use UDP-activated *N*-acetylglucosamine. Both synthases incorporate these sugars into a growing glycan chain by catalyzing the formation of β -(1,4)-glycosidic bonds. Due to their similar reaction mechanism both synthases are classified into the broad group of family 2 GTs, according to the Carbohydrate Active enZYme database (CAZy; Lombard *et al.*, 2014).

In enteric bacteria cellulose biosynthesis is performed by a protein complex of three subunits: BcsA, BcsB, and BcsC (Ross *et al.*, 1991). BcsA is an integral inner membrane protein with an intracellular catalytic domain, BcsB is a membrane-associated periplasmic protein, while BcsC is predicted to form a pore in the outer membrane. Only BcsA and BcsB are essential for cellulose synthesis *in vitro*, however, also the action of BcsC and the cellulase BcsZ are required for synthesis *in vivo* (Römling, 2002; Römling and Galperin, 2015). In 2013 the catalytically-active BcsA-BcsB complex of *Rhodobacter sphaeroides* was crystalized, which also contained the polysaccharide that was being synthesized (Morgan *et al.*, 2013). The structure revealed that BcsA contains eight transmembrane (TM) helices, of which TM3

to TM8 form a narrow channel for transport of this polysaccharide over the plasma membrane (Fig. 1A). The active site of BcsA is located between TM helices 4 and 5, and adopts a canonical glycosyltransferase A (GT-A) fold (Charnock and Davies, 1999; Breton *et al.*, 2006). The intracellular C-terminus of the protein contains a PilZ domain that can bind cyclic-di-GMP, thereby inducing a conformational change in BcsA leading to activation of the complex. BcsB is largely located on the periplasmic side and interacts via carbohydrate binding domains with the polysaccharide.

The crystal structure of BcsA provides important insight in the role of the highly conserved residues of the characteristic D,D,D,Q(Q/R)XRW signature present in all processive β glycosyltransferases (Saxena *et al.*, 1995; Morgan *et al.*, 2013; Gloster, 2014). In BcsA, the first two variably spaced aspartic acid residues of the signature (Asp179 and Asp246), located in the DDG and DXD motifs, coordinate UDP-glucose in the active site, while the

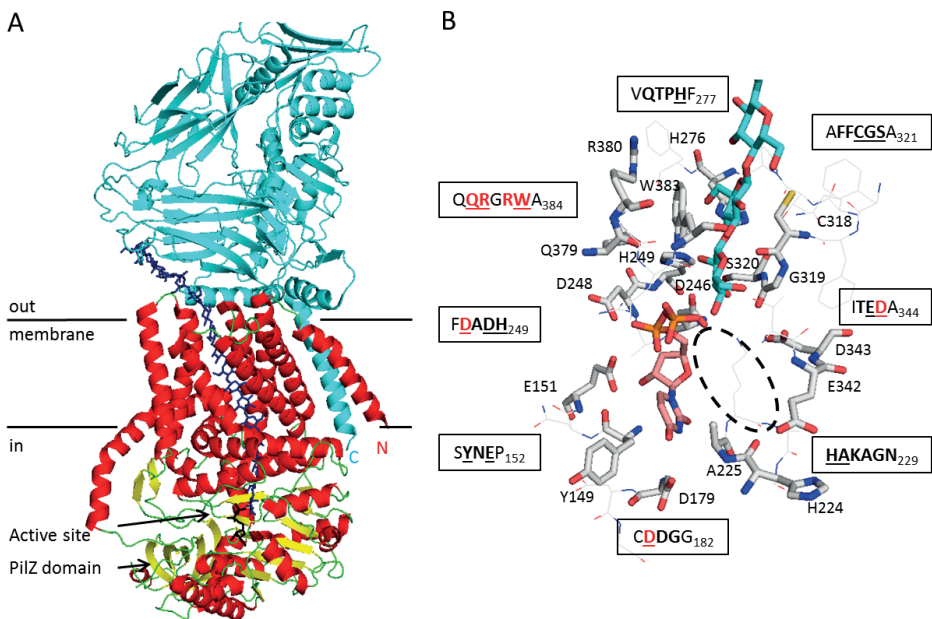


Figure 1. Architecture of the BcsA-B complex from *Rhodobacter sphaeroides* (Morgan *et al.*, 2013). **A**) Crystal structure of the BcsA-BcsB complex, with BcsB colored in cyan. BcsA helices are shown in red, while loops and strands are shown in green and yellow, respectively. The translocating glucan is shown in dark blue and the UDP-moiety is shown in black in the active site. **B**) Active site residues of BcsA are engaged in coordinating the UDP moiety of UDP-glucose and the terminal disaccharide of the translocating glucan. The organic molecules are represented in sticks with UDP in orange and the glucan in cyan. Conserved amino acids are represented in grey colored sticks and belong to sequence motifs shown in single letter code. Conserved residues are highlighted in bold and the depicted residues are underlined. The residues of the glycosyltransferase signature are shown in red letters. The likely position of the donor Glc is indicated by a dashed ellipsoid. Images were recreated in PyMol based on figures from Morgan *et al.* (2013).

third aspartic acid (Asp343), located in the TED motif, probably acts as the catalytic base (Morgan *et al.*, 2013; Fig. 1B). The Q(Q/R)XRW part of the signature is located at the interface between the cytosol and the membrane. There, Trp383 interacts with the penultimate sugar moiety of the acceptor glycan.

In addition to the processive glycosyltransferase signature also the role of certain cellulose synthase-specific motifs is shown by the crystal structure. The amino acid residues of the FFCGS motif are engaged in coordinating the ultimate glucose moiety of the growing chain (Fig. 1B). The QTPH cellulose synthase-motif is also involved in positioning the translocating glycan as it is within hydrogen bonding distance to the penultimate glucose via the histidine, which in turn is positioned properly by the proline residue contained in this motif. Residues in the HXKAG motif are involved in coordinating UDP-glucose in the binding pocket together with the glutamate of the TED motif (Fig. 1B).

The filamentous soil bacterium *Streptomyces lividans* contains a family 2 GT called CslA_{SL} for cellulose synthase-like protein. The CslA_{SL} protein makes a glycan at hyphal tips with multiple roles during growth and development; it is required for the formation of aerial hyphae on solid media (Xu *et al.*, 2008), and also for the formation of large mycelial aggregates, called pellets, in liquid-grown cultures (Xu *et al.*, 2008; Chaplin *et al.*, 2015). Furthermore, the CslA-derived glycan is involved in the attachment of hyphae to hydrophobic surfaces (de Jong *et al.*, 2009). Despite its importance, the true identity of the glycan produced by CslA_{SL} remains to be discovered. Preliminary experimental evidence suggested that cellulose-like polymers are formed at apical sites. This is based on 1) the CslA_{SL}-dependent hyphal tip staining with calcofluor white (CFW), which stains β -(1,3)- and β -(1,4)-coupled glycans including cellulose and chitin, and 2) the abolishment in hyphal attachment of the wild-type strain when grown in the presence of cellulase, which mimics the phenotype of a *cslA_{SL}* mutant (Xu *et al.*, 2008; de Jong, Wösten, *et al.*, 2009). However, the purity of enzyme preparations and also the specificity of the enzymes themselves is often questionable (Schiavone *et al.*, 2014).

Purification and characterization of the glycan produced by CslA_{SL} is hampered by the relative little amount of this polymer that appears to be produced compared to peptidoglycan (PG), which is the major constituent of the *Streptomyces* cell wall. To circumvent these problems, we here describe an innovative PG-independent synthesis platform for characterization of unknown glycans, with the polymer produced by CslA as a proof-of-concept. Preliminary data using this system indicated that the CslA polymer could be composed of glucose and/or *N*-acetylgalactosamine. We anticipate that our system may be applied for the synthesis and purification of glycans from other bacterial sources that in their endogenous hosts are only produced in limited amount.

Results

Gene synteny correlates $csIA_{SL}$ to polysaccharide biosynthetic genes

The genetic organization around $csIA_{SL}$ is different from the *bcsABZC* cellulose biosynthesis operon in enteric bacteria (Römling, 2002), since $csIA_{SL}$ (SLI_3187) is organized in a cluster with $glxA_{SL}$ (SLI_3188) for a radical copper oxidase and $csIZ$ (SLI_3189) for a β -(1,4)-endoglucanase (Liman *et al.*, 2013). In terms of gene synteny, conserved genes are found in close proximity to this gene cluster in nearly all streptomycetes (Fig. 2A): SLI_3182 encodes a copper-dependent lytic polysaccharide monooxygenase (LPMO), which typically play important roles in the degradation of polysaccharides (Nakagawa *et al.*, 2015); SLI_3183 encodes a protein with a flotillin domain, which is implicated in localizing large multiprotein complexes to the membrane; SLI_3184 encodes a protein with a peptidoglycan-binding domain and an uncharacterized NLPC_P60 domain that is found in some hydrolases; SLI_3192 encodes for sortase E (SrtE), an enzyme that covalently couples proteins to the cell wall, with SLI_3193 encoding such a putative sortase E substrate; and SLI_3194 encodes NagD, a possible ribonucleotide monophosphatase, which might play a role in recycling UDP when liberated by the action of glycosyltransferases on UDP-activated sugar moieties (Tremblay *et al.*, 2006). Thus, several genes in this genetic location are involved in polysaccharide synthesis and/or modification.

Bioinformatics analysis and structural modeling of $CsIA_{SL}$

$csIA_{SL}$ was annotated as a cellulose synthase-like gene based on similarity to the catalytic subunits of cellulose synthases from other bacteria and plants (Xu *et al.*, 2008). Careful bioinformatics analyses, based on new prediction programs and increased understanding of these synthases, indicated that $CsIA_{SL}$ is an integral membrane protein with six transmembrane (TM) helices (Fig. 2B), in contrast to the earlier prediction of seven TM helices (Xu *et al.*, 2008). Both the N- and the C-terminus of the protein are predicted to reside in the cytoplasm. The first two TM helices are followed by a large cytoplasmic region (aa 143 – 425) that contains a CESA_CelA-like domain (aa 168 – 406), which is also found in the known cellulose synthases $CsIA_{GX}$ of *Gluconacetobacter xylinus*, CelA of *Agrobacterium tumefaciens* and BcsA of *R. sphaeroides* (Saxena *et al.*, 1990; Matthyse *et al.*, 1995; Morgan *et al.*, 2013). The other four TM helices follow this cytoplasmic domain and are near the Cterminus of the protein.

Alignment of the amino acid sequences of the cytoplasmic domain of *S. lividans* $CsIA_{SL}$ against those of the above-mentioned cellulose synthases indicates that the D,D,D,Q(Q/R)XRW signature is present (Xu *et al.*, 2008; Fig. 2C), confirming $CsIA_{SL}$ as a

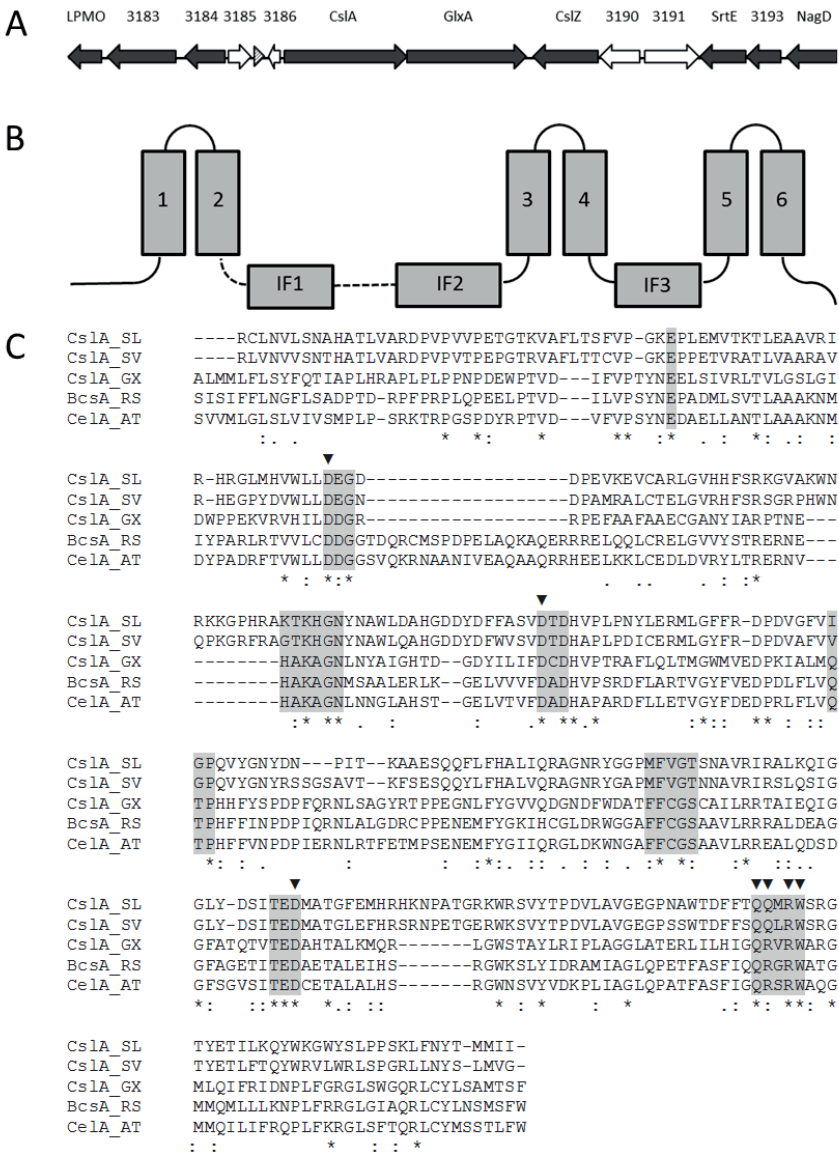


Figure 2. Bioinformatics analysis of $CslA_{SL}$. **A)** Gene organization around $cslA_{SL}$ in *S. lividans*. The filled arrows represent genes that are conserved in this region in nearly all streptomycetes. The open arrows represent genes that are not conserved, while the dashed arrowhead represents a tRNA locus. Numbers correspond to the SLI number as given by Cruz-Morales et al. (2013). **B)** Schematic representation of the six transmembrane helices (1-6) and three interfacial helices (IF1-3) of $CslA_{SL}$ as predicted by TMHMM 2.0 and Phyre. The catalytic site is conserved in the cytoplasmic region between transmembrane helices 2 and 4. **C)** Protein sequence alignment of the catalytic regions of $CslA_{SL}$ of *S. lividans* (EOY47900) with $CslA_{SV}$ of *S. viridifaciens*, $CslA_{GX}$ of *Gluconacetobacter xylinus* (CAA38487.1), $BcsA$ of *Rhodobacter spaeroides* (WP_041669585.1) and $CelA$ of *Agrobacterium tumefaciens* (NP_533806.1) with Clustal Omega. Conserved motifs are highlighted in grey. The residues of the D,D,D,Q(Q/R)XRW signature are indicated with arrow heads above the alignment.

processive glycosyltransferase. However, some other motifs uniquely found in cellulose synthases are less well conserved (*vide infra*). We then used the Phyre2 server (Kelley *et al.*, 2015) to predict the 3D structure of CslA_{SL}. The highest scoring structural template used for 3D conformation modeling of CslA_{SL} is the crystal structure of the cellulose synthase BcsA from *R. spaeroides*, which has a 24% identity score in the aligned region. Modeling of 529 residues of CslA_{SL} (i.e. residues 79-608) leads to the structure prediction shown in Fig. 3. Comparison of this model with the 3D-structure of BcsA (Fig. 1) indicates that the six TM helices of CslA_{SL} form the glycan-translocating channel, while the cytoplasmic CESA_CelA_{SL}-like domain in CslA_{SL} has a similar fold as the comparable domain in BcsA. However, BcsA has two additional N-terminal TM helices, which are not present in CslA_{SL}. One of these two helices may interact with the C-terminal TM helix of BcsB, which is missing in *S. lividans*. Also absent in CslA_{SL} is the C-terminal PilZ domain of BcsA, which is involved in activation of the protein via interaction with c-di-GMP (Morgan *et al.*, 2014).

Detailed analysis of the active site of CslA_{SL} indicates that the organization of the D,D,D,Q(Q/R)XRW signature is very similar to the organization in BcsA (Fig. 3B). However, the hydrophobic alanine underlined in the HAKAG motif that flanks the binding pocket for UDP-Glc in BcsA is substituted by a larger, polar threonine in CslA_{SL} (KTKHG). Changes in the

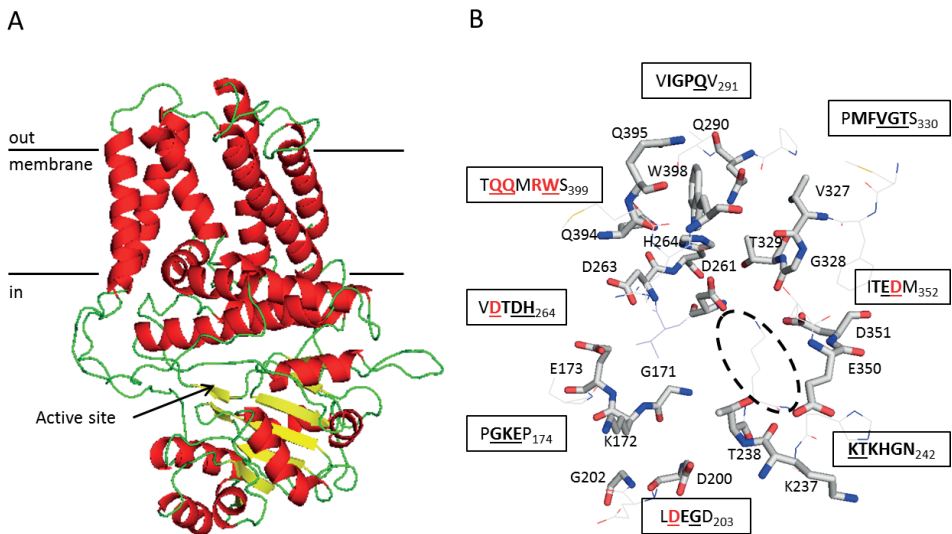


Figure 3. Computational model and the active site interacting residues of CslA_{SL} from *S. lividans*. **A)** Cartoon representation with CslA_{SL} colored according to its predicted secondary structure with helices in red, loops in green and strands in yellow. Horizontal bars indicate the membrane boundaries. **B)** Conserved amino acids of the predicted active site of CslA_{SL} are represented in grey colored sticks and belong to sequence motifs shown in single letter code. Conserved residues are highlighted in bold and the depicted residues are underlined. The residues of the glycosyltransferase signature are shown in red letters. The likely position of the donor sugar is indicated by a dashed ellipsoid. Images were prepared in PyMol.

conserved active site residues YNE possibly affect interactions with the UDP-site of the activated sugar. Also interactions with the acceptor glycan chain appear to be different due to differences in the QTPH/IGPQ motif, where the polar Gln290 residue is distinct from the positively charged His276 residue, and the FFCGS/MFVGI motif, where Thr329 is larger than Ser320. Note hereby that CslA_{SL} is modeled along the backbone of BcsA and that changes in the backbone orientation might occur that are not visible in this predicted 3D-structure.

Taken together, CslA_{SL} shows the characteristics of a cell membrane-embedded processive glycosyltransferase with an overall fold very similar to that of BcsA. However, the changes in several residues near the catalytic site of CslA_{SL} may lead to different substrate specificity in CslA_{SL}.

Cellulase or chitinase treatment abolish hyphal attachment

Attachment of *S. coelicolor* hyphae to surfaces is dependent on the activity of CslA (de Jong, *et al.*, 2009). In agreement, deletion of *cslA*_{SL} in *S. lividans* reduces attachment to 53 ± 5% of the wild type, while deletion of the functionally-related *glxA*_{SL} gene reduces hyphal attachment to 32 ± 6% (Fig. 4A). Considering that CslA_{SL} is a processive glycosyltransferase, we then assessed attachment of the wild-type strain in the presence of increasing amounts of cellulase and chitinase. Growth in the presence of cellulase abolished attachment, consistent with earlier results in *S. coelicolor* (Fig. 4B). Notably, growth in the presence of increasing amounts of chitinase lead to a similar loss of adhesion (Fig. 4B). In contrast, O-glycosidase, which catalyzes the removal of O-linked disaccharides from glycoproteins, had no effect on attachment (data not shown).

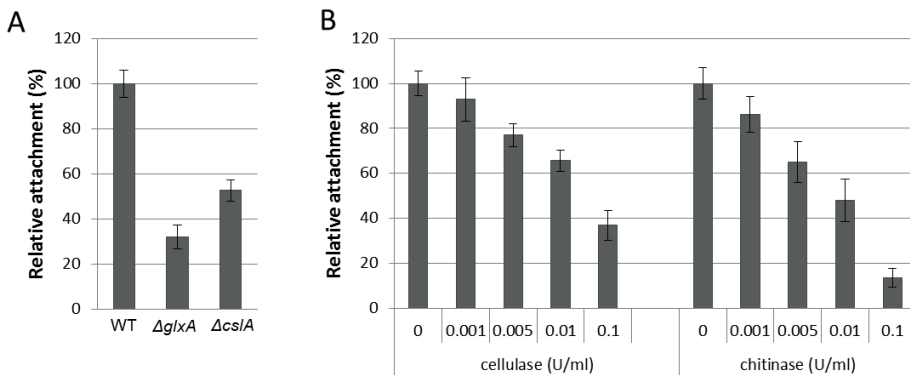


Figure 4. Attachment of mycelium to hydrophobic surfaces. **A)** *S. lividans* *cslA*_{SL} and *glxA*_{SL} deletion mutants show reduced attachment in liquid standing mNNMP cultures. **B)** Increasing amounts of cellulase or chitinase reduce the attachment of hyphae to hydrophobic surfaces. Error bars indicate standard error of the mean measured from thirteen biological replicates in A and eight biological replicates in B.

Peptidoglycan hampers the characterization of the *CslA_{SL}*-dependent glycan

Cell walls of the parental strain *S. lividans* 1326 and its *cslA_{SL}* deletion derivative were isolated and ground with potassium bromide for analysis with Fourier transform infrared spectroscopy (FTIR), which is commonly used for the identification of carbohydrates (Kumirska *et al.*, 2010). Both samples showed a similar spectrum with strong absorbance bands of amide I (1650 cm^{-1}) and amide II (1550 cm^{-1} ; Fig. 5) characteristic of the presence of *N*-acetyl groups. Given the presence of these signals in both strains, we anticipate that they result from *N*-acetylglucosamine (GlcNAc) and *N*-acetylmuramic acid (MurNAc) residues in the peptidoglycan.

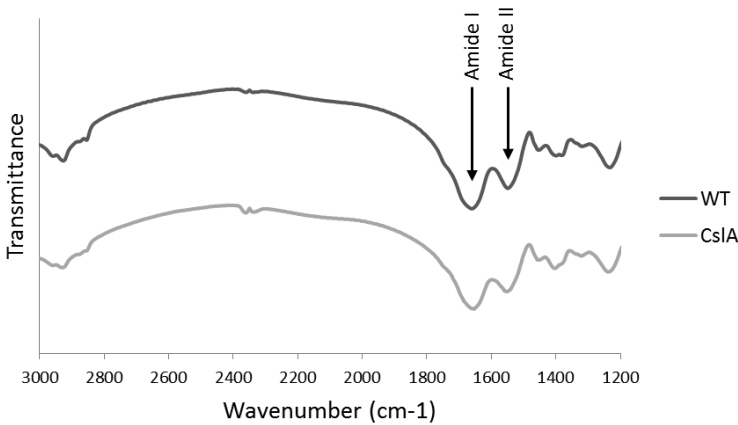


Figure 5. FTIR spectra of cell wall fractions of *S. lividans* WT and $\Delta cslA_{SL}$ are identical. The specific amide I ($\sim 1650 \text{ cm}^{-1}$) and amide II ($\sim 1550 \text{ cm}^{-1}$) absorbance bands are indicated by arrows.

We also analysed cell walls using ^{13}C CPMAS solid-state NMR, which provides information on composition and glycan structure (Fig. 6). The spectra of *S. lividans* 1326 (A) and $\Delta cslA_{SL}$ (B) showed almost the same peak pattern. To understand the origin of these rather complex spectra we used the same approach to analyse peptidoglycan from *Bacillus subtilis* (C), purified chitin (D) or cellulose (E). The spectrum of cellulose shows the peaks of sugar carbon atoms, while in the spectrum of chitin two additional characteristic peaks resulting from the *N*-acetyl groups of GlcNAc were seen: The very sharp signal at 22.6 ppm is from the methyl carbon atoms, and the peak at 173.1 ppm is from the carbonyl carbon atoms. In the spectrum of peptidoglycan the peaks are broader than in the spectra of cellulose and chitin because peptidoglycan is not as crystalline. In addition to the sugar carbons of GlcNAc and MurNAc in the peptidoglycan backbone, also the carbon atoms of the peptide bridges contribute to the peaks in the spectrum, where they overlap with the before mentioned carbonyl carbon, sugar carbon and methyl carbon peaks (Bougault *et al.*, 2012). The spectra

of *S. lividans* 1326 (A) and $\Delta csIA_{SL}$ (B) most likely result from a similar combination of peaks derived from cell wall peptidoglycan, including peaks resulting from sugar carbons, *N*-acetyl groups and peptide carbons. As both spectra show a virtually identical peak pattern it seems that the amount of glycan produced by *CsIA* is only small in respect to the abundant peptidoglycan.

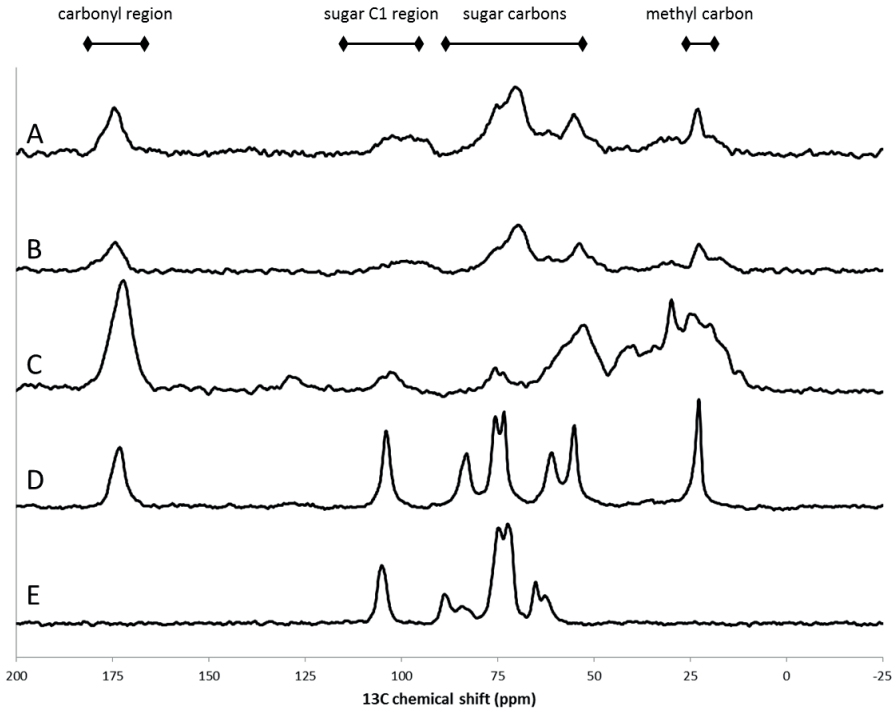


Figure 6. Solid-state ^{13}C CP-MAS NMR spectra of cell wall fractions of *S. lividans* WT (A) and $\Delta csIA_{SL}$ (B), peptidoglycan from *Bacillus subtilis* (C), chitin (D) and cellulose (E). Main regions that can be detected in the NMR spectra of peptidoglycan or polysaccharide are indicated above the graph, with horizontal lines indicating the corresponding region.

To analyse the monosaccharide composition of cell walls in more detail, we methanolyzed cell wall fractions of the *S. lividans* wild-type strain and compared these to fractions obtained from strains lacking $csIA_{SL}$ or $glxA_{SL}$. The biological replicates showed considerable differences both in monosaccharide composition and in the percentage of the total sugars content, which varied from 18 to 79 % in the $glxA_{SL}$ mutant (Fig. 7). The analysis showed that the cell walls of the $csIA_{SL}$ and $glxA_{SL}$ deletion mutants mainly consist of GlcNAc or sugars that are converted into this sugar during the methanolysis process (such as MurNAc). The wild-type samples contained 36 % and 23 % glucose respectively, unlike the mutant strains where glucose was hardly detectable (Fig. 7). This indicates that the polysaccharide composition of the cell wall is changed in the absence either $csIA_{SL}$ or $glxA_{SL}$.

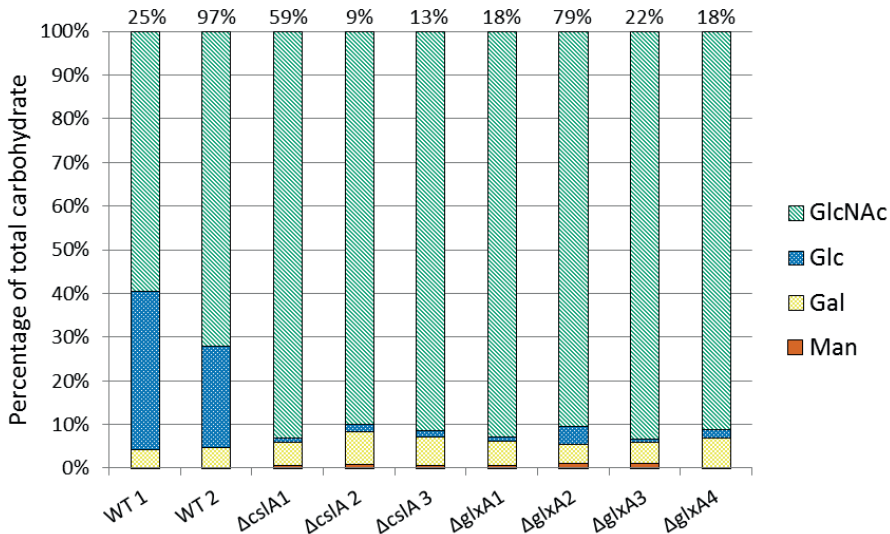


Figure 7. Carbohydrate monomer composition of cell walls from TSBS cultures of *S. lividans* WT, $\Delta cslA_{SL}$ and $\Delta glxA_{SL}$, as detected after acid hydrolysis and GLC-MS quantification of pentose and hexose sugars (colored as indicated in figure legend). Values are represented as a mole-based percentage of total recovered carbohydrate. Percentages above each bar represent the fraction of carbohydrate as a percentage of the total weight of the sample. The abbreviations used are: GlcNAc, N-acetylglucosamine; Glc, glucose; Gal, galactose; Man, mannose.

Use of cell wall deficient L-forms for glycan identification

Our data indicate that the presence of PG complicates the analysis of the glycan produced by $CslA_{SL}$. We therefore considered developing a platform in which the synthesis of PG is abolished. Growth without PG results in the formation of so-called L-forms, which have been created in several actinomycetes, including *Streptomyces viridifaciens* (Innes and Allan, 2001). Based on phylogenetic analysis and genome comparisons this species has recently been shown to belong to the genus of *Kitasatospora* (Girard *et al.*, 2014), which is closely related to the genus *Streptomyces* in the family Streptomycetaceae (Labeda *et al.*, 2012). Bioinformatic analysis shows that the $cslA_{SL}-glxA_{SL}$ gene cluster is conserved in *S. viridifaciens*, encoding proteins that share 53% and 52% aa identity to $CslA_{SL}$ and $GlxA_{SL}$, respectively. Amino acid alignment of the catalytic domain of $CslA_{SV}$ shows that the glycosyltransferase-specific signature is completely conserved (Fig. 2B). Moreover, all amino acids of $CslA_{SL}$ that are predicted to interact with the UDP-sugar moiety or the translocating glycan are conserved in $CslA_{SV}$ (Fig. 2B, Fig. 3B). The genetic organization around the $cslA_{SV}-glxA_{SV}$ cluster is similar to the organization in *S. lividans*, showing the neighborhood of NagD and a gene encoding an endoglucanase (Fig. 8A, Table 2). Together, this gives a strong indication that these homologues fulfill the same biological role.

To test the biological role of *csIA_{sv}* or *glxA_{sv}*, deletion mutants were created in *S. viridifaciens* and compared to the corresponding *S. lividans* mutants. Both the *S. viridifaciens* and *S. lividans* wild-type strains form a robust aerial mycelium and produce spores after four days of growth on MYM plates (Fig. 8B-C). Deletion of *glxA* blocks aerial growth in both organisms, while aerial mycelium formation and sporulation is greatly reduced in the *csIA* deletion mutants. Morphology of the mutants was also studied in liquid-grown cultures. In contrast to *S. lividans*, *S. viridifaciens* does not form dense pellets in liquid-grown cultures

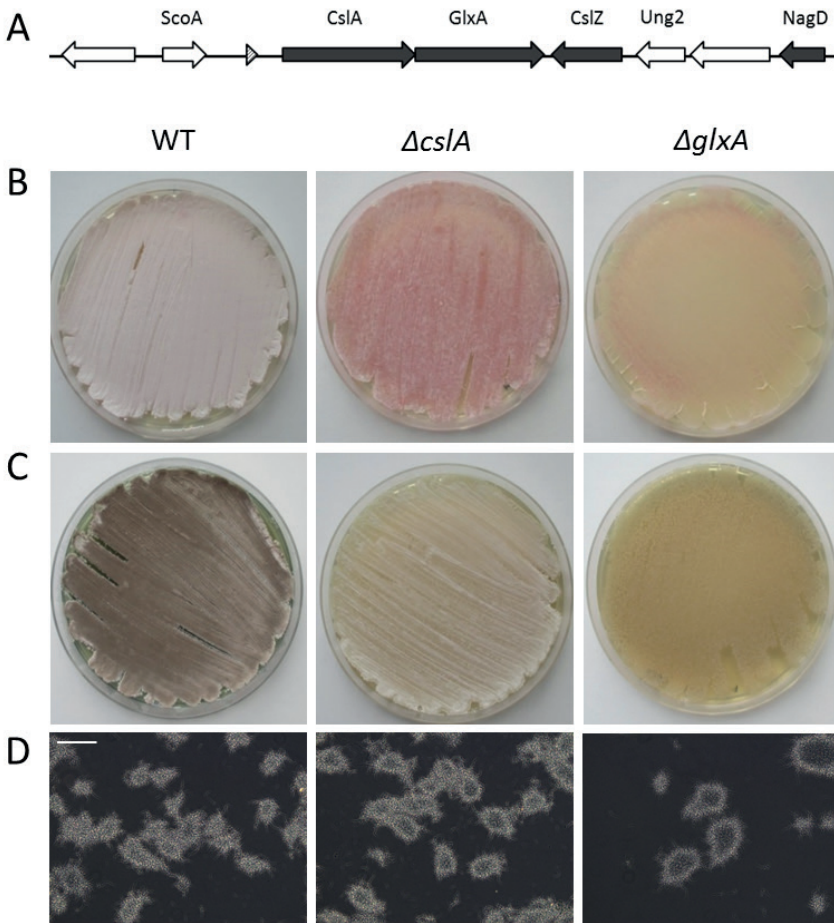


Figure 8. The *S. viridifaciens* *csIA_{sv}-glxA_{sv}* gene cluster. **A)** Gene organization around *csIA_{sv}*. The filled arrows represent genes that are conserved in this region in nearly all streptomycetes. The open arrows represent genes that are not conserved, while the dashed arrowhead represents a tRNA locus. **B-C)** Phenotypes WT, $\Delta cslA$ and $\Delta glxA$ strains of *S. lividans* (**B**) and *S. viridifaciens* (**C**) after 4 days of growth on MYM agar plates. Note that the *glxA* mutants do not produce any aerial mycelium, while the *csIA* mutants are severely delayed in aerial mycelium and spore formation. **D)** Morphology of *S. viridifaciens* WT, $\Delta cslA_{sv}$ and $\Delta glxA_{sv}$ strains after 1 day of growth in liquid shaken TSBS. Scale bar is 100 μ m.

(Fig. 8D). As a consequence, deletion of $csIA_{sv}$ or $glxA_{sv}$ had no effect on mycelial architecture, unlike the absence of the corresponding genes in *S. lividans*, which prevents the formation of pellets (Xu *et al.*, 2008; Chaplin *et al.*, 2015). Taken together, the strong similarity of the $CsIA_{sl}$ and $CsIA_{sv}$ active sites, and the equivalent morphological defects of the $csIA$ mutants infer that both synthases have a comparable role and produce a similar glycan.

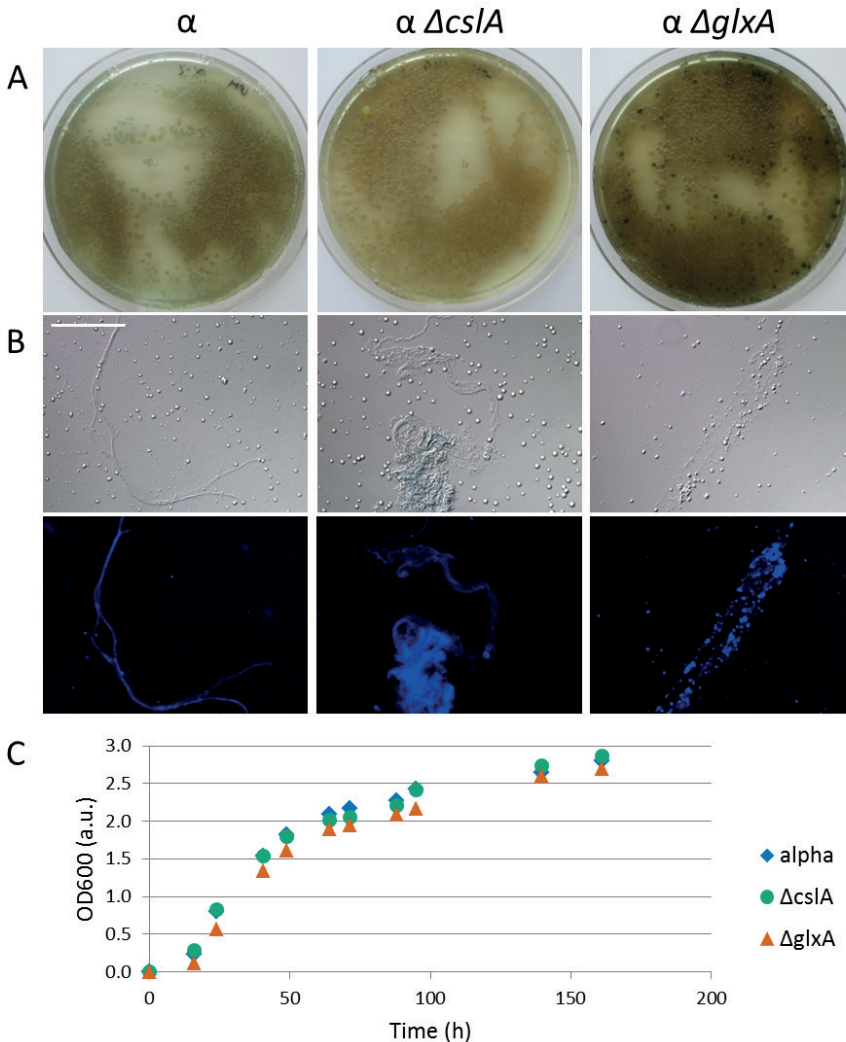


Figure 9. Phenotypic analysis of L-form $\Delta csIA_{sv}$ and $\Delta glxA_{sv}$ mutants. **A)** Morphology of *S. viridifaciens* L-form strains alpha (parental strain), $\Delta csIA_{sv}$ and $\Delta glxA_{sv}$ after 3 days of growth on LPM agar plates. **B)** L-forms and produced fibers stained with CFW from a 7 days old LPB culture. Upper row are the brightfield images, lower row is CFW fluorescence signal. Scale bar is 100 μm . **C)** Growth curves of L-forms strains in LPB is measured by OD600 and corrected for the absorption of the green pigment.

In order to study glycan production in the L-form background, which supposedly lacks PG, we constructed a series of control strains in which the *csA_{sv}* and *glxA_{sv}* genes were replaced by an apramycin resistance cassette (see M&M for details). Mutants were grown on LPM agar plates and compared to the parental strain. Growth of the wild-type and mutant L-form strains resulted in the formation of colonies with a smooth, glossy surface that were similar in appearance (Fig. 9A). Also, the morphology and growth rate in liquid LPB medium were similar between the three strains (Fig. 9C). Following a phase of relatively fast growth during the first 2 days, growth slowed and cells entered the stationary phase after 7 days of growth (Fig. 9C). Notably, after 7 days of growth fibrils were observed in the supernatant of all cultures, which were remarkably long as compared to the size of the L-forms themselves. Interestingly, fibers in all strains could be stained with CFW (Fig. 9B), indicating that they contain β -(1,3)- or β -(1,4)-glycosidic bonds.

To determine the monosaccharide composition of the glycan(s) produced by the L-form strains, insoluble substances were isolated from the parental strain and the *csA_{sv}* and *glxA_{sv}* deletion mutants in triplicate. Typically, from a 100 ml 7-day-old culture approximately 1 mg of product was obtained. However, for one wild-type sample and two *csA_{sv}* mutant samples the amounts were insufficient for analysis. The monosaccharide composition of the other samples is shown in Fig. 10. Notably, the fraction of GlcNAc in the *S. viridifaciens* L-form

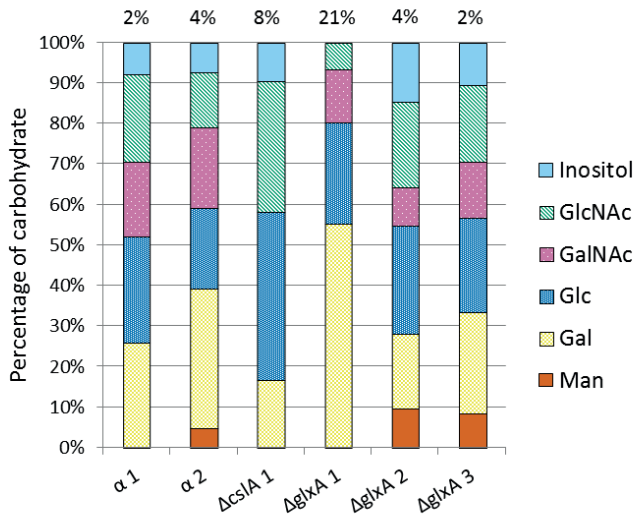


Figure 10. Carbohydrate monomer composition of insoluble particles in L-forms cultures of *S. viridifaciens* alpha (parental strain), ΔcsA_{sv} and $\Delta glxA_{sv}$ as detected after acid hydrolysis and GLC-MS quantification of pentose and hexose sugars (colored as indicated in figure legend). Values are represented as a mole-based percentage of total recovered carbohydrate. Percentages above each bar represent the fraction of carbohydrate as a percentage of the total weight of the sample. The abbreviations used are: GlcNAc, N-acetylglucosamine; GalNAc, N-acetylgalactosamine; Glc, glucose; Gal, galactose; Man, mannose.

samples varies between 10-30% compared to 60-90% for *S. lividans* growing as a mycelium (see Fig. 7). As a consequence, sugars that are derived from glycans which are produced in (very) low quantities compared to the abundance of peptidoglycan now make up a significant part of the total fraction. An example is galactose, which comprises 4 to 8% of the monosaccharides from the *S. lividans* mycelial samples, in contrast to the samples from L-forms where the percentage of galactose ranged from 16 to 55%. Excitingly, no GalNAc was detected in the sample obtained from the *csIA_{sv}* mutant L-forms. This may indicate that the polymer produced by CslA contains GalNAc residues, an observation that awaits verification. The strong reduction in the levels of GlcNAc due to the absence of PG shows the potential of L-forms for the characterization of glycans produced in small amounts.

Discussion

Glycans are formed in all kingdoms of life, where they play pivotal roles during growth and development. They mostly occur in the extracellular space, where they contribute to providing structural integrity of the surrounded cells. Some polysaccharides, such as the cell wall constituent peptidoglycan, are abundantly synthesized, while others are produced at barely detectable levels. The characterization of glycan structures is often limited by the amounts and purity of the isolated glycan (Mulloy *et al.*, 2009). In this study we aimed to characterize a glycan produced by the *Streptomyces* CslA protein, which appears to represent only a minor fraction of the cell wall matrix. To this end, we developed a cell wall deficient L-form platform that due to the absence of PG simplifies glycan purification and characterization. Preliminary analyses using this innovative platform hints that the glycan produced by CslA may contain GalNAc.

Limitations in bioinformatics and indirect approaches to determine glycosyltransferase specificity

The key enzymes in the production of glycans are the glycosyltransferases (GTs), which catalyze glycosidic linkage formation between the sugar moieties of activated nucleotide sugars and glycosyl acceptor molecules. Combining sequence- and network- based computational predictions can unveil insight in the donor and acceptor molecules, which can be growing glycan chains, lipids, peptidoglycan or proteins (Sánchez-Rodríguez *et al.*, 2014). Bioinformatics analysis shows that *CslA_{sl}* is a processive glycosyltransferase that couples monosaccharides to a growing glycan chain, which is transported through the membrane into the extracellular environment. Genome synteny analysis supports the role of *CslA_{sl}* as a polysaccharide producing protein, based on the observation that the *csIA_{sl}* gene is surrounded by a number of genes that encode proteins functioning in carbohydrate metabolism. However, predicting the specificity of GTs is still complicated especially for GTs

of Gram-positive bacteria, for which clear sequence motifs determining substrate specificity are largely unknown (Weerapana and Imperiali, 2006). For example, the active site of CslA_{SL} is very similar to the established bacterial cellulose synthases BcsA (Morgan *et al.*, 2013), but contains a number of amino acid substitutions in crucial motifs, which makes it unreliable to conclude that CslA_{SL} synthesizes cellulose.

In addition to computational analyses, polysaccharides are often studied using indirect methods, including the use of fluorescent stains, antibodies, lectins and hydrolytic enzymes (Cummings and Etzler, 2009; Mulloy *et al.*, 2009). Likewise, CslA_{SL} was predicted to produce cellulose, based on 1) the CslA_{SL}-dependent hyphal tip staining with calcofluor white (CFW), which stains β -(1,3)- and β -(1,4)-glycans including cellulose and chitin (Wood, 1980), and 2) the abolishment in hyphal attachment of the wild-type strain when grown in the presence of cellulase, which mimics the phenotype of a *csIA*_{SL} mutant (Xu *et al.*, 2008; de Jong, Wösten, *et al.*, 2009). Our work shows that not only treatment with cellulases, but also treatment with chitinases is able to abolish attachment of hyphae to hydrophobic surfaces. These data can be interpreted in different ways: 1) the polymer produced by CslA may contain stretches of both cellulose and chitin; 2) the hydrolytic enzyme preparations are not pure or specific enough and may therefore hydrolyse different types of carbohydrates (Schivone *et al.*, 2014); or 3) cellulose and chitin are produced during adhesion, both of which are required for attachment. The only way to discriminate between these options is to purify the glycan followed by characterization of its composition and structure.

L-forms as a platform to overcome the PG barrier for glycan characterization

Synthesis of the CslA_{SL}-dependent glycan occurs at growing hyphal tips (Xu *et al.*, 2008; de Jong, Wösten, *et al.*, 2009; Chaplin *et al.*, 2015), which are subject to constant remodeling during the process of tip extension, and which poses a threat to the integrity of the entire hypha. During tip growth, nascent layers of peptidoglycan are deposited outside the cell, which subsequently become cross-linked by transpeptidase activity, thereby leading to the formation of mature PG. The glycan produced by CslA is thought to provide protection by forming an extracellular bandage-like structure, which may protect the site where PG is still present in a nascent form (Chater *et al.*, 2010). Having fulfilled its protective role, the polymer may be degraded again sub-apically, for instance by the CslZ protein being part of the *csIA-glxA* gene cluster (Liman *et al.*, 2013). Cell-wall analysis with FTIR and NMR did not result in significant differences between *S. lividans* 1326 and its Δ *csIA* mutant. Furthermore, the monosaccharide analysis of the cell walls showed predominantly the sugar GlcNAc. These results strongly imply the high relative abundance of peptidoglycan, and are supportive for a model in which the CslA_{SL}-dependent glycan is only transiently present, or only comprises a marginal fraction of the total amount of glycan present at the cell surface. An L-form cell line that is derived from the strain of interest has the advantage

that precursors for glycan synthesis are created by the organism itself; other unknown essential proteins for glycan synthesis are conserved; and deletion mutants of homologous genes can be created for comparison. As expected, monosaccharide analysis revealed that the amount of GlcNAc in L-forms is dramatically reduced, indicating that the majority of PG is absent. The loss of the cell wall has an additional benefit as it leads to the secretion of otherwise cell wall-associated glycans in the culture broth, which greatly facilitates their purification and subsequent characterization. We therefore anticipate that this platform will be useful for studying GTs from many different organisms, in particular if the glycan only comprises a marginal fraction of the total amount of glycans produced by the natural host. In this context it is interesting to mention that the molecular techniques for manipulating L-forms have already been developed.

What is the composition of the CslA-dependent glycan?

The monosaccharide composition analysis of cell walls from WT and *csIA_{SL}* and *glxA_{SV}* deletion mutants suggests with a decrease in the amount of glucose upon gene deletion that CslA might indeed produce cellulose. In contrast, analysis of the L-form strains only showed the remarkable absence of GalNAc in the *csIA_{SV}* mutant, while glucose remained constant. We could speculate that CslA produces a glucose based polymer with incorporation of other monosaccharides like GalNAc under certain conditions. This type of substrate promiscuity of GTs is not uncommon in bacteria as is demonstrated by the incorporation of GlcNAc by the cellulose synthase of *Glucanoactebacter xylinus* (Lee *et al.*, 2001; Sánchez-Rodríguez *et al.*, 2014). Interestingly, the active site of processive glycosyltransferases can give rise to two separate types of glycosidic bonds (May *et al.*, 2012), suggesting that CslA may produce a glycan with alternating glycosidic linkages. Overexpression of the the *csIA-glxA* gene cluster in the L-form platform would be the next step towards characterizing the CslA-produced glycan.

Materials and Methods

Bacterial strains and growth conditions

The bacterial strains used in this study are presented in Table 1. *E. coli* K12 strains JM109 (Sambrook *et al.*, 1989) and ET12567 (MacNeil *et al.*, 1992) were used for plasmid propagation and were grown and transformed using standard procedures (Sambrook *et al.*, 1989). Soy flour mannitol (MS; Kieser *et al.*, 2000) agar plates were used for the isolation of spores from *Streptomyces lividans* wild-type (1326) and mutant strains. For phenotypical characterization and growth of *Streptomyces viridifaciens* wild-type (DSM40239) and mutant strains, MYM agar plates (Jakeman *et al.*, 2006) or TSBS liquid medium were used.

30 ml liquid cultures were inoculated with 10^6 WT or $\Delta csIA_{SV}$ spores per ml or with 1ml of precultured $\Delta glxA_{SV}$ culture and analysed after 24h of growth.

For growth of all *S. viridifaciens* L-form strains, liquid L-phase broth (LPB) and solid L-phase medium (LPM) were used. LPB is a mixture of 50 % TSBS and 50 % YEME supplemented with 25 mM $MgCl_2$ (Kieser *et al.*, 2000). L-phase medium (LPM) contains 200 g sucrose, 5 g glucose, 5 g yeast extract, 5 g peptone, 0.1 g $MgSO_4$, and 7.5 g Iberian agar per liter, and is supplemented with 25 mM $MgCl_2$ and 5 % horse serum (Sigma Aldrich) after autoclaving. L-form cultures were shaken at 100 rpm, and, if necessary, inoculated in fresh LPB (1:100 dilution) after one week.

Table 1 Strains used in this study

Strains	Description	Reference or source
<i>S. lividans</i> strains		
1326	<i>Streptomyces lividans</i> 1326	(Hopwood <i>et al.</i> , 1985)
1326 $\Delta csIA_{SL}$	<i>S. lividans</i> 1326 $\Delta csIA_{SL}$ marker-less	(Chaplin <i>et al.</i> , 2015)
1326 $\Delta glxA_{SL}$	<i>S. lividans</i> 1326 $\Delta glxA_{SL}$ marker-less	(Chaplin <i>et al.</i> , 2015)
<i>S. viridifaciens</i> mycelial strains		
DSM40239	<i>Streptomyces viridifaciens</i> DSM40239	(Soliveri <i>et al.</i> , 1993)
DSM40239 $\Delta csIA_{SV}$	<i>S. viridifaciens</i> DSM40239 $csIA_{SV}::ApraLoxP$	This study
DSM40239 $\Delta glxA_{SV}$	<i>S. viridifaciens</i> DSM40239 $glxA_{SV}::ApraLoxP$	This study
<i>S. viridifaciens</i> L-form strains		
α	<i>S. viridifaciens</i> DSM40239 L-form cell line	K. Ramijan, <i>unpublished</i>
$\alpha \Delta csIA_{SV}$	<i>S. viridifaciens</i> DSM40239 $\alpha csIA_{SV}::ApraLoxP$	This study
$\alpha \Delta glxA_{SV}$	<i>S. viridifaciens</i> DSM40239 $\alpha glxA_{SV}::ApraLoxP$	This study
<i>E. coli</i> strains		
JM109	See reference	(Sambrook <i>et al.</i> , 1989)
ET12567	See reference	(MacNeil <i>et al.</i> , 1992)

Attachment assay

Attachment of hyphae to polystyrene surface was assessed and quantified as earlier described (de Jong, *et al.*, 2009). Briefly, 25-well plates were filled with 3 ml mNMMP (van Keulen *et al.*, 2003) containing 10^6 spores per ml. After the addition of spores, different amounts of chitinase from *Trichoderma viride* (Sigma Aldrich) or cellulase from *Trichoderma reesei* (Sigma Aldrich) were added. Plates were then sealed with parafilm to prevent dehydration. After 7 days of growth 100 μ l of crystal violet solution (0.5%; Acros Organics) was added to each well and plates were left at room temperature for 10 min. Subsequently, the supernatant with free floating biomass was removed and plates were vigorously washed with running tap water and dried at 50 °C. Crystal violet was extracted from the attached biomass with 4

ml of 10% SDS during 30 min incubation at room temperature. The OD₅₇₀ of 100 µl aliquots was determined using a spectrophotometer. For each enzyme treatment eight biological replicates were analysed and for the attachment of the *S. lividans* wild-type *csIA_{sl}* and *glxA_{sl}* mutants thirteen biological replicates were analysed. The relative attachment was calculated by normalizing the data with the mean attachment of the untreated or wild-type samples in the same 25-well plate.

Generation of S. viridifaciens ΔcsIA_{sv} and ΔglxA mutants

The *csIA_{sv}* and *glxA_{sv}* null-mutants were created in *S. viridifaciens* DSM40239, and in the stable L-form derivative strain called α. The *csIA_{sv}* and *glxA_{sv}* genes were replaced via homologous recombination, with an apramycin resistance cassette (*aacC4*) flanked with *loxP* sequences using the unstable pWHM3 plasmid (Świątek *et al.*, 2012). In the *csIA_{sv}* null-mutants nucleotides +195 to +2037 relative to the start of *csIA_{sv}* were replaced, while in the *glxA_{sv}* mutants nucleotides +164 to +1587 relative to the start of *glxA_{sv}* were replaced. L-forms were transformed using an adjusted protocol for protoplast transformation (Kieser *et al.*, 2000): L-forms from 1 ml of a three days-old LPM culture were washed with, and subsequently resuspended in 1 ml P-buffer. For each transformation 50 µl of washed L-forms were mixed with 0.5 µg of plasmid DNA and 200 µl 25% PEG in P-buffer, after which the suspension was plated on LPM agar plates. Following transformation, mutants were selected that were thiostrepton-sensitive and apramycin-resistant. All mutants were verified by PCR analysis (see Table 2 for primer sequences).

Growth of L-forms

Growth of L-form cultures was measured using a spectrophotometer (BioRad) operated at a wavelength of 600 nm. Measurements were corrected for the absorbance of a (unknown) green pigment that is produced by L-forms, by subtracting the OD₆₀₀ measurement of the supernatant obtained after 10 min centrifugation at 16,000 *g*.

Microscopy of L-forms

Morphology of L-forms was analysed by light microscopy using an Axioplan 2 (Zeiss) equipped with a DKC-5000 digital camera (Sony). Insoluble fibers were stained by incubating 9 µl of L-form culture with 1 µl calcofluor white solution (Sigma Aldrich) for 5 min. Stained samples were analysed using fluorescence microscopy equipped with a mercury lamp and Omega Optical Filter set XF06.

Table 2 Primers used in this study

Primer name	Primer sequence	Restriction site
CsIA-P1-HindIII	GACAAGCTTAAGGAGGTGAGGGAGTTC	HindIII
CsIA-P2-XbaI	GACTCTAGAGAAGTGACCGTAGTCATAGG	XbaI
CsIA-P3-XbaI	GACTCTAGAACACGACGAAACAGCGACAC	XbaI
CsIA-P4-EcoRI	GACGAATTCCTCGGGTCGTAGACCTCGTTG	EcoRI
CsIA-INT-FW	GGAACCGCAAGCACAAACGTGAG	
CsIA-INT-RV	AACACCACCGCCAGAACAG	
Delcheck CsIA-FW	GCCGTCCCAACCGTACAAG	
Delcheck CsIA-RV	CACGTACTGGTGGTACTG	
Apra-primer	ATTCGGGGATCCGTCGACC	
GlxA-P1-FW	GACGAATTCAGAATCCGCTCGTCCAGTC	EcoRI
GlxA-P2-REV	GACTCTAGAAAGTGGCCGTACTGTCCCTTG	XbaI
GlxA-P3-FW	GACTCTAGAGAGCAGCGCATCGAGATCTAC	XbaI
GlxA-P4-REV	GATAAGCTTAGGTGGCTTCTCTACCAG	HindIII
GlxA-INT-FW	ATGTTCTGCGGCGGTACAC	
GlxA-INT-REV	TGCCCTGGTAGTCTGCTTG	
Delcheck GlxA-FW	ACGACGAACAGCGACAC	
Delcheck GlxA-RV	CGTCCGTCAGGAACAACATGTACC	

Bioinformatics analyses

Genetic synteny analysis was performed with SyntTax (Oberto, 2013), using the CsIA sequence of *S. lividans* (CsIA_{SL}, accession number: EOY47900) as input. Protein topology predictions were made with TMHMM version 2.0 (Krogh *et al.*, 2001). Protein sequence comparisons were made by aligning CsIA_{SL} with BcsA of *Rhodobacter spaeroides* (WP_041669585.1), CelsA of *Agrobacterium tumefaciens* (NP_533806.1) and CsIA_{AX} of *Acetobacter xylinus* (also known as *Komagataeibacter xylinus*, CAA38487.1) with Clustal Omega (Sievers *et al.*, 2011). The 3D-structure of CsIA_{SL} was predicted using Phyre2 (<http://www.sbg.bio.ic.ac.uk/phyre2>; Kelley *et al.*, 2015). The crystal structure of BcsA (c4hg6A) formed the highest scoring template and was used for homology modeling of CsIA_{SL} omitting the low confidence regions with high disorder prediction, which are the N-terminus (amino acid 1-78) and C-terminus (amino acid 590-653). The 3D-model was checked for accuracy with the build in Phyre investigator, showing that the general fold of the 3D-model of CsIA_{SL} is reasonable.

FTIR spectroscopy

Fourier Transform Infrared (FTIR) spectroscopy was performed on cell walls of the *S. lividans* wild-type strain and the Δ *csIA*_{SL} mutant. Therefore, total mycelium obtained from 5 ml

broth of 24 h TSBS cultures was washed twice with demineralized water and sonicated (5s on/5s off) until the mycelium was broken (as visualized using microscopy). The insoluble cell walls were obtained by centrifugation, and subsequently washed with demineralized water, acetone and ether before being lyophilized (Lee *et al.*, 2001). 2 mg of cell walls were manually blended with 100 mg of dried KBr powder and pressed into a tablet. FTIR transmittance spectra of both samples were recorded with a Bio-Rad (Excalibur series) FTS4000 spectrometer between 4,000-500 cm^{-1} (64 scans, resolution 2 cm^{-1}) and corrected for background signals.

Solid state CPMAS-NMR

For NMR analysis mycelium was harvested from 24h TSBS grown cultures and lysed with a French pressure cell (Stansted Fluid Power Ltd.). Cell walls were harvested by centrifugation at 16,000 *g*, washed three times with 10 mM Tris-HCL pH 7.0 and freeze-dried overnight. Solid-state ^{13}C NMR studies were performed on a Bruker AV-750 spectrometer with a 17.6 Tesla magnetic field, in which carbon nuclei resonate at 188.64 MHz, respectively. A triple resonance MAS probe head of 4 mm with a standard ZrO_2 rotor was used to spin till 13 kHz. For ^1H to ^{13}C CPMAS with TPPM decoupling, we used 49.1 kHz and a ramp from 80 kHz to 100kHz RF field frequencies in the ^{13}C and ^1H channels, respectively, for CP. The contact time was 2 ms, and the repetition time was 1 s for 512 scans. Chemical shift references (0 ppm) were externally referenced with TMS for ^1H and ^{13}C .

Monosaccharide analysis by GLC-MS

For monosaccharide analysis, mycelium from 30 ml 24h TSBS grown cultures was collected and lysed with a French pressure cell (Stansted Fluid Power Ltd.). Cell walls were harvested by centrifugation at 12,000 *g* for 30 min and resuspended in DNase buffer (10 mM Tris-HCl, 2.5mM MgCl_2 , 0.5mM CaCl_2 , pH7.6). Cell walls were treated with 5 μl DNase and 5 μl RNase (Thermo Scientific) for 1 h at 30 °C. After 20 min centrifugation at 12,000 *g*, pellets were resuspended in protein extraction buffer (2% SDS, 40mM β -mercaptoethanol, 50 mM Tris/HCl, 5 mM EDTA, pH7.4; Gastebois *et al.*, 2010; van Munster *et al.*, 2013) and incubated for 10 min at RT. After centrifugation for 20 min at 12,000 *g*, cell walls were washed twice with demineralized water and lyophilized.

Fibers produced by L-forms were isolated by spinning down (12,000 *g* for 30 min) insoluble material present in 50 ml of 7-day-old liquid-grown cultures. The pellet fraction, containing L-forms and fibers, was resuspended in DNase buffer, thereby lysing the L-forms. The lysate was further processed as described above. Samples containing a relatively high level of deoxyribose indicative of ineffective DNase and RNase treatment were excluded from

further analysis.

The method for monosaccharide analysis was previously described by Van Leeuwen *et al.* (2008). The polysaccharide containing samples were subjected to methanolysis (1.0 M methanolic HCl, 24 h, 85 °C), followed by re-*N*-acetylation and trimethylsilylation (1:1:5 hexamethyldisilazane–trimethylchlorosilane–pyridine; 30 min, room temperature). The mixture of trimethylsilylated (methyl ester) methyl glycosides were analysed by GLC on an ZB-1HT column (30 m × 0.25 mm; Phenomenex, Utrecht, The Netherlands), using a Trace 1300 gas chromatograph with flame-ionization detection (Fisher Scientific, Amsterdam, The Netherlands; temperature program 140 – 240 °C, 4 °C/min). The identification of the monosaccharide derivatives was confirmed by GLC-EI-MS analysis on a QP2010 Plus system (Shimadzu, 's-Hertogenbosch, The Netherlands), using the same column and temperature program.

7

General Discussion

The microbial world consists of millions of organisms with a wonderful variability of morphologies. They can range from single-celled individuals, such as yeasts and many bacterial species, to chains of cells and large multicellular communities, such as bacterial biofilms. One of the most sophisticated groups of bacteria is formed by the streptomycetes. These saprophytic bacteria thrive predominantly in soil habitats, where they colonize dead and living organic material. Unlike most other bacteria, streptomycetes grow by forming thread-like structures called hyphae, that together form a branched mycelial network. This filamentous growth enables the bacterium to burrow into neighbouring materials that would otherwise be inaccessible. After a period of vegetative growth, the onset of morphological differentiation is triggered by a lack of nutrients. This leads to the formation of a reproductive aerial mycelium, that ultimately gives rise to the formation of millions of spores that can withstand harsh environmental conditions.

Morphological differentiation is coupled to the production of a large arsenal of antibiotics to protect the non-motile *Streptomyces* colony from predation by other microbes. From an applied perspective we are interested in streptomycetes due to their ability to synthesize antibiotics and many other secondary metabolites used in medicine, biotechnology and agriculture, including antitumor, antifungal and anthelmintic compounds (Hopwood, 2007). In addition, as saprophytes these bacteria produce a large number of hydrolytic enzymes, which can be employed for industrial use (Chater *et al.*, 2010). However, optimal growth and production in bioreactors is complicated by the filamentous mode-of-growth of the bacteria, that results in the formation of complex mycelial structures. Especially macromolecules on the cell surface are important for bacterial morphology. The subject of this thesis was the formation of these extracellular macromolecules and their influence on morphogenesis, with a special emphasis on glycan production by genes of the *csIA-glxA* gene cluster. The

new knowledge derived from my work may lead to improved production of secondary metabolites or enzymes by streptomycetes.

Heterogeneity in Streptomyces pellets

Growth of streptomycetes in bioreactors results in the formation of intertwined clumps of hyphae called pellets. *Streptomyces* pellets can reach sizes over a millimetre in diameter and are therefore too large for analysis with regular flow cytometers. In Chapter 3 for the first time a Complex Object Parametric Analyser and Sorter (COPAS) was used to quantitatively analyse pellet sizes of different streptomycetes. Interestingly, we observed the presence of two populations of pellets in liquid-grown cultures of *Streptomyces lividans*, *Streptomyces coelicolor*, *Streptomyces scabies*, and *Streptomyces griseus*, that differ in size and probably also in function (see below). The average size of the particles belonging to the population of small mycelia had a constant mean diameter of approximately 260 μm . In contrast, the particles belonging to the population of large mycelia showed more variation in size, with *S. scabies* having pellets with the largest mean diameter of 557 μm . The diameter of the population of small mycelia of *S. coelicolor* was not affected by culture age and medium composition, whereas the size of the larger pellets did vary. Our data suggest that especially in the population of larger pellets the particle diameter is dependent on external parameters. These parameters may include the composition of the growth medium, pH, viscosity, surface tension, agitation speed, dissolved oxygen levels, temperature and inoculum (Tough and Prosser, 1996; Celler *et al.*, 2012; van Dissel *et al.*, 2014).

Proteomic comparison of large and small *S. coelicolor* pellets revealed an overrepresentation of proteins involved in antibiotic production in the population of large pellets (Chapter 3). This is consistent with the concept that larger mycelial structures are better for antibiotic production (Martin and Bushell, 1996). The overrepresentation of stress-related proteins in the larger pellets may be explained by the reduced availability of oxygen or nutrients in the centre of large pellets, which may in fact be triggers to induce antibiotic production. These stress-related proteins include the response regulator SCO0204 and the universal stress protein USP (SCO0200), which is part of the SCO0204 regulon (Urem *et al.* manuscript in preparation). Low levels of oxygen or nutrients in the centre of these larger mycelia might constrain growth and primary metabolism. In agreement, the small pellets contained more proteins involved in active growth, such as those involved in DNA metabolism and organization. Given that small pellets probably grow faster than large pellets makes them more suitable for the production of industrial relevant enzymes. This would be consistent with the increased growth speed and enzyme production observed upon induced fragmentation by the cell division activator protein SsgA (van Wezel *et al.*, 2006).

The size of pellets increases by tip growth and branching, while fragmentation and lysis leads

to a decrease in their size. Because these processes occur simultaneously in a bioreactor, pellets are heterogeneous in size. In filamentous fungi pellets originate from aggregated spores and germlings (Lin *et al.*, 2008), which implies that surface properties of spores and hyphae affect pellet size (van Veluw *et al.*, 2013). In streptomycetes the secreted chaplin proteins are known to decorate spores with a hydrophobic layer (Claessen *et al.*, 2003; Elliot *et al.*, 2003), while the cellulose synthase-like protein CslA produces an extracellular glycan at hyphal tips that could become part of the spore surface (Xu *et al.*, 2008). Deletion of *cslA* or the genes encoding for the chaplins resulted in a large decrease in the average size of mycelia, although sizes were still heterogenic (Chapter 3). Size heterogeneity was also observed when cultures were inoculated with pre-grown mycelia or synchronously germinated spores. These results show that, similarly to filamentous fungi, cell surface properties are crucial for pellet architecture, although their influence in spore and germling aggregation is not the only factor giving rise to two differentially sized populations of pellets (Chapter 3). This infers that other factors explain the heterogeneity in mycelial size, with shear force leading to random fragmentation being a likely candidate.

Structural cell-surface components involved in pellet architecture

Pellet integrity is challenged by the strong shear forces in bioreactors. This is especially important in pellets that have initiated programmed cell death, which leads to the partial degradation of pre-existing hyphae in the central part of these structures (Rioseras *et al.*, 2014). This may be compensated for by the synthesis of a number of glycans, such as those produced by CslA, that could form an adhesive, extracellular matrix that contributes to pellet integrity. Recently, the *mat* gene cluster was identified as a locus that is required for pellet growth of streptomycetes (van Dissel *et al.*, 2015). Homology of the *mat* cluster with the *ica* operon of *Staphylococcus* spp. suggests that it encodes a polysaccharide synthase complex that produces a polysaccharide containing β -(1,6)-linked *N*-acetylglucosamine molecules (van Dissel *et al.*, 2015). A third secreted polysaccharide possibly involved in pellet integrity is hyaluronic acid (Kim and Kim, 2004), a glucosaminoglycan consisting of repeating units of D-glucuronic acid and D-*N*-acetylglucosamine, linked via alternating β -(1,4)- and β -(1,3)-glycosidic bonds. Treatment of pellets with hyaluronidase makes the structures very fragile (Kim and Kim, 2004), although the purity and specificity of the enzyme preparation that was used is unknown. The SLI_5327-SLI_5330 gene cluster is a candidate for synthesis of hyaluronic acid in *S. lividans*. Deletion of this gene cluster, however, had no major effect on pellet morphology under the conditions tested (our unpublished results).

In addition to glycans, an extracellular pellet matrix may also contain other macromolecules. Many biofilm-forming bacteria secrete DNA in the environment that contributes to biofilm architecture (Whitchurch *et al.*, 2002). Likewise, extracellular DNA has been suggested to be involved in shaping *Streptomyces* pellets (Kim and Kim, 2004). Moreover, matrices often

contain adhesive proteins, including amyloid-forming proteins such as curli in *Escherichia coli* and TasA in *Bacillus subtilis* (López *et al.*, 2010). The effect on *Streptomyces* pellet morphology caused by deletion of the amyloid-forming chaplin proteins (Chapter 3), illustrates the similarity in extracellular matrix between pellets and bacterial biofilms.

So far, it is not clear how all these extracellular components collaborate in the establishment and maintenance of pellet integrity. Since chaplins and the cellulose-like structure produced by CslA were shown to cooperate in the attachment of hyphae to hydrophobic surfaces (de Jong *et al.*, 2009) it is likely that this also happens in the process of pellet formation. In addition, one can easily imagine interaction between the different polysaccharides produced in the pellet matrix. For example, it is shown that fibril association and crystallinity of the cellulosic network produced by *Glucanoacetobacter xylinus* strains is influenced by the presence of non-cellulosic exopolysaccharides (Fang and Catchmark, 2015). Furthermore, diverse covalent bonds are present between different polysaccharides in the arabinogalactan-peptidoglycan complex in the mycobacterial cell envelope (Crick *et al.*, 2001). Since the glycan produced by CslA is directly produced in the growing tip (Chapter 4; Xu *et al.*, 2008), it might serve as a scaffold to efficiently organize other macromolecules in the extracellular matrix. However, this awaits further experimental evidence.

Structural cell-surface components in aerial growth

Structural cell-surface molecules are also important for morphological differentiation on solid substrates. Vegetative hyphae of streptomycetes elongate via tip extensions at the cell pole, while new hyphae emerge via branching of sub-apical compartments. Hydrostatic pressure acting on the extension zones drives the hyphal elongation process at the tips, which are the sites where the cell wall is constantly being remodelled (Prosser and Tough, 1991). This means that growing hyphal tips are relatively weak compared to the remainder of the hyphae that are surrounded by mature peptidoglycan. To control cell integrity during growth many proteins function together in the so-called tip-organizing centre (Holmes *et al.*, 2013). One of the crucial proteins is the polar localized protein DivIVA that plays an essential role in apical growth by orchestration of the cell wall synthesis process (Flärdh, 2003a; Flärdh *et al.*, 2012). Protein-protein interactions showed that DivIVA binds to CslA, suggesting that the glycan produced by CslA is required during cell wall synthesis. Its putative function is to provide protection to the growing tips (Xu *et al.*, 2008; Chater *et al.*, 2010). Although deletion mutants of *csA* are able to establish a vegetative mycelium, the erection of rigid hyphae into the air requires the presence of CslA (Chapter 4, (Xu *et al.*, 2008)). Immediately after the onset of aerial mycelium formation expression from the promoter upstream of *csA* is dramatically reduced (Liman *et al.*, 2013).

In this thesis also the morphological role of the radical copper oxidase GlxA was extensively

studied. The *glxA* gene is located immediately downstream of *csIA* in an operon-like manner that is highly conserved in streptomycetes (Liman *et al.*, 2013). Both CslA and GlxA are required for hyphal tip staining with the glycan-binding stain calcofluor white, suggesting that GlxA cooperates with CslA in the synthesis, anchoring and/or modification of a glycan at the growing tips (Chapter 4). This is strongly supported by the observations that *glxA* deletion mutants grow as dispersed mycelia in liquid cultures and are unable to produce an aerial mycelium as was shown for *csIA* deletion mutants (Chapter 4 and 5 and (Xu *et al.*, 2008; Liman *et al.*, 2013)). Finally, deletion of either *csIA* or *glxA* reduces the attachment to hydrophobic surfaces in liquid standing cultures (Chapter 6). Thus, the *glxA* mutant is a phenocopy of the *csIA* mutant under various conditions. The crystal structure of GlxA contains tunnels that are sufficiently large for a polysaccharide strand to stretch from the protein surface all the way to the active site of the enzyme (Chapter 4). We envision a scenario whereby the nascent glycan produced by CslA is fed into one of these tunnels, orientated in the substrate pocket, oxidised and then released through another tunnel. Notably, small differences in development can be observed between the *csIA* and *glxA* mutants under specific conditions. For instance, the *csIA* mutant is severely delayed in aerial growth on MYM medium, while the *glxA* mutant fails to form aerial hyphae altogether (Chapter 6). This hints at a CslA-independent role for GlxA in development, which is supported by the identification of a second promoter in the *csIA* coding sequence that drives transcription of the *glxA* gene independent of *csIA* (Liman *et al.*, 2013). On the other hand, the phenotype of the *csIA* deletion mutant is more severe on relatively low osmolyte media, suggesting that at least under those conditions GlxA is not essential for CslA function (Liman *et al.*, 2013).

As discussed in Chapter 2 the formation of an aerial mycelium also strongly depends on the secretion of the lantibiotic-like peptide SapB and the chaplin proteins, both of which act as surfactants to lower the water surface tension enabling aerial growth (Claessen *et al.*, 2003; Willey *et al.*, 2006; Capstick *et al.*, 2007). Together with the rodlin proteins, the chaplins have a second role in development by assembling into a hydrophobic layer surrounding the aerial hyphae and spores (Claessen *et al.*, 2002 and 2003; Elliot *et al.*, 2003). The capacity to initiate aerial growth relates to three crucial factors: the turgor pressure inside the hyphae, the rigidity of the hyphal wall and the surface tension barrier at the medium-air interface. Deletion of *csIA* or *glxA* probably affects the rigidity of the vegetative hyphal wall, deletion of the chaplin genes or the *ram* gene cluster (required for SapB biosynthesis) prevents the required reduction in surface tension, while changes in the medium composition influences all three factors. Considering the combined effect of these factors underlying aerial growth may explain why the block in development of the *csIA* mutant (less rigid hyphae) could be rescued by the addition of chaplins (thereby further reducing the surface tension; Xu *et al.*, 2008), why a reduction in osmolarity (thereby increasing turgor pressure and (slightly) reducing surface tension) enables the *glxA* mutant (with less rigid walls) to establish an aerial mycelium (Liman *et al.*, 2013), why SapB is not essential in low osmolyte media

(during which hyphae can generate more turgor pressure) and why *csA* deletion mutants are able to erect aerial hyphae on some media, while they cannot on others (Chapter 4 and 5). Thereby, the structural cell wall components that are involved in hyphal rigidity also seem to contribute to aerial mycelium formation, while others like the polysaccharides produced by the *mat* cluster are only important for pellet formation.

The role of copper in morphogenesis

S. lividans displays a distinct dependence on copper (Cu) to fully initiate morphological development. The work in this thesis shows that GlxA is the principle extracytoplasmic cuproenzyme that is essential for morphogenesis. Cu plays an essential role in the activity of GlxA as it forms one of the two redox centres in the active site of the protein. The other redox centre is formed by a nearby cross-link between a Cys residue and one of the Cu-coordinating Tyr residues (Chapter 4). *In vitro* data showed that the Tyr-Cys cross-link is only formed in the presence of Cu (Chapter 5). With the combined redox centres GlxA can access three oxidation states: Cu(I)-Tyr-Cys (reduced), Cu(II)-Tyr-Cys (semi-reduced) and Cu(II)-Tyr-Cys• (fully oxidized). GlxA should therefore be able to catalyse the two-electron oxidation of a substrate (Chapter 4).

The GlxA crystal structure shows a lid-like structure that protects both the redox centres in the active site and the substrate binding pocket (Chapter 4). However, this raised the question how GlxA acquires and incorporates Cu. Using Western Blot analysis, the acquisition of Cu by GlxA could be detected, due to a change in electrophoretic mobility when the Cu dependent Tyr-Cys cross-link is formed (Chapter 5). Further analysis showed that *in vivo* GlxA maturation depends on the extracytoplasmic copper chaperone Sco. Sco was already known to deliver Cu to the active site of an aa_3 -type of cytochrome c oxidase (CcO). However, the lack of aerial mycelium formation in the *sco* deletion mutant could not be explained by its role in Cu transfer to CcO, as the *cco* mutant develops normally (Blundell *et al.*, 2013; Blundell *et al.*, 2014). GlxA being a second target of Sco fits with the identical defects of both mutants including the lack of aerial growth on solid media, and the absence of pellet formation in liquid cultures (Chapter 5). Only when copper is available in high concentrations GlxA will not rely on the presence of Sco, thereby enabling the *sco* deletion mutant to erect aerial hyphae and to create small pellets (Chapter 5).

In turn, Sco receives its Cu ion from the extracytoplasmic Cu chaperone ECuC in a unidirectional manner (Blundell *et al.*, 2014). The transfer takes place in the cuprous form (Cu(I)) of the ion, but the oxidation state after transfer is unknown (Blundell *et al.*, 2014). Interestingly, transfer from Sco towards CcO required the cupric (Cu(II)) oxidation state of the metal (Blundell *et al.*, 2013), while the required oxidation state for incorporation in GlxA is not known. Both the morphological defects and reduced CcO activity are less pronounced

in the *ecuc* mutant compared to the *sco* mutant, suggesting that Sco can scavenge Cu(II) directly from extracytoplasmic pools (Chapter 5). Efficient loading probably does require ECuC as a Cu(I) donor and the subsequent action of an oxidizing molecule or protein to create Cu(II). The nature of this molecule or protein is unknown.

sco (SLI_4214) and *ecuc* (SLI_4213) are the first two genes of an operon that also contains a gene encoding a putative Cu transport protein (SLI_4212) as well as *dtpA* for a Dyp-type peroxidase (SLI_4211, Chapter 5). Interestingly, deletion of *dtpA* also results in a developmental arrest coinciding with impaired GlxA maturation (Chapter 5). The morphological defects of *dtpA* mutants can be overcome by high levels of Cu, as is the case for the *sco* mutant (Chapter 5). The physiological role of Dyp-type peroxidases is still relatively unclear, although they are widely distributed amongst fungi and bacteria (Singh and Eltis, 2015). One possibility would be that GlxA and DtpA act in a coupled assay, whereby DtpA activates or stabilizes GlxA via protein-protein interactions or via the removal of H₂O₂ produced by GlxA. Such a cooperation of a cognate peroxidase with an oxidase has been reported in some fungal systems (Hamilton *et al.*, 1978; Kersten, 1990; Takano *et al.*, 2010). We showed that DtpA can act as a peroxidase in the presence of active GlxA *in vitro* (Chapter 5). *In vivo*, these proteins could potentially also function together as GlxA is an extracellular membrane-associated protein (Chapter 4), while also DtpA is secreted into the extracellular environment via the twin-arginine translocation pathway (Chapter 5). This transport pathway is known for the secretion of folded proteins, especially when these proteins contain a cofactor, such as the haem in DtpA. However, no strong physical interaction between GlxA and DtpA could be observed *in vitro*, and DtpA did not boost the activity of GlxA in a peroxidase coupled enzymatic assay compared with the regularly used horse radish peroxidase (Chapter 5).

Alternatively, DtpA could function in the Cu-trafficking pathway towards GlxA. We could speculate that DtpA is the oxidizing protein that creates Cu(II) from Sco-bound Cu(I). This would not only explain why GlxA maturation is impaired in a comparable manner to the *sco* mutant (Chapter 5), but also why the CcO activity is reduced in a *dtpA* mutant in *S. coelicolor* (Fujimoto *et al.*, 2012). Sco proteins are known to be able to bind both Cu(I) and Cu(II) and it is not unlikely that Cu transfer to acceptor proteins is dependent on the oxidation state of the metal (Banci *et al.*, 2007). A role for DtpA in oxidizing metal ions would be very similar to the function of the Dyp-type peroxidase EfeB, which oxidizes Fe(II) to Fe(III) before cellular uptake (Miethke *et al.*, 2013).

Cu is not the only redox-active metal that is important for morphology in streptomycetes. Especially the role of iron (Fe) has gained a lot of interest since this metal plays essential roles in house-keeping functions, such as DNA replication, protein synthesis and respiration (Cornelis and Andrews, 2010; Lambert *et al.*, 2014). Many microbes secrete iron-chelating

molecules called siderophores, which are important for the acquisition of the poorly soluble Fe(III). The siderophore desferrioxamine (DFO) has recently been shown to be essential for growth of *S. coelicolor* on medium with low levels of Fe (Lambert *et al.*, 2014). In addition, many of the classical *bld* mutants, which are unable to erect an aerial mycelium under certain conditions, show altered DFO-mediated Fe utilization (Lambert *et al.*, 2014). The availability of Fe might also influence the Cu-dependent morphology pathway, given the presence of the Fe-containing haem group in DtpA. This thesis describes a range of new *bld* mutants, all of which are affected in Cu utilization and trafficking. Taken together, this implicates an essential role for metals in morphological differentiation. One question that remains to be answered is how Cu is sequestered and transported into the cell. The only known copper-acquisition compound in nature is Methanobactin, which is produced and secreted by the methanobacterium *Methylosinus trichosporum* (Kim *et al.*, 2004). Whether streptomycetes produce comparable molecules that can acquire copper remains to be discovered.

Future directions

Despite the various roles of CslA in morphogenesis the true identity of the produced glycan remains to be discovered. New bioinformatics tools confirm that CslA is a processive glycosyltransferase, which adds sugar moieties to the growing end of a linear polysaccharide without releasing the acceptor substrate (Chapter 6). The overall conformation and the fold of the active site of the protein are similar to those of the cellulose synthase BcsA of *Rhodobacter spaeroides* (Chapter 6). This shows that CslA combines the intracellular synthesis of a glycan directly with its transport through the cytoplasmic membrane. However, amino acid substitution of residues that interact with the sugar binding pocket or the growing glycan chain suggest an altered specificity of CslA compared to that of BcsA (Chapter 6).

In the direct vicinity of the *csIA-glxA* operon lie several genes that relate functionally to carbohydrate metabolism, including *csIZ*, for a glycosyl hydrolase of family 6 that encompasses mainly cellulases and cellobiohydrolases, *nagD* for a possible ribonucleotide monophosphatase, which are implicated in recycling UDP when liberated by the action of glycosyltransferases on UDP-activated sugars (Tremblay *et al.*, 2006), and SLI_3183 encoding a lytic polysaccharide monoxygenase (LPMO), which are enzymes known to target crystalline surfaces of polysaccharides. In Chapter 4 I showed that GlxA and CslA cooperate in the synthesis and modification of an extracellular glycan, which is likely composed of $\beta(1,3)$ or $\beta(1,4)$ glycosidic linkages based on calcofluor white staining assays. The best *in vitro* activity of GlxA was measured using glycoaldehyde as the substrate, which is the smallest molecule to contain both an aldehyde and a hydroxyl group (Chapter 4). Identification of polysaccharide substrates for CslZ, SLI_3183 and/or GlxA is required to further our understanding of the nature of the polymer produced, modified and degraded by the joint

action of these enzymes. Conversely, characterization of the polymer could lead to a better understanding of the chemical conversions performed by these enzymes.

Direct characterization of the glycan synthesized by CslA was hampered by the relative little amount that is produced in comparison to the abundance of peptidoglycan in the *Streptomyces* cell wall (Chapter 6). Use of a newly developed peptidoglycan-independent synthesis platform showed potential for characterization of bacterial glycans that are produced only in limited amounts in their endogenous (Gram-positive) hosts (Chapter 6). Preliminary data using this system indicated that the CslA polymer could be composed of glucose and/or *N*-acetylgalactosamine moieties (Chapter 6). The first step to fully characterize both the composition and the structure of the glycan would be to overproduce the glycan in this peptidoglycan-independent synthesis platform by increased expression of the *csIA-glxA* gene cluster using a strong promoter.

A major discovery described in this thesis is the importance of DtpA for development. Undoubtedly, work must be continued to better understand the precise function of this protein and the other described proteins involved in copper-dependent morphogenesis. Interestingly, the morphology of *sco* or *dtpA* deletion mutants shows new opportunities to manipulate bacterial growth in bioreactors by simply changing the concentration of Cu in the culture broth. Low levels of copper result in growth of a more dispersed mycelium, which probably results in faster growth and good enzyme production, while high levels of copper result in the formation of pellets, which will be beneficial for antibiotic production. The work presented in this thesis provides a foundation for the further research on the role of cell-surface components in controlling *Streptomyces* morphology. This is of fundamental importance for understanding the determinants of growth and development of this exciting multicellular model organism, and at the same time may help us to further optimize their exploitation for the industrial production of secondary metabolites and enzymes.

N

Nederlandse Samenvatting

De microbiële wereld bestaat uit miljoenen organismen met een prachtige verscheidenheid aan verschijningsvormen. Deze kunnen variëren van eencelligen, zoals gisten en vele bacterie soorten, tot ketens van cellen, zoals bij schimmeldraden, of grote meercellige gemeenschappen, zoals bacteriële biofilms, die je misschien kent van tandplak. Eén van de meest fascinerende groepen van bacteriën wordt gevormd door de streptomyceten. Deze bacteriën leven voornamelijk in de grond, waar ze zowel dood als levend organisch materiaal kunnen koloniseren. In tegenstelling tot de meeste andere bacteriën groeien streptomyceten door het vormen van draadvormige structuren, die hyfen worden genoemd. Deze hyfen vertakken zich tot een zogenaamd mycelium, een complex netwerk van draden. De filamenteuze groei stelt de bacterie in staat om bodem- en plantenmateriaal binnen te groeien en voedingsstoffen op te nemen die anders onbereikbaar zijn. Wanneer er een tekort aan voedingsstoffen ontstaat, schakelt de bacterie over tot het vormen van een voortplantingsmycelium. Dit mycelium steekt recht uit de grond de lucht in en zorgt ervoor dat uiteindelijke miljoenen sporen gevormd worden die bestand zijn tegen de verslechterde omstandigheden.

De vorming van het voortplantingsmycelium is nauw gekoppeld aan de productie van een groot arsenaal aan antibiotica die dienen om de *Streptomyces* kolonie te verdedigen tegen predatie van andere microben. Vanuit toegepast oogpunt zijn wij voornamelijk geïnteresseerd in streptomyceten vanwege hun vermogen tot het synthetiseren van antibiotica en vele andere zogenaamde secundaire metabolieten die gebruikt kunnen worden in de geneeskunde, biotechnologie en landbouw, zoals middelen tegen tumoren, schimmels en parasieten (Hopwood, 2007). Daarnaast produceren deze bacteriën een groot aantal hydrolytische enzymen, die gebruikt worden in de industrie voor bijvoorbeeld de productie van biobrandstoffen, papier of textiel (Chater *et al.*, 2010). Optimale groei en productie in bioreactoren wordt echter bemoeilijkt door de filamenteuze groeivorm van de bacterie, die leidt tot de vorming van complexe myceliumstructuren. Verschillende macromoleculen die zich op het celoppervlak bevinden zijn belangrijk voor de totstandkoming van de morfologie van deze bacterie. In dit proefschrift heb ik de vorming van een aantal van deze externe macromoleculen en hun invloed op *Streptomyces* morfologie beschreven. Hierbij ligt de nadruk op de productie van een glycaan (suikerpolymeer) door genen van het *csla-glxA* cluster. De kennis opgedaan uit mijn werk kan leiden tot verbeterde productie van secundaire metabolieten en enzymen door streptomyceten.

Heterogeniteit in Streptomyces pellets

Groei van streptomyceten in bioreactoren resulteert in de vorming van verweven klompjes van hyfen, genaamd pellets. *Streptomyces* pellets kunnen in diameter meer dan een millimeter groot worden en zijn daarmee te groot voor analyse met reguliere flow cytometrie. In hoofdstuk 3 werd voor de eerste keer de Complex Object Parametric Analyser and Sorter (COPAS) gebruikt voor het kwantitatief analyseren van pellet groottes van verschillende streptomyceten. Interessant is de observatie dat twee populaties van pellets in vloeibare culturen van *Streptomyces lividans*, *Streptomyces coelicolor*, *Streptomyces scabies* en *Streptomyces griseus* aanwezig zijn, die verschillen in grootte en waarschijnlijk ook in functie (zie onderstaand). De gemiddelde grootte van deeltjes horend bij de populatie van kleine mycelia had een constante gemiddelde diameter van ongeveer 260 μm . Daarentegen toonden de deeltjes horend bij de populatie van grote mycelia meer variatie in grootte, met de grootste gemiddelde diameter van 557 μm voor de pellets van *S. scabies*. De diameter van de populatie van kleine mycelia van *S. coelicolor* werd niet beïnvloed door leeftijd van de culture of medium compositie, terwijl dit wel van invloed was op de populatie van grote pellets. Daarmee suggereert onze data dat de pellet diameter voornamelijk in de populatie van grote pellets afhankelijk is van externe parameters, zoals de samenstelling van het groeimedium, pH, viscositeit, oppervlakte spanning, roersnelheid, opgeloste zuurstof concentraties, temperatuur en de grootte en samenstelling van het inoculum (Tough and Prosser, 1996; Celler *et al.*, 2012; van Dissel *et al.*, 2014).

Een proteoom vergelijking tussen de kleine en grote *S. coelicolor* pellets liet zien dat de eiwitten die betrokken zijn bij het maken van antibiotica in hogere mate aanwezig zijn in de populatie van grote pellets (Hoofdstuk 3). Dit komt overeen met het concept dat grote mycelium structuren beter geschikt zijn voor antibiotica productie (Martin and Bushell, 1996). Daarnaast waren er relatief meer stress-gerelateerde eiwitten aanwezig in de grote pellets, wat wellicht te verklaren is door de verminderde beschikbaarheid van zuurstof of nutriënten in de kern van de grote pellets. Deze stress signalen zouden wellicht schakelaars kunnen zijn die leiden tot de vorming van antibiotica. Deze stress-gerelateerde eiwitten omvatten de respons regulator SCO0204 en het universele stress eiwit USP (SCO0200), dat deel is van het SCO0204 regulon (Urem *et al.* manuscript in voorbereiding). Lage niveaus van zuurstof of nutriënten in de kern van deze grotere mycelia kunnen mogelijk groei en primair metabolisme remmen. Daarmee in overeenstemming bevatten de kleine pellets naar verhouding meer eiwitten die betrokken zijn bij actieve groei. Zo zijn er aanmerkelijk meer eiwitten aanwezig die functioneren in DNA metabolisme en de organisatie van het DNA. Aangezien kleine mycelia vermoedelijk sneller groeien dan grote pellets zijn ze meer geschikt voor de industriële productie van enzymen. Dit zou consistent zijn met de toename in groeisnelheid en enzymproductie die is waargenomen bij het stimuleren van het SsgA eiwit, dat betrokken is bij celdelings activatie, leidend tot fragmentatie (van Wezel *et al.*,

2006).

Pellets groeien door middel van hyfen die zich verlengen aan de hyfetoppen, en het vormen van vertakkingen, terwijl fragmentatie en afbraak leidt tot een afname in hun grootte. Pellets zijn heterogeen in grootte, omdat deze processen gelijktijdig plaatsvinden in een bioreactor. In filamenteuze schimmels ontstaan pellets van origine uit geaggregeerde sporen en kiemen (Lin *et al.*, 2008), wat impliceert dat oppervlakte eigenschappen van sporen en hyfen de pellet grootte beïnvloeden (van Veluw *et al.*, 2013). In streptomyceten zijn de uitgescheiden chaplin eiwitten bekend om de decoratie van sporen met een hydrofobe laag (Claessen *et al.*, 2003; Elliot *et al.*, 2003) en produceert het cellulose synthase-achtige eiwit CslA een extracellulair glycaan aan de hyfetoppen. Net als de chaplins is ook dit glycaan een onderdeel van het oppervlak van sporen (Xu *et al.*, 2008). Deletie van *csIA* of de genen die coderen voor de chaplins resulteert in een afname in de gemiddelde grootte van mycelia, maar heeft geen effect op de culture heterogeniteit (Hoofdstuk 3). Heterogeniteit in grootte werd ook geobserveerd als cultures werden beënt met voorgegroeiende mycelia of synchronoon ontkiemde sporen. Dit resultaat toont aan dat net als bij filamenteuze schimmels, macromoleculen op het celoppervlak cruciaal zijn voor pellet architectuur in streptomyceten, alhoewel hun invloed in aggregatie van sporen en kiemen niet de enige factor is die leidt tot de vorming van twee populaties pellets met verschillende groottes (Hoofdstuk 3). Hieruit valt af te leiden dat andere factoren betrokken zijn bij de totstandkoming van de heterogeniteit, met als mogelijke kandidaat de sterke wrijvingskrachten die op de pellets werken en die leiden tot fragmentatie.

Structurele celoppervlak componenten betrokken in pellet architecture

Pellet integriteit wordt op de proef gesteld door de sterke wrijving in bioreactors. Dit is met name het geval in pellets die een proces van geprogrammeerde celdood ondergaan, dat leidt tot de gedeeltelijke afbraak van bestaande hyfen in het centrale deel van deze structuren (Rioseras *et al.*, 2014). Hiervoor kan gecompenseerd worden met de synthese van een aantal glycanen, zoals die geproduceerd door CslA, die bijdragen aan pellet integriteit door het vormen van een hechtende, extracellulaire matrix. Recentelijk is ontdekt dat het *mat* gen cluster noodzakelijk is voor pellet groei van streptomyceten (van Dissel *et al.*, 2015). Homologie van het *mat* cluster met het *ica* operon van *Staphylococcus* spp. suggereert dat het codeert voor een polysaccharide synthese complex dat een polysaccharide produceert van β -(1,6)-gelinkte *N*-acetylglucosamine moleculen (van Dissel *et al.*, 2015). Een derde gesecreteerd polysaccharide dat mogelijk betrokken is bij pellet integriteit is hyaluronzuur (Kim and Kim, 2004), een glucosaminoglycaan bestaand uit D-glucuronzuur en *N*-acetyl-D-glucosamine, die afwisselend met elkaar verbonden zijn via β (1,4) en β (1,3) glycoside bindingen. Behandeling van pellets met hyaluronidase maakt de structuren erg kwetsbaar (Kim and Kim, 2004), alhoewel de zuiverheid en specificiteit van het gebruikte

enzym preparaat onbekend is. Het SLI_5327-SLI_5330 gen cluster is een kandidaat voor de synthese van hyaluronzuur in *S. lividans*. Deletie van dit gen cluster had echter geen groot effect op pellet morfologie onder de geteste condities (onze niet gepubliceerde data).

Een extracellulaire pellet matrix kan naast glycanen ook bestaan uit andere macromoleculen. Veel biofilm-vormende bacteriën secreteren DNA dat bijdraagt aan biofilm architectuur (Whitchurch *et al.*, 2002). Evenzo is gesuggereerd dat extracellulair DNA betrokken is bij het vormen van *Streptomyces* pellets (Kim and Kim, 2004). Matrices bevatten bovendien vaak hechtende eiwitten, inclusief amyloid-vormende eiwitten zoals curli in *Escherichia coli* en TasA in *Bacillus subtilis* (López *et al.*, 2010). Het effect op *Streptomyces* pellet morfologie veroorzaakt door deletie van HyaS, een enzym met amine oxidase activiteit dat stevige fusie-achtige contacten induceert tussen substraat hyfen (Koebsch *et al.*, 2009), of de amyloid-vormende chaplin eiwitten (Hoofdstuk 3) illustreert de overeenkomsten in extracellulaire matrix tussen pellets en bacteriële biofilms.

Tot nu toe is het onduidelijk hoe al deze extracellulaire componenten samenwerken in het opbouwen en waarborgen van pellet integriteit. Aangezien een samenwerking tussen de chaplins en het cellulose-achtige glycaan geproduceerd door CslA is aangetoond in de hechting van hyfen aan hydrofobe oppervlakten (de Jong *et al.*, 2009), is het aannemelijk dat dit ook plaatsvindt in het proces van pelletvorming. Daarnaast zijn interacties tussen verschillende polysachariden in de pellet matrix gemakkelijk voor te stellen. Zo is bijvoorbeeld aangetoond dat vezelassociatie en kristalliniteit van het cellulose netwerk geproduceerd door *Glucanoacetobacter xylinus* stammen beïnvloed worden door de aanwezigheid van polysachariden die niet bestaan uit cellulose (Fang and Catchmark, 2015). Daarnaast zijn verschillende covalente bindingen aanwezig tussen diverse polysachariden in het arabinogalactaan-peptidoglycaan complex in de mycobacteriële celenvlop (Crick *et al.*, 2001). Omdat het glycaan geproduceerd door CslA direct geproduceerd wordt in de groeiende hyfetop (Chapter 4; Xu *et al.*, 2008), kan deze dienen als een fundering voor de efficiënte organisatie van andere macromoleculen in de extracellulaire matrix. Meer experimenteel bewijs is echter nodig om dit te testen.

Structurele celoppervlak componenten in groei van een luchtmycelium

Moleculen op het celoppervlak zijn ook belangrijk voor morfologische differentiatie bij groei op een vaste ondergrond. Vegetatieve hyfen van streptomyceten worden langer door extensie van de hyfetop, terwijl nieuw hyfen ontstaan door zijwaartse vertakkingen. Hydrostatische druk op de extensie zones drijft het proces van verlenging in de hyfetop, waar ook de celwand constant wordt geherstructureerd (Prosser and Tough, 2008). Dit zorgt ervoor dat een groeiende hyfetop relatief zwak is in vergelijking met de door peptidoglycaan omringde hyfe. Veel eiwitten functioneren samen in het tip-organisatie centrum (TIPOC)

om cel integriteit te waarborgen tijdens groei (Holmes *et al.*, 2013). Eén van de cruciale eiwitten is het polair gelokaliseerde eiwit DivIVA dat een essentiële rol speelt in topgroei door het coördineren van het celwand synthese proces (Flårdh, 2003; Flårdh *et al.*, 2012). Eiwit-eiwit interacties tonen aan dat DivIVA bindt aan CslA, wat suggereert dat de glycaan geproduceerd door CslA noodzakelijk is tijdens celwand synthese. Haar vermeende functie is de versterking van groeiende hyfetoppen (Xu *et al.*, 2008; Chater *et al.*, 2010). Alhoewel deletie mutanten van *csIA* in staat zijn een vegetatief mycelium te bouwen, vereist de vorming van een sterk luchtmycelium de aanwezigheid van CslA (Chapter 4, (Xu *et al.*, 2008)). Onmiddellijk na de aanzet tot luchtmycelium formatie daalt de expressie van *csIA* drastisch (Liman *et al.*, 2013).

In dit proefschrift is ook de rol van de radicale koper-oxidase GlxA uitgebreid bestudeerd. Het *glxA* gen ligt onmiddellijk achter het *csIA* gen in een operon dat sterk is geconserveerd in streptomyceten (Liman *et al.*, 2013). Zowel CslA als GlxA zijn noodzakelijk voor de kleuring van hyfetoppen met de glycaan-bindende kleurstof calcofluor wit. Dit suggereert dat GlxA samenwerkt met CslA in de synthese, verankering en/of modificatie van het glycaan aan de groeiende hyfetoppen (Hoofdstuk 4). Dit wordt sterk ondersteund door de observatie dat *glxA* deletie mutanten niet in staat zijn een luchtmycelium te produceren op vaste ondergrond en ook geen pellets vormen in vloeibare cultures, maar groeien als een open netwerk van hyfen, zoals ook was aangetoond voor *csIA* deletie mutanten (Hoofdstuk 4 en 5, (Xu *et al.*, 2008; Liman *et al.*, 2013)). Daarnaast hechten zowel *csIA* als *glxA* mutanten verminderd aan hydrofobe oppervlakken in staande vloeibare cultures (Hoofdstuk 6). Kortom, de *glxA* mutant gedraagt zich vergelijkbaar als een *csIA* mutant onder verschillende omstandigheden. De kristal structuur van GlxA bevat tunnels die groot genoeg zijn voor een polysaccharide om van het eiwitoppervlak helemaal tot aan het actieve centrum van het eiwit te rijden (Hoofdstuk 4). We stellen ons hierbij de mogelijkheid voor dat het glycaan geproduceerd door CslA in één van de tunnels wordt geleid, georiënteerd en geoxideerd wordt in de substraat bindingsplaats, en vervolgens wordt vrijgelaten door een andere tunnel. Opmerkelijk genoeg worden er wel kleine verschillen in ontwikkeling tussen de *csIA* en *glxA* mutant waargenomen onder specifieke omstandigheden. Zo is de *csIA* mutant bijvoorbeeld vertraagd in de groei van een luchtmycelium op MYM medium, terwijl de *glxA* mutant dan helemaal geen luchtmycelium meer kan maken (Hoofdstuk 6). Dit wijst erop dat GlxA een CslA-onafhankelijke rol heeft in ontwikkeling, wat in overeenstemming is met de aanwezigheid van een tweede promotor in de *csIA* coderende sequentie, die de transcriptie van het *glxA* gen kan aansturen onafhankelijk van *csIA* (Liman *et al.*, 2013). Aan de andere kant is het fenotype van de *csIA* mutant juist ernstiger dan dat van de *glxA* mutant op media met een relatief lage osmolariteit, wat suggereert dat onder die omstandigheden GlxA niet essentieel is voor het functioneren van CslA (Liman *et al.*, 2013).

Zoals besproken in hoofdstuk 2 is de vorming van een luchtmycelium ook sterk afhankelijk van

de secretie van het lantibioticum-achtige peptide SapB en de chaplin eiwitten, die allebei als oppervlakte-actieve stoffen te werk gaan aan de verlaging van de oppervlaktetenspanning om groei van een luchtmycelium mogelijk te maken. Samen met de rodlin eiwitten hebben de chaplin eiwitten een tweede rol in ontwikkeling in de samenstelling van een hydrofobe laag rondom de luchthyfen en sporen. De mogelijkheid om de lucht in te groeien is afhankelijk van drie cruciale factoren: de turgor druk in de hyfen, de rigiditeit van de celwand en de oppervlaktetenspanning op het grensvlak van het groeimedium en de lucht. Deletie van *csIA* of *glxA* heeft waarschijnlijk effect op de rigiditeit van de vegetatieve hyfe-wand, deletie van de chaplin genen of het *ram* gen cluster (verantwoordelijk voor SapB biosynthese) verhindert de benodigde verlaging in oppervlakte spanning, terwijl veranderingen in medium compositie invloed hebben op alle drie de factoren. Het combineren van deze effecten, die ten grondslag liggen aan luchtgroei kan verhelderen waarom een blokkade in de ontwikkeling van een *csIA* mutant (minder sterke hyfen) gered kan worden door de toevoeging van chaplins (waarbij de oppervlaktetenspanning verder verlaagd wordt, Xu *et al.*, 2008), waarom een verlaging van de osmolariteit (waarbij de turgor druk verhoogt wordt en de oppervlakte spanning (licht) verlaagd) een *glxA* mutant (minder sterke hyfen) in staat stelt om een luchtmycelium te groeien (Liman *et al.*, 2013), waarom SapB niet essentieel is op media met een lage osmolariteit (waarop hyfen meer turgordruk kunnen opbouwen) en waarom *csIA* deletie mutanten een luchtmycelium kunnen bouwen op sommige media, maar niet op andere (Hoofdstuk 4 en 5). Daarbij lijken de structurele celwand componenten die betrokken zijn bij de integriteit van hyfen ook bij te dragen aan de groei van een luchtmycelium, terwijl anderen, zoals HyaS en het polysaccharide geproduceerd door het *mat* cluster, enkel belangrijk zijn voor pellet vorming.

De rol van koper in morfogenese

S. lividans toont een onderscheidende afhankelijkheid van koper (Cu) om volledige morfologische ontwikkeling te initiëren. Het werk in dit proefschrift toont dat GlxA het belangrijkste extracellulaire koperenzym is dat deze behoefte verklaard. Cu speelt een onmisbare rol in de activiteit van GlxA omdat het één van de twee redox centra vormt in het actieve gedeelte van het eiwit. Het andere redox centrum wordt gevormd door een dichtbijgelegen covalente verbinding tussen een Cysteïne en één van de Cu-coördinerende Tyrosines (Hoofdstuk 4). *In vitro* data toont aan dat de Tyr-Cys verbinding alleen gevormd wordt in de aanwezigheid van Cu (Hoofdstuk 5). Door de gecombineerde redox centra heeft GlxA toegang tot drie oxidatietoestanden: Cu(I)-Tyr-Cys (gereduceerd), Cu(II)-Tyr-Cys (half gereduceerd) en Cu(II)-Tyr-Cys• (volledig geoxideerd). GlxA zou daarom in staat moeten zijn om de twee-elektron oxidatie van een substraat te katalyseren (Hoofdstuk 4).

De GlxA kristalstructuur toont een dekselachtig domein dat beide redox centra en het actieve deel met de substraat bindingsplaats beschermt (Hoofdstuk 4). Dit roept echter de

vraag op hoe GlxA Cu verkrijgt en inbouwt. Middels Western Blot analyse kan de verwerving van Cu door GlxA gedetecteerd worden door een verandering in electroforetische mobiliteit wanneer de Cu-afhankelijke Tyr-Cys verbinding wordt gevormd (Hoofdstuk 5). Nadere analyse toont dat GlxA maturatie *in vivo* afhankelijk is van de extracytoplasmatische Cu chaperonne Sco. Sco was al bekend voor het leveren van Cu aan het actieve deel van een aa_3 -type cytochrome c oxidase (CcO). Omdat een *cco* mutant zich normaal ontwikkeld, kon het gebrek aan luchtmycelium vorming van de *sco* mutant niet verklaard worden door haar rol in Cu levering aan CcO. (Blundell *et al.*, 2013; Blundell *et al.*, 2014). Het idee dat GlxA een tweede doel is van Sco is in overeenstemming met de identieke defecten van beide mutanten, inclusief het onvermogen om luchthyfen te vormen op vaste media en de afwezigheid van pellets in vloeibare cultures (Hoofdstuk 5). Alleen wanneer koper aanwezig is in hoge concentraties zal GlxA niet afhankelijk zijn van Sco, waardoor een *sco* deletie mutant dan zowel een luchtmycelium als kleine pellets kan vormen (Hoofdstuk 5).

Op haar beurt ontvangt Sco een Cu ion van de extracytoplasmatische Cu chaperonne ECuC via een eenrichtingsproces (Blundell *et al.*, 2014). De overdracht vindt plaats in de Cu(I) vorm van het ion, maar de oxidatiestaat na overdracht is onbekend (Blundell *et al.*, 2014). Interessant is dat de overdracht van Sco naar CcO de Cu(II) oxidatietoestand van het metaal vereist (Blundell *et al.*, 2013), terwijl de benodigde oxidatietoestand voor opname in GlxA niet bekend is. Zowel de morfologische defecten als de verminderde CcO activiteit zijn minder uitgesproken in de *ecuc* mutant vergeleken met de *sco* mutant, wat suggereert dat Sco Cu(II) direct kan vergaren uit de omgeving (Hoofdstuk 5). ECuC is waarschijnlijk wel als Cu(I) donor belangrijk voor een efficiënte lading van Sco, gevolgd door de actie van een oxiderend molecuul of eiwit om Cu(II) te creëren. De natuur van dit molecuul of eiwit is onbekend.

Sco (SLI_4214) en *ecuc* (SLI_4213) zijn de eerste twee genen van een operon dat ook een gen bevat dat codeert voor een mogelijk Cu transporteiwit (SLI_4212) als ook voor *dtpA* (SLI_4211) dat codeert voor een Dyp-type peroxidase (Hoofdstuk 5). Opmerkelijk is dat deletie van *dtpA* een morfologische ontwikkeling blokkeert, wat samengaat met de afwezigheid van GlxA maturatie (Hoofdstuk 5). De morfologische defecten van *dtpA* mutanten kunnen gecompenseerd worden door hoge concentraties Cu, zoals ook het geval was voor de *sco* mutant (Hoofdstuk 5). Over de fysiologische rol van Dyp-type peroxidases is nog veel onduidelijk, alhoewel ze wijdverspreid voorkomen in schimmels en bacteriën (Singh and Eltis, 2015). Een mogelijkheid zou zijn dat GlxA en DtpA samenwerken in een gekoppeld proces waarbij DtpA GlxA activeert of stabiliseert via eiwit-eiwit interacties, of door verwijdering van H_2O_2 geproduceerd door GlxA. Zo'n samenwerking tussen een verwante peroxidase en oxidase is eerder waargenomen in sommige schimmels (Hamilton *et al.*, 1978; Kersten, 1990; Takano *et al.*, 2010). Wij toonden aan dat DtpA als peroxidase kan werken in de aanwezigheid van actief GlxA *in vitro* (Hoofdstuk 5). *In vivo* kunnen deze eiwitten

in potentie ook samenwerken omdat GlxA een extracellulair membraan-geassocieerd eiwit is (Hoofdstuk 4), terwijl DtpA wordt uitgescheiden in het extracellulaire milieu door het twin-arginine translocatie proces (Hoofdstuk 5). Dit eiwittransport is vooral bekend doordat het gevouwen eiwitten kan uitscheiden, voornamelijk als deze een cofactor bevatten zoals de haem groep in DtpA. Op dit moment hebben we geen aanwijzingen voor een sterke fysieke interactie tussen GlxA en DtpA, en ook verhoogt DtpA niet de activiteit van GlxA in een peroxidase-gekoppelde test in vergelijking met de regulier gebruikte mierikswortel peroxidase (Hoofdstuk 5).

Een andere mogelijkheid is dat DtpA functioneert in het Cu transport richting GlxA. We kunnen speculeren dat DtpA het oxiderende eiwit is dat Cu(II) creëert van Sco-gebonden Cu(I). Dit zou niet alleen verklaren waarom GlxA maturatie verstoord is op een vergelijkbare manier als bij de *sco* mutant (Hoofdstuk 5), maar ook waarom de CcO activiteit verminderd is in een *dtpA* mutant in *S. coelicolor* (Fujimoto *et al.*, 2012). Sco eiwitten zijn bekend om zowel Cu(I) als Cu(II) te kunnen binden en het is niet onwaarschijnlijk dat Cu overdracht naar accepterende eiwitten afhankelijk is van de oxidatie staat van het metaal (Banci *et al.*, 2007). Een rol voor DtpA in het oxideren van metaal ionen zou erg gelijkend zijn op de functie van de Dyp-type peroxidase EfeB, die Fe(II) oxideert tot Fe(III) voor cellulaire opname (Miethke *et al.*, 2013).

Cu is niet het enige redox-actieve metaal dat belangrijk is in de morfologie van streptomyceten. Vooral de rol van ijzer (Fe) heeft veel aandacht gekregen, omdat dit metaal een belangrijk rol speelt in tal van huishoud-functies, zoals DNA replicatie, eiwit synthese en ademhaling (Cornelis and Andrews, 2010; Lambert *et al.*, 2014). Veel microben secreteren ijzer-chelerende moleculen genaamd sideroforen, die belangrijk zijn voor het verkrijgen van het slecht oplosbare Fe(III). Recentelijk is aangetoond dat de siderofoor desferrioxamine (DFO) essentieel is voor de groei van *S. coelicolor* op media met lage Fe niveaus (Lambert *et al.*, 2014). Daarnaast blijken veel klassieke *bld* mutanten, die niet in staat zijn een luchtmycelium op te richten onder bepaalde condities, verstoord in hun ijzerhuishouding gerelateerd aan hun onvermogen om DFO te maken (Lambert *et al.*, 2014). De beschikbaarheid van Fe kan ook invloed hebben op het Cu-afhankelijke morfologie proces gezien de aanwezigheid van het Fe-bevattende haem in DtpA. Dit proefschrift beschrijft een aantal nieuwe *bld* mutanten die allen aangedaan zijn in Cu gebruik en transport. Gezamenlijk impliceert dit een essentiële rol van metalen in morfologische verandering. Een vraag die nog beantwoord moet worden is hoe Cu wordt verzameld en getransporteerd naar de cel. De enige bekende Cu-verwervende stof in de natuur is Methanobactin, die wordt geproduceerd en uitgescheiden door de methaanbacterie *Methylosinus trichosporum* (Kim *et al.*, 2004). Of streptomyceten ook vergelijkbare Cu verwervende moleculen produceren is nog onbekend.

Toekomstig onderzoek

Ondanks de vele rollen van CslA in morfologie moet de ware identiteit van het geproduceerde glycaan nog ontdekt worden. *In silico* analyses bevestigen dat CslA een glycaan synthase is, die suikers toevoegt aan het groeiende uiteinde van een lineair polysaccharide zonder daarbij het accepterende substraat los te laten (Hoofdstuk 6). De algehele opbouw en vouwing van het actieve deel van het eiwit zijn vergelijkbaar met die van de cellulose synthase BcsA van *Rhodobacter spaeroides* (Hoofdstuk 6). Dit toont aan dat CslA de intracellulaire synthese van een glycaan combineert met het transport ervan door het cytoplasmatisch membraan. Echter, de veranderde aminozuren die interactie aangaan met de suikerbindende holte of de groeiende glycaanketen suggereert dat CslA een veranderde specificiteit kan hebben als BcsA (Hoofdstuk 6).

In de directe omgeving van het *csIA-glxA* operon ligt een aantal genen dat functioneel gerelateerd is aan koolwaterstof metabolisme, waaronder *cslZ* voor een glycosyl hydrolase van familie 6 die vooral cellulases en cellobiohydrolases bevat, *nagD* voor een mogelijke ribonucleotide monofosfatase, die betrokken kan zijn in het recyclen van UDP na vrijlating van UDP-geactiveerde suikers door de actie van glycosyltransferases (Tremblay *et al.*, 2006), en SLI_3183 voor een lytische polysaccharide mono-oxygenase (LPMO), wat enzymen zijn die zich richten op kristallijne oppervlakten van polysacchariden. In hoofdstuk 4 toonde ik aan dat CslA en GlxA samenwerken in de synthese en modificatie van een extracellulair glycaan, dat waarschijnlijk bestaat uit $\beta(1,3)$ of $\beta(1,4)$ glycoside bindingen gebaseerd op calcofluor wit kleuringen. De beste *in vitro* activiteit van GlxA is gemeten met glycoaldehyde als substraat, wat het kleinste molecuul is dat zowel een aldehyde als een hydroxyl groep heeft (Hoofdstuk 4). Identificatie van polysaccharide substraten voor CslZ, SLI_3183 en/of GlxA is van belang om meer kennis te verkrijgen over het polymeer dat geproduceerd, aangepast en afgebroken wordt door de gezamenlijke actie van deze enzymen. Andersom zal karakterisatie van het polymeer leiden tot meer kennis van de chemische omzettingen uitgevoerd door deze enzymen.

Directe karakterisatie van de glycaan gesynthetiseerd door CslA wordt bemoeilijkt door de relatief kleine hoeveelheid die geproduceerd wordt in vergelijking met de overvloed aan peptidoglycaan in de *Streptomyces* celwand (Hoofdstuk 6). Gebruik van een nieuw ontwikkeld peptidoglycaan-onafhankelijk synthese platform toont de potentie voor karakterisatie van bacteriële glycanen die slechts geproduceerd worden in kleine hoeveelheden door het hun oorspronkelijke organisme (Hoofdstuk 6). De eerste voorlopige resultaten laten zien dat het CslA polymeer zou kunnen bestaan uit glucose en/of *N*-acetylgalactosamine groepen (Hoofdstuk 6). De volgende stap tot volledige karakterisatie van zowel de samenstelling als de structuur van het glycaan zou de overproductie ervan zijn in het peptidoglycaan-onafhankelijke synthese platform, door de expressie van het *csIA-glxA* gen cluster te

verhogen.

Een grote ontdekking beschreven in dit proefschrift is het belang van DtpA in de biologie van *Streptomyces*. Ongetwijfeld moet het werk voortgezet worden om de precieze functie van dit eiwit en de andere beschreven eiwitten betrokken in Cu-afhankelijke morfogenese beter te begrijpen. De morfologie van de *sco* en *dtpA* deletie mutanten toont interessante nieuwe mogelijkheden om bacteriële groei in bioreactoren te manipuleren door simpelweg de Cu concentratie in de culture aan te passen. Lage niveaus van Cu resulteren in groei van een minder dicht hyfen netwerk, wat waarschijnlijk leidt tot snellere groei en goede enzym productie, terwijl hoge niveaus van Cu resulteren in de vorming van pellets, die voordelig zijn voor de productie van antibiotica. Het werk beschreven in dit proefschrift vormt de basis voor verder onderzoek naar de rol van macromoleculen op het celoppervlak en de manipulatie hiervan voor het controleren van de morfologie. Dit is van fundamenteel belang voor het begrijpen van de bepalende factoren die ten grondslag liggen aan groei en ontwikkeling van dit bijzondere modelorganisme, en voor het verbeteren van streptomyceten voor industriële productie van secundaire metabolieten en enzymen.

R

References

- Alteri, CJ, Xicohtencatl-Cortes, J, Hess, S, Caballero-Olín, G, Girón, JA, and Friedman, RL (2007) *Mycobacterium tuberculosis* produces pili during human infection. *Proc Natl Acad Sci U S A* **104**: 5145–50.
- Anné, J, Maldonado, B, Van Impe, J, Van Mellaert, L, and Bernaerts, K (2012) Recombinant protein production and streptomycetes. *J Biotechnol* **158**: 159–67.
- Antholine, W (2005) Low frequency EPR of Cu²⁺ in proteins. In *Biological Magnetic Resonance*. Eaton, SR, Eaton, GR, and Berliner, LJ (eds). Springer-Verlag, New York. pp. 417–454.
- Arends, IWCE, Gamez, P, and Sheldon, RA (2006) Green oxidation of alcohols using biomimetic Cu complexes and Cu enzymes as catalysts. *Adv Inorg Chem* **58**: 235–279.
- Avigad, G, Amaral, D, Asensio, C, and Horecker, BL (1962) The D-galactose oxidase of *Polyporus circinatus*. *J Biol Chem* **237**: 2736–43.
- Bagos, PG, Nikolaou, EP, Liakopoulos, TD, and Tsigirig, KD (2010) Combined prediction of Tat and Sec signal peptides with hidden Markov models. *Bioinformatics* **26**: 2811–7.
- Bagos, PG, Tsigirig, KD, Liakopoulos, TD, and Hamdrakas, SJ (2008) Prediction of lipoprotein signal peptides in Gram-positive bacteria with a Hidden Markov Model. *J Proteome Res* **7**: 5082–93.
- Banci, L, Bertini, I, Cavallaro, G, and Rosato, A (2007) The functions of Sco proteins from genome-based analysis. *J Proteome Res* **6**: 1568–1579.
- Barnes, AMT, Ballering, KS, and Leibman, RS (2012) *Enterococcus faecalis* produces abundant extracellular structures. *mBio* **3**: 1–9.
- Baron, AJ, Stevens, C, Wilmot, C, Seneviratne, KD, Blakeley, V, Dooley, DM, et al. (1994) Structure and mechanism of galactose oxidase. The free radical site. *J Biol Chem* **269**: 25095–105.
- Battye, TGG, Kontogiannis, L, Johnson, O, Powell, HR, and Leslie, AGW (2011) iMOSFLM: a new graphical interface for diffraction-image processing with MOSFLM. *Acta Crystallogr D Biol Crystallogr* **67**: 271–81.
- Bekker, C de, Veluw, GJ van, Vinck, A, Wiebenga, LA, and Wösten, HAB (2011) Heterogeneity of *Aspergillus niger* microcolonies in liquid shaken cultures. *Appl Environ Microbiol* **77**: 1263–7.
- Bendtsen, JD, Nielsen, H, Widdick, D, Palmer, T, and Brunak, S (2005) Prediction of twin-arginine signal peptides. *BMC Bioinformatics* **6**: 167.
- Bentley, SD, Chater, KF, Cerdeño-Tárraga, A-M, Challis, GL, Thomson, NR, James, KD, et al. (2002) Complete genome sequence of the model actinomycete *Streptomyces coelicolor* A3(2). *Nature* **417**: 141–147.
- Berardo, C Di, Capstick, DS, Bibb, MJ, Findlay, KC, Buttner, MJ, and Elliot, MA (2008) Function and redundancy of the chaplin cell surface proteins in aerial hypha formation, rodlet assembly, and viability in *Streptomyces coelicolor*. *J Bacteriol* **190**: 5879–5889.
- Bereman, RD, and Kosman, DJ (1977) Stereoelectronic properties of metalloenzymes. 5. Identification and assignment of ligand hyperfine splittings in the electron spin resonance spectrum of galactose oxidase. *J Am Chem Soc* **99**: 7322–5.

References

- Berliner, LJ, Khrantsov, V, Fujii, H, and Clanton, TL (2001) Unique *in vivo* applications of spin traps. *Free Radic Biol Med* **30**: 489–99.
- Berner, I, Konetschny-Rapp, S, Jung, G, and Winkelmann, G (1988) Characterization of ferrioxamine E as the principal siderophore of *Erwinia herbicola* (*Enterobacter agglomerans*). *Biol Met* **1**: 51–56.
- Bewick, MW, Williams, ST, and Veltkamp, C (1976) Growth and ultrastructure of *Streptomyces venezuelae* during chloramphenicol production. *Microbios* **16**: 191–9.
- Bibb, MJ, Domonkos, A, Chandra, G, and Buttner, MJ (2012) Expression of the chaplin and rodlin hydrophobic sheath proteins in *Streptomyces venezuelae* is controlled by σ^{BldN} and a cognate anti-sigma factor, RsbN. *Mol Microbiol* **84**: 1033–49.
- Bierman, M, Logan, R, O'Brien, K, Seno, ET, Rao, RN, and Schoner, BE (1992) Plasmid cloning vectors for the conjugal transfer of DNA from *Escherichia coli* to *Streptomyces* spp. *Gene* **116**: 43–9.
- Blake, C, and Serpell, L (1996) Synchrotron X-ray studies suggest that the core of the transthyretin amyloid fibril is a continuous beta-sheet helix. *Structure* **4**: 989–998.
- Blanco, LP, Evans, ML, Smith, DR, Badtke, MP, and Chapman, MR (2012) Diversity, biogenesis and function of microbial amyloids. *Trends Microbiol* **20**: 66–73.
- Blundell, KLIM, Hough, MA, Vijgenboom, E, and Worrall, JAR (2014) Structural and mechanistic insights into an extracytoplasmic copper trafficking pathway in *Streptomyces lividans*. *Biochem J* **459**: 525–38.
- Blundell, KLIM, Wilson, MT, Svistunenko, DA, Vijgenboom, E, and Worrall, JAR (2013) Morphological development and cytochrome c oxidase activity in *Streptomyces lividans* are dependent on the action of a copper bound Sco protein. *Open Biol* **3**: 120163.
- Boersema, PJ, Raijmakers, R, Lemeer, S, Mohammed, S, and Heck, AJR (2009) Multiplex peptide stable isotope dimethyl labeling for quantitative proteomics. *Nat Protoc* **4**: 484–494.
- Bokhove, M, Claessen, D, De Jong, W, Dijkhuizen, L, Boekema, EJ, and Oostergetel, GT (2013) Chaplins of *Streptomyces coelicolor* self-assemble into two distinct functional amyloids. *J Struct Biol* **184**: 301–9.
- Bougault, C, Hediger, S, and Simorre, J-P (2012) Solid-state NMR of the bacterial cell wall. In *Bacterial Glycomics: Current Research, Technology and Applications*. Horizon Scientific Press, p. 270.
- Breton, C, Snajdrová, L, Jeanneau, C, Koca, J, and Imberty, A (2006) Structures and mechanisms of glycosyltransferases. *Glycobiology* **16**: 29R–37R.
- Capstick, DS, Jomaa, A, Hanke, C, Ortega, J, and Elliot, MA (2011) Dual amyloid domains promote differential functioning of the chaplin proteins during *Streptomyces aerial* morphogenesis. *Proc Natl Acad Sci U S A* **108**: 9821–6.
- Capstick, DS, Willey, JM, Buttner, MJ, and Elliot, MA (2007) SapB and the chaplins: connections between morphogenetic proteins in *Streptomyces coelicolor*. *Mol Microbiol* **64**: 602–13.
- Celler, K, Picioareanu, C, Loosdrecht, MCM van, and Wezel, GP van (2012) Structured morphological modeling as a framework for rational strain design of *Streptomyces* species. *Antonie Van Leeuwenhoek* **102**: 409–23.
- Chao, JD, Papavinasasundaram, KG, Zheng, X, Chávez-Steenbock, A, Wang, X, Lee, GQ, and Av-Gay, Y (2010) Convergence of Ser/Thr and two-component signaling to coordinate expression of the dormancy regulon in *Mycobacterium tuberculosis*. *J Biol Chem* **285**: 29239–29246.
- Chaplin, AK, Petrus, MLC, Mangiameli, G, Hough, MA, Svistunenko, DA, Nicholls, P, *et al.* (2015) GlxA is a new structural member of the radical copper oxidase family and is required for glycan deposition at hyphal tips and morphogenesis of *Streptomyces lividans*. *Biochem J* **469**: 433–444.
- Charnock, SJ, and Davies, GJ (1999) Structure of the nucleotide-diphospho-sugar transferase, SpsA from *Bacillus subtilis*, in native and nucleotide-complexed forms. *Biochemistry* **38**: 6380–5.

- Chater, KF (1972) A morphological and genetic mapping study of white colony mutants of *Streptomyces coelicolor*. *J Gen Microbiol* **72**: 9–28.
- Chater, KF (1998) Taking a genetic scalpel to the *Streptomyces* colony. *Microbiology* **144**: 1465–1478.
- Chater, KF (2006) *Streptomyces* inside-out: a new perspective on the bacteria that provide us with antibiotics. *Philos Trans R Soc Lond B Biol Sci* **361**: 761–8.
- Chater, KF, Biró, S, Lee, KJ, Palmer, T, and Schrempf, H (2010) The complex extracellular biology of *Streptomyces*. *FEMS Microbiol Rev* **34**: 171–98.
- Chater, KF, and Losick, R (1997) Mycelial life style of *Streptomyces coelicolor* A3(2) and its relatives. In *Bacteria as multicellular organisms*. Shapiro, J.A., and Dworkin, M. (eds). Oxford University Press, New York. pp. 149–182.
- Chauhan, S, Sharma, D, Singh, A, Surolia, A, and Tyagi, JS (2011) Comprehensive insights into *Mycobacterium tuberculosis* DevR (DosR) regulon activation switch. *Nucleic Acids Res* **39**: 7400–7414.
- Cheah, IK, and Halliwell, B (2012) Ergothioneine; antioxidant potential, physiological function and role in disease. *Biochim Biophys Acta* **1822**: 784–93.
- Chen, C, Shrestha, R, Jia, K, Gao, PF, Geisbrecht, B V, Bossmann, SH, et al. (2015) Characterization of dye-decolorizing peroxidase (DyP) from *Thermomonospora curvata* reveals unique catalytic properties of A-type DyPs. *J Biol Chem* **290**: 23447–63.
- Chovancova, E, Pavelka, A, Benes, P, Strnad, O, Brezovsky, J, Kozlikova, B, et al. (2012) CAVER 3.0: a tool for the analysis of transport pathways in dynamic protein structures. *PLoS Comput Biol* **8**: e1002708.
- Claessen, D, Jong, W de, Dijkhuizen, L, and Wösten, HAB (2006) Regulation of *Streptomyces* development: reach for the sky! *Trends Microbiol* **14**: 313–9.
- Claessen, D, Rink, R, De Jong, W, Siebring, J, De Vreugd, P, Boersma, FGH, et al. (2003) A novel class of secreted hydrophobic proteins is involved in aerial hyphae formation in *Streptomyces coelicolor* by forming amyloid-like fibrils. *Genes Dev* **17**: 1714–1726.
- Claessen, D, Rozen, DE, Kuipers, OP, Sjøgaard-Andersen, L, and Van Wezel, GP (2014) Bacterial solutions to multicellularity: a tale of biofilms, filaments and fruiting bodies. *Nat Rev Microbiol* **12**: 115–24.
- Claessen, D, Stokroos, I, Deelstra, HJ, Penninga, NA, Bormann, C, Salas, JA, et al. (2004) The formation of the rodlet layer of streptomycetes is the result of the interplay between rodlines and chaplins. *Mol Microbiol* **53**: 433–43.
- Claessen, D, Wösten, HAB, Van Keulen, G, Faber, OG, Alves, AMCR, Meijer, WG, and Dijkhuizen, L (2002) Two novel homologous proteins of *Streptomyces coelicolor* and *Streptomyces lividans* are involved in the formation of the rodlet layer and mediate attachment to a hydrophobic surface. *Mol Microbiol* **44**: 1483–1492.
- Cleveland, L, Coffman, RE, Coon, P, and Davis, L (1975) An investigation of the role of the copper in galactose oxidase. *Biochemistry* **14**: 1108–1115.
- Colpa, DI, Fraaije, MW, and Bloois, E van (2014) DyP-type peroxidases: a promising and versatile class of enzymes. *J Ind Microbiol Biotechnol* **41**: 1–7.
- Cornelis, P, and Andrews, SC (eds) (2010) *Iron uptake and homeostasis in microorganisms*. Caister Academic Press, Norfolk, UK.
- Cot, M, Ray, A, Gilleron, M, Vercellone, A, Larrouy-Maumus, G, Armau, E, et al. (2011) Lipoteichoic acid in *Streptomyces hygroscopicus*: structural model and immunomodulatory activities. *PLoS One* **6**: e26316.
- Coutinho, PM, Deleury, E, Davies, GJ, and Henrissat, B (2003) An evolving hierarchical family classification for glycosyltransferases. *J Mol Biol* **328**: 307–317.

References

- Cox, J, and Mann, M (2008) MaxQuant enables high peptide identification rates, individualized p.p.b.-range mass accuracies and proteome-wide protein quantification. *Nat Biotechnol* **26**: 1367–1372.
- Cox, J, Neuhauser, N, Michalski, A, Scheltema, RA, Olsen, J V., and Mann, M (2011) Andromeda: A peptide search engine integrated into the MaxQuant environment. *J Proteome Res* **10**: 1794–1805.
- Crick, DC, Mahapatra, S, and Brennan, PJ (2001) Biosynthesis of the arabinogalactan-peptidoglycan complex of *Mycobacterium tuberculosis*. *Glycobiology* **11**: 107R–118R.
- Cruz-Morales, P, Vijgenboom, E, Iruegas-Bocardo, F, Girard, G, Yáñez-Guerra, LA, Ramos-Aboites, HE, *et al.* (2013) The genome sequence of *Streptomyces lividans* 66 reveals a novel tRNA-dependent peptide biosynthetic system within a metal-related genomic island. *Genome Biol Evol* **5**: 1165–75.
- Cui, YQ, Okkerse, WJ, Lans, RGJM Van Der, and Luyben, KCAM (1998) Modeling and measurements of fungal growth and morphology in submerged fermentations. *Biotechnol Bioeng* **60**: 216–229.
- Cummings, RD, and Etzler, ME (2009) Antibodies and lectins in glycan analysis. In *Essentials of Glycobiology*. 2nd edition. Varki A, Cummings RD, Esko JD, *et al.* (ed.). Cold Spring Harbor Laboratory Press, New York.
- Davis, IW, Leaver-Fay, A, Chen, VB, Block, JN, Kapral, GJ, Wang, X, *et al.* (2007) MolProbity: all-atom contacts and structure validation for proteins and nucleic acids. *Nucleic Acids Res* **35**: W375–W383.
- Deacon, SE, and McPherson, MJ (2011) Enhanced expression and purification of fungal galactose oxidase in *Escherichia coli* and use for analysis of a saturation mutagenesis library. *Chembiochem* **12**: 593–601.
- Van Dissel, D, Claessen, D, Roth, M, and Van Wezel, GP (2015) A novel locus for mycelial aggregation forms a gateway to improved *Streptomyces* cell factories. *Microb Cell Fact* **14**: 44.
- Van Dissel, D, Claessen, D, and Van Wezel, GP (2014) Morphogenesis of *Streptomyces* in submerged cultures. *Adv Appl Microbiol* **89**: 1–45.
- Dueholm, MS, Petersen, S V., Sønderkær, M, Larsen, P, Christiansen, G, Hein, KL, *et al.* (2010) Functional amyloid in pseudomonas. *Mol Microbiol* **77**: 1009–1020.
- Duong, A, Capstick, DS, Berardo, C Di, Findlay, KC, Hesketh, A, Hong, H-J, and Elliot, MA (2012) Aerial development in *Streptomyces coelicolor* requires sortase activity. *Mol Microbiol* **83**: 992–1005.
- Ekkers, DM, Claessen, D, Galli, F, and Stamhuis, E (2014) Surface modification using interfacial assembly of the *Streptomyces* chaplin proteins. *Appl Microbiol Biotechnol* **98**: 4491–4501.
- Elliot, MA, and Talbot, NJ (2004) Building filaments in the air: Aerial morphogenesis in bacteria and fungi. *Curr Opin Microbiol* **7**: 594–601.
- Elliot, MA, Karoonuthaisiri, N, Huang, J, Bibb, MJ, Cohen, SN, Kao, CM, and Buttner, MJ (2003) The chaplins: A family of hydrophobic cell-surface proteins involved in aerial mycelium formation in *Streptomyces coelicolor*. *Genes Dev* **17**: 1727–1740.
- Emsley, P, and Cowtan, K (2004) Coot: model-building tools for molecular graphics. *Acta Crystallogr D Biol Crystallogr* **60**: 2126–32.
- Errington, J (2003) Regulation of endospore formation in *Bacillus subtilis*. *Nat Rev Microbiol* **1**: 117–126.
- Errington, J, Daniel, RA, and Scheffers, D-J (2003) Cytokinesis in bacteria. *Microbiol Mol Biol Rev* **67**: 52–65, table of contents.
- Evans, PR, and Murshudov, GN (2013) How good are my data and what is the resolution? *Acta Crystallogr D Biol Crystallogr* **69**: 1204–14.
- Fang, L, and Catchmark, JM (2015) Characterization of cellulose and other exopolysaccharides produced from *Gluconacetobacter* strains. *Carbohydr Polym* **115**: 663–9.

- Flårdh, K (2003a) Growth polarity and cell division in *Streptomyces*. *Curr Opin Microbiol* **6**: 564–571.
- Flårdh, K (2003b) Essential role of DivIVA in polar growth and morphogenesis in *Streptomyces coelicolor* A3(2). *Mol Microbiol* **49**: 1523–36.
- Flårdh, K, and Buttner, MJ (2009) *Streptomyces* morphogenetics: dissecting differentiation in a filamentous bacterium. *Nat Rev Microbiol* **7**: 36–49.
- Flårdh, K, Richards, DM, Hempel, AM, Howard, M, and Buttner, MJ (2012) Regulation of apical growth and hyphal branching in *Streptomyces*. *Curr Opin Microbiol* **15**: 737–43.
- Fujimoto, M, Yamada, A, Kurosawa, J, Kawata, A, Beppu, T, Takano, H, and Ueda, K (2012) Pleiotropic role of the Sco1/SenC family copper chaperone in the physiology of *Streptomyces*. *Microb Biotechnol* **5**: 477–488.
- Gaskell, AA, Giovinazzo, JA, Fonte, V, and Willey, JM (2012) Multi-tier regulation of the streptomycete morphogenetic peptide SapB. *Mol Microbiol* **84**: 501–515.
- Gastebois, A, Mouyna, I, Simenel, C, Clavaud, C, Coddeville, B, Delepierre, M, *et al.* (2010) Characterization of a new beta-(1-3)-glucan branching activity of *Aspergillus fumigatus*. *J Biol Chem* **285**: 2386–96.
- Gebbink, MFBG, Claessen, D, Bouma, B, Dijkhuizen, L, and Wösten, HAB (2005) Amyloids - a functional coat for microorganisms. *Nat Rev Microbiol* **3**: 333–41.
- Gerasimova, A, Kazakov, AE, Arkin, AP, Dubchak, I, and Gelfand, MS (2011) Comparative genomics of the dormancy regulons in mycobacteria. *J Bacteriol* **193**: 3446–3452.
- Girard, G, Willemsse, J, Zhu, H, Claessen, D, Bukarasam, K, Goodfellow, M, and Van Wezel, GP (2014) Analysis of novel kitasatosporae reveals significant evolutionary changes in conserved developmental genes between *Kitasatospora* and *Streptomyces*. *Antonie Van Leeuwenhoek* **106**: 365–80.
- Gloster, TM (2014) Advances in understanding glycosyltransferases from a structural perspective. *Curr Opin Struct Biol* **28**: 131–41.
- Goldman, E, and Green, LH (eds) (2008) *Practical Handbook of Microbiology, Second Edition*. CRC Press, Boca Raton.
- Goosens, VJ, Monteferrante, CG, and Van Dijk, JM (2014) The Tat system of Gram-positive bacteria. *Biochim Biophys Acta - Mol Cell Res* **1843**: 1698–1706.
- Goosens, VJ, Otto, A, Glasner, C, Monteferrante, CC, Van der Ploeg, R, Hecker, M, *et al.* (2013) Novel twin-arginine translocation pathway-dependent phenotypes of *Bacillus subtilis* unveiled by quantitative proteomics. *J Proteome Res* **12**: 796–807.
- Gras, SL, and Dennis, C (2014) Functional amyloid fibrils: lessons from microbes. In *Natural products analysis: instrumentation, methods, and applications*. Havlicek, V., and Spizek, J. (eds). Wiley, New York.
- Gubbens, J, Janus, M, Florea, BI, Overkleeft, HS, and Van Wezel, GP (2012) Identification of glucose kinase-dependent and -independent pathways for carbon control of primary metabolism, development and antibiotic production in *Streptomyces coelicolor* by quantitative proteomics. *Mol Microbiol* **86**: 1490–1507.
- Güssow, HT (1914) The systematic position of the organism of the common potato scab. *Science* **39**: 431–3.
- Hamilton, GA, Adolf, PK, Jersey, J De, DuBois, GC, Dyrkacz, GR, and Libby, RD (1978) Trivalent copper superoxide and galactose oxidase. *J Am Chem Soc* **100**: 1899–1912.
- Hammer, ND, Schmidt, JC, and Chapman, MR (2007) The curli nucleator protein, CsgB, contains an amyloidogenic domain that directs CsgA polymerization. *Proc Natl Acad Sci U S A* **104**: 12494–9.
- Hengge, R (2009) Principles of c-di-GMP signalling in bacteria. *Nat Rev Microbiol* **7**: 263–273.
- Hengst, CD den, Tran, NT, Bibb, MJ, Chandra, G, Leskiw, BK, and Buttner, MJ (2010) Genes essential for morphological development and antibiotic production in *Streptomyces coelicolor* are targets of BldD during vegetative

- growth. *Mol Microbiol* **78**: 361–379.
- Holmes, NA, Walshaw, J, Leggett, RM, Thibessard, A, Dalton, KA, Gillespie, MD, *et al.* (2013) Coiled-coil protein Scy is a key component of a multiprotein assembly controlling polarized growth in *Streptomyces*. *Proc Natl Acad Sci U S A* **110**: E397–406.
- Hong, H-J, Paget, MSB, and Buttner, MJ (2002) A signal transduction system in *Streptomyces coelicolor* that activates the expression of a putative cell wall glycan operon in response to vancomycin and other cell wall-specific antibiotics. *Mol Microbiol* **44**: 1199–1211.
- Hopwood, DA (2007) *Streptomyces in Nature and Medicine: The Antibiotic Makers*. Oxford University Press, New York.
- Hopwood, DA, Bibb, MJ, Chater, KF, Kieser, T, Lydiate, DJ, Smith, CP, *et al.* (1985) *Genetic manipulation of streptomyces — A laboratory manual*. The John Innes Foundation and Cold Spring Harbour Laboratory, Norwich, UK.
- Hopwood, DA, Kieser, T, Wright, HM, and Bibb, MJ (1983) Plasmids, recombination and chromosome mapping in *Streptomyces lividans* 66. *J Gen Microbiol* **129**: 2257–69.
- Hughes, AH, Hancock, IC, and Baddiley, J (1973) The function of teichoic acids in cation control in bacterial membranes. *Biochem J* **132**: 83–93.
- Hull, TD, Ryu, M-H, Sullivan, MJ, Johnson, RC, Klena, NT, Geiger, RM, *et al.* (2012) Cyclic-di-GMP phosphodiesterases RmdA and RmdB are involved in regulating colony morphology and development in *Streptomyces coelicolor*. *J Bacteriol* **194**: 4642–51.
- Hunt, AC, Servín-González, L, Kelemen, GH, and Buttner, MJ (2005) The *bldC* developmental locus of *Streptomyces coelicolor* encodes a member of a family of small DNA-binding proteins related to the DNA-binding domains of the MerR family. *J Bacteriol* **187**: 716–728.
- Hutter, KJ, and Eipel, HE (1979) Microbial determinations by flow cytometry. *J Gen Microbiol* **113**: 369–375.
- Innes, CMJ, and Allan, EJ (2001) Induction, growth and antibiotic production of *Streptomyces viridifaciens* L-form bacteria. *J Appl Microbiol* **90**: 301–308.
- Ito, N, Phillips, SE, Stevens, C, Ogel, ZB, McPherson, MJ, Keen, JN, *et al.* (1991) Novel thioether bond revealed by a 1.7 Å crystal structure of galactose oxidase. *Nature* **350**: 87–90.
- Ito, N, Phillips, SE, Yadav, KD, and Knowles, PF (1994) Crystal structure of a free radical enzyme, galactose oxidase. *J Mol Biol* **238**: 794–814.
- Jahn, CE, Selimi, DA, Barak, JD, and Charkowski, AO (2011) The *Dickeya dadantii* biofilm matrix consists of cellulose nanofibres, and is an emergent property dependent upon the type III secretion system and the cellulose synthesis operon. *Microbiology* **157**: 2733–44.
- Jakeman, DL, Graham, CL, Young, W, and Vining, LC (2006) Culture conditions improving the production of jadomycin B. *J Ind Microbiol Biotechnol* **33**: 767–772.
- Jakimowicz, D, and Van Wezel, GP (2012) Cell division and DNA segregation in *Streptomyces*: How to build a septum in the middle of nowhere? *Mol Microbiol* **85**: 393–404.
- De Jong, W, Manteca, A, Sanchez, J, Bucca, G, Smith, CP, Dijkhuizen, L, *et al.* (2009) NepA is a structural cell wall protein involved in maintenance of spore dormancy in *Streptomyces coelicolor*. *Mol Microbiol* **71**: 1591–603.
- De Jong, W, Vijgenboom, E, Dijkhuizen, L, Wösten, HAB, and Claessen, D (2012) SapB and the rodlinins are required for development of *Streptomyces coelicolor* in high osmolarity media. *FEMS Microbiol Lett* **329**: 154–159.
- De Jong, W, Wösten, HAB, Dijkhuizen, L, and Claessen, D (2009) Attachment of *Streptomyces coelicolor* is mediated by amyloid fimbriae that are anchored to the cell surface via cellulose. *Mol Microbiol* **73**: 1128–40.

- Käll, L, Krogh, A, and Sonnhammer, ELL (2004) A combined transmembrane topology and signal peptide prediction method. *J Mol Biol* **338**: 1027–36.
- De Keersmaecker, S, Van Mellaert, L, Lammertyn, E, Vrancken, K, Anné, J, and Geukens, N (2005) Functional analysis of TatA and TatB in *Streptomyces lividans*. *Biochem Biophys Res Commun* **335**: 973–982.
- De Keersmaecker, S, Vrancken, K, Van Mellaert, L, Anné, J, and Geukens, N (2007) The Tat pathway in *Streptomyces lividans*: interaction of Tat subunits and their role in translocation. *Microbiology* **153**: 1087–94.
- Keijser, BJ, Van Wezel, GP, Canters, GW, Kieser, T, and Vijgenboom, E (2000) The ram-dependence of *Streptomyces lividans* differentiation is bypassed by copper. *J Mol Microbiol Biotechnol* **2**: 565–74.
- Kelemen, GH, and Buttner, MJ (1998) Initiation of aerial mycelium formation in *Streptomyces*. *Curr Opin Microbiol* **1**: 656–662.
- Kelleher, FM, and Bhavanandan, VP (1986) Re-examination of the products of the action of galactose oxidase. Evidence for the conversion of raffinose to 6''-carboxyraffinose. *J Biol Chem* **261**: 11045–8.
- Kelley, LA, Mezulis, S, Yates, CM, Wass, MN, and Sternberg, MJE (2015) The Phyre2 web portal for protein modeling, prediction and analysis. *Nat Protoc* **10**: 845–858.
- Kelley, WL (2006) Lex marks the spot: The virulent side of SOS and a closer look at the LexA regulon. *Mol Microbiol* **62**: 1228–1238.
- Kendrick, KE, and Ensign, JC (1983) Sporulation of *Streptomyces griseus* in submerged culture. *J Bacteriol* **155**: 357–66.
- Kershaw, MJ, and Talbot, NJ (1998) Hydrophobins and repellents: proteins with fundamental roles in fungal morphogenesis. *Fungal Genet Biol* **23**: 18–33.
- Van Keulen, G, Jonkers, HM, Claessen, D, Dijkhuizen, L, and Wösten, HAB (2003) Differentiation and anaerobiosis in standing liquid cultures of *Streptomyces coelicolor*. *J Bacteriol* **185**: 1455–8.
- Khurana, R, Uversky, VN, Nielsen, L, and Fink, AL (2001) Is Congo red an amyloid-specific dye? *J Biol Chem* **276**: 22715–21.
- Kieser, T, Bibb, MJ, Buttner, MJ, Chater, KF, and Hopwood, DA (2000) *Practical Streptomyces Genetics*. The John Innes Foundation, Norwich.
- Kieser, T, and Hopwood, DA (1991) Genetic manipulation of *Streptomyces*: integrating vectors and gene replacement. *Methods Enzymol* **204**: 430–58.
- Kim, HJ, Graham, DW, DiSpirito, AA, Alterman, MA, Galeva, N, Larive, CK, et al. (2004) Methanobactin, a copper-acquisition compound from methane-oxidizing bacteria. *Science* **305**: 1612–5.
- Kim, SJ, and Shoda, M (1999) Purification and characterization of a novel peroxidase from *Geotrichum candidum* dec 1 involved in decolorization of dyes. *Appl Environ Microbiol* **65**: 1029–35.
- Kim, Y-M, and Kim, J (2004) Formation and dispersion of mycelial pellets of *Streptomyces coelicolor* A3(2). *J Microbiol* **42**: 64–7.
- Kirima, K, Tsuchiya, K, Sei, H, Hasegawa, T, Shikishima, M, Motobayashi, Y, et al. (2003) Evaluation of systemic blood NO dynamics by EPR spectroscopy: HbNO as an endogenous index of NO. *Am J Physiol Heart Circ Physiol* **285**: H589–96.
- Kirschner, DA, Abraham, C, and Selkoe, DJ (1986) X-ray diffraction from intraneuronal paired helical filaments and extraneuronal amyloid fibers in Alzheimer disease indicates cross-beta conformation. *Proc Natl Acad Sci U S A* **83**: 503–7.
- Kleinschnitz, E-M, Latus, A, Sigle, S, Maldener, I, Wohlleben, W, and Muth, G (2011) Genetic analysis of SCO2997, encoding a TagF homologue, indicates a role for wall teichoic acids in sporulation of *Streptomyces coelicolor*

References

- A3(2). *J Bacteriol* **193**: 6080–5.
- Kodani, S, Hudson, ME, Durrant, MC, Buttner, MJ, Nodwell, JR, and Willey, JM (2004) The SapB morphogen is a lantibiotic-like peptide derived from the product of the developmental gene *ramS* in *Streptomyces coelicolor*. *Proc Natl Acad Sci U S A* **101**: 11448–53.
- Kodani, S, Lodato, MA, Durrant, MC, Picart, F, and Willey, JM (2005) SapT, a lanthionine-containing peptide involved in aerial hyphae formation in the streptomycetes. *Mol Microbiol* **58**: 1368–1380.
- Koebisch, I, Overbeck, J, Piepmeyer, S, Meschke, H, and Schrempf, H (2009) A molecular key for building hyphae aggregates: the role of the newly identified *Streptomyces* protein HyaS. *Microb Biotechnol* **2**: 343–360.
- Kozlikova, B, Sebestova, E, Sustr, V, Brezovsky, J, Strnad, O, Daniel, L, et al. (2014) CAVER Analyst 1.0: graphic tool for interactive visualization and analysis of tunnels and channels in protein structures. *Bioinformatics* **30**: 2684–5.
- Krogh, A, Larsson, B, Von Heijne, G, and Sonnhammer, EL (2001) Predicting transmembrane protein topology with a hidden Markov model: application to complete genomes. *J Mol Biol* **305**: 567–80.
- Kumar, N, and Borth, N (2012) Flow-cytometry and cell sorting: An efficient approach to investigate productivity and cell physiology in mammalian cell factories. *Methods* **56**: 366–374.
- Kumirska, J, Czerwicka, M, Kaczyński, Z, Bychowska, A, Brzozowski, K, Thöming, J, and Stepnowski, P (2010) Application of spectroscopic methods for structural analysis of chitin and chitosan. *Mar Drugs* **8**: 1567–636.
- Labeda, DP, Goodfellow, M, Brown, R, Ward, AC, Lanoot, B, Vannanneyt, M, et al. (2012) Phylogenetic study of the species within the family Streptomycetaceae. *Antonie Van Leeuwenhoek* **101**: 73–104.
- Lairson, LL, Henrissat, B, Davies, GJ, and Withers, SG (2008) Glycosyltransferases: structures, functions, and mechanisms. *Annu Rev Biochem* **77**: 521–55.
- Lambert, S, Traxler, MF, Craig, M, Maciejewska, M, Ongena, M, Van Wezel, GP, et al. (2014) Altered desferrioxamine-mediated iron utilization is a common trait of bald mutants of *Streptomyces coelicolor*. *Metallomics* **6**: 1390–9.
- Lee, JW, Deng, F, Yeomans, WG, Allen, AL, Gross, RA, and Kaplan, DL (2001) Direct incorporation of glucosamine and N-acetylglucosamine into exopolymers by *Gluconacetobacter xylinus* (= *Acetobacter xylinum*) ATCC 10245 : Production of chitosan-cellulose and chitin-cellulose exopolymers. *Appl Environ Microbiol* .
- Lee, Y-K, Whittaker, MM, and Whittaker, JW (2008) The electronic structure of the Cys-Tyr(*) free radical in galactose oxidase determined by EPR spectroscopy. *Biochemistry* **47**: 6637–49.
- Van Leeuwen, SS, Kralj, S, Van Geel-Schutten, IH, Gerwig, GJ, Dijkhuizen, L, and Kamerling, JP (2008) Structural analysis of the alpha-D-glucan (EPS180) produced by the *Lactobacillus reuteri* strain 180 glucansucrase GTF180 enzyme. *Carbohydr Res* **343**: 1237–50.
- Liman, R, Facey, PD, Van Keulen, G, Dyson, PJ, and Sol, R Del (2013) A laterally acquired galactose oxidase-like gene is required for aerial development during osmotic stress in *Streptomyces coelicolor*. *PLoS One* **8**: e54112.
- Lin, PJ, Grimm, LH, Wulkow, M, Hempel, DC, and Krull, R (2008) Population balance modeling of the conidial aggregation of *Aspergillus niger*. *Biotechnol Bioeng* **99**: 341–350.
- Lombard, V, Golaconda Ramulu, H, Drula, E, Coutinho, PM, and Henrissat, B (2014) The carbohydrate-active enzymes database (CAZy) in 2013. *Nucleic Acids Res* **42**: D490–5.
- López, D, Vlamakis, H, and Kolter, R (2010) Biofilms. *Cold Spring Harb Perspect Biol* **2**: a000398.
- Lugones, LG, Jong, JF De, Vries, OMH De, Jalving, R, Dijksterhuis, J, and Wösten, H a B (2004) The SC15 protein of *Schizophyllum commune* mediates formation of aerial hyphae and attachment in the absence of the SC3 hydrophobin. *Mol Microbiol* **53**: 707–716.

- MacNeil, DJ, Gewain, KM, Ruby, CL, Dezeny, G, Gibbons, PH, and MacNeil, T (1992) Analysis of *Streptomyces avermitilis* genes required for Avermectin biosynthesis utilizing a novel integration vector. *Gene* **111**: 61–68.
- Manteca, A, Alvarez, R, Salazar, N, Yagüe, P, and Sanchez, J (2008) Mycelium differentiation and antibiotic production in submerged cultures of *Streptomyces coelicolor*. *Appl Environ Microbiol* **74**: 3877–86.
- Martin, SM, and Bushell, ME (1996) Effect of hyphal micromorphology on bioreactor performance of antibiotic-producing *Saccharopolyspora erythraea* cultures. *Microbiology* **142**: 1783–1788.
- Matthysse, AG (1986) Initial interactions of *Agrobacterium tumefaciens* with plant host cells. *Crit Rev Microbiol* **13**: 281–307.
- Matthysse, AG, White, S, and Lightfoot, R (1995) Genes required for cellulose synthesis in *Agrobacterium tumefaciens*. *J Bacteriol* **177**: 1069–75.
- May, JF, Levengood, MR, Splain, RA, Brown, CD, and Kiessling, LL (2012) A processive carbohydrate polymerase that mediates bifunctional catalysis using a single active site. *Biochemistry* **51**: 1148–59.
- McCoy, AJ, Grosse-Kunstleve, RW, Adams, PD, Winn, MD, Storoni, LC, and Read, RJ (2007) Phaser crystallographic software. *J Appl Crystallogr* **40**: 658–674.
- McNicholas, S, Potterton, E, Wilson, KS, and Noble, MEM (2011) Presenting your structures: the CCP4mg molecular-graphics software. *Acta Crystallogr D Biol Crystallogr* **67**: 386–94.
- Merrick, MJ (1976) A morphological and genetic mapping study of bald colony mutants of *Streptomyces coelicolor*. *J Gen Microbiol* **96**: 299–315.
- Messing, J, Crea, R, and Seeburg, PH (1981) A system for shotgun DNA sequencing. *Nucleic Acids Res* **9**: 309–21.
- Miethke, M, Monteferrante, CG, Marahiel, MA, and Van Dijk, JM (2013) The *Bacillus subtilis* EfeUOB transporter is essential for high-affinity acquisition of ferrous and ferric iron. *Biochim Biophys Acta - Mol Cell Res* **1833**: 2267–2278.
- Millard, WA (1922) Common scab of potatoes. *Ann Appl Biol v. 9* (1922): 70–88.
- Monteferrante, CG, MacKichan, C, Marchadier, E, Prejean, M-V, Carballido-López, R, and Van Dijk, JM (2013) Mapping the twin-arginine protein translocation network of *Bacillus subtilis*. *Proteomics* **13**: 800–11.
- Morgan, JLW, McNamara, JT, and Zimmer, J (2014) Mechanism of activation of bacterial cellulose synthase by cyclic-di-GMP. *Nat Struct Mol Biol* **21**: 489–96.
- Morgan, JLW, Strumillo, J, and Zimmer, J (2013) Crystallographic snapshot of cellulose synthesis and membrane translocation. *Nature* **493**: 181–6.
- Mulloy, B, Hart, GW, and Stanley, P (2009) Structural analysis of glycans. In *Essentials of Glycobiology. 2nd edition*. Varki A, Cummings RD, Esko JD, et al. (ed.). Cold Spring Harbor Laboratory Press, New York.
- Van Munster, JM, Nitsche, BM, Krijgsheld, P, Van Wijk, A, Dijkhuizen, L, Wösten, HAB, et al. (2013) Chitinases CtcB and CfcI modify the cell wall in sporulating aerial mycelium of *Aspergillus niger*. *Microbiology* **159**: 1853–1867.
- Murshudov, GN, Vagin, AA, and Dodson, EJ (1997) Refinement of macromolecular structures by the maximum-likelihood method. *Acta Crystallogr D Biol Crystallogr* **53**: 240–55.
- Nakagawa, YS, Kudo, M, Loose, JSM, Ishikawa, T, Totani, K, Eijsink, VGH, and Vaaje-Kolstad, G (2015) A small lytic polysaccharide monoxygenase from *Streptomyces griseus* targeting α - and β -chitin. *FEBS J* **282**: 1065–79.
- Newcomb, WD, and Rimstidt, JD (2002) Trace element distribution in US groundwaters: a probabilistic assessment using public domain data. *Appl Geochemistry* **17**: 49–57.
- Nielsen, J (1996) Modelling the morphology of filamentous microorganisms. *Trends Biotechnol* **14**: 438–443.

References

- Nielsen, J, and Johansen, C (1995) Pellet formation and fragmentation in submerged cultures of *Penicillium chrysogenum* and its relation to penicillin production. *Biotechnol Prog* **11**: 93–98.
- Nieminen, L, Webb, S, Smith, MCM, and Hoskisson, PA (2013) A flexible mathematical model platform for studying branching networks: experimentally validated using the model actinomycete, *Streptomyces coelicolor*. *PLoS One* **8**: e54316.
- Noens, EE, Mersinias, V, Willemse, J, Traag, BA, Laing, E, Chater, KF, *et al.* (2007) Loss of the controlled localization of growth stage-specific cell-wall synthesis pleiotropically affects developmental gene expression in an *ssgA* mutant of *Streptomyces coelicolor*. *Mol Microbiol* **64**: 1244–1259.
- Oberto, J (2013) SyntTax: a web server linking synteny to prokaryotic taxonomy. *BMC Bioinformatics* **14**: 4.
- Ostash, B, Shashkov, A, Streshinskaya, G, Tul'skaya, E, Baryshnikova, L, Dmitrenok, A, *et al.* (2014) Identification of *Streptomyces coelicolor* M145 genomic region involved in biosynthesis of teichulosonic acid-cell wall glycopolymer. *Folia Microbiol (Praha)* **3**: 355–360.
- Palmer, T, and Berks, BC (2012) The twin-arginine translocation (Tat) protein export pathway. *Nat Rev Microbiol* **10**: 483–96.
- Pastor, MT, Esteras-Chopo, A, and Serrano, L (2007) Hacking the code of amyloid formation: the amyloid stretch hypothesis. *Prion* **1**: 9–14.
- Paul, GC, and Thomas, CR (1998) Characterisation of mycelial morphology using image analysis. *Adv Biochem Eng Biotechnol* **60**: 1–59.
- Peisach, J, and Blumberg, WE (1974) Structural implications derived from the analysis of electron paramagnetic resonance spectra of natural and artificial copper proteins. *Arch Biochem Biophys* **165**: 691–708.
- Perrakis, A, Morris, R, and Lamzin, VS (1999) Automated protein model building combined with iterative structure refinement. *Nat Struct Biol* **6**: 458–63.
- Petersen, TN, Brunak, S, Heijne, G von, and Nielsen, H (2011) SignalP 4.0: discriminating signal peptides from transmembrane regions. *Nat Methods* **8**: 785–6.
- Petrus, MLC, and Claessen, D (2014) Pivotal roles for *Streptomyces* cell surface polymers in morphological differentiation, attachment and mycelial architecture. *Antonie Van Leeuwenhoek* **106**: 127–139.
- Petrus, MLC, Van Veluw, GJ, Wösten, HAB, and Claessen, D (2014) Sorting of *Streptomyces* cell pellets using a complex object parametric analyzer and sorter. *J Vis Exp* e51178.
- Phillips, AP, and Martin, KL (1983) Immunofluorescence analysis of *Bacillus* spores and vegetative cells by flow cytometry. *Cytometry* **4**: 123–131.
- Piette, A, Derouaux, A, Gerkens, P, Noens, EEE, Mazzucchelli, G, Vion, S, *et al.* (2005) From dormant to germinating spores of *Streptomyces coelicolor* A3(2): New perspectives from the *crp* null mutant. *J Proteome Res* **4**: 1699–1708.
- Potekhina, NV, Streshinskaya, GM, Tul'skaya, EM, and Shashkov, AS (2011) Cell wall teichoic acids in the taxonomy and characterization of Gram-positive bacteria. In *Methods in Microbiology*. pp. 132–164.
- Prosser, JI, and Tough, AJ (1991) Growth mechanisms and growth kinetics of filamentous microorganisms. *Crit Rev Biotechnol* **10**:4, 253-274
- Rahman, O, Cummings, SP, and Sutcliffe, IC (2009) Phenotypic variation in *Streptomyces* sp. DSM 40537, a lipoteichoic acid producing actinomycete. *Lett Appl Microbiol* **48**: 226–9.
- Rioseras, B, López-García, MT, Yagüe, P, Sánchez, J, and Manteca, A (2014) Mycelium differentiation and development of *Streptomyces coelicolor* in lab-scale bioreactors: Programmed cell death, differentiation, and lysis are closely linked to undecylprodigiosin and actinorhodin production. *Bioresour Technol* **151**: 191–8.

- Rogers, MS, Tyler, EM, Akyumani, N, Kurtis, CR, Spooner, RK, Deacon, SE, *et al.* (2007) The stacking tryptophan of galactose oxidase: a second-coordination sphere residue that has profound effects on tyrosyl radical behavior and enzyme catalysis. *Biochemistry* **46**: 4606–18.
- Romero, D, Aguilar, C, Losick, R, and Kolter, R (2010) Amyloid fibers provide structural integrity to *Bacillus subtilis* biofilms. *Proc Natl Acad Sci U S A* **107**: 2230–4.
- Römling, U (2002) Molecular biology of cellulose production in bacteria. *Res Microbiol* **153**: 205–12.
- Römling, U, and Galperin, MY (2015) Bacterial cellulose biosynthesis: diversity of operons, subunits, products, and functions. *Trends Microbiol* .
- Rose, RW, Brüser, T, Kissinger, JC, and Pohlschröder, M (2002) Adaptation of protein secretion to extremely high-salt conditions by extensive use of the twin-arginine translocation pathway. *Mol Microbiol* **45**: 943–50.
- Ross, P, Mayer, R, and Benziman, M (1991) Cellulose biosynthesis and function in bacteria. *Microbiol Rev* **55**: 35–58.
- Sambrook, J, Fritsch, EF, Maniatis, T, Fritsch, EF, Sambrook, Fritsch, E.F and Maniatis, T, and J (1989) *Molecular Cloning: A Laboratory Manual*. Cold Spring Harbor Laboratory Press, New York.
- Sancar, A (1996) DNA excision repair. *Annu Rev Biochem* **65**: 43–81.
- Sánchez-Rodríguez, A, Tytgat, HLP, Winderickx, J, Vanderleyden, J, Lebeer, S, and Marchal, K (2014) A network-based approach to identify substrate classes of bacterial glycosyltransferases. *BMC Genomics* **15**: 349.
- Sarrà, M, Casas, C, Poch, M, and Gòdia, F (1999) A simple structured model for continuous production of a hybrid antibiotic by *Streptomyces lividans* pellets in a fluidized-bed bioreactor. *Appl Biochem Biotechnol* **80**: 39–50.
- Sawyer, EB, Claessen, D, Gras, SL, and Perrett, S (2012) Exploiting amyloid: how and why bacteria use cross- β fibrils. *Biochem Soc Trans* **40**: 728–34.
- Sawyer, EB, Claessen, D, Haas, M, Hurgobin, B, and Gras, SL (2011) The assembly of individual chaplin peptides from *Streptomyces coelicolor* into functional amyloid fibrils. *PLoS One* **6**: e18839.
- Saxena, IM, Brown, RM, Fevre, M, Geremia, RA, and Henriessat, B (1995) Multidomain architecture of β -glycosyl transferases: Implications for mechanism of action. *J Bacteriol* **177**: 1419–1424.
- Saxena, IM, Lin, FC, and Brown, RM (1990) Cloning and sequencing of the cellulose synthase catalytic subunit gene of *Acetobacter xylinum*. *Plant Mol Biol* **15**: 673–83.
- Schaerlaekens, K, Van Mellaert, L, Lammertyn, E, Geukens, N, and Anné, J (2004) The importance of the Tat-dependent protein secretion pathway in *Streptomyces* as revealed by phenotypic changes in *tat* deletion mutants and genome analysis. *Microbiology* **150**: 21–31.
- Schaerlaekens, K, Schierová, M, Lammertyn, E, Geukens, N, Anné, J, and Van Mellaert, L (2001) Twin-arginine translocation pathway in *Streptomyces lividans*. *J Bacteriol* **183**: 6727–32.
- Schäffer, C, and Messner, P (2005) The structure of secondary cell wall polymers: how Gram-positive bacteria stick their cell walls together. *Microbiology* **151**: 643–51.
- Schatz, A, Bugle, E, and Waksman, SA (1944) Streptomycin, a substance exhibiting antibiotic activity against Gram-positive and Gram-negative bacteria. *Exp Biol Med* **55**: 66–69.
- Schiavone, M, Vax, A, Formosa, C, Martin-Yken, H, Dague, E, and François, JM (2014) A combined chemical and enzymatic method to determine quantitatively the polysaccharide components in the cell wall of yeasts. *FEMS Yeast Res* **14**: 933–47.
- Schneewind, O, and Missiakas, DM (2012) Protein secretion and surface display in Gram-positive bacteria. *Philos Trans R Soc Lond B Biol Sci* **367**: 1123–39.
- Schneider, CA, Rasband, WS, and Eliceiri, KW (2012) NIH Image to ImageJ: 25 years of image analysis. *Nat Methods*

References

9: 671–675.

- Scholtmeijer, K, Vocht, ML de, Rink, R, Robillard, GT, and Wösten, HAB (2009) Assembly of the fungal SC3 hydrophobin into functional amyloid fibrils depends on its concentration and is promoted by cell wall polysaccharides. *J Biol Chem* **284**: 26309–14.
- Seebeck, FP (2010) In vitro reconstitution of mycobacterial ergothioneine biosynthesis. *J Am Chem Soc* **132**: 6632–6633.
- Serra, DO, Richter, AM, and Hengge, R (2013) Cellulose as an architectural element in spatially structured *Escherichia coli* biofilms. *J Bacteriol* **195**: 5540–54.
- Sezer, M, Genebra, T, Mendes, S, Martins, LO, and Todorovic, S (2012) A DyP-type peroxidase at a bio-compatible interface: structural and mechanistic insights. *Soft Matter* **8**: 10314.
- Shashkov, AS, Kosmachevskaya, LN, Streshinskaya, GM, Evtushenko, LI, Bueva, O V, Denisenko, VA, *et al.* (2002) A polymer with a backbone of 3-deoxy-D-glycero-D-galacto-non-2-ulopyranosonic acid, a teichuronic acid, and a beta-glucosylated ribitol teichoic acid in the cell wall of plant pathogenic *Streptomyces* sp. VKM Ac-2124. *Eur J Biochem* **269**: 6020–5.
- Shimon, LJ, Bayer, EA, Morag, E, Lamed, R, Yaron, S, Shoham, Y, and Frolow, F (1997) A cohesin domain from *Clostridium thermocellum*: the crystal structure provides new insights into cellulosome assembly. *Structure* **5**: 381–390.
- Sievers, F, Wilm, A, Dineen, D, Gibson, TJ, Karplus, K, Li, W, *et al.* (2011) Fast, scalable generation of high-quality protein multiple sequence alignments using Clustal Omega. *Mol Syst Biol* **7**: 539.
- Silakowski, B, Ehret, H, and Schairer, HU (1998) *fbfB*, a gene encoding a putative galactose oxidase, is involved in *Stigmatella aurantiaca* fruiting body formation. **180**: 1241–1247.
- Silakowski, B, Pospiech, A, Neumann, B, and Schairer, HU (1996) *Stigmatella aurantiaca* fruiting body formation is dependent on the *fbfA* gene encoding a polypeptide homologous to chitin synthases. *J Bacteriol* **178**: 6706–13.
- Sillitoe, I, Cuff, AL, Dessailly, BH, Dawson, NL, Furnham, N, Lee, D, *et al.* (2013) New functional families (FunFams) in CATH to improve the mapping of conserved functional sites to 3D-structures. *Nucleic Acids Res* **41**: D490–8.
- Simm, R, Morr, M, Kader, A, Nimtz, M, and Römling, U (2004) GGDEF and EAL domains inversely regulate cyclic di-GMP levels and transition from sessility to motility. *Mol Microbiol* **53**: 1123–1134.
- Singh, R, and Eltis, LD (2015) The multihued palette of dye-decolorizing peroxidases. *Arch Biochem Biophys* **574**: 56–65.
- Smits, WK, Kuipers, OP, and Veening, J-W (2006) Phenotypic variation in bacteria: the role of feedback regulation. *Nat Rev Microbiol* **4**: 259–271.
- Soliveri, J, Vijgenboom, E, Granozzi, C, Plaskitt, KA, and Chater, KF (1993) Functional and evolutionary implications of a survey of various actinomycetes for homologues of two *Streptomyces coelicolor* sporulation genes. *J Gen Microbiol* **139**: 2569–78.
- Stein, N (2008) CHAINSAW : a program for mutating pdb files used as templates in molecular replacement. *J Appl Crystallogr* **41**: 641–643.
- Studier, FW (2005) Protein production by auto-induction in high density shaking cultures. *Protein Expr Purif* **41**: 207–34.
- Sugano, Y, Sasaki, K, and Shoda, M (1999) cDNA cloning and genetic analysis of a novel decolorizing enzyme, peroxidase gene *dyp* from *Geotrichum candidum* Dec 1. *J Biosci Bioeng* **87**: 411–417.
- Sugano, Y, Muramatsu, R, Ichiyanagi, A, Sato, T, and Shoda, M (2007) DyP, a unique dye-decolorizing peroxidase, represents a novel heme peroxidase family: ASP171 replaces the distal histidine of classical peroxidases. *J*

- Biol Chem 282: 36652–8.
- Sun, L, Bulter, T, Alcalde, M, Petrounia, IP, and Arnold, FH (2002) Modification of galactose oxidase to introduce glucose 6-oxidase activity. *Chembiochem* **3**: 781–3.
- Sunde, M, Serpell, LC, Bartlam, M, Fraser, PE, Pepys, MB, and Blake, CC (1997) Common core structure of amyloid fibrils by synchrotron X-ray diffraction. *J Mol Biol* **273**: 729–739.
- Świątek, MA, Tenconi, E, Rigali, S, and Van Wezel, GP (2012) Functional analysis of the *N*-acetylglucosamine metabolic genes of *Streptomyces coelicolor* and role in control of development and antibiotic production. *J Bacteriol* **194**: 1136–44.
- Takano, M, Nakamura, M, and Yamaguchi, M (2010) Glyoxal oxidase supplies hydrogen peroxide at hyphal tips and on hyphal wall to manganese peroxidase of white-rot fungus *Phanerochaete crassa* WD1694. *J Wood Sci* **56**: 307–313.
- Takano, M, Hayashi, N, Nakamura, M, Yamaguchi, M (2009) Extracellular peroxidase reaction at hyphal tips of white-rot fungus *Phanerochaete crassa* WD1694 and in fungal slime. *J. Wood Sci.* **55**, 302–307.
- Talbot, NJ (1997) Growing into the air. *Curr Biol* **7**: R78–R81.
- Talbot, NJ, Ebbole, DJ, and Hamer, JE (1993) Identification and characterization of MPG1, a gene involved in pathogenicity from the rice blast fungus *Magnaporthe grisea*. *Plant Cell* **5**: 1575–90.
- Talbot, NJ, Kershaw, MJ, Wakley, GE, De Vries, O, Wessels, J, and Hamer, JE (1996) MPG1 encodes a fungal hydrophobin involved in surface interactions during infection-related development of *Magnaporthe grisea*. *Plant Cell* **8**: 985–999.
- Tillotson, RD, Wösten, HA, Richter, M, and Willey, JM (1998) A surface active protein involved in aerial hyphae formation in the filamentous fungus *Schizophillum commune* restores the capacity of a bald mutant of the filamentous bacterium *Streptomyces coelicolor* to erect aerial structures. *Mol Microbiol* **30**: 595–602.
- Tough, AJ, and Prosser, JI (1996) Experimental verification of a mathematical model for pelleted growth of *Streptomyces coelicolor* A3(2) in submerged batch culture. *Microbiology* **142**: 639–648.
- Tran, NT, Hengst, CD, Den, Gomez-Escribano, JP, and Buttner, MJ (2011) Identification and characterization of CdgB, a diguanylate cyclase involved in developmental processes in *Streptomyces coelicolor*. *J Bacteriol* **193**: 3100–8.
- Tremblay, LW, Dunaway-Mariano, D, and Allen, KN (2006) Structure and activity analyses of *Escherichia coli* K-12 NagD provide insight into the evolution of biochemical function in the haloalkanoic acid dehalogenase superfamily. *Biochemistry* **45**: 1183–93.
- Tresner, HD, Hayes, JA, and Backus, EJ (1967) Morphology of submerged growth of streptomycetes as a taxonomic aid. I. Morphological development of *Streptomyces aureofaciens* in agitated liquid media. *Appl Microbiol* **15**: 1185–91.
- Tul'skaya, EM, Shashkov, AS, Streshinskaya, GM, Senchenkova, SN, Potekhina, N V, Kozlova, YI, and Evtushenko, LI (2011) Teichuronic and teichulosonic acids of actinomycetes. *Biochem Biokhimiā* **76**: 736–44.
- Ueda, K, Oinuma, K-I, Ikeda, G, Hosono, K, Ohnishi, Y, Horinouchi, S, and Beppu, T (2002) AmfS, an extracellular peptidic morphogen in *Streptomyces griseus*. *J Bacteriol* **184**: 1488–92.
- Ueda, K, Tomaru, Y, Endoh, K, Beppu, T (1997) Stimulatory effect of copper on antibiotic production and morphological differentiation in *Streptomyces tanashiensis*. *J. Antibiot. (Tokyo)*. **50**, 693–5.
- Vara, J, Lewandowska-Skarbek, M, Wang, YG, Donadio, S, and Hutchinson, CR (1989) Cloning of genes governing the deoxysugar portion of the erythromycin biosynthesis pathway in *Saccharopolyspora erythraea* (*Streptomyces erythreus*). *J Bacteriol* **171**: 5872–81.
- Vecht-Lifshitz, SE, Magdassi, S, and Braun, S (1990) Pellet formation and cellular aggregation in *Streptomyces*

References

- tendae*. *Biotechnol Bioeng* **35**: 890–6.
- Veening, J-W, Smits, WK, and Kuipers, OP (2008) Bistability, epigenetics, and bet-hedging in bacteria. *Annu Rev Microbiol* **62**: 193–210.
- Van Veluw, GJ, Petrus, MLC, Gubbens, J, De Graaf, R, De Jong, IP, Van Wezel, GP, *et al.* (2012) Analysis of two distinct mycelial populations in liquid-grown *Streptomyces* cultures using a flow cytometry-based proteomics approach. *Appl Microbiol Biotechnol* **96**: 1301–12.
- Van Veluw, GJ, Teertstra, WR, De Bekker, C, Vinck, A, Van Beek, N, Muller, WH, *et al.* (2013) Heterogeneity in liquid shaken cultures of *Aspergillus niger* inoculated with melanised conidia or conidia of pigmentation mutants. *Stud Mycol* **74**: 47–57.
- Vijgenboom, E, Woudt, LP, Heinstra, PW, Rietveld, K, Van Haarlem, J, Van Wezel, GP, *et al.* (1994) Three *tuf*-like genes in the kirromycin producer *Streptomyces ramocissimus*. *Microbiology* **140** (Pt 4): 983–98.
- Vinck, A, Terlouw, M, Pestman, WR, Martens, EP, Ram, AF, Van Den Hondel, CAMJJ, and Wösten, HAB (2005) Hyphal differentiation in the exploring mycelium of *Aspergillus niger*. *Mol Microbiol* **58**: 693–699.
- De Vocht, ML, Reviakine, I, Ulrich, W-P, Bergsma-Schutter, W, Wösten, HAB, Vogel, H, *et al.* (2002) Self-assembly of the hydrophobin SC3 proceeds via two structural intermediates. *Protein Sci* **11**: 1199–1205.
- Vrancken, K, and Anné, J (2009) Secretory production of recombinant proteins by *Streptomyces*. *Future Microbiol* **4**: 181–188.
- Wardell, JN, Stocks, SM, Thomas, CR, and Bushell, ME (2002) Decreasing the hyphal branching rate of *Saccharopolyspora erythraea* NRRL 2338 leads to increased resistance to breakage and increased antibiotic production. *Biotechnol Bioeng* **78**: 141–146.
- Weerapana, E, and Imperiali, B (2006) Asparagine-linked protein glycosylation: from eukaryotic to prokaryotic systems. *Glycobiology* **16**: 91R–101R.
- Weidenmaier, C, and Peschel, A (2008) Teichoic acids and related cell-wall glycopolymers in Gram-positive physiology and host interactions. *Nat Rev Microbiol* **6**: 276–87.
- Wessel, D, and Flüggé, UI (1984) A method for the quantitative recovery of protein in dilute solution in the presence of detergents and lipids. *Anal Biochem* **138**: 141–143.
- Van Wezel, GP, Krabben, P, Traag, BA, Keijsers, BJF, Kerster, R, Vijgenboom, E, *et al.* (2006) Unlocking *Streptomyces* spp. for use as sustainable industrial production platforms by morphological engineering. *Appl Environ Microbiol* **72**: 5283–5288.
- Van Wezel, GP, and McDowall, KJ (2011) The regulation of the secondary metabolism of *Streptomyces*: new links and experimental advances. *Nat Prod Rep* **28**: 1311–1333.
- Whitchurch, CB, Tolker-Nielsen, T, Ragas, PC, and Mattick, JS (2002) Extracellular DNA required for bacterial biofilm formation. *Science* **295**: 1487.
- White, AP, Gibson, DL, Collinson, SK, Banser, PA, and Kay, WW (2003) Extracellular polysaccharides associated with thin aggregative fimbriae of *Salmonella enterica* serovar enteritidis. *J Bacteriol* **185**: 5398–407.
- Whittaker, MM, Kersten, PJ, Cullen, D, and Whittaker, JW (1999) Identification of catalytic residues in glyoxal oxidase by targeted mutagenesis. *J Biol Chem* **274**: 36226–32.
- Whittaker, MM, and Whittaker, JW (1988) The active site of galactose oxidase. *J Biol Chem* **263**: 6074–80.
- Whittaker, MM, and Whittaker, JW (1990) A tyrosine-derived free radical in apogalactose oxidase. *J Biol Chem* **265**: 9610–3.
- Whittaker, MM, and Whittaker, JW (1993) Ligand interactions with galactose oxidase: mechanistic insights. *Biophys J* **64**: 762–72.

- Whittaker, MM, and Whittaker, JW (2003) Cu(I)-dependent biogenesis of the galactose oxidase redox cofactor. *J Biol Chem* **278**: 22090–101.
- Whittaker, MM, and Whittaker, JW (2006) *Streptomyces coelicolor* oxidase (SCO2837p): a new free radical metalloenzyme secreted by *Streptomyces coelicolor* A3(2). *Arch Biochem Biophys* **452**: 108–18.
- Widdick, DA, Dilks, K, Chandra, G, Bottrill, A, Naldrett, M, Pohlschröder, M, and Palmer, T (2006) The twin-arginine translocation pathway is a major route of protein export in *Streptomyces coelicolor*. *Proc Natl Acad Sci U S A* **103**: 17927–32.
- Widdick, DA, Eijlander, RT, Van Dijl, JM, Kuipers, OP, and Palmer, T (2008) A facile reporter system for the experimental identification of twin-arginine translocation (Tat) signal peptides from all kingdoms of life. *J Mol Biol* **375**: 595–603.
- Wildermuth, H, Wehrli, E, and Horne, RW (1971) The surface structure of spores and aerial mycelium in *Streptomyces coelicolor*. *J Ultrastruct Res* **35**: 168–80.
- Willemse, J, Borst, JW, Waal, E De, Bisseling, T, and Van Wezel, GP (2011) Positive control of cell division: FtsZ is recruited by SsgB during sporulation of *Streptomyces*. *Genes Dev* **25**: 89–99.
- Willemse, J, Ruban-Ośmiałowska, B, Widdick, D, Celler, K, Hutchings, MI, Van Wezel, GP, and Palmer, T (2012) Dynamic localization of Tat protein transport machinery components in *Streptomyces coelicolor*. *J Bacteriol* **194**: 6272–81.
- Willey, J, Santamaria, R, Guijarro, J, Geistlich, M, and Losick, R (1991) Extracellular complementation of a developmental mutation implicates a small sporulation protein in aerial mycelium formation by *S. coelicolor*. *Cell* **65**: 641–50.
- Willey, JM, Willems, A, Kodani, S, and Nodwell, JR (2006) Morphogenetic surfactants and their role in the formation of aerial hyphae in *Streptomyces coelicolor*. *Mol Microbiol* **59**: 731–742.
- Wood, PJ (1980) Specificity in the interaction of direct dyes with polysaccharides. *Carbohydr Res* **85**: 271–287.
- Worrall, JAR, and Vijgenboom, E (2010) Copper mining in *Streptomyces*: enzymes, natural products and development. *Nat Prod Rep* **27**: 742–56.
- Wösten, H, De Vries, O, and Wessels, J (1993) Interfacial self-assembly of a fungal hydrophobin into a hydrophobic rodlet layer. *Plant Cell* **5**: 1567–1574.
- Wösten, HAB, Schuren, FH, and Wessels, JG (1994) Interfacial self-assembly of a hydrophobin into an amphipathic protein membrane mediates fungal attachment to hydrophobic surfaces. *EMBO J* **13**: 5848–54.
- Wösten, HAB, Van Wetter, M-A, Lugones, LG, Van der Mei, HC, Busscher, HJ, and Wessels, JGH (1999) How a fungus escapes the water to grow into the air. *Curr Biol* **9**: 85–88.
- Xu, H, Chater, KF, Deng, Z, and Tao, M (2008) A cellulose synthase-like protein involved in hyphal tip growth and morphological differentiation in *Streptomyces*. *J Bacteriol* **190**: 4971–8.
- Yamanaka, K, Oikawa, H, Ogawa, HO, Hosono, K, Shinmachi, F, Takano, H, *et al.* (2005) Desferrioxamine E produced by *Streptomyces griseus* stimulates growth and development of *Streptomyces tanashiensis*. *Microbiology* **151**: 2899–2905.
- Yeats, C, Bentley, S, and Bateman, A (2003) New knowledge from old: In silico discovery of novel protein domains in *Streptomyces coelicolor*. *BMC Microbiol* **3**: 3.
- Zogaj, X, Nimtz, M, Rohde, M, Bokranz, W, Römling, U, and Römling, U (2001) The multicellular morphotypes of *Salmonella typhimurium* and *Escherichia coli* produce cellulose as the second component of the extracellular matrix. *Mol Microbiol* **39**: 1452–1463.

C

Curriculum Vitae

Maria Louise Catharina (Marloes) Petrus was born on the 8th of January, 1988, in Heemskerk, The Netherlands. In 2006, she graduated from the Kennemer College in Beverwijk with honor. In September of that same year she started her Life, Science & Technology studies at Leiden University and Delft University of Technology. As part of the Bachelor program she completed an internship at the Leiden University Medical Centre in the group of Prof. Dr. Rob C. Hoeben under supervision of Dr. Danijela Koppers-Lalic. During this internship she identified epitopes of the Adenovirus capsule proteins that are recognized by human immunoglobulins. After obtaining her Bachelor degree she continued with her Master's in Life Science & Technology at Leiden University in 2009. During her Master's internship in the Molecular Biotechnology group under supervision of Prof. Dr. Gilles P. van Wezel and Dr. Magdalena A. Świątek she was introduced to the research on streptomycetes. Marloes accomplished her Master program with honor in August 2011. In September of that year she started as a PhD-student at the Institute of Biology (Leiden University) under supervision of Dr. Dennis Claessen and Prof. dr. Gilles P. van Wezel. The work done as a PhD student is described in this thesis. Currently Marloes is working as a Scientist Discovery for BioMarin Nederland B.V.

P

Publications

Petrus, MLC, Vijgenboom, E, Chaplin, AK, Worrall, JAR, Van Wezel, GP, and Claessen, D (2016) The DyP-type peroxidase DtpA is a Tat-substrate required for GlxA maturation and morphogenesis in *Streptomyces*. *Open Biology* **6**: (1) p. 150149

Chaplin, AK, **Petrus, MLC**, Mangiameli, G, Hough, MA, Svistunenko, DA, Nicholls, P, *et al.* (2015) GlxA is a new structural member of the radical copper oxidase family and is required for glycan deposition at hyphal tips and morphogenesis of *Streptomyces lividans*. *Biochem J* **469**: 433–444.

Petrus, MLC, and Claessen, D (2014) Pivotal roles for *Streptomyces* cell surface polymers in morphological differentiation, attachment and mycelial architecture. *Antonie Van Leeuwenhoek* **106**: 127–139.

Petrus, MLC, Van Veluw, GJ, Wösten, HAB, and Claessen, D (2014) Sorting of *Streptomyces* cell pellets using a complex object parametric analyzer and sorter. *J Vis Exp* e51178.

Van Veluw*, GJ, **Petrus***, **MLC**, Gubbens*, J, De Graaf, R, De Jong, IP, Van Wezel, GP, *et al.* (2012) Analysis of two distinct mycelial populations in liquid-grown *Streptomyces* cultures using a flow cytometry-based proteomics approach. *Appl Microbiol Biotechnol* **96**: 1301–12.

